INFORMATION TO USERS

This was produced from a copy of a document sent to us for microfilming. While the most advanced technological means to photograph and reproduce this document have been used, the quality is heavily dependent upon the quality of the material submitted.

The following explanation of techniques is provided to help you understand markings or notations which may appear on this reproduction.

1. The sign or "target" for pages apparently lacking from the document photographed is "Missing Page(s)". If it was possible to obtain the missing page(s) or section, they are spliced into the film along with adjacent pages. This may have necessitated cutting through an image and duplicating adjacent pages to assure you of complete continuity.

2. When an image on the film is obliterated with a round black mark it is an indication that the film inspector noticed either blurred copy because of movement during exposure, or duplicate copy. Unless we meant to delete copyrighted materials that should not have been filmed, you will find a good image of the page in the adjacent frame.

3. When a map, drawing or chart, etc., is part of the material being photographed the photographer has followed a definite method in "sectioning" the material. It is customary to begin filming at the upper left hand corner of a large sheet and to continue from left to right in equal sections with small overlaps. If necessary, sectioning is continued again—beginning below the first row and continuing on until complete.

4. For any illustrations that cannot be reproduced satisfactorily by xerography, photographic prints can be purchased at additional cost and tipped into your xerographic copy. Requests can be made to our Dissertations Customer Services Department.

5. Some pages in any document may have indistinct print. In all cases we have filmed the best available copy.

PLEASE NOTE:

In all cases this material has been filmed in the best possible way from the available copy. Problems encountered with this document have been identified here with a check mark ✓.

1. Glossy photographs _____

2. Colored illustrations _____

3. Photographs with dark background _____

4. Illustrations are poor copy _____

5. Print shows through as there is text on both sides of page _____

6. Indistinct, broken or small print on several pages _____ throughout _____

7. Tightly bound copy with print lost in spine _____

8. Computer printout pages with indistinct print ✓_____

9. Page(s) _____ lacking when material received, and not available from school or author _____

10. Page(s) _____ seem to be missing in numbering only as text follows _____

11. Poor carbon copy _____

12. Not original copy, several pages with blurred type _____

13. Appendix pages are poor copy _____

14. Original copy with light type _____

15. Curling and wrinkled pages _____

16. Other _____

7908187

NADEL, LAWRENCE DENNIS
   AN INVESTIGATION OF THE PULSE-SCATTER IMAGING
TECHNIQUE FOR MEDICAL ULTRASONIC IMAGING AND
   TISSUE CHARACTERIZATION.

THE OHIO STATE UNIVERSITY, PH.D., 1978

AN INVESTIGATION OF THE PULSE-SCATTER

IMAGING TECHNIQUE FOR MEDICAL ULTRASONIC

IMAGING AND TISSUE CHARACTERIZATION

DISSERTATION

Presented in Partial Fulfillment of the Requirements for

the Degree Doctor of Philosophy in the Graduate

School of the Ohio State University
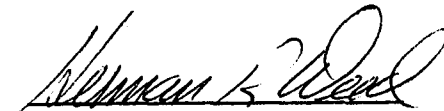
by

Lawrence Dennis Nadel, B.S.E.E., M.Sc.

* * * * *

The Ohio State University

1978

Reading Committee:

Dr. Richard Campbell
Dr. Dean Davis
Dr. Karl Graff
Dr. Atis Freimanis
Dr. Hsiung Hsu
Prof. Herman Weed

Approved By

Adviser
Department of Electrical
Engineering

ACKNOWLEDGEMENTS

Many people have contributed both directly and indirectly to the success of this dissertation. Unfortunately, not everyone can be mentioned or given their due credit in the sentences which follow. Those who are not mentioned or just mentioned briefly, however, I hope will realize my grateful appreciation for their technical assistance, personal cooperation and friendship.

I must first express my gratitude to Professor Herman Weed, my academic adviser and "chief consultant" throughout my years at Ohio State, while pursuing both the masters and doctoral degrees. In addition to his lectures in the classroom, academic guidance, moral support and his tending to the neverending administrative affairs, Professor Weed offered the special qualities of personal understanding and friendship, helping to make my attendance at Ohio State both worthwhile and enjoyable.

With respect to this dissertation in particular, the foremost person responsible for its success is Dr. Stephen Tehon, Consulting Engineer for Solid State Acoustics at the GE E-Lab. It was through Steve that I was first invited to participate in the E-Lab's summer employment program. Somehow, Steve managed to find time in his hectic schedule (generally after working hours) to serve as a highly competent and professional educator and primary technical consultant. Quite an impossible task, Steve coordinated what was essentially

ii

VITA

March 1, 1952 . . . .   Born - Brooklyn, New York

1973 . . . .   B.S.E.E., Polytechnic Institute of Brooklyn,
                               Brooklyn, New York

1973-1978 . . . .   Graduate Research Associate, Bio-Medical
                               Engineering Center, The Ohio State University,
                               Columbus, Ohio

1975 . . . .   M.Sc. (EE-BME), The Ohio State University,
                               Columbus, Ohio

1977-78 . . . .   Research Intern, General Electric Company,
                               Electronics Laboratory, Syracuse, New York

PUBLICATIONS

"A Hybrid Computer System for Use in Cardiology", IEEE 27th ACEMB Proceedings, October, 1974.

"A Remotely Located Hybrid Computer System for Use in Cardiology", AAMI Conference Proceedings, March, 1976.

"Computerized Cardiac Catheterization Analysis Via a Remotely Located Hybrid Computer System", IEEE 29th ACEMB Proceedings, November, 1976.

"A Hybrid Computer System for Use in Cardiology", Medical Progress Through Technology, 4(4), April, 1977, pp. 185-191.

"PSI-- A New Ultrasonic Imaging Technique", IEEE 31st ACEMB Proceedings, November, 1978.

FIELDS OF STUDY

Major Field: Electrical Engineering

Studies in Bio-Medical Engineering. Professors Herman R. Weed and
Richard M. Campbell

Minor Fields:

Studies in Digital and Computer Systems. Professor Robert B. Lackey

Studies in Medicine (Cardiology). Professor Mary Beth Fontana, M.D.

Studies in Statistics. Dean Thomas A. Willke

TABLE OF CONTENTS

TABLE OF CONTENTS (cont.)

LIST OF FIGURES

LIST OF FIGURES (cont.)

LIST OF FIGURES (cont.)

LIST OF FIGURES (cont.)

LIST OF TABLES

CHAPTER I. INTRODUCTION

A. INVESTIGATION PERSPECTIVE

The most widely used ultrasonic imaging technique in medical diagnosis today is the pulse-echo B-scan. This method results in the production of cross-sectional images of the body, utilizing ultrasonic energy incident upon and reflected from tissue structures in a normal direction. Biological tissue is generally (i.e. depending upon the frequency and lateral dimensions of the sound beam used) specular with respect to diagnostic ultrasound and so unless normal incidence and reception of the ultrasonic beam using the pulse-echo mode is achieved, essentially none of the acoustic energy impinging upon a particular tissue surface will be received. Since most of the tissue structures being insonified by a given pulse of acoustic energy will, by sheer probability considerations, lie non-normally to the incident beam, only a small portion of the transmitted energy will contribute to the B-scan image. In order to increase signal reception and, thus, the information contained in the B-scan image, the concept of Pulse-Scatter Imaging (PSI) [1] is hereby being investigated. As will be described in detail in Chapter IV of this dissertation, the PSI technique, rather than use a single transmit/receive transducer as in B-scan, utilizes a circular array of ultrasonic transducers in which each transducer is pulsed once in succession around the array while, following each pulsed transmission, all

1

transducers are utilized as receivers. Therefore, in addition to receiving the standard pulse-echo signals, the pulse-scattered signals are received and incorporated into the image as well.

In conducting this investigation of PSI, a previous computer simulation and report on the proposed concept was available for review, however, no prior work had been done with real data [1]. Thus, after establishment of a general protocol, it was necessary to conduct a preliminary computer simulation of the reconstruction method, itself, followed by development of both a facility and capability for PSI data collection, processing and display. Hardware development centered around design and fabrication of the physical apparatus for calibrated transducer and specimen manipulation. A minimal amount of electronic circuitry had to be designed as well. In addition to the main PSI reconstruction algorithm, general software routines were written to enable automatic control of acoustic data acquisition via a digitizing transient recorder, pre-reconstruction data processing, and post-reconstruction image analysis and processing. As will be shown by the photographs in Chapters V and VI (please note that unless the printed reproduction of these photos maintains a high quality gray scale, many of the images may appear washed out and not show the details discussed in the text), both biological and non-biological objects (e.g. metal rods, Plexiglas triangle, transistor heat sink, natural sponge, home-made polyurethane gel/polyethylene tubing tissue phantom, chicken heart) were imaged with reasonable success, especially when taking into account the fact that the overall PSI system as investigated was a "non-tuned" version, in only its initial stage of development.

Briefly, several hypothesized advantages of the PSI technique in medical imaging may be itemized as follows:

(i) Rapid scan time/minimal patient exposure -- each transducer in array need be excited on the order of a microsecond, only once. All scattered signals are received simultaneously, for a given transducer excitation.

(ii) More image information due to the incorporation of scattered data in addition to the standard pulse-echo data.

(iii) Transducer beam dimensions are less crucial since a fan beam rather than a pencil beam is required; resolution depends upon the reconstruction process and the ability to measure signal time differences of arrival.

(iv) The use of a three-dimensional annular transducer array along with digital storage of the original data will enable display and magnification of an arbitrary oblique cross-section.

(v) Electronic scanning of the transducer array eliminates the operator variability experienced in manual procedures.

(vi) Incorporation of a rapid electronic switching and data processing capability could enable real-time display; a pseudo-real-time display could be reconstructed from the stored scans via synchronization with a signal such as EKG.

B.   HISTORICAL INTRODUCTION

Scientific interest in the principles of ultrasonic waves (i.e. sound waves of greater frequency than the human audible limit of approximately 20 kHz) had its firmest roots in the 1800's when researchers such as Savart and Despretz

developed ultrasonic generators, and others such as Dr. Francis Galton became curious as to the limits of hearing in humans and animals. [2] During the latter 1800's and early 1900's, Lord Rayleigh carried out investigations culminating in his renowned Theory of Sound [3], which still stands as the fundamental description of acoustic behavior. It was also in the 19th century when the basic ideas behind electro-mechanical ultrasonic transduction were developed -- Joule with his work on magnetostriction around 1842 and the Curie brothers, Jacques and Pierre, with their investigations of piezoelectricity around 1880 [2].

The first attempts at any sort of ultrasonic imaging were made by researchers such as the Frenchman, Langevin, the Russian, Chilowsky, and the Englishmen, Rutherford and Boyle, who worked on sonar systems for the detection of submarines in World War I. It was not until World War II that the newly developed electronic sophistication and better quality ultrasonic transducers enabled the development of a reliable sonar detection system. Sokolov, during the 1930's, is recognized for the first major attempt at ultrasonic nondestructive testing (NDT) of materials for flaws, with the introduction of his "shadow method" [2]. Dussik is considered the "father of medical ultrasound" for his work in the 1940's dealing with medical ultrasonic transmission imaging [57].

Firestone, while at the University of Michigan, is credited with the first American attempt at ultrasonic NDT, with the development of the "supersonic reflectoscope" [4], [5], which produced an A-mode display. With the announcement of this device, Smith recognized the potential for visualization of soft biological tissues (not visible with X-rays) using reflected ultrasound [6]. Although unable to secure funds to support research, Smith's observation was one of the first of many, which between 1950 and the present, spurred by the rapid advances in electronic technology, have led to the development of ultrasonic

diagnostic imaging systems capable of A, B, C and M scans in both real and non-real time. In fact, the tremendous interest in medical ultrasonic imaging generated by the preliminary work in NDT has resulted in such rapid advances in the medical systems, particularly in the last decade, that equipment and techniques developed in the medical arena are now being re-applied to NDT procedures.

C.   MOTIVATION FOR MEDICAL ULTRASONIC IMAGING

The past decade has seen a rapidly increasing utilization of clinical ultrasonic imaging procedures. The two primary motivating factors, in conjunction with the higher quality of commercially available equipment, have been (i) the (presumed) biological safety of ultrasound at currently used diagnostic power levels, as compared with the hazards of long-existing imaging techniques using ionizing radiation such as X-ray, and (ii) the highly effective ability of ultrasound to visualize soft-tissues.

In the case of fetal examination, for example, the potential damaging effects of X-rays have been generally accepted. Although various studies around the country are currently in progress to rigorously demonstrate the safety of diagnostic ultrasound [7], the limited studies to date have failed to demonstrate any harmful effects of ultrasound when administered at current diagnostic power levels [8]. As a result, ultrasound is now routinely used to monitor fetal development periodically during gestation (as well as to monitor fetal heart sounds via doppler techniques).

Up until the introduction of computerized X-ray tomography (CT) several years ago [9], ultrasound provided essentially the only means for discrimination of soft tissues. Even now, however, ultrasound still possesses a greater

capability for soft tissue visualization and characterization than does CT (which strictly relies on a tissue's ability to absorb X-rays) due to the fact that ultrasonic interaction with body tissues relies on numerous parameters, some of which will be discussed in Chapters II and III.

D. CHRONOLOGICAL PERSPECTIVE OF DISSERTATION

The work on this dissertation can essentially be divided into three phases. The first phase extended from January, 1977 - June, 1977, when full-time was spent on the O.S.U. campus. During this time, clinical exposure and experience as well as an education on the aspects of medical ultrasound were obtained under the guidance of Dr. Atis Freimanis, Professor and Chairman of the Ohio State University Department of Radiology, and the ultrasound staff. Concurrently, a state-of-the-art review of ultrasonic imaging techniques (medical and industrial) along with a survey and examination, where possible, of ultrasonic imaging equipment, was undertaken.

July, 1977 through June, 1978 encompassed the second phase of this work, where full time was spent conducting the bulk of this investigation at the General Electric Company's Electronics Laboratory, under the leadership of Dr. Stephen Tehon, Consulting Engineer in Solid State Acoustics.

Finally, this dissertation was written and final data gathered during July, 1978-December, 1978 when full-time periods were spent both on the Ohio State campus and at General Electric.

E. PURPOSE OF INVESTIGATION

The concept of Pulse-Scatter Imaging (PSI) was conceived during the summer of 1976 at the General Electric Company's Electronics Laboratory in Syracuse, New York in an academic/industrial cooperative effort under the leadership of Dr. Stephen Tehon [1]. A generalized mathematical approach

for the implementation of the PSI concept was suggested and a preliminary computer simulation examining the geometry involved was developed [10] . A six-transducer ring was constructed and preliminary data taken; however, attempts at image reconstruction were limited and unsuccessful. Essentially, no further work was carried out on this project until June, 1977, when another student, Mr. Larry Browning, PhD candidate in Physics at Purdue University, and the author were given the responsibility of starting an investigation of the PSI technique, as part of a summer employment program. Prior to returning to school at the beginning of August, Mr. Browning had written a preliminary program for reconstructing an image using the PSI technique on a Varian mini-computer. The author's efforts were spent developing a manual PSI data acquisition and data processing capability using the limited laboratory equipment available.

Around the end of the summer, a minimal amount of funds became available to support the construction of some rather crude experimental hardware. With the Electronics Laboratory's purchase of a high speed digital transient recorder, the potential for a complete data acquisition and processing system, utilizing a PDP-11 minicomputer, became available, and it was suggested by academic advisers at Ohio State and GE staff that the author carry out his dissertation in medical ultrasonic imaging at General Electric, to investigate the validity and feasibility of the PSI technique for ultrasonic imaging and in particular, as applied to medical imaging, as well as to derive a theoretical description of the technique. These tasks, which comprise the bulk of this dissertation, are described in detail throughout Chapters IV-VIII, in addition to the following brief categorization —

    i)   review PSI concept, previously untested, as well as applicable acoustic theory

ii) design experimental protocol and associated hardware/software
to test the PSI concept

iii) develop a theoretical basis for PSI

iv) modify PSI concept as necessary and repeat experiment

v) evaluate PSI technique as to its potential usefulness and feasibility
as a clinical imaging procedure.

The next two chapters (II and III) will provide a summary of the theoretical
acoustic considerations for ultrasonic imaging, as well as a review of existing
techniques used both in clinical and research environments for ultrasonic imaging.
Since PSI results in a reconstructed image, Chapter IV will reference several
somewhat related techniques, such as computerized X-ray tomography (CT)
and military radar detection systems using a reconstruction-like approach.

CHAPTER II. BACKGROUND ACOUSTIC THEORY

A. INTRODUCTION

In the non-destructive evaluation of materials, flaw or structural detection by ultrasonic means may be accomplished by both transmission and reflection techniques, since any material discontinuity will tend to intercept and scatter the ultrasonic beam, which can produce any or a combination of reflection, refraction, diffraction, and traveling wave mode conversion. Such effects will vary with changes in sample properties. Thus, transmission techniques indicate flaws by a smaller received signal than would otherwise be expected, taking standard transmission properties of the material into account, whereas reflection systems will exhibit an echo or reflected wave. For simple non-destructive testing, transmission techniques have the drawback of requiring access to more than one surface of the given object.

In general, reflective techniques predominate in the United States, whereas transmission techniques have found more widespread use abroad. The remainder of this chapter is devoted to a review and edited compilation of both general ultrasonic theory and acoustic scattering phenomena.

B. WAVE AND TRANSMISSION THEORY OF ULTRASONIC SIGNALS

In utilizing ultrasonics for materials inspection three general assumptions are made, namely,

(i) the ultrasonic beam consists of plane wave fronts

9

(ii)   elastic moduli are independent of stress amplitude, frequency and direction

(iii)   when frequency is a parameter, particle motion is continuous and sinusoidal.

These assumptions are reasonably valid unless very short or very large amplitude pulses are utilized [11] .

Depending upon a material's state of matter, various modes of ultrasonic vibration may be supported, with individualized material/mode specific velocities. Acoustic velocity, frequency and wavelength are governed by the following relation (CGS units shown)

$$v = f\lambda \tag{2-1}$$

where v = velocity (cm/sec)

f = frequency (Hz)

λ = wavelength (cm)

Velocity is frequency dependent except in cases where one or more material dimensions approach a wavelength and phasing effects can occur [11] .

The two primary acoustic wave modes, which we are concerned with in materials evaluation, are longitudinal and transverse propagation. Longitudinal waves exhibit particle motion in the direction of the applied force (compression) while transverse waves produce motion perpendicular to the direction of wave travel (shear) (see Figure 2-1). No net particle movement is exhibited except for such phenomena as liquid streaming. Longitudinal waves are readily supported in gases, liquids and solids, whereas shear waves are generally restricted to solids (and fluids with appreciable viscosity). The longitudinal and transverse modes may exist either individually or in combination depending upon the material properties and geometry.

(a) LONGITUDINAL WAVES

(b) TRANSVERSE WAVES

DIRECTION OF TRAVEL ⟶
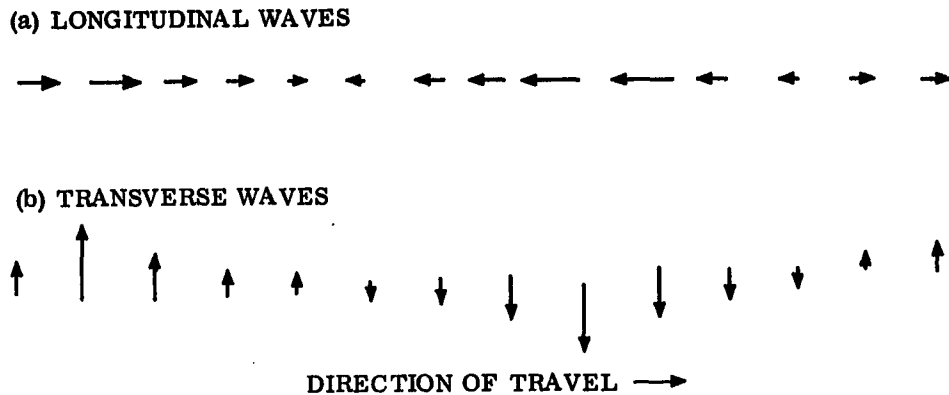
Figure 2-1. Particle motion in longitudinal and transverse (shear) waves.
Arrows represent velocity vector of the particles in the medium
at a given instant of time. (Adapted from Hussey [14] , p. 20).

Before proceeding any further, it would be worthwhile to define the dif-
ferences between acoustic amplitude, energy, intensity and power. The acoustic
amplitude is essentially the degree of instantaneous excursion about their resting
points undergone by the particles of the insonified medium. For example, when
receiving an emitted acoustic signal with another piezoelectric transducer,
one would measure acoustic amplitude in terms of the electrical voltage of
the received signal.

The particles in an insonified medium (assumed lossless) normally
undergo simple harmonic motion, and as a result, do not experience any net
movement (unless, for example, acoustic streaming occurs). Thus, the total
energy of the system, comprised of the sum of the potential and kinetic com-
ponents, is constant over time, and is equal to

$$e = \frac{1}{2} m v_o^2 \tag{2-2}$$

where   m = mass of particle

   v_o = velocity of particle at reference displacement

   (i.e. maximum velocity of particle)

The energy density, E, equal to the total energy of all particles in a given volume is calculated by replacing the mass of a single particle, m, in Equation (2-2), by the mass per unit volume, otherwise defined as density, ρ.

$$E = \frac{1}{2} \rho v_o^2 \tag{2-3}$$

Now, the ultrasonic intensity, I, is defined as the energy traveling through a unit area (perpendicular to beam direction) in unit time (i.e. rate of flow of energy through unit area). Given the wave velocity, c (measured in distance per unit time), a unit volume then equals area $\times$ c. Thus, intensity is computed as

$$I = cE \tag{2-4}$$

$$= \frac{1}{2} \rho c v_o^2 \tag{2-5}$$

$$= \frac{1}{2} Z v_o^2 \tag{2-6}$$

where "Z" is the acoustic impedance, to be defined in Equation (2-8).

Finally, the power of an acoustic signal is the rate of energy flow through the entire ultrasonic beam cross-section. Therefore,

$$P = I \times A \tag{2-7}$$

where   P = ultrasonic power (watts)

   I = ultrasonic intensity (watts - cm^2)

   A = beam cross-sectional area (cm^2)

One must specify whether a given power measurement is peak or time-averaged. For diagnostic ultrasound signals, peak power is typically 5-50 watts whereas average power is generally in the neighborhood of 5 mW [12] .

The characteristic acoustic impedance, Z, of a substance, (referred to in Equation (2-6)), defined by the relation

$$Z = \rho v \tag{2-8}$$

where ρ = density (g/cm^3)

   v = velocity (cm/sec),

is useful in describing ultrasonic behavior at material boundaries. The quantity and direction of energy reflected/transmitted at a plane boundary depends both on the respective acoustic impedances and the beam angle of incidence.

No sudden discontinuities can exist in either particle velocity or particle pressure in a traveling wave, thus establishing a set of boundary conditions for a wave impinging upon an interface between two media. Such conditions ensure that physical contact between the media is maintained. Formation of both an equation relating the vector sum of the normal components of the incident, transmitted and reflected waves, and a pressure equality sum, meets the above continuity requirements. Thus,

$$v_i \cos \theta_i - v_r \cos \theta_r = v_t \cos \theta_t \tag{2-9}$$

and $$p_i + p_r = p_t \tag{2-10}$$

where v = velocity

   p = pressure

   θ = angle with respect to normal

   i = incident wave

   r = reflected wave

   t = transmitted wave

(see Figure 2-2).
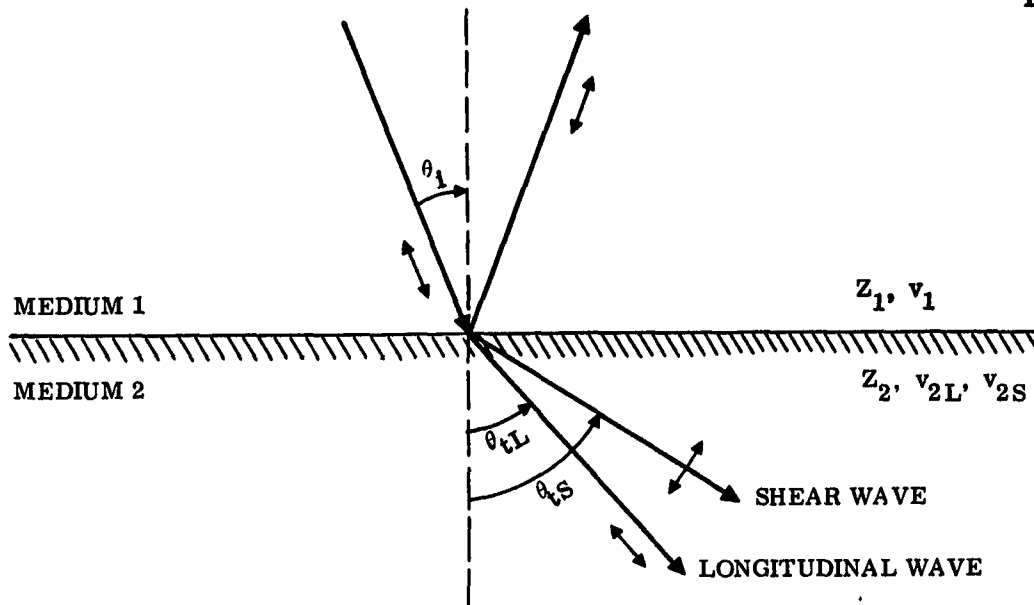
Figure 2-2. Some possible waves generated from oblique incidence at a plane interface - reflection, refraction and mode conversion.

Now, the Ohm's Law analogy in acoustics is

$$p = Z v \tag{2-11}$$

Incorporating Equation (2-8) into the above, results in

$$p = \rho c v \tag{2-12}$$

Thus, Equation (2-9) can be written as

$$\left(\frac{p_i}{Z_1}\right) \cos \theta_i - \left(\frac{p_r}{Z_1}\right) \cos \theta_i = \left(\frac{p_t}{Z_2}\right) \cos \theta_i \tag{2-13}$$

where the wave is traveling from a medium with impedance, Z_1 to one with impedance Z_2.

Solving Equations (2-10) and (2-13) simultaneously results in

$$\frac{p_r}{p_i} = \frac{Z_2 \cos \theta_i - Z_1 \cos \theta_t}{Z_2 \cos \theta_i + Z_1 \cos \theta_t} \tag{2-14}$$

and

$$\frac{p_t}{p_i} = \frac{2 Z_2 \cos \theta_i}{Z_2 \cos \theta_i + Z_1 \cos \theta_t} \tag{2-15}$$

Under circumstances of normal incidence, $\theta_i = \theta_t = 0$, resulting in

$$\frac{p_r}{p_i} = \frac{(Z_2 - Z_1)}{(Z_2 + Z_1)} \tag{2-16}$$

and

$$\frac{p_t}{p_i} = \left(\frac{2 Z_2}{Z_2 + Z_1}\right) \tag{2-17}$$

Therefore, for perfect impedance matching, $Z_1 = Z_2$ and $p_r/p_i = 0$, specifying no reflected wave. When $Z_2 > Z_1$, $p_r/p_i = (+)$ and so the incident and reflected waves are in phase; for $Z_2 < Z_1$, $p_r/p_i = (-)$, resulting in a 180° out-of-phase relationship.

Next, in order to ascertain the relationship for acoustic intensity,

$$v_o^2 = \frac{p_o^2}{\rho^2 c^2} \tag{2-18}$$

from Equation (2-12). Substitution into Equation (2-5) results in

$$I = \frac{1}{2} \frac{p_o^2}{\rho_c} \tag{2-19}$$

Thus, intensity is proportional to (pressure)^2 and so Equations (2-13) and (2-14) may be rewritten as

$$\frac{I_r}{I_t} = \left(\frac{Z_2 \cos \theta_i - Z_1 \cos \theta_t}{Z_2 \cos \theta_i + Z_1 \cos \theta_t}\right)^2 \tag{2-20}$$

and

$$\frac{I_t}{I_i} = \frac{4 Z_2 Z_1 \cos \theta_i \cos \theta_t}{\left(Z_2 \cos \theta_i + Z_1 \cos \theta_t\right)^2} \tag{2-21}$$

The ratio I_r/I_t is termed the reflection coefficient, R, and I_t/I_i, the transmission coefficient, T. For the case of normal incidence

$$R = \frac{I_r}{I_t} = \left(\frac{Z_2 - Z_1}{Z_2 + Z_1}\right)^2 = \left(\frac{\frac{Z_2}{Z_1} - 1}{\frac{Z_2}{Z_1} + 1}\right) = \left(\frac{r-1}{r+1}\right)^2 \tag{2-22}$$

where r = impedance mismatch factor, Z_2/Z_1. Likewise, for normal incidence

$$T = \frac{I_t}{I_i} = 1 - R = \frac{4 Z_2 Z_1}{\left(Z_2 + Z_1\right)^2} = \frac{4r}{\left(r+1\right)^2} \qquad (2\text{-}23)$$

Thus, the better the impedance match, the less the reflection and greater the transmission, and vice versa. Furthermore, for an impedance mismatch with identical velocities, all angles from the normal are equal, i.e. the angles of incidence, reflection and refraction are the same.

Refraction of the ultrasonic beam occurs under conditions of non-normal incidence and unequal sound velocities; additional beams may simultaneously be generated via mode conversion, as shown in Figure 2-2. So, what has thus far been referred to as the "transmitted wave" may, in fact, be several waves. As in optics, the angle of refraction is governed by Snell's Law

$$\frac{\sin \theta_1}{v_1} = \frac{\sin \theta_2}{v_2} \qquad (2\text{-}24)$$

where each variable is defined as depicted in the figure. For total reflection, $\theta_2 = 90^{\circ} \rightarrow \sin \theta_2 = 1$. Therefore, for $v_2 > v_1$, the critical incident angle, $\theta_c = \sin^{-1} (v_1/v_2)$, beyond which total reflection is achieved. Beyond the intended detail of the present discussion, amplitude calculations for multimode situations can be calculated using the set of continuity relations known as Knott's equations [11]. One other consideration worthy of note is that, upon refraction, a circular beam, for example, tends to become elliptical and narrower, thus producing a more intense beam [11].

The overall reduction in energy of an ultrasonic beam as it travels through a given material is termed attenuation. This term generally lumps together all factors such as absorption, grain boundary scattering, beam non-uniformity, couplant mismatch, and instrumentation variables, to name a few, which result in a reduced signal reception, for transmission through a material. For plane wave propagation, the attenuation factor, α, is constant and related as in Equation (2-25).

$$A_x = A_0 e^{-\alpha x} \tag{2-25}$$

$$\alpha = -\frac{1}{x} \ln\left(\frac{A_x}{A_0}\right) \text{ nepers/cm} \tag{2-26}$$

$$\alpha = \frac{-8.686}{x} \ln\left(\frac{A_x}{A_0}\right) \text{ dB/cm} \tag{2-27}$$

where A_0 = wave peak amplitude at $x = 0$

        A_x = wave peak amplitude at a specific value of 'x'

An alternative representation for Equation (2-25) is

$$I_1 = I_0 e^{-2\alpha x} \tag{2-28}$$

$$\alpha = -\frac{1}{2x} \ln \frac{I_1}{I_0} \tag{2-29}$$

$$= \frac{0.5}{x} \ln\left(\frac{I_0}{I_1}\right) \text{ nepers/cm} \tag{2-30}$$

where: I_0 = reference intensity at $x = 0$

        I_1 = intensity at $x = x_1$ $(I_0 > I_1)$

Absorption, as mentioned earlier, is only one of many factors contributing to a signal's attenuation. The delay occurring between the instantaneous pressure in the acoustic-wave and the resultant change in density of the propagating medium is related to a material's absorption. Depending on the specific material, various amounts of energy are absorbed, increasing the energy level of the component molecules. In addition, energy is expended in overcoming the

frictional or viscous forces which oppose the periodic particle motion of ultra-sonic vibration. This energy exchange arrangement is based on the mechanism termed relaxation. Energy in the ultrasonic system can exist in various forms, e.g. lattice vibrational, molecular vibrational, translational, etc. If the energy present were to be reversibly transformed from one energy type to another, so that at the end of the vibrational cycle all energy would be in initial form, no energy losses would occur. However, since return of energy to original states is not complete or instantaneous, energy returns out of phase, cancelling part of the travelling wave, and results in a net loss of energy from the system, primarily in the form of heat [13].

The time required for energy to transfer from one state to another and back again is termed relaxation time. Since the relaxation process involves a characteristic time, the process has maximum effectiveness at a particular frequency, known as the relaxation frequency.

Energy loss also occurs during relative motion between various struc-tures and the surrounding medium. This effect is primarily due to the influence of radiation pressure acting on an interface at which there is a change in char-acteristic impedance. Finally, hysteresis loss is the mechanism whereby energy is lost due to the fact that the given medium is not perfectly elastic. Both of the above mechanisms involve loss of energy primarily in the form of heat.

Absorption, aside from being temperature dependent [14], is a disper-sive process owing to such factors as relaxation frequency. In water, absorp-tion is approximately proportional to $(frequency)^2$, primarily due to frictional and viscous losses. In soft tissues, the attenuation is generally proportional to frequency, but is greater and somewhat anisotropic in muscle tissue de-pending on fiber orientation [15].

Due to the multitude of factors involved, with respect to NDT of materials (for example, as opposed to medical tissue characterization) standard test blocks and materials have been used for equipment calibration, rather than initiate exhaustive efforts at isolating, in detail, each of the parameters involved. For ultrasonic tissue characterization, however, researchers have been attempting to identify the individual factors contributing to attenuation. Only limited results have been obtained thus far.

C.   SCATTERING OF THE ULTRASONIC SIGNAL

When an obstacle is placed in the midst of an ultrasonic beam, the object will interact with the undisturbed sound pattern via such processes as reflection, diffraction and shadow formation, to form a new sonic pattern termed the scattered wave field.

In the classical analysis of an ultrasonic field, so long as one is dealing with an interface that is large compared with the ultrasonic wavelength, one considers the ultrasonic source to be composed of an array of Huygen's point sources. The sonic field may then be calculated from the diffraction pattern produced by the coincident spatial and temporal distributions of the equivalent Huygen's sources. For example, such a procedure is applicable for determining the beam pattern of an ultrasonic transducer, as mentioned in the next section.

Converse to the preceding situation, the scattered wave field may be determined by placing an obstacle in an infinite plane wave field. In this case, the resultant field is formed by the diffraction pattern of the incident wave field and the obstacle field, formed by distributing a set of Huygen's wave sources over the object's surface. The scattering object is said to possess a scattering cross-section, S, as defined in Equation (2-31).

$$S = \frac{P_S}{I_i}$$ (2-31)

where P_S = total power scattered by obstacle

I_i = incident wave intensity.

When the obstacle dimensions (D, cross-sectional diameter) are much greater than the sonic wavelength (λ), specular reflection and shadow formation result. For a perfect reflector, S = 1. When $D << \lambda$ (the Rayleigh scattering condition), uniform omnidirectional scattering occurs. Now, in the case of a spherical reflector, for example, $S \propto k^4 a^6$, where $k = 2\pi f$, f = frequency and a = radius of sphere [15]. In the situation where $D \approx \lambda$, the resultant field pattern has a critical dependence on both the dimensions and characteristic impedance of the obstacle. Sonic energy, for example, may be absorbed by the obstacle and then re-radiated, depending upon object characteristics. Development of a detailed mathematical model of the scattering process under various conditions is beyond the scope of this current dissertation. A summary of results from works strictly devoted to investigation of the scattering process will be presented in the following paragraphs. For the corresponding mathematical treatments, the references cited should be consulted.

Scattering is an involved process comprised of various factors as mentioned above, and is further complicated by such behavior as absorption, especially if one is attempting to obtain quantitative results. Although relatively minimal work has been done in determining a quantified scattering behavior, researchers have used both inanimate objects and tissue samples in investigating scattering phenomena.

Faran has investigated, both mathematically and experimentally, sound scattering by isotropic, metallic circular cylinders and spheres in water, using a frequency of approximately 1 MHz, for the case where $D \approx \lambda$ [16] . In general it cannot be assumed that a solid scatterer in a liquid medium is rigid and immovable (i.e. a perfect reflector) and thus, sound wave penetration and subsequent partial mode conversion to shear waves is taken into account. In order to depict behavior typical of what might be expected, some of Faran's results have been reproduced in Figure 2-3. Particularly note in part (c) of the figure, the deviations in scattering pattern with slight changes in frequency (wavelength). Similar work has been conducted by Davis et al using silicone rubber cylinders and spheres, demonstrating a negligible effect of shear in silicone [17] . Alkier, using a stiffened aluminum plate, demonstrates the generation of scattered waves from internally guided longitudinal stress waves [18] . Finally, Tittmann, using the technique of metallic diffusion bonding was able to create controllable voids without evidence of a bond line in metals and examine their interaction with ultrasonic waves [19] . The separate angular dependence of scattering and mode conversion was demonstrated.

Recent interest in ultrasonic materials characterization has resulted in some attempts at isolating individual scattering and absorption parameters. Inhomogeneous gels of ethanol-glycerine and plastic spheres of approximately 0.5 mm diameter have been used as a human tissue phantom, in conjunction with a technique of transmitting and receiving bi-directionally from water through the sample in order to separate out the scattering and absorption coefficients with respect to scatterer location within the sample [20] . Whereas
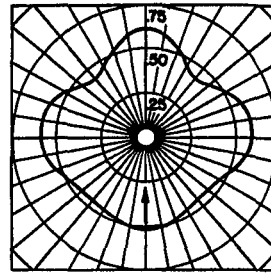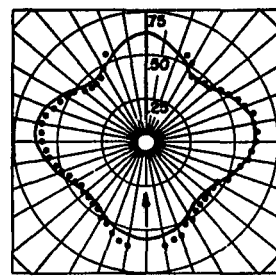
(a) D = 0.5453 λ
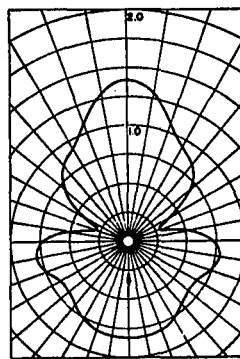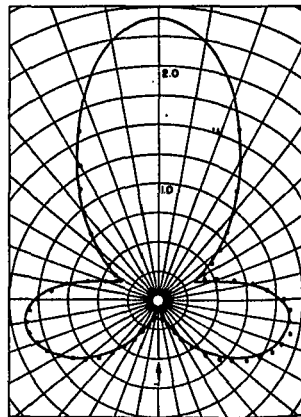
(b) D = 1.058 λ
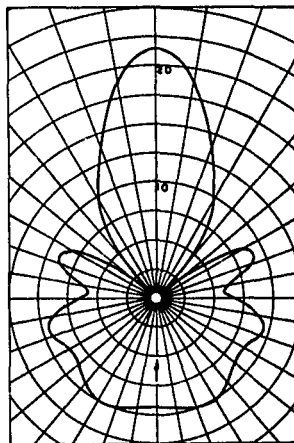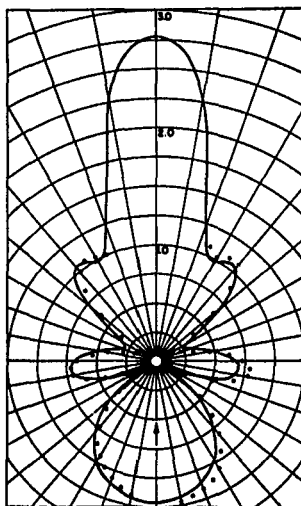
(c) D = 1.575 λ

BRASS CYLINDER   RIGID IMMOVABLE CYLINDER

Z = 3.8 x 10^7 Kg m^2 - s   Z = ∞ (i.e. PERFECT REFLECTOR)

Figure 2-3. Scattering dependence on object diameter (D) and acoustic
            wavelength (λ) for brass and rigid cylinders. (From data
            of Faran [16] .)

this approach uses a single interrogating frequency (1 MHz), on-going research at the University of Rochester has been involved with the use of a swept frequency signal (1-8 MHz sinusoidal burst, wideband transducer centered at 5 MHz) to insonify scatterers of monofilament nylon, fine metal wire and various sized Sephadex (cross-linked dextran particles which absorb water and scatter weakly) particles [21], [22]. The ultrasonic data acquisition system, which collects angle-scanned data, is similar to that used for the PSI investigation, to be described in Chapter V. The Rochester system, however, also examines the scatterers optically, followed by digitization and subsequent Fourier analysis for comparison with the ultrasonic data. As can be observed in Figure 2-4, reduced scatterer sizes for a fixed frequency tend to produce a lesser focused, omni-directional scattering, consistent with classical theory. Each of the Fourier spectra of Figure 2-5 contains a ring whose diameter gives average particle spacing and whose width indicates variation in particle size. After examining the wires and arrays of such, it was determined that slight beam misalignment was inconsequential for the disc transducers used, as were near-field beam non-uniformities when using the far-field model to determine scatterer spacing. As a result, it is believed that diffraction (i.e. scattering) based ultrasonic techniques will prove useful for determining structure on a scale corresponding to the wavelength employed [22].

Until recently, the inadvertent scattering (i.e. other than backscatter) of ultrasound when trying to image the body was looked upon as a process which only served to deteriorate the B-scan image and conflict with the single ray assumptions utilized. Current interest in ultrasonic tissue characterization, however, has motivated scientists to better understand the scattering process in the hope of determining tissue-specific behavior for both normal and diseased
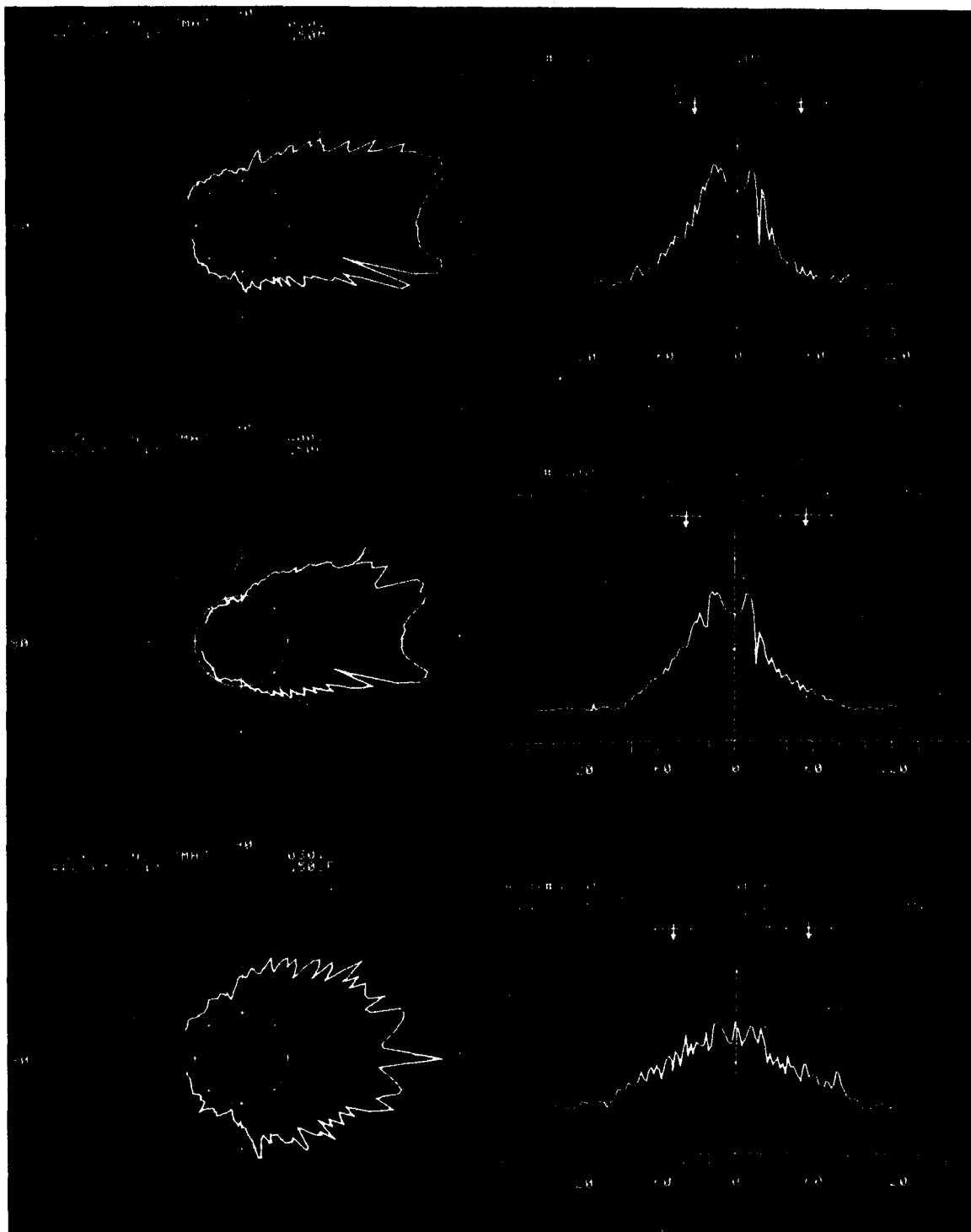
Figure 2-4. Polar and Cartesian plots of average scattered acoustic intensity
as a function of scattering angle for distributions of Sephadex
medium (G50M, 86-257 μm), fine (G50F, 34-137 μm) and super-
fine (G50SF, 17-68 μm) sized particles. Arrows on Cartesian
plots denote mean scattering angles while the bars represent
standard deviation from the mean. (Data plots courtesy of Dr.
R.C. Waag, University of Rochester (NY), [31].)
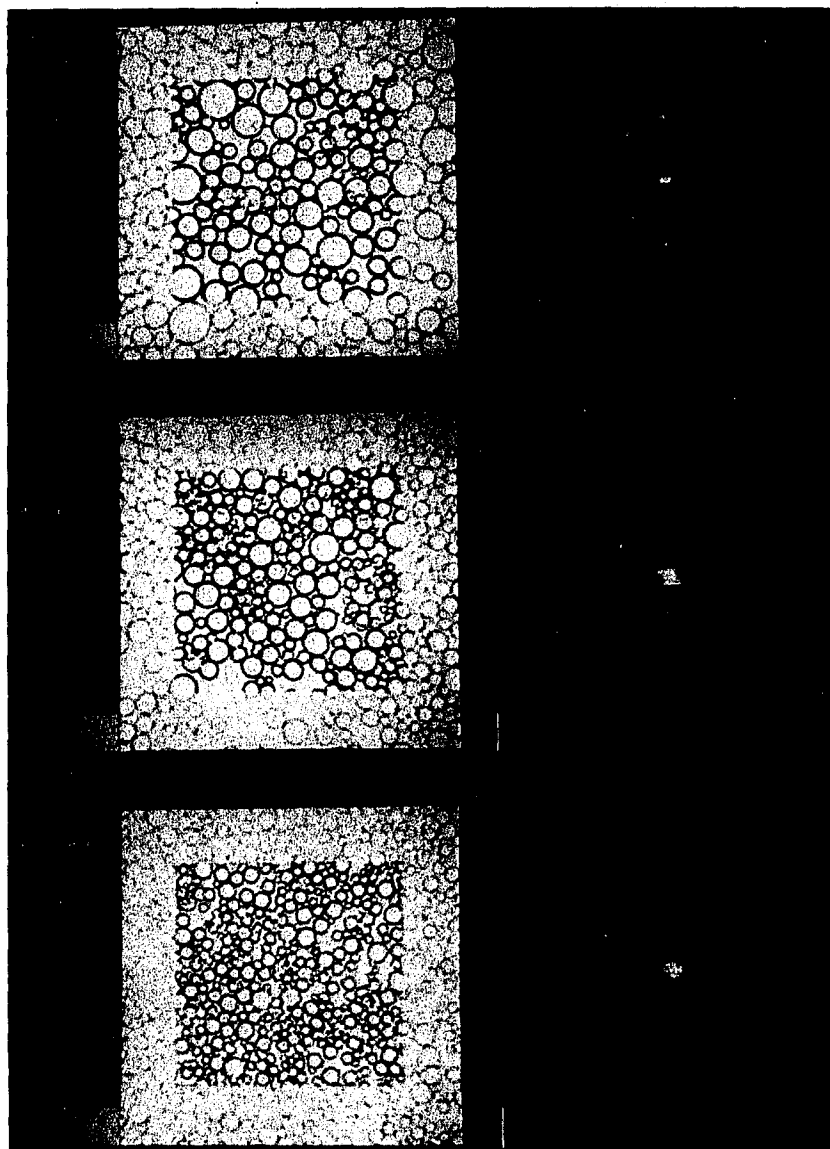
Figure 2-5. Typical digitized cross-sectional optical images (central region enhanced by histogram equalization) and corresponding Fourier log magnitude spectra for scattering by Sephadex particles as described in Figure 2-4. (Photos courtesy of Dr. R.C. Waag, University of Rochester (NY), [31].)

states. The relatively sparse data presently available do indicate that different tissues exhibit different angular scattering patterns and spectra [23], [24].

Mathematical models of varying degrees of detail have been developed to describe the phenomena of ultrasonic scattering in tissues [25]-[33]. In general, most of the models utilize plane wave and far field conditions, generally reasonable assumptions when comparing the resultant analytical and experimental results [31]. Unlike the models previously mentioned for scattering by cylinders and arrays, tissue models have assumed shear components to be negligible. To date, little attention has been paid to shear waves in tissues and further studies will be necessary to better determine the role of this mechanism. Similarly, most models address the situation of volume scattering and thus neglect the presence of large specular echoes. Here, the assumption is made that the use of compression amplifiers, to achieve a large dynamic range, along with the use of a narrow enough transmitted pulse width, will enable reception of both specular and volume-scattered echoes.

The following paragraphs are intended to serve as a cross-section of experimental results that have been obtained by various researchers concerning scattering from biological tissues. As touched upon earlier, one of the most comprehensive studies of ultrasonic scattering is being conducted in the United States at the University of Rochester, by Waag et al. [21], [22], [24], [28], [29], [30], [31], [34]. This work was originally motivated by techniques in X-ray crystallography and atmospheric probing by radar, in order to determine structure in tissue on the order of a wavelength. At the outset is it noted that absorption, an approximately linearly increasing function of frequency, will reduce the high frequency components of the scattered waves and thus give more weight to scattering from closely spaced centers. Ultrasonic interrogation of excised human liver, a) cirrhotic, b) normal and c) infiltrated

by myelogenous leukemia, by 1-8 MHz swept frequency sinusoidal bursts
measured at a 96° scattering angle resulted in the data portrayed in Figure
2-6. (It should be noted that swept-frequency scanning is identical to angle
scanning at a fixed frequency so long as the sample insonified is isotropic,
since path length differences are varied by changing orientation between the
beam and scatterers. By definition, Bragg diffraction depends on the construc-
tive or destructive phase interference resulting from path length differences be-
tween the transmitted and received waveforms [32] .) The scattered power from
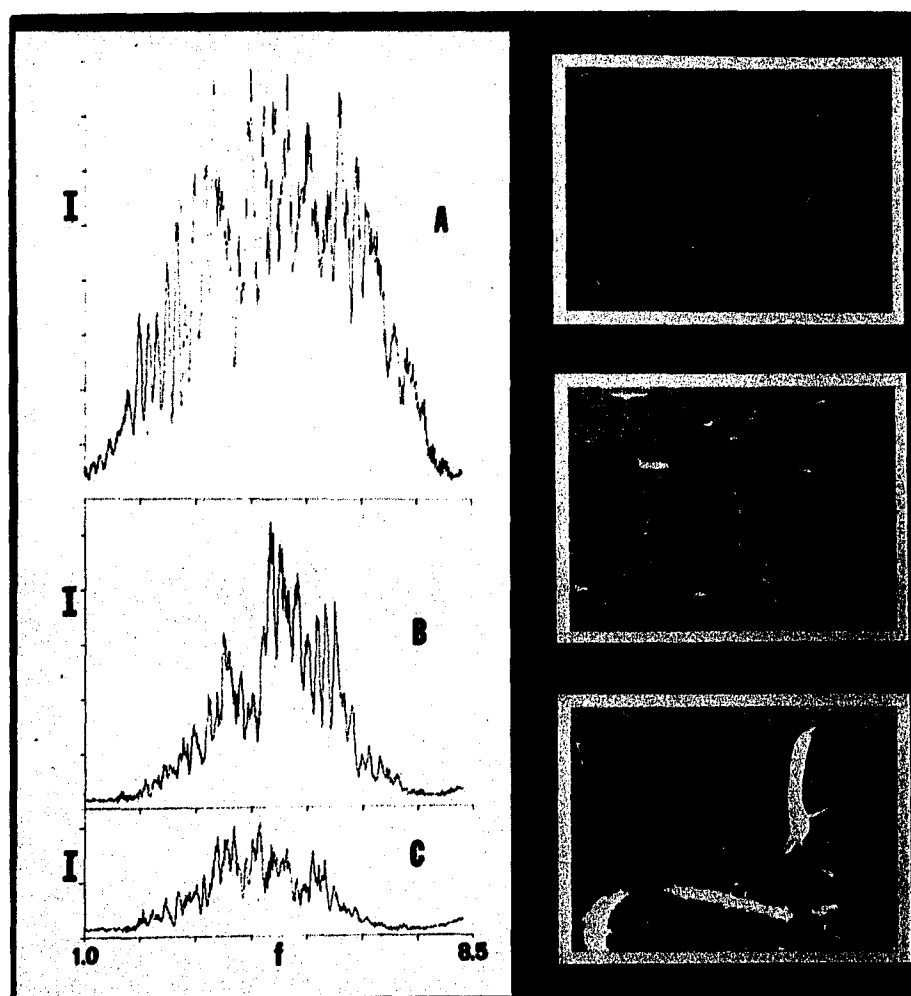
Figure 2-6. Swept-frequency (1.0-8.5 MHz) averaged scattering spectra
from liver - (a) cirrhotic, (b) normal, (c) infiltrated by
myelogenous leukemia cells, and corresponding optical photo-
micrographs. All three intensity scales are identical. (Courtesy
of Dr. R.C. Waag, University of Rochester (NY), [31].)

cirrhotic liver was significantly greater than that from normal, probably due

to the higher cirrhotic collagen content and resultant increase in local elasticity.

The cirrhotic data periodicities also imply a mean scatterer spacing considerably

greater than in normal liver, consistent with the associated histology of small

nodules surrounded by fibrous septae. Similar analysis holds for liver infil-

trated with myelogenous leukemia cells where less power was scattered and

increased reflector spacing indicated, probably due to alteration of structure

by the invading disease processes. Performing swept frequency scanning of

normal liver samples using various sample orientations, demonstrated normal

liver isotropy by the almost identical spectral patterns obtained at each speci-

men orientation. Finally, Figure 2-7 illustrates an angle scan performed at

3 MHz by the Rochester team. Comparison of this plot with that shown in

Figure 2-4 implies that the liver tissue is composed of scatters similar in size

to the Dextran particles (10-300 μm). Note that significantly more energy is

scattered at small angles than in the backscattered mode. Swept frequency

scans in the 1-8 MHz range of normal and infarcted cardiac tissue demonstrated
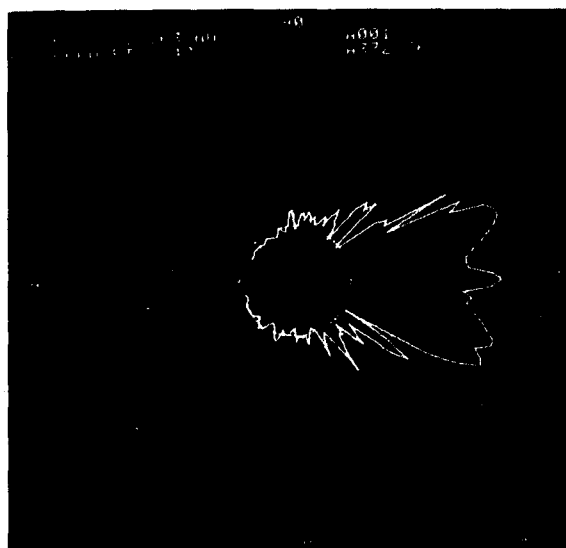
Figure 2-7. Log amplitude polar plot of angle-scan scattering data obtained
from liver insonified at 3 MHz. (Courtesy of Dr. R.C. Waag,
University of Rochester (NY), [31].)

greater high-frequency scattering possibly due to structural disruption in the infarcted tissue.

Shung and Reid have been investigating backscattering coefficients (i.e. the power scattered by a unit volume scatterer in the backward direction, 180°, per solid angle per unit incident intensity) in excised calf myocardium and liver [23]. They determined that while the backscattering coefficient increases with frequency, the myocardium exhibits a much steeper dependence (proportional to f^3, where f = frequency) than liver, in the 3-10 MHz frequency range. At the lower end of the frequency range observed, liver exhibits a much stronger backscattering coefficient as compared with myocardium. The liver dependence was not a simple function of frequency, suggesting the contribution of various specialized intrahepatic tissue contribution to the backscattering. The myocardial frequency dependence suggests that scatterer size is less than 20 μm. Since the cardiac muscle fibers are of the order of 10 μm, it is suggested that the basic myocardial scattering unit is the muscle fiber. Investigation of myocardial and liver aging properties showed ultrasonic velocity to decrease after the third day post-excision probably due to diffusion of body fluids out of the tissue samples; however, backscattering properties remained constant (between measurements, tissues were stored in normal saline at 4°-6^OC). Tissues fixed in 10% formaldehyde exhibited an increase in backscattering due to the fact that fixation hardens the tissue structure. Lele et al report similar changes in backscattering with fixation, i.e., increased backscattering, but no change in frequency dependence [32].

Additional work by Lele et al, in agreement with the previously discussed studies, demonstrated increased scattered intensities with increased insonifying frequency, for as the scatterer dimension becomes much less than the insonifying wavelength, there is a greater tendency for omnidirectional scattering and thus, on the average, any one receiver position will pick up a greater amount of

ultrasonic energy than for the case of a lower frequency [25],[32]. Scattering

profiles correlated well with surface roughness. The Bragg scattering con-

dition, discussed earlier, was used to predict scatterer spacing. Discrepan-

cies were explained by the fact that scatterers are probably not spaced in

perfectly orderly arrays for dimensions corresponding to the ultrasonic wave-

length (submillimeter to millimeter range). Furthermore examination of

various orientations of skeletal muscle fibers with respect to the ultrasonic

signal demonstrated skeletal muscle anisotropy, a situation which was not seen

in cardiac muscle, since there is no predominant fiber orientation in heart

muscle.

Hill has been studying the relationships, both by modeling and clinical

investigation, of acoustic frequency and axial orientation on volume backscat-

tering, with the final goal of clinical implementation [35]. His findings thus

far appear to be in agreement with the authors already discussed.

Finally, Shung, Sigelmann and Reid [26],[33] have been studying ultrasonic

angular scattering by blood utilizing pulse-burst insonification of an Arenberg

generator, as discussed in Chapter V, as being used for investigation of PSI.

It has been determined that the primary scatterer in blood is the red blood cell.

With an average radius of 2.75 μm, the red blood cell may be treated as a

Rayleigh scatterer. The backscattering coefficient varied as the fourth power

of frequency. By way of comparison, scattering from a unit volume of eryth-

rocytes is approximately 70 dB below reflection off a flat stainless steel plate.

Angular scattering varied significantly depending on blood compressibility and

density. It has, therefore, been suggested that measurements of angular scat-

tering might provide a means for determining an abnormal blood condition such

as sickle cell anemia, where the presence of hemoglobin of increased viscosity results in reduced erythrocyte elasticity and greater blood viscosity. Finally, scattering was not found to be a linear function of hematocrit (percent packed red blood cell volume in a sample of blood). The scattering coefficient exhibits approximately a linear increase with hematocrits up to about 8%, then increases non-linearly to a maximum at a hematocrit of about 26%, and then decreases with greater values of hematocrit.

D. TRANSDUCERS AND ULTRASOUND GENERATION

The following qualitative review is intended to be an overview of the general factors one considers in selecting a transducer for ultrasonic imaging. For a more in depth and mathematical description of the characterization of transducer materials and their incorporation into a practical transducer, the reader is particularly referred to references [36]-[39], among others in the bibliography, as well as the commercial manufacturers (e.g. K.B. Aerotech, Panametrics, Dapco). Many factors were considered when "home-made" transducers were going to be attempted. However, since only commercial transducers were used in the results reported in this dissertation, details such as the wave physics behind transducer construction are beyond the scope of the present discussion.

The ultrasonic transducer transforms high frequency electrical energy into high frequency mechanical energy and vice versa. The two most common methods of generating ultrasonic vibrations are via magnetostrictive (expansion and contraction of magnetic materials under the influence of varying magnetic fields) and piezoelectric (expansion and contraction of crystalline and ceramic substances under the influence of electric fields) means. Magnetostrictive transducers are suitable for generating ultrasonic signals less than approximately

100 kHz and so are generally not considered for the purposes of materials testing. These transducers find wider use in sonar and underwater signaling applications.

Piezoelectric transducers, on the other hand, capable of oscillating at tens of MHz, are rather easily fabricated. Prior to World War II, only naturally-occurring quartz and Rochelle salt crystals were used as piezoelectric elements. Since that time, the development of synthetic crystalline and ceramic materials such as lithium sulfate monohydride, barium titanate and lead metaniobate has enabled greater transducer variety. Selection of the best piezoelectric element depends upon the specific application, including such factors as input signal drive, output frequency, signal bandwidth, transducer sensitivity, transducer efficiency and input and output coupling impedance.

Being anisotropic, a piezoelectric material allows for the interaction of bound electric charge with an applied electric field to produce a mechanical stress. Simply stated, for a piezoelectric material, mechanical deformation results in a generated voltage, while an applied voltage results in mechanical deformation. A piezoelectric element may be designed to vibrate in various directional modes depending on either the particular crystalline cut (for crystalline elements) or the direction in which the element has been poled (for synthetic materials, i.e. ferroelectrics). Poling is the process used for aligning the molecular dipoles of a ceramic element in a direction such that the application of an electric-field across the element will result in the desired orientation and degree of expansion or contraction. This polarization process involves heating the ceramic above its Curie Point (the temperature above which the ceramic material suffers complete loss of its electromechanical coupling or piezoelectric

activity) and then subjecting the given element to an intense DC electric field (e.g. 2 kV/mm), applied in the direction of desired dipole alignment, as the element cools to room temperature. Internal alignment is maintained, except for the consideration of aging, which is generally logarithmic with time [9], as long as the ceramic is operated at a temperature well below the Curie Point.

Most presently used piezoelectric transducers used for pulse echo analysis are made of lead zirconate titanate (PZT-4 or PZT-5) or lead metaniobate. Referring to some of the parameters listed in Appendix A, Table A-1, a comparison of lead metaniobate and PZT indicate a better water coupling (lower acoustic-impedance) and wider bandwidth (lower Q) for lead metaniobate, however, PZT excels in efficiency and sensitivity. As already mentioned, one must weigh the importance of each of the particular parameters for the given application, in deciding upon the appropriate transducer material to be used. At this point, it should be noted that two other transducer materials of great potential use particularly in the medical area are polyvinylidene fluoride (PVDF) and to a lesser extent, cadmium sulfide. PVDF exhibits the properties, among others, of low Q (Q = 3), desirable for broadband operation, and a characteristic impedance only several times that of water, to provide excellent matching capabilities [13], [40], [41]. Monocrystalline cadmium sulfide, although only suitable as a receiver, essentially responds to the energy in an acoustic signal and not the phase [42]. Such a phase-insensitive receiver would be useful both for power measurements as well as in imaging, so that the particular gray scale assignment might correspond to the absolute energy in a scattered signal rather than to the complex sum of signals impinging upon a given cross-sectional area, namely, that of the transducer element.

The piezoelectric ultrasonic transducer is essentially an electromecha-nical transformer and as represented by the equivalent circuit of Figure 2-8 , can be used both as a transmitter and receiver. The analagous electrical and mechanical units are shown in Table 2-1 [36], [43], [44]. Equivalent circuits such as shown, when utilized at an appropriate degree of complexity, are useful design tools for both electrical and mechanical impedance matching to enable maximum transfer of energy to or from the transducer. With respect to com-

IDEAL
N : 1
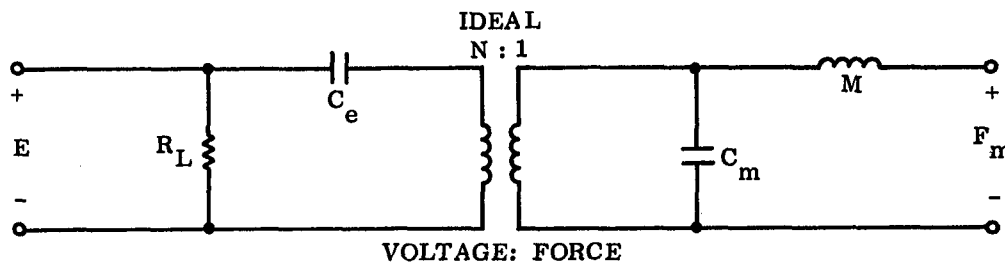
VOLTAGE: FORCE

E = APPLIED ELECTRICAL VOLTAGE
R_L = TRANSDUCER ELECTRICAL INPUT RESISTANCE
C_e = TRANSDUCER ELECTRICAL INPUT CAPACITANCE

M = VIBRATING MASS OF PIEZOELECTRIC ELEMENT
C_m = MECHANICAL COMPLIANCE
F_m^m = OUTPUT MECHANICAL FORCE

Figure 2-8. Simplified piezoelectric transducer equivalent circuit

TABLE 2-1. TRANSDUCER EQUIVALENT CIRCUIT ELECTROMECHANICAL ANALOGIES

Electrical Unit	Mechanical Unit
voltage	force
current	velocity
charge	displacement
capacitance	compliance
inductance	mass
impedance	mechanical impedance

mercially available transducers, as are being used in this project, electrical input impedance is specified at a nominal 50 Ω, at the transducer's center or resonant frequency. Many times, a small coil is included within the transducer casing and is electrically connected at the input, in order to cancel out any capacitance associated with the piezoelectric element and electrical connections, and thus create as nearly an input impedance of 50 + j0 ohms as possible. In this way, maximum electrical power will be transferred to the transducer when driven by a standard generator with a 50 Ω (matching) output impedance. As the generator frequency is varied about the center frequency, poorer matching results. Improvement at a particular frequency may be obtained by connecting an appropriately valued coil, externally, in series or parallel with the transducer input in order to null out the input capacitance. (Input capacitance, in particular, degrades high frequency performance.) Similarly, in order to maximize electrical reception, the receiving or pulse-echo transducer should be electrically matched to the impedance of the receiving amplifier or recording device. The goal is to null out any stray capacitance (at the operating frequency) while feeding into a 50 ohm input receiver. Obviously, for broadband applications as in pulse-echo work, impedance matching is of a more limited value than for single frequency or tuned narrowband operation.

Analogous to the electrical situation, mechanical impedance matching should be done between the transducer and medium into which it is transmitting. Again, this matching is frequency-specific; the usual technique is to place a quarter-wave thickness layer, generally of an epoxy material of high 'Q', of acoustic impedance equal to the geometric mean of the acoustic impedance of the transducer element and loading medium [43]. This layer also serves as a protective coating on the transducer element itself.

It is generally desired that ultrasonic transducers radiate energy from only a single face (i.e. the front face). An acoustic insulator is inserted around the sides of the piezoelectric element to reduce the effects of radial radiation (and vibration of transducer casing), whereas a backing layer is used on the rear face. For transducers which operate in a resonant, narrowband mode, the back face may simply be air backed, causing total reflection of the backwards traveling energy back into the transducer so that it can combine in-phase (due to the half-wave thickness of the piezoelectric element) with the forward traveling wave and contribute to the resonant mode of operation. The output signal will be of relatively large amplitude when driven by a continuous wave (C.W.) signal with frequency that of transducer resonance. For broadband operation, as is desired for pulse-echo work, for example, rather than back the transducer element with a perfect reflector, one wishes to use an acoustically absorbing (damping) backing. When operated via pulsed excitation, the output signal will be of a damped sinusoidal-like form, the number of cycles ('ringing') in the signal inversely proportional to the degree of damping (see Figure 2-9).
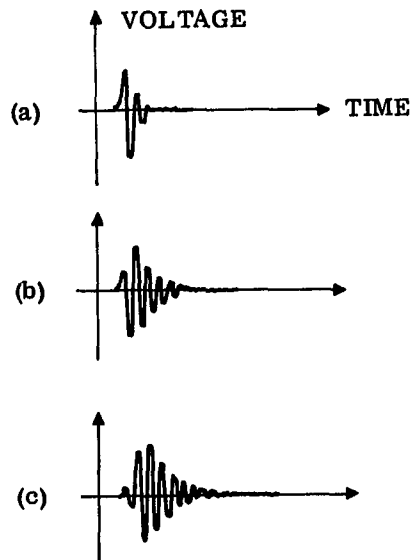
Figure 2-9. Output voltages obtained from typical piezoelectric transducers with shock pulse excitation and (a) heavy, (b) medium, (c) light internal damping

The damping layer is generally an epoxy resin loaded with metallic particles
(e.g. tungsten) of low acoustic impedance. Figure 2-10 shows a cutaway view of
a typical diagnostic probe. With respect to broadband transducers, the greatest
bandwidth currently achievable in commercially prepared transducers is approxi-
mately 60% (i.e. ±30 percent of center frequency). The price one pays for
broadband operation is decreased sensitivity at any one particular frequency [45].
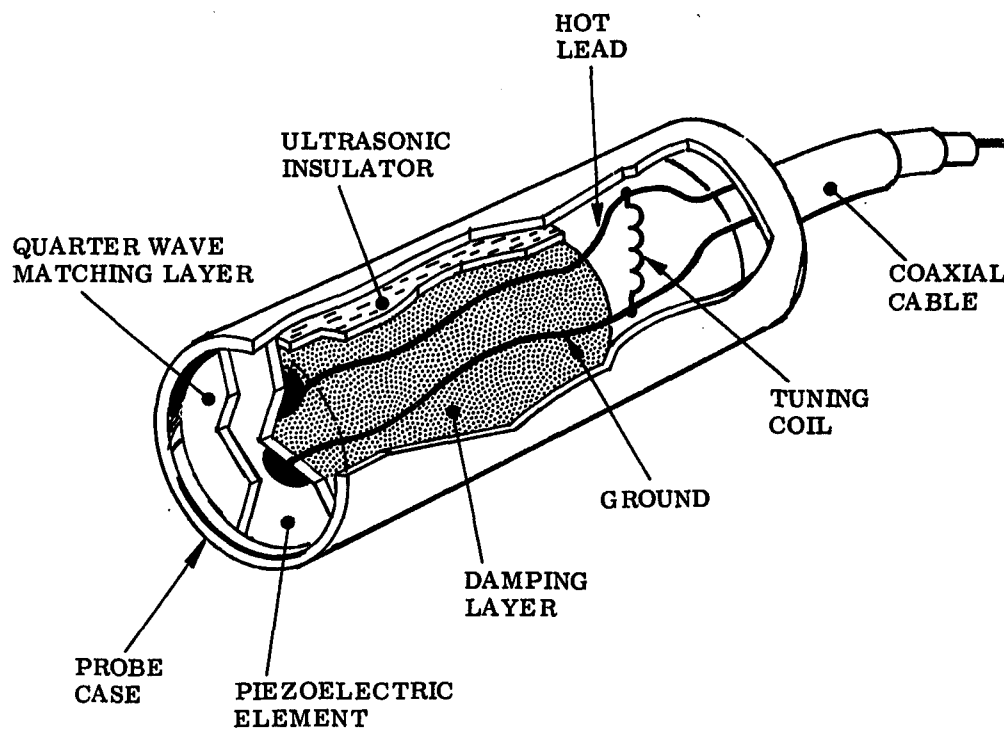
Figure 2-10. Cutaway view of a typical diagnostic piezoelectric transducer
probe. (Adapted from Wells [13], p. 69).

In order to obtain reliable and quantitative results from ultrasonic imaging,
one must be aware of the acoustic field produced by the particular transducer
used. Ideally, the beam pattern should be uniform, i.e. the acoustic intensity
at all points a given distance from the transducer is constant. In general, no
two transducers will have exactly the same field characteristics and thus, the
fabrication goal when more than one transducer is needed for a given procedure

is to achieve transducers which have as nearly "similar" characteristics as possible.

The acoustic pattern produced by an ultrasonic transducer can be described in terms of its near or Fresnel field and its far or Fraunhoffer field. As for light beam analysis, Huygen's principle, stating that energy is radiated in all directions from a point source, applies to the ultrasonic transducer, where the transducer face is assumed to be comprised of a large number of point sources in tandem. For continuous wave operation, the near field effects predominate throughout the acoustic field, whereas in the pulsed system, both near and far fields exist. The near field is a complex acoustic pattern formed by the phase interference of wavelets emitted by the transducer. In the pulsed system, proceeding further away from the transducer, these interference effects attenuate, resulting in a more regular beam pattern (see Figure 2-11). Furthermore, in the far field region, the acoustic environment can be assumed to consist of plane waves over distances greater than or comparable to wavelength.

Figure 2-12 illustrates Huygen construction of an ultrasonic field from a two-point source model of a radiating transducer. As depicted in Figure 2-13, for a typical field pattern, if one were to move towards the transducer along its central axis from infinity, a gradual increase in intensity would be perceived until a maximum would be reached, known as the "Y_{+0}" point. Similarly, moving closer to the transducer, the first minimum will be reached, known as the "Y_{-1}" point. Proceeding further towards the transducer, other maxima (Y_{+1}, Y_{+2}, ..., Y_{+n}) and minima (Y_{-2}, Y_{-3}, ...Y_{-n}) will be perceived. Moving away from the transducer, the field beyond Y_{-1} and Y_{+0} demarks the beginning of the far field.

(a)
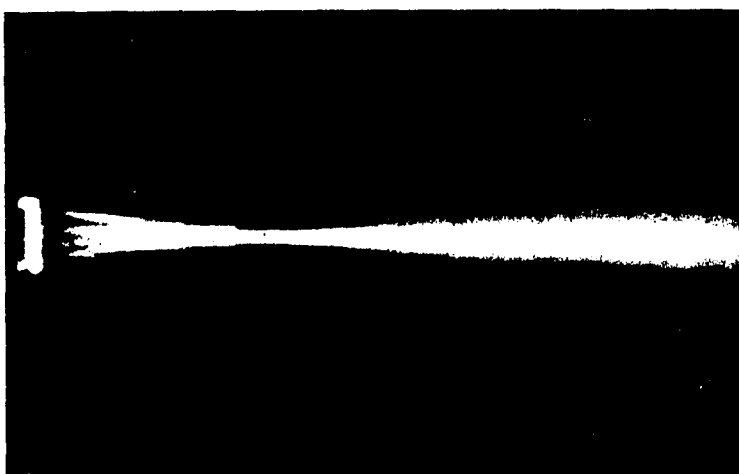
(b)

Figure 2-11. (a) Schlieren pattern of sound beam from a non-focused transducer
with $D/\lambda = 6.7$ (Photo from Krautkramer and Krautkramer [46] ,
p. 63.)
(b) Beam pattern of a transducer with focusing lens on front face.
(Photo from King [47] , p. 30.)
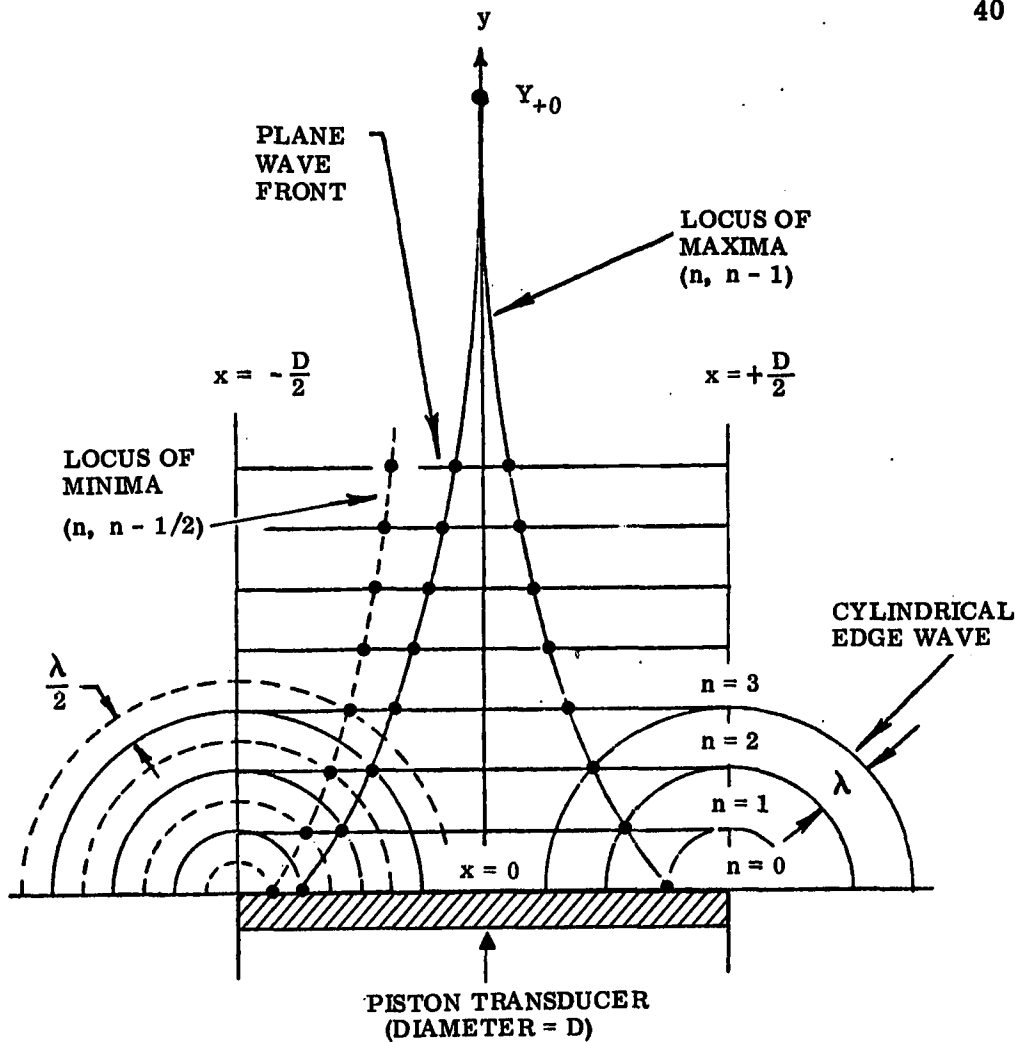
Figure 2-12. Huygen's reconstruction of ultrasonic field from a piston radiator utilizing a two point source model ($D \gg \lambda$). Assume plane waves over transducer face and cylindrical waves at edges. (Adapted from McMaster [11].)
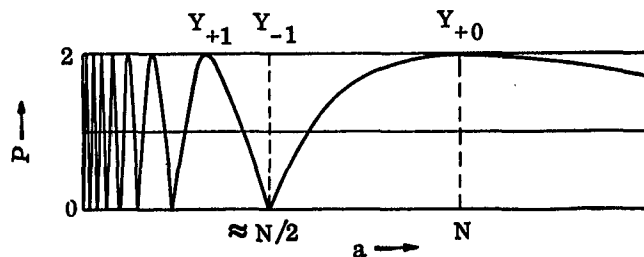
Figure 2-13. Axial beam pattern for a typical ultrasonic transducer - acoustic pressure (P) vs. distance from transducer (a). See corresponding three dimensional beam cross-sections in Figure 2-14. (Adapted from Krautkramer and Krautkramer [46], p. 65.)

The distance of the Y_{+0} point from the face of the unfocused, circular transducer depends on the transducer diameter to wavelength relationship, namely [46]

$$N = \frac{d^2 - \lambda^2}{4\lambda} \qquad (2-32)$$

where: d = transducer element diameter

N = length of near field for a circular piston

λ = wavelength

For the case of d $>>\lambda$ (which is generally true for diagnostic transducers) λ^2 can be neglected in the numerator to give

$$N = \frac{d^2}{4\lambda} \qquad (2-33)$$

Since d = 2r, where r = radius

$$N = \frac{4r^2}{4\lambda} = \frac{r^2}{\lambda} \qquad (2-34)$$

It should be emphasized that the near field to far field transition is not instantaneous and so Equation (2-34) really implies a transition region, not a single coordinate. Figure 2-14(a), depicts the theoretical near field along the central axis of an ideal piston oscillator, along with a simulated gray scale cross-section of the beam to emphasize the circular symmetry of the field. In this case d/λ = 16 and so Equation (2-33) applies.

Figure 2-14(b) shows a similar plot, but for the case where d/λ = 4 (therefore, Equation (2-32) holds). Note the more rapid beam divergence in this case than in the former. It is then obvious why commercially available diagnostic transducers are used in wider diameters at low frequencies (i.e. long wavelengths) and narrower diameters at higher frequencies. For maximum pulse-echo lateral resolution in conventional diagnostic procedures one desires as small an element diameter as possible. However, d/λ must be kept
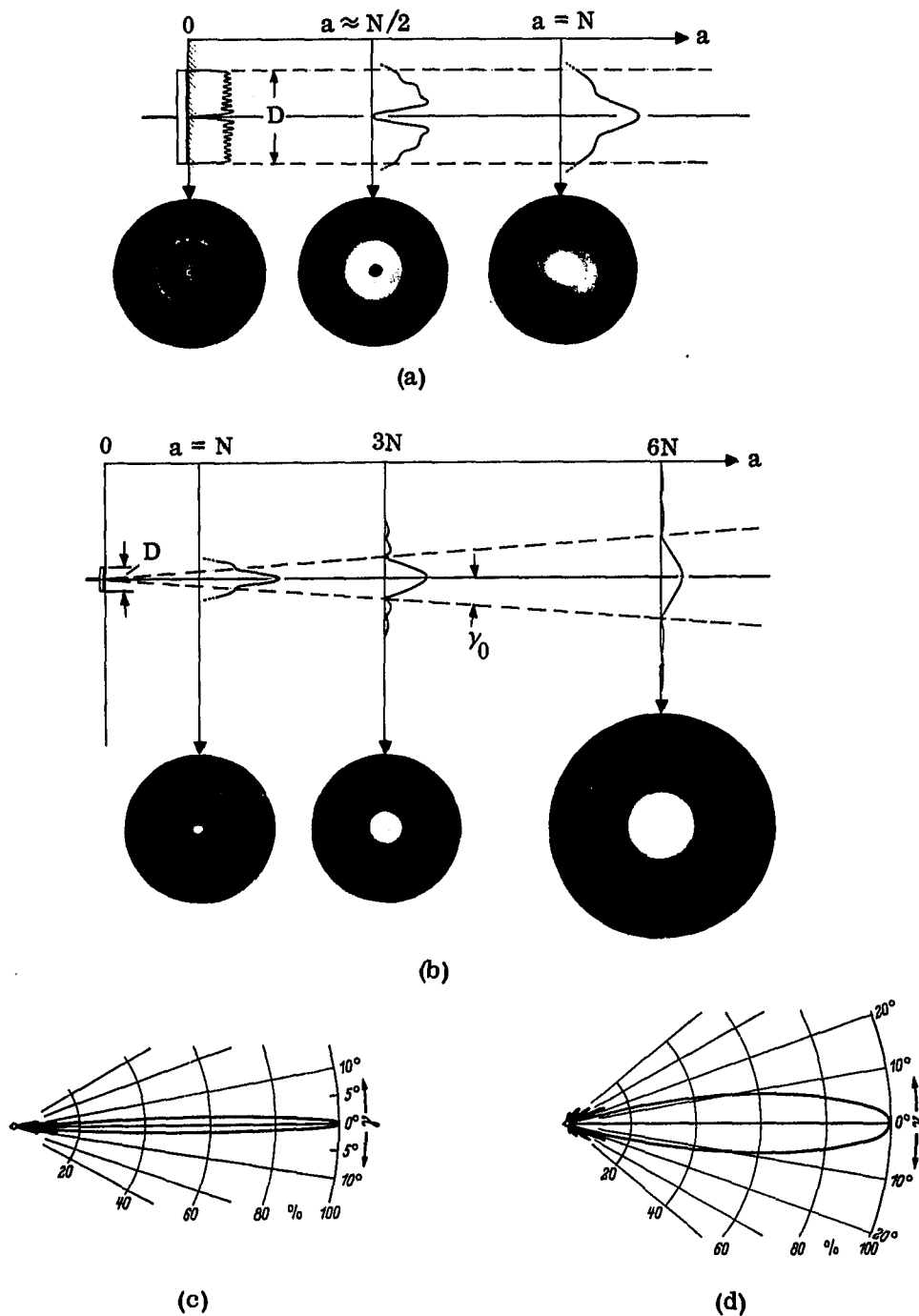
Figure 2-14. (a) Three dimensional cross-sectional beam pattern in front of
typical ultrasonic transducer with $D/\lambda =16$. Near field. High
brightness regions correspond to areas of high acoustic
pressure.

(b) Same as (a) except with $D/\lambda = 4$. Near field to far field
transition.

(c) Polar plot of directional characteristic for (a).

(d) Polar plot of directional characteristic for (b).

(Reproduced from Krautkramer and Krautkramer [46],
pp. 64-65, 68.)

sufficiently large in order not to achieve too rapid a beam divergence in the region of interest. As illustrated in Figure 2-14(b), even in the far field, although greatly reduced in amplitude, sidelobe energy is still present and can provide misleading results if one is not aware of its presence. As depicted in the same figure, γ_0, the half angle beam divergence, may be calculated as

$$\sin \gamma_0 = 1.2 \; \frac{\lambda}{d} \qquad\qquad (2\text{-}35) \; [46\,]$$

where: $d \gg \lambda$

Figure 2-14(c-d) shows the corresponding polar plots of directional characteristic corresponding to the two d/λ cases already discussed.

Figure 2-15 illustrates the effect of intensity, for a given d/λ, on beam width. Part (i) of the figure was determined such that an omni-directional point target could be detected when placed at the most sensitive point in the field, for a reference gain of 10 dB. Data sets (ii) and (iii) are calculated for successive increases in gain of 10 dB and 20 dB, respectively.

The final beam characteristic appropriate to mention at this time is the beam focus. As shown in Figure 2-16, although focusing results in increased field divergence beyond the focal region, within the focal zone a concentrated beamwidth much narrower than transducer diameter may be achieved, an advantageous situation to improve lateral resolution, in the pulse-echo B-scan, for example, or in the case where a high intensity spot of ultrasound is desired as in various types of ultrasonic surgery. Focusing, which moves the point of maximum intensity towards the transducer, is achieved with a plano-concave lens whereas de-focusing (as in producing a fan beam) requires a lens which is plano-convex. The ultrasonic lens may either be affixed to the front of the transducer
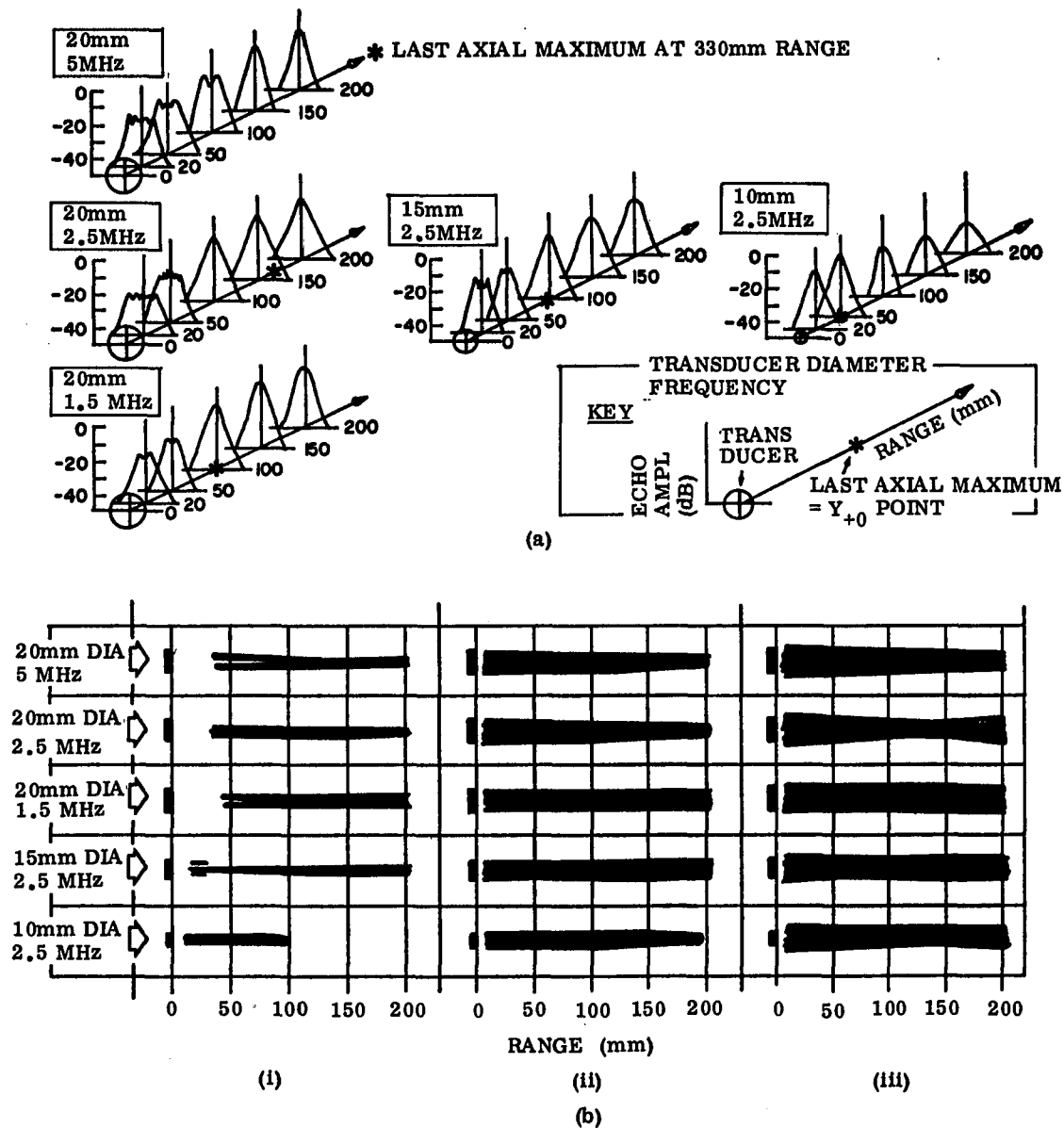
Figure 2-15. (a) Axial beam profiles for some transducers determined by
reflection off a 6.3 mm steel sphere in water

(b) Effective beamwidths of transducers with various dynamic
ranges.(i) 10 dB (ii) 20 dB (iii) 30 dB

(Adapted from Wells [13] , pp. 151,153.)
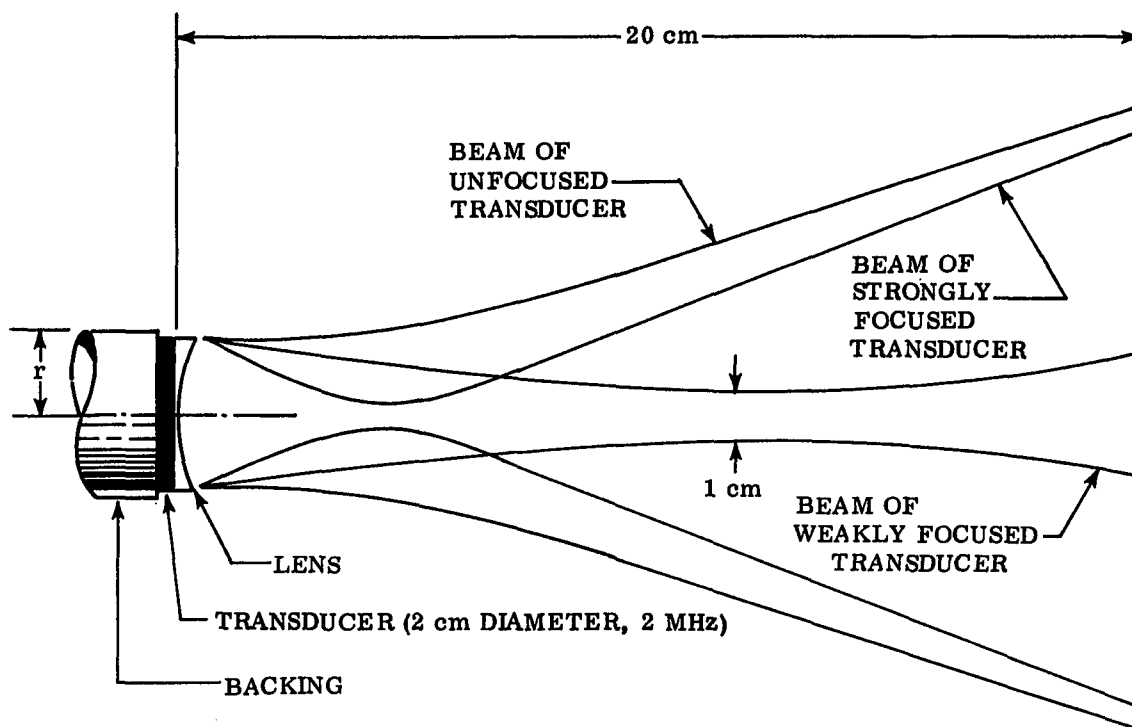
Figure 2-16. Beam shapes for various degrees of ultrasonic transducer focusing. (After Hubelbank [48] , p. 29.)

or be in the form of a shaped transducer element. As touched upon earlier, for maximum coupling to the object being examined, the lens material should have a matched acoustic impedance and be of quarter wavelength thickness.

Given the foregoing factors with which an instrument designer is concerned about for ultrasound generation and reception, the factors of interest to the clinical user of a conventional pulse-echo B-scan device include:

(i) impedance matching to water or tissue

(ii) focal region, beamwidth -- lateral resolution

(ii) resonant or center frequency -- depth or axial resolution

(iv) frequency bandwidth

The first two factors have already been discussed in detail and so the remainder of the chapter will be devoted to the last two items above. The resonant or center frequency is that frequency(s), for a given input level, where

maximum transducer output is obtained. This value also corresponds to the

frequency of minimum electrical impedance. The transducer bandwidth (BW)

corresponds to the frequency range about the resonant frequency (f_o) where the

sound amplitude has declined by 3 dB of the output at resonance (i.e. equals

0.707 times output at resonance). The quality factor or selectivity, Q, equals

f_o/BW. Therefore, high "Q" devices are highly selective and exhibit sharply

peaked amplitude versus frequency characteristics. Low "Q" devices, on the

other hand are broadband and consequently possess a relatively "flat" amplitude

characteristic (see Figure 2-17). Since piezoelectric elements by themselves

are generally high "Q" (e.g. 20,000) devices resulting in "ringing" and

consequently pulse broadening after excitation, utilization of a backing layer,

as discussed earlier, will result in damping out of this lengthy tail. In the

process, the overall transducer characteristic will become broader band, thus

enabling shorter output pulses (although at reduced amplitude), enabling greater

depth resolution.

(a) HIGH "Q"
 NARROW BANDWIDTH

(b) LOW "Q"
 WIDE BANDWIDTH

$$BANDWIDTH = f_u - f_\ell$$

$$QUALITY\ FACTOR = \frac{f_c}{f_u - f_\ell}$$
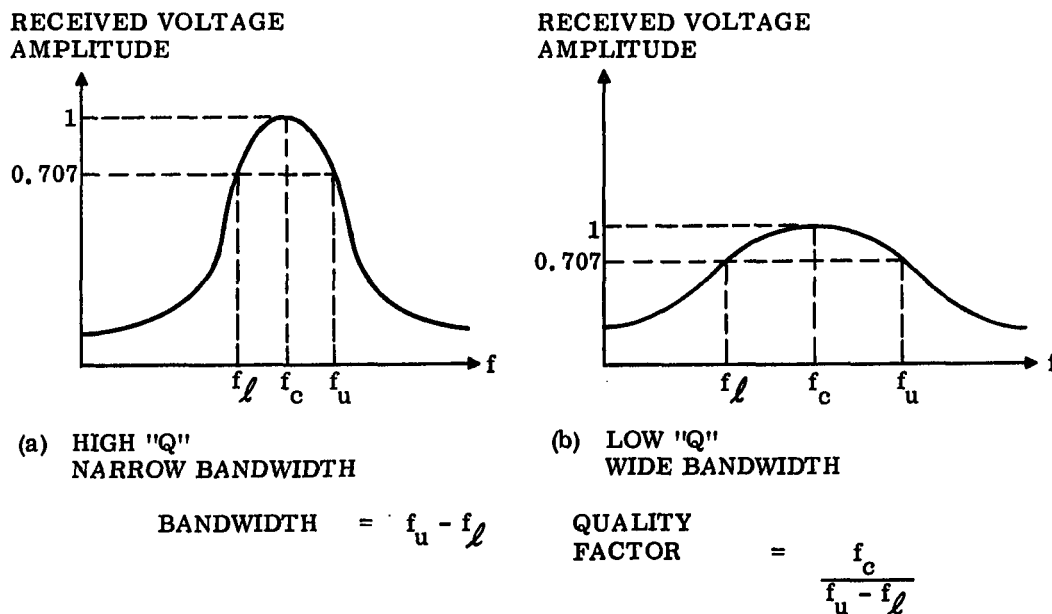
Figure 2-17. Frequency characteristics for (a) narrowband and (b) wideband
transducers. Voltages normalized for 0-1 volt range

CHAPTER III. ULTRASOUND AS A MODALITY FOR MEDICAL-IMAGING

A. PHYSICAL ASPECTS

In order to ultrasonically interrogate the body tissues to determine their medical condition, one must efficiently couple the sonic energy between the body and transducer in order to minimize boundary energy losses. As discussed in Chapter II(D), a good transducer is designed so as to provide as close an impedance match to the tissues as possible, and thus minimize boundary losses. In order to take advantage of such characteristics, during use, the transducer must make intimate contact with the body, since if air, for example, were to get between the transducer and tissue, the transducer would then see the characteristic impedance of air rather than that of the tissue. The comparatively low acoustic impedance of air will result in almost total reflection of the ultrasonic signal, whether it be travelling from transducer to tissue or vice versa. As a result, in order to guarantee effective coupling, in the case of abdominal scanning, for example, a gel or oil is placed between the transducer and body to serve as coupling medium. Although common mineral oil is inexpensive and serves as an excellent couplant it tends to run quite easily, making it rather messy and require replacement often throughout an exam. Various companies manufacture a coupling gel which is comparable to mineral oil in performance, quite a bit more costly, but somewhat more convenient to work with depending

47

on the particular procedure being performed. These gels are generally water soluble and easily wash out of clothing. The simplest of all couplants is water and although not conveniently used for conventional abdominal scanning (i.e. the water runs all over) it is commonly used in the form of a water bath placed over the eye with the patient in a supine position, for opthalmic exams.

One aspect of ultrasound which has received only little attention until recently is the aspect of biological safety. The policy adopted by the American Institute of Ultrasound in Medicine (AIUM) and commonly accepted by the medical community is that diagnostic ultrasound (as opposed to ultrasound used for surgery or therapy) at currently used power levels is biologically safe [8]. This conclusion is based on only the limited research conducted to date, with such data being predominantly from non-human subjects. Various studies, such as one being conducted by the Ohio State University Bio-Medical Engineering Center on the safety of ultrasound on pigs and their offspring, are in progress to determine both the short and long term (i.e. genetic) damaging effects on the body, if any, resulting from ultrasonic imaging. When evaluating the results of any such study, one must ascertain whether peak or average power (i.e. temporal distribution) is being specified. Furthermore, one should also be aware of the beam pattern as it exists in the tissue being examined in order to determine whether the measurement given is spatially peak or average.

Since biological damage has not been reported at current diagnostic levels (<100 mW/cm^2 average and 1-30 W/cm^2 peak power) it would be instructive to touch upon the mechanisms of damage which have been recorded at higher power levels. The reader should be reminded that various types of surgery or therapy utilize high power ultrasound and rely on these mechanisms to achieve

desired results. Six basic effects have been reported and may be summarized as [49]:

(i) heating - related to the absolute spatial and temporal distribution of insonification. The higher the acoustic intensity, the greater the motion imparted to the tissues, atoms and molecules, resulting in increased heat production due to frictional losses. Furthermore, ultrasonic absorption mechanisms such as relaxation result in the transformation of acoustic energy to heat energy at micromolecular levels. Thus, as is absorption, heat production is an increasing function of frequency. Heating may impart such effects as the actual burning of tissue, enzyme denaturation and variations in nervous conduction velocity, to name a few.

(ii) cavitation - results in bubble formation in liquids. Two mechanisms have been described, namely, vaporous or transient cavitation where vapor-filled cavities are formed during the rarefactive part of the ultrasonic wave and then collapse during compression phase, and gaseous or stable cavitation whereby dissolved gases come out of solution. Increasing either the acoustic frequency, liquid viscosity or external pressure decreases the chances for cavitation to occur as a finite amount of time is needed for cavitation to develop. Depending on the circumstances, a cavitation threshold may be described below which cavitation will not occur. Finally, cavitation may also cause temperature increases of several hundred degrees with adiabatic compression of the gas bubbles during positive pressure peaks [50] .

(iii) chemical changes - chemical reactions which do not generally occur, result presumably due to such effects as increased molecular agitation and local temperature. For example, enzyme activity has been found to be enhanced at low intensities (e.g. better mixing) and discouraged at higher energy levels (e.g. enzyme breakdown).

(iv) mechanical agitation - the oscillating acoustic energy sets tissue particles in motion. Aside from heat generation, various structures may be torn apart by the forces generated.

(v) streaming - results in the movement of liquid or particles in liquid since not all particles displaced during liquid deformation are returned to their original positions during the following quarter-cycle.

(vi) other effects - effects such as sonoluminescence, whereby some ultrasonically insonified liquids under transient cavitation emit light once each acoustic cycle, presumably due to electron excitation in water, have also been reported.

The specific acoustic parameters such as velocity, attenuation, etc., discussed in Chapter II with respect to materials in general, equally apply to biological tissues, and so another discussion tailored to biological materials is unnecessary at this time. One point worthy of re-emphasis, however, since it is such an important consideration in medical imaging, is the fact that ultrasound attenuation is an increasing function of frequency and generally follows the relationship

$$\alpha = a \, f^n \tag{3-1}$$

where: α = attenuation in dB/cm

a = constant

f = frequency in Hz

n = generally a value between 1.0-2.0 for biological structures.

Figure 3-1 illustrates the frequency dependence of attenuation for several biological substances. Since this plot is log-log, the frequency dependence parameter, "n" above, for each specific substance may be determined

ATTENUATION (dB/cm)

10

5

1

0.5

0.1

BONE

LIVER

BRAIN

BLOOD

DISTILLED
WATER

0.5   1   5   10
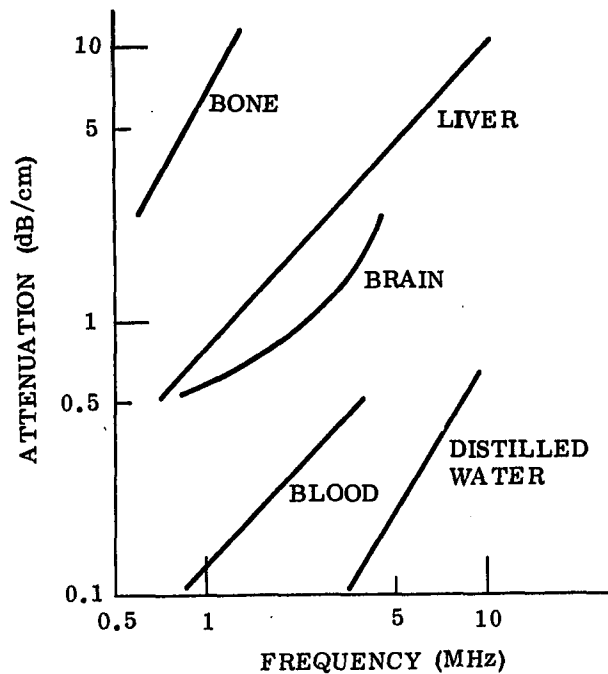
FREQUENCY (MHz)

Figure 3-1. Frequency dependence of attenuation for several biological
substances. (After Hubelbank [48], p. 21.)

directly from the slope of the particular curve. It will be noted that the liver

and blood tissue exhibit a linear dependence on "f", brain tissue on approximately

linear "f" dependence, and water and bone approximately an "f^2" dependence

characteristic of classical viscous absorption in liquids. Even though the

clinician wants to image with as high a frequency as possible in order to

maximize axial resolution, an upper frequency limit will exist corresponding

to the desired depth of penetration.

Another ramification of frequency dependent attenuation is that for broad-

band (i.e. shock excitation) pulse-echo techniques, the transmitted pulse will

contain a wide range of frequency components. Since the higher frequency

components attenuate most rapidly, essentially the tissues nearest the trans-

ducer will receive broadband insonification, while the deeper regions receive

only the lower frequency components. The deeper structures will thus exhibit

poorer resolution. In order to compensate for such effects, ideally a frequency

selection time-gain compensation (TGC) is required rather than the broadband

TGC used in conventional B-scanners.

B. CONVENTIONAL MEDICAL ULTRASONIC IMAGING PRINCIPLES AND TECHNIQUES

An ultrasonic image of some portion of the body may be obtained via

transmission or scattering (e.g. reflection) techniques. However, conventional

clinical imaging relies almost solely on backscattering. These techniques will

be discussed in the present and following section, whereas experimental and

research techniques will be briefly summarized in sections D and E of this

chapter.

Data collection for backscattering or so-called pulse-echo techniques

relies simply on the fact that knowledge of the acoustic signal velocity and total

time of flight enables one to calculate the distance from the face of the trans-

ducer to where the given echo originated (see Equation (3-1)).

$$d = v \times \frac{t}{2} \tag{3-1}$$

where: d = distance of echo producer from acoustic-source

            v = velocity of sound propagation

            t = round-trip signal time-of-flight

This calculation relies on the fact that the echo resulted from straight-line

travel between transducer and reflector (i.e. no multipath). Furthermore,

precise knowledge of velocity is required. Although the velocity of sonic

propagation has been fairly well determined for many of the body's tissues,

velocity is, nevertheless, tissue-specific. Thus, since the sound beam gen-

erally passes through numerous tissues before returning to the transducer as

an echo, the best that has been done to date is the assumption of an average

tissue velocity of 1540 m/sec [12] . Figure 3-2 illustrates the velocity

variation in soft tissues. Worst case positional errors in soft tissue may be

calculated assuming representative high and low velocities.

Average velocity in soft tissue = 1540 meters/second

Representative low velocity (adipose tissue) = 1476 meters/second

Representative high velocity (across muscle fibers) = 1592 meters/second

[14]

For medical imaging, interested in maximum path of 30 cm or a 60 cm round-trip.
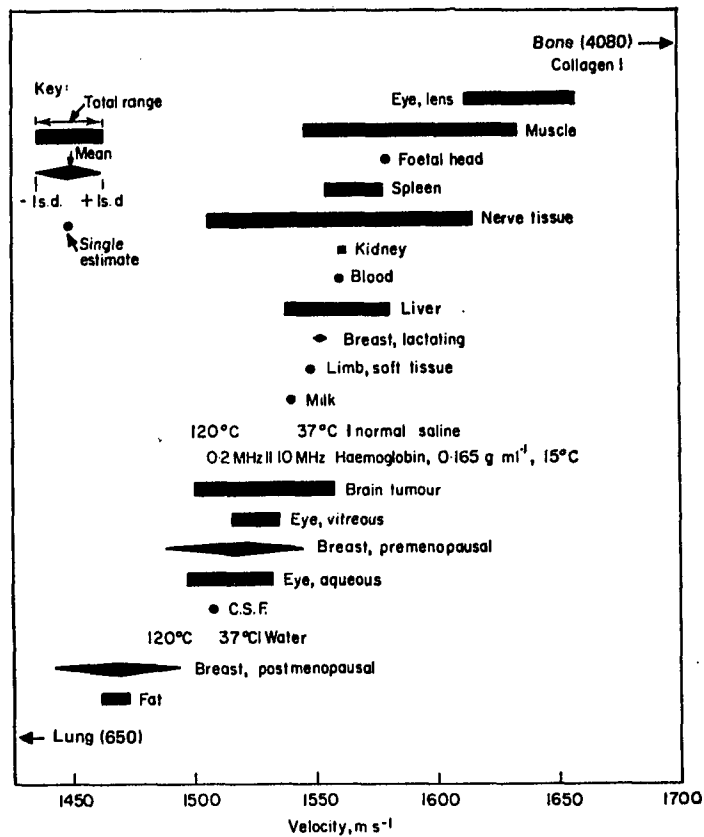
Figure 3-2. Velocity of sound in some biological substances. (Adapted from Wells [13], p. 125.)

Average: 60 cm = 0.6 m

$$0.6 \text{ m} \times 1 \text{ sec}/1540 \text{ m} = 389.6 \text{ } \mu\text{sec to travel } 60 \text{ cm} = t_{avg}$$

Low: $0.6 \text{ m} \times 1 \text{ sec}/1476 \text{ m} = 406.5 \text{ } \mu\text{sec to travel } 60 \text{ cm} = t_{low}$

Therefore, $t_{avg} - t_{low} = 406.5 - 389.6 = 16.9 \text{ } \mu\text{sec}$

Using the assumed average velocity of sound (1540 m/sec),
this time discrepancy results in a position (distance)
error of $1540 \text{ m}/10^6 \text{ } \mu\text{sec} \times 16.9 \text{ } \mu\text{sec} = 26 \text{ mm shorter}$

High: $0.6 \text{ m} \times 1 \text{ sec}/1592 \text{ m} = 376.9 \text{ } \mu\text{sec to travel } 60 \text{ cm} = t_{high}$

Therefore, $t_{avg} - t_{high} = 389.6 - 376.9 = 12.7 \text{ } \mu\text{sec}$

Using the assumed average velocity of sound (1540 m/sec)
this time discrepancy results in a positional (distance)
error of $1540 \text{ m}/10^6 \text{ } \mu\text{sec} \times 12.7 \text{ } \mu\text{sec}. = 19.6 \text{ mm farther}$

Therefore, the worst case positioned error for a maximum distance of 30 cm is (-13 mm, + 9.8 mm). Over shorter path lengths (which will be the general case) this error would be proportionately reduced. Furthermore, since the typical pulse-echo signal passes through numerous tissues, velocity will tend to average out, resulting in positional errors much less than worst-case.

For the pulse-echo technique, although it is possible to receive multipath data, the transducers used are generally highly directional and narrow beam. As a result, an echo will only be received if it deviates by approximately $\leq 2^o$ to either side of the original beam direction (see Figure 3-3). In this case, then, reception of a multipath signal is generally unlikely. Multipath reception, when it does occur, will of course be interpreted as a straight line path, thus indicating that the reflector is further from the transducer than it really is.

Acoustic reverberation will produce similar errors. Reverberation occurs when the acoustic-pulse bounces back and forth between the transducer and reflector, resulting in several pulses, equally spaced in time and successively
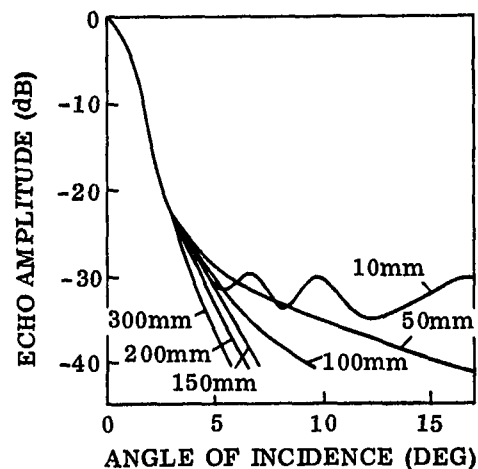
Figure 3-3. Relationship between echo amplitude and angle of incidence, for a
flat target in water at various ranges. Each curve is relative to
0 dB at normal incidence. Zero-crossing frequency, 1.7 MHz;
transducer diameter, 20 mm. (Reproduced from Wells [13],
p. 159.)

more highly attenuated. Such a result would be interpreted as there being one

reflector corresponding to each pulse received.

Various display modes have been used to aid in interpretation of the ultra-

sonic echo. The simplest display, termed (amplitude) A-mode, is a plot of echo

envelope voltage amplitude versus time. As shown in the block diagram of

Figure 3-4 of a generalized A-mode pulse-echo system, the original echo is

an RF signal which is then envelope-detected to produce the signal character-

istic of the A-mode display. Most systems today possess a variable or fixed

time-gain compensation (TGC) or swept-gain capability in an attempt to null out

the effects of ultrasonic absorption. As discussed earlier, the display indicates

that two objects any closer than a single pulse-width cannot be resolved.

Proceeding one step further is the (brightness) B-mode display, presenting

reflector location in an X-Y Cartesian plane, and echo amplitude in terms of

Z-axis intensity modulation (i.e. brightness of the point in the X-Y plane cor-

responds to the amplitude of the received echoes). Knowing the exact location of
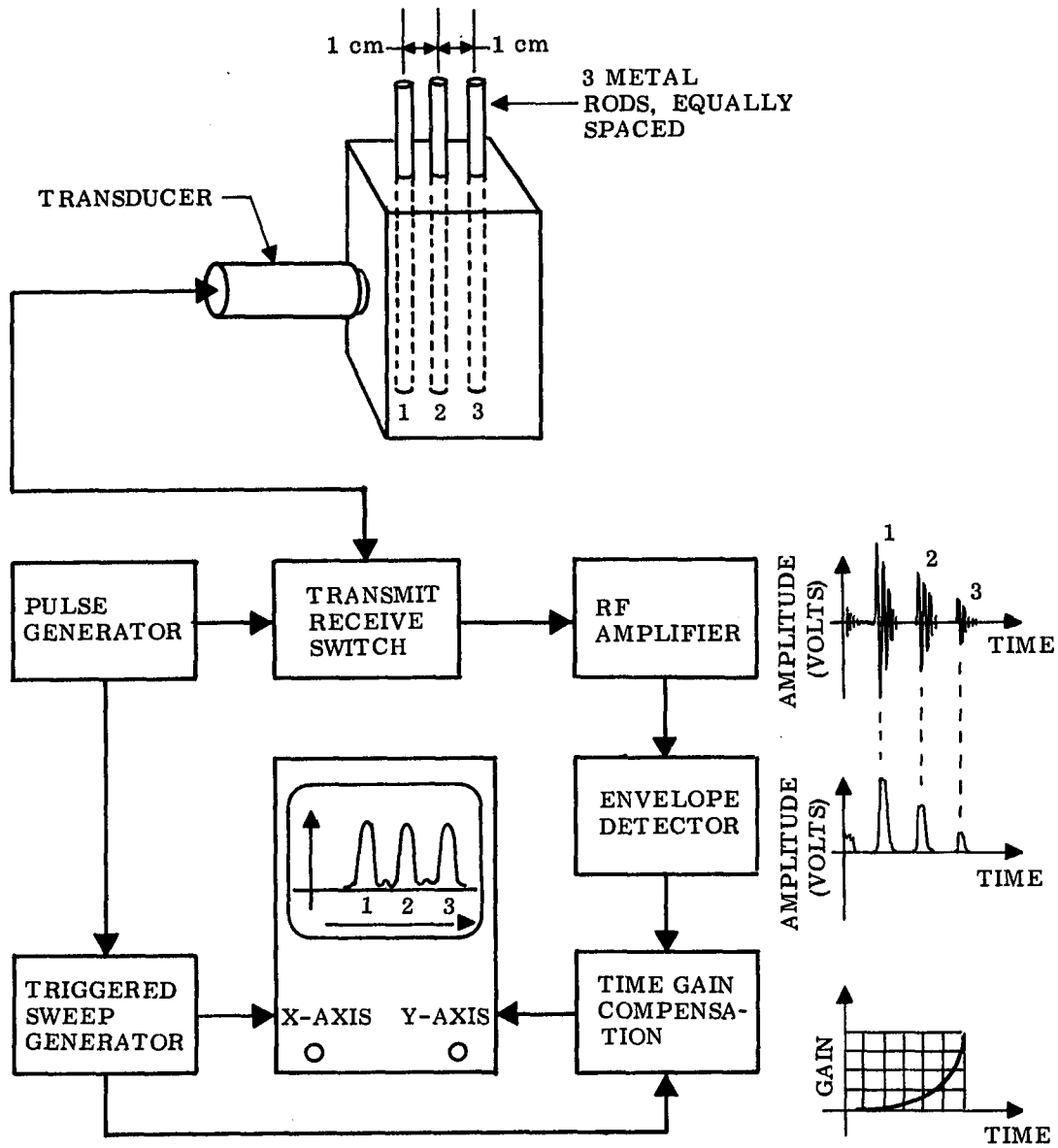
Figure 3-4. Generalized A-mode pulse-echo system

the sound beam as it cuts through the X-Y plane represented (determined from the outputs of three sine-cosine potentiometers), the A-mode waveform is simply "written" down by assigning the proper shade of gray to each display resolution element (pixel) covered by the beam. Scanning the transducer over a particular circumferential plane of the body in an attempt at covering each resolution element with an A-mode will result in an image of a particular body cross-section, as depicted in Figure 3-5. As discussed earlier and illustrated in Figure 3-3, in order to examine each resolution element of tissue, the sound beam must impinge normally. In scanning a transducer across the body to form a B-scan, it is evident that echoes from many of the tissue elements will not be received due to off normal scattering. Such is one of the prime motivations behind the pulse-scattering technique investigated in this dissertation.

Early B-scanners utilized storage oscilloscopes for display, which operated in a bistable mode; echo presence was indicated by a bright spot and lack of echoes by darkness. Development of analog and most recently, digital scan converter systems has allowed gray scale display of generally sixteen levels on a cathode ray screen. Figure 3-6 illustrates various schemes for associating grade shade with signal amplitude. Although the recent trend has been towards digital storage and processing of the ultrasonic data, more conveniently enabling gray scale assignment (gamma function) and additional signal analysis and image processing, most systems in clinical use utilize only a linear gamma. The "best" gamma to choose depends on the particular range and distribution of the signals acquired. Such considerations will be mentioned in Section IV (B) with regard to computerized X-ray tomography.

Now, let an A-mode signal (transducer position is fixed) be displayed as an intensity modulated line (as in B-scan) and oriented on an X-Y display at X = 0 and parallel with the Y-axis. Let the X-axis represent time and locate
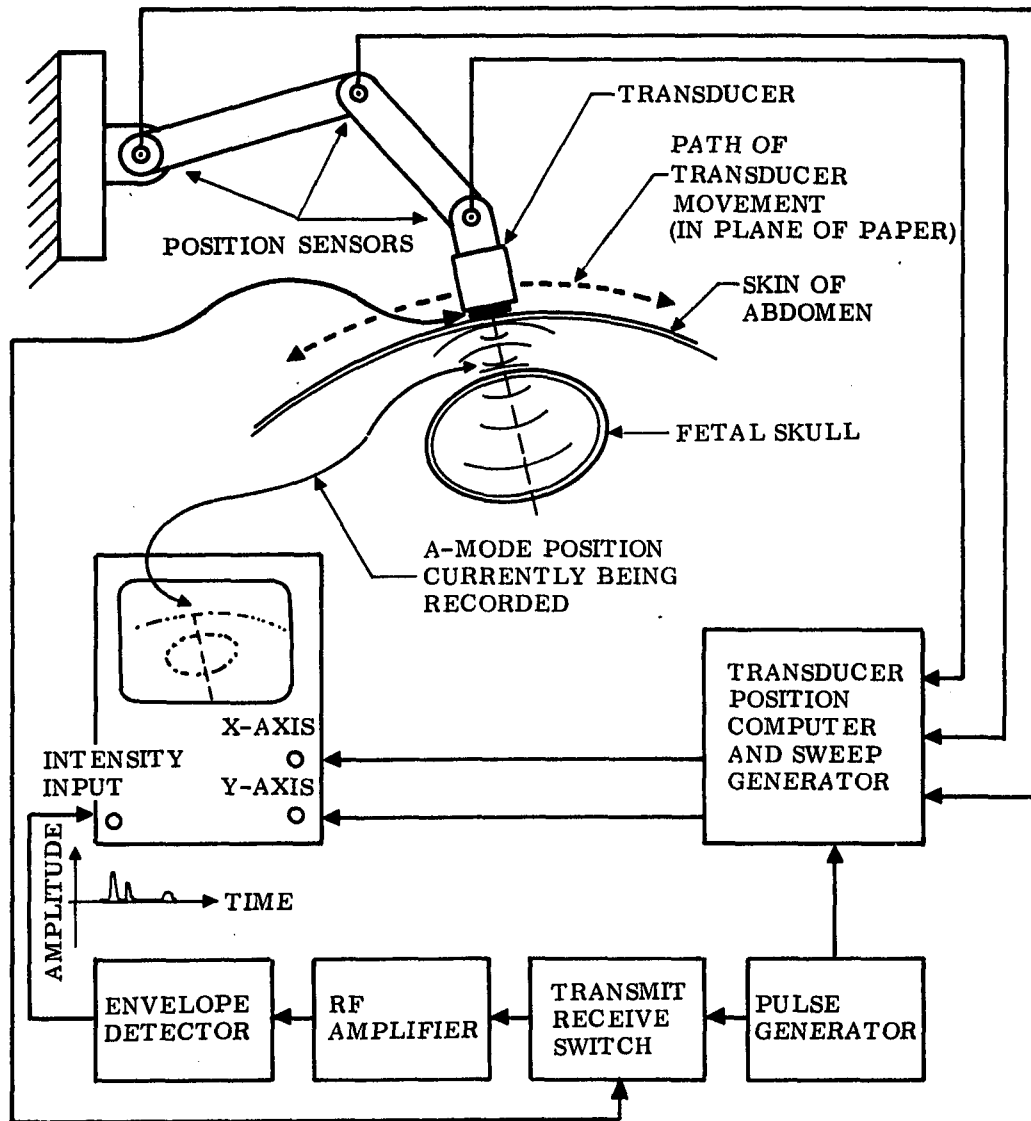
Figure 3-5. Generalized B-scan system (bistable display)
(After Hubelbank [48], p. 13.)
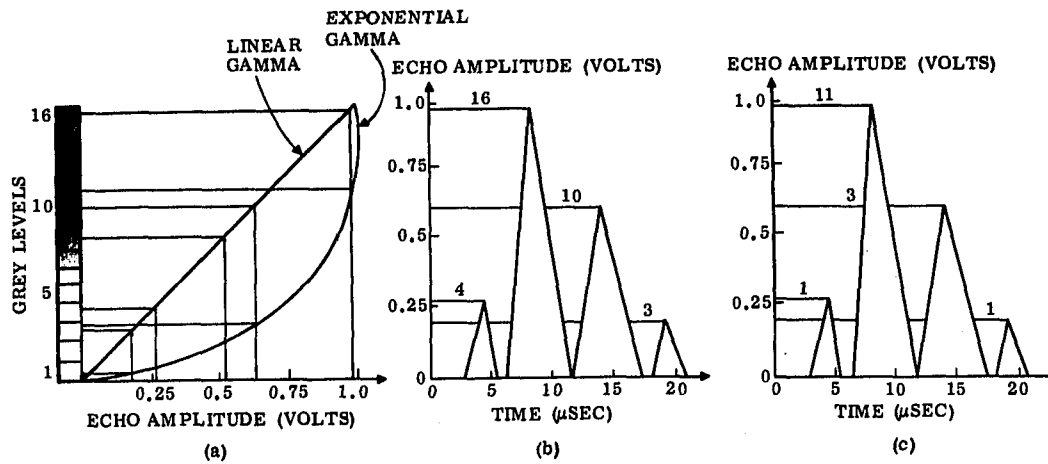
Figure 3-6. Various schemes for gray scale assignment
(a) Gamma assignment curves
(b) Linear gamma
(c) Exponential gamma

each succeeding intensity-modulated A-mode signal at the corresponding

abscissa. In this manner, a (motion) M-mode scan is formed, whereby the

motion of the structure being insonified by the "pencil beam" can be seen with

advancing time (see Figure 3-7).

Although not conventional, two other display modes have been used

routinely in certain clinics, which essentially present B-scan in slightly dif-

ferent formats. Color coding, pioneered in ultrasound by Baum [51], involves

assigning colors, rather than gray shades to represent echo amplitude on a B-

scan plot. Depending on the pattern displayed, the eye generally cannot dif-

ferentiate sixteen shades of gray. Sixteen bright colors, however, can easily

be viewed. Color coding has generally been rejected for two reasons, namely,

(i) there is no obvious relationship between color and amplitude and (ii) the

visual amplitude averaging which can be done for gray shades cannot readily be

done for colors. Although various coloring schemes have been suggested to

enable more obvious association of color and shade of gray, color coding has

thus far failed to gain wide acceptance.
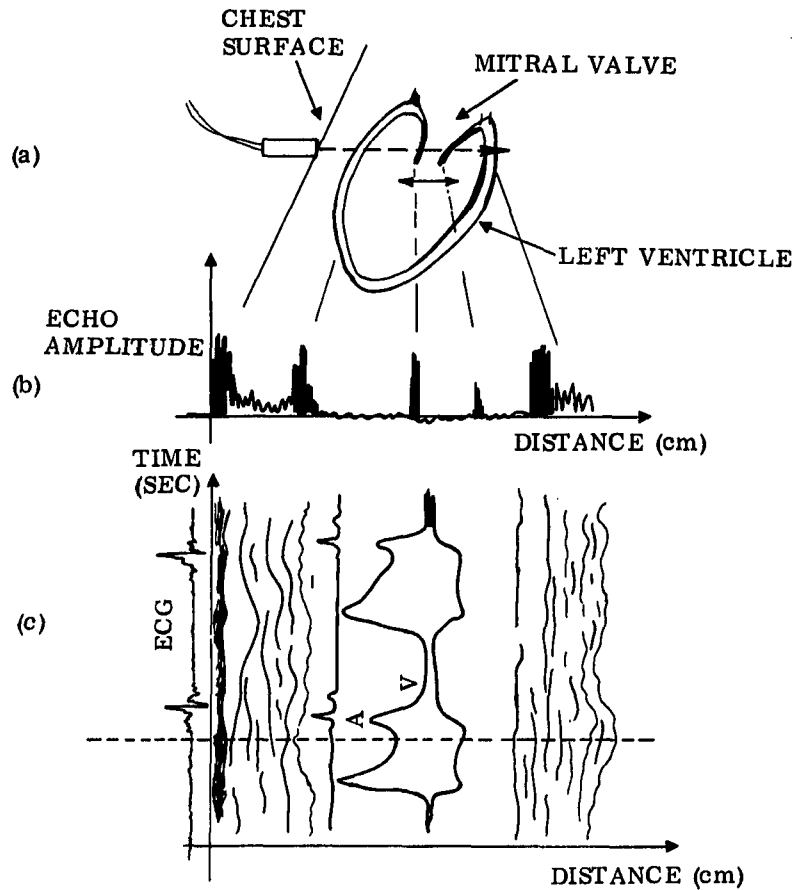
Figure 3-7. Illustration of M-mode display.
(a) Transducer placed on chest in alignment with valve leaflets
(b) A-mode display
(c) M-mode display; position of A-mode waveform on M-scan represented by horizontal dotted line. Valve leaflets open at atrial systole (A) and close at ventricular systole (V).
(Adapted from King [47], p. 42)

Finally, an isometric or perspective plot may be presented in which two spatial dimensions are presented in what appears to be the plane of the image, while a third dimension, echo amplitude, is plotted so as to appear to be extending out of the display plane [52]. Such a display does not exhibit the relatively coarse amplitude quantization necessary for gray-scale assignment.

The goal of each of the abovementioned modes is to display ultrasonic data so that obvious correlations can be made between the display appearance and the

physiological state of the tissue being imaged. The best display to use depends on the specific parameters of interest (e.g. do they vary with time?) as well as the ultrasonographer's preference.

During the present decade, techniques have been developed to enable so-called "real-time" ultrasonic imaging. In short, these techniques display B-scans which are constantly updated with time. As long as the display updates faster than any motion occurs in the subject, then all motion will be observed in the image. When subject motion occurs faster than image update, the resultant display will appear more as a sequence of stop-action shots. Data acquisition for real time display is attained either via the earlier method of rapid mechanical scanning ("wobbling") of an individual transducer or, more recently, by sequential high speed switching of the individual transducers comprising a linear array which spans the tissue region of interest. Exciting the component transducers in a properly phased sequence, either individually or in multi-combination, dynamic focusing and beam steering can effectively be obtained [53]-[56]. Together with digital storage and image processing of traditional B-scan data, imaging with linear and phased arrays comprise the state-of-the-art in commercially available ultrasonic imagers. Thus far, real time techniques have been most successfully used for cardiac imaging.

C. CLINICAL ULTRASONIC IMAGING – SOME ILLUSTRATIVE EXAMPLES

Thus far, the general physical concepts behind ultrasonic imaging have been reviewed, in addition to the conventional medical ultrasonic imaging techniques, in particular. While ultrasonic techniques have been utilized to image or characterize a major portion of the body's tissues, current ultrasonic imaging, in particular, B-scan, finds most widespread use in the areas of

abdominal, pelvic and ophthalmic scanning. In order to place the discussions and results of this dissertation in better perspective, several illustrative examples in these areas will now be presented.

Figure 3-8 illustrates a series of longitudinal (i.e. saggital) sections imaged with a Picker 80L B-scan unit and a 2.25 MHz focused transducer at various distances from the mid-line (ML), e.g. "R9" means 9 cm to the right of ML. As indicated in the figure, vascular or fluid-filled structures are clearly echo-free. Normal liver, being a relatively homogeneous tissue, exhibits a regular speckled pattern. As for the kidney, the medullary calices appear as strong echo producers whereas the outer cortical region is much less echogenic.

Figure 3-9 illustrates several saggital, abdominal scans of a 21 year old human male, taken at approximately 6 cm to the right of midline for 2.25, 5.0 and 10.0 MHz on a Picker digital B-scanner to demonstrate image dependence on transducer frequency. While indicating many of the structures observed in the previous figure, it is seen that ultrasonic penetration is reduced with increased frequency, while resolution is clearly improved.

Figure 3-10 illustrates B-scan sections similar to those already presented, except for a pregnant woman. As indicated by the two sections shown, the fetus is situated laterally with its head at the mother's right (left side of photo) and feet at the mother's left. These two scans show exceedingly good fetal detail. Particularly note the "wiggly line" (in the region of the "H" in the lower photo) indicating cardiac motion. This line is most likely the interventricular septum.

Ultrasonic B-scan is also widely used for ophthalmic diagnosis. This technique is especially useful for cases such as cataracts where the physician cannot see into the eye due to its resultant opacity to light. The fact that the
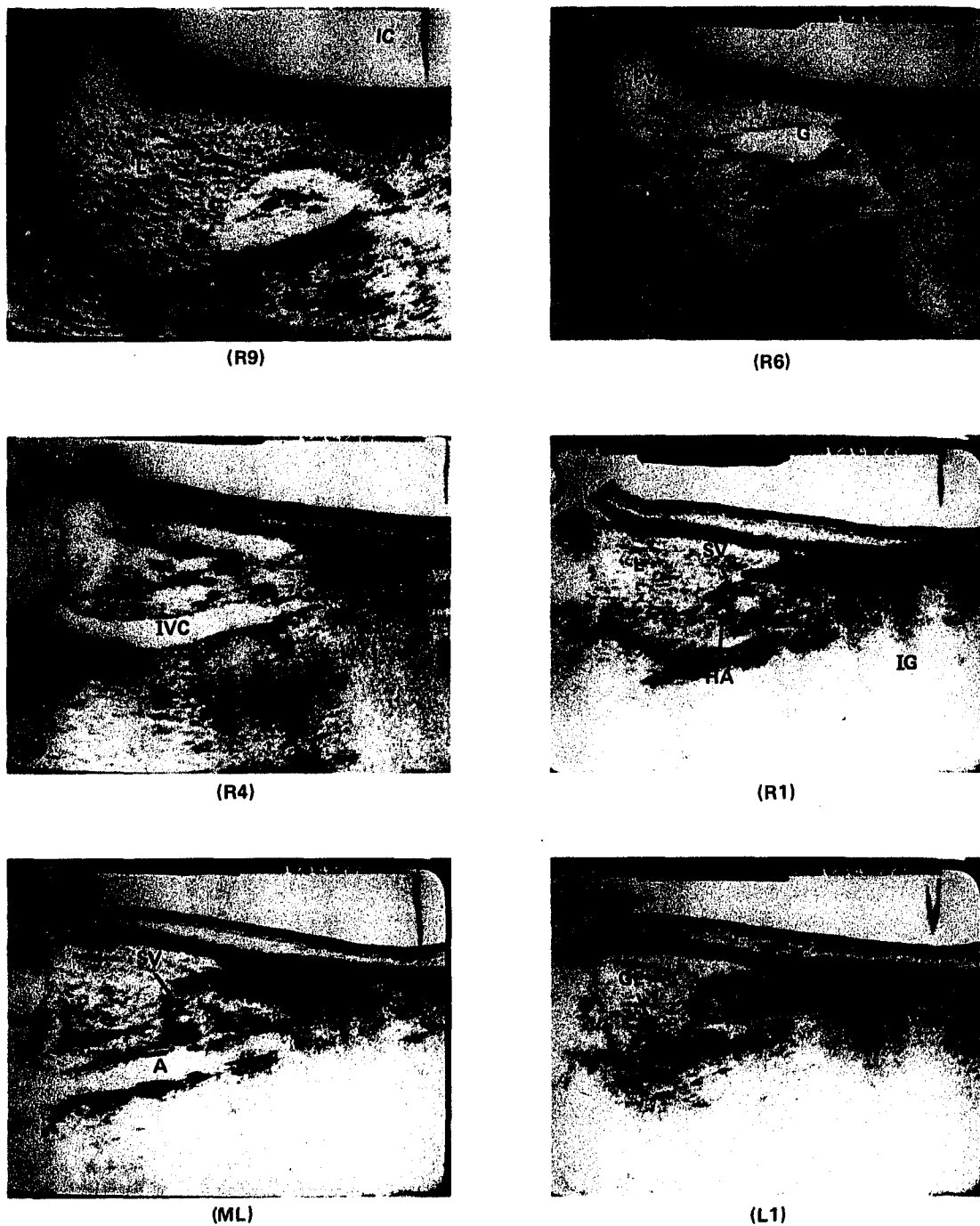
Figure 3-8. Normal longitudinal abdominal B-scan taken with a Picker 80-L
scanner and 2.25 MHz transducer for the various sections indi-
cated. Some of the structures clearly seen are the diaphragm (D),
liver (L), kidney (K), portal vein (PV), hepatic-vein (HV), cystic
duct (CD), gallbladder (G), inferior vena cava (IVC), aorta (A),
splenic vein (SV), hepatic-artery (HA), pancreas (P) and gastro-
esophogeal junction (GE). The iliac-crest (IC) is denoted for
geographical reference. Intestinal gas (IG) is indicated by the
streaked patterns and characteristic reverberation.
(Photos courtesy of Atis Freimanis, MD, Chairman, Ohio State
University Department of Radiology.)

2.25 MHz

5.0 MHz
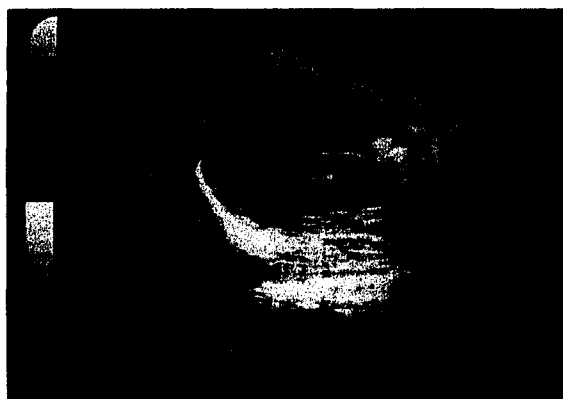
10.0 MHz
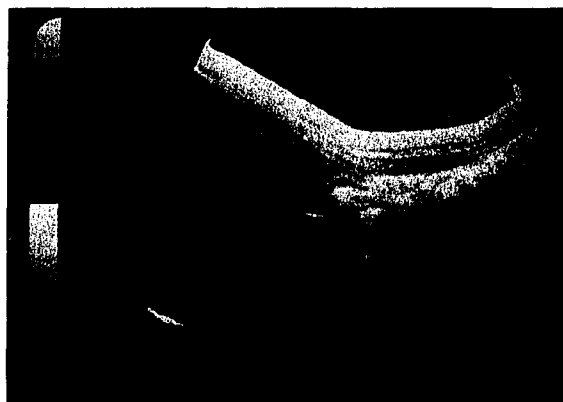
Figure 3-9. Saggital abdominal B-scan (human male, 21 years old) taken at
approximately 6 cm to the right of mid-line at 2.25, 5.0 and
10 MHz. The diaphragm (D), liver (L), kidney (K) and some
hepatic vessels (HV) can clearly be seen. Increased resolution
and decreased penetration can be seen with increasing frequency.
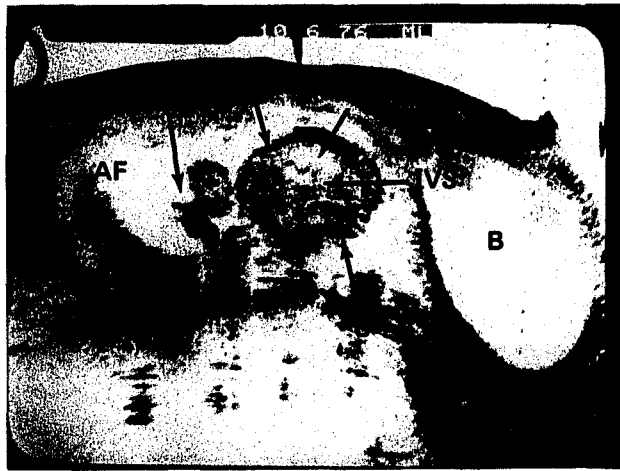
LONGITUDINAL SECTION (ML)

TRANSVERSE SECTION (IC)

Figure 3-10. Longitudinal (mid-line, ML) and transverse (iliac crest, IC) sections of a pregnant woman illustrating fetal detail and associated anatomy – placenta (P), amniotic fluid (AF), small parts (SP), trunk cross-section (T), heart (H), interventricular septum (IVS), fetal head (HE) and Mother's bladder (B)

eye offers such relatively little attenuation to ultrasound, scanning with a 10 MHz

signal produces excellent results. Ultrasonic examination is of particular value

for isolating a detached retina, vitreous hemorrhage and various melanomas.

As a final clinical illustration, Figure 3-11 shows a fundus photograph (where

the retinal blood vessels are visualized by fluorescein injection) and associated

A- and B-scans demonstrating a small choroidal melanoma. In Figure 3-12,

the melanoma has enlarged and resulted in the complication of retinal detach-

ment. In the fundus photograph of Figure 3-12, the extremely raised character-

istic of the melanoma (easily visualized by the B-scan cross-section) is indicated

by the large degree with which the mass is out of focus with the rest of the

choroid in view.

D.   EXPERIMENTAL TECHNIQUES AND RESEARCH ACTIVITIES IN
     ULTRASONIC IMAGING AND TISSUE CHARACTERIZATION

Within the past decade, efforts devoted to research in medical ultrasound

have increased at a phenomenal rate. Ultrasound has seen a wide range of appli-

cations, including surgical procedures, various treatment and therapy techniques,

blood flow profiles and non-invasive imaging. The tremendous advances being

made in electronics technology resulting in high speed, low cost and compact

digital processing and memory components, and in particular, microcomputer

processing and control systems, has resulted in the development of real time

ultrasonic imaging systems based on linear and phased arrays [58]. Additional

systems have been using spectral analysis and multiple frequency techniques,

computerized X-ray technology principles (see Chapter IV (B), ultrasonic trans-

mission tomography), as well as techniques such as Bragg diffraction and

acoustical holography. Rapid advances in digital imaging processing, originally

an outgrowth of the space program, has opened up a wide range of analytical
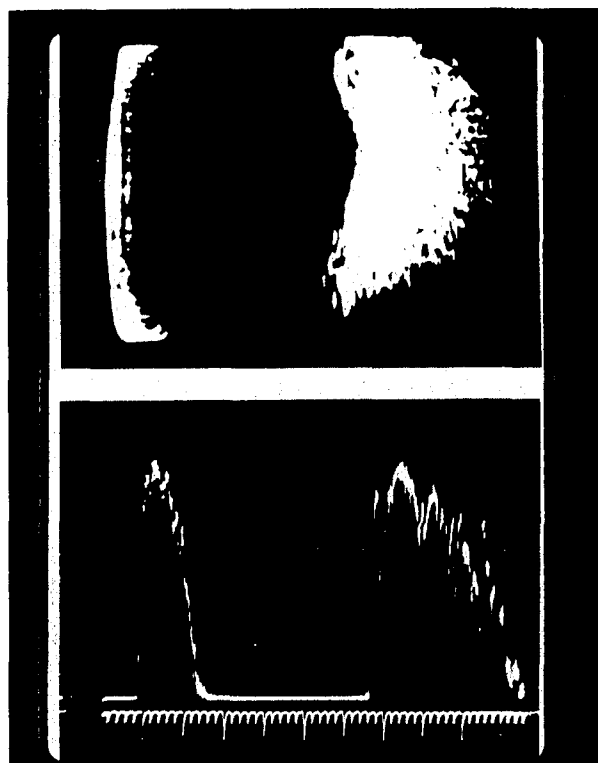
Figure 3-11. (Top) Fundus photograph illustrating optic disc (bright spot in upper, right corner), retinal blood vessels (made visible with fluorescein injection), and a relatively small choroidal melanoma. (Bottom) Ultrasonic B- and A-scans indicative of the melanoma shown. The ultrasound enters the eye through the lens at the right of the B-scan photo.
(Photos courtesy of Mick Clark and Holly Taylor, O.S.U. Dept. of Ophthalmology.)

Figure 3-12. (Top) Fundus photograph illustrating a large choroidal melanoma
and detached retina. Note the raised state of the tumor, as
indicated by its blurred appearance compared with the rest of
the figure.
(Bottom) B- and A-scan indicative of the above situation. Note
the large mass and detached retina in the B-scan presented.
(Photos courtesy of Mick Clark and Holly Taylor, O.S.U.
Dept. of Ophthalmology.)

possibilities for not only improving image quality, but more importantly, to provide an additional tool for ultrasonic tissue characterization. While most of these techniques are still in laboratory development, many of these methods have undergone successful but limited clinical testing. No doubt many of these systems will come into more widespread use in the very near future.

A written summary of the literature which has been reviewed related to the material encompassed in the above paragraph would require that literally an additional volume be added to this dissertation. As a result, the interested reader is recommended to several excellent review references which have been found to be quite up to date [13],[59],[60],[61],[62], [63]. More detailed descriptions may be found in some of the citations in the List of References and related papers and texts.

CHAPTER IV. THE PULSE-SCATTER IMAGING TECHNIQUE

A. INTRODUCTION

As mentioned in the introductory chapter of this dissertation, I(E), the concept of Pulse-Scatter Imaging (PSI) was proposed during the summer of 1976 as part of a joint industrial/academic National Science Foundation Facility Participation Program at the General Electric Company's Electronics Laboratory in Syracuse, N.Y. The prime participants in the program were

> Dr. Stephen Tehon, GE Consulting Engineer for Solid State Acoustics
>
> Mr. Robert Glusick, GE Senior Engineer for Display Systems
>
> Dr. Abraham Liboff, Chairman, Department of Medical Physics, Oakland University, Rochester, Michigan
>
> Dr. Frederick Terry, Chairman, Department of Electrical Engineering, Christian Brothers College, Memphis, Tennessee.

The hypothesis was made that although ultrasonic imaging, B-mode presentation in particular, had revolutionized the field of non-invasive medical imaging, the pulse-echo data utilized represented only a small amount of the information generated with this procedure. Most of the acoustic energy, rather than be backscattered to the pulse-echo transducer, was scattered away in various other directions depending upon the exact specimen imaged. Scattering theory, as reviewed in Section II(C), completely supports this hypothesis. It

70

was thus suggested that in order to capture this lost information, additional ultrasonic transducers be equally spaced in a circular array about the object to be imaged [1] . In this way, both the usual pulse-echo as well as non-backscattered signals could be recovered and incorporated into an image. Recovery of all scattered data in this fashion would require an extremely large number (the exact number depending on the desired resolution) of omni-directional receivers. Furthermore, as previously discussed, depending upon the particular tissue being imaged, scattering behavior may vary with direction of insonification, requiring omni-directional insonification for complete scat-terer imaging. Taking these physical criteria into account, the compromise of using a circular array of equally spaced fan beam transducers was suggested in order to obtain a reasonable amount of omni-directional insonification and reception, with a minimum number of transducers and data handling. Each transducer is successively pulsed, allowing the subject to be viewed at varying incident angles. Immediately following each excitation pulse, all transducers become ultrasonic receivers, in order to monitor the scattered signals (in-cluding pulse-echo). Each receiver outputs an A-mode signal specifying an amplitude and time-of-flight for each echo received. Assuming a constant acoustic-velocity, the measured time defines the path length traveled by the received echo. Also, knowing the coordinates of the specific transmitter/ receiver pair, the loci of all points which could have possibly caused a given single scatter based solely on time-of-flight considerations (assuming no multipath transmission), is an ellipse with foci at the transducer locations. Therefore, the A-mode signal corresponding to each transmit/receive pair will produce a family of cofocal ellipses, one ellipse per scattering event (echo), with each ellipse being assigned a gray-scale intensity corresponding

to the amplitude of the received signal. Linear superposition (i.e. intensity summation) of all ellipses will result in an image where true scattering events will intersect and reinforce each other, while artifactual data and noise will lack such reinforcement and fade into the background.

Having presumed the above hypothesis, some minimal analysis was performed and data taken using an 8" diameter aluminum ring supporting six transducers built at General Electric. Although a reconstruction algorithm had not yet been designed, image data was taken of a plastic bottle filled with water, having an o.d. of 6.07 cm and i.d. of 5.91 cm. Simple data analysis suggested reasonable system performance. In a separate effort, a computer program was designed to simulate PSI image reconstruction of some simple objects, using the ellipse superposition technique on a 320 × 320 pixel, 10-bit internal resolution, 16 shade gray scale GE computerized X-ray tomography CRT display. Successful results demonstrated the validity of the PSI approach suggested, but also illustrated the image smearing effects prevalent in image reconstruction via computerized X-ray tomography (CT).

Essentially no other work was performed on this project until June, 1977, when another student, Mr. Larry Browning, PhD candidate in Physics at Purdue University, and the author were given the responsibility of starting an investigation of the PSI technique, as part of a summer employment program at the General Electric Electronics Laboratory. Prior to returning to school at the beginning of August, Mr. Browning had written a preliminary computer program for reconstructing an image using the PSI technique on a Varian minicomputer. The author's efforts were spent developing a manual PSI data acquisition and pre-processing capability using the limited equipment available. In all, such efforts failed to demonstrate the physical validity and feasibility of the

PSI technique, beyond the results obtained, during the previous summer's computer simulation carried out by Mr. Glusick.

At the suggestion of General Electric personnel in conjunction with the author's academic advisers at Ohio State University, the author decided to concentrate his PhD dissertation effort on investigating the validity and feasibility of PSI for medical ultrasonic imaging, as well as to derive a theoretical description of the technique. These tasks comprise the bulk of this dissertation and are presented in the following sections. As listed in Chapter I, the following is a brief categorization of this effort -

i)   review PSI concept, previously untested, as well as applicable acoustic theory

ii)   design experimental protocol and associated hardware/software to test the PSI concept

iii)   develop a theoretical basis for PSI

iv)   modify PSI concept as necessary and repeat experiments

v)   evaluate PSI as to its potential usefulness and feasibility as a clinical imaging procedure.

B.   PSI - RELATED IMAGING TECHNIQUES

For completeness, prior to discussing the PSI investigation itself, a summary of techniques found in the literature that bear some, although minimal, similarities to PSI will be presented. Four references have been found, two in the area of radar and one each in geophysics and acoustic imaging.

The radar system, "Loran" (Long Range Navigation), was originally developed during World War II as a navigational aid to both sea and air forces [64],[65]. Various "Loran-C" ground stations, currently located around the world, are utilized as an aid to marine navigation. Loran-C is an updated version of Loran, utilizing a lower frequency carrier signal to obtain

greater range and accuracy due to more stable LF propagation characteristics.
Utilizing at least three reference stations, generally a master transmitter and
two slave transmitters (triggered by the master after a known time delay)
variously coded pulse bursts (to minimize multipath ambiguities) are trans-
mitted to and received by the traveling vessel. At the receiver, distance
"differences" are calculated between the vessel and transmitter pairs. A
hyperbola with foci located at the transmitter locations (modified appropriately
for the slave transmitter, to take into account trigger delay) defines the locus
of all vessel locations from which the particular distance difference could have
been measured (see Figure 4-1). Measuring such distances from two pairs
of transmitters (hence the need for at least three transmitters in all) will
result in an intersection of two hyperbolas, thus defining a position-fix.

The second system, termed "multilateration radar" is an airborne-based
radar system which bears quite a bit more resemblance to PSI [66]. As depicted
in Figure 4-2, an aircraft possessing a wide antenna pattern (analogous to the PSI
fan beam) flies at a constant velocity in a straight line path past the region to be
imaged. Either narrow or pulse-compressed pulses (to maximize range
resolution) are transmitted, with corresponding echoes being reflected off
any targets in the field of view, prior to reception back at the plane. Assuming
that the plane's velocity is such that receiving the resultant echoes at positions
slightly beyond the original transmitter location results in a negligible change
in the echo times of arrival, the received echo times can be translated into
circular bands, centered at the transmitter location, possessing radii equal
to the distance corresponding to the particular echo time of flight. The width
of the band corresponds to the range resolution dictated by the transmitted pulse
width. Superimposing these annular rings on a suitable storage medium, inter-
sections of these rings at reflector locations will result in an image build-up at
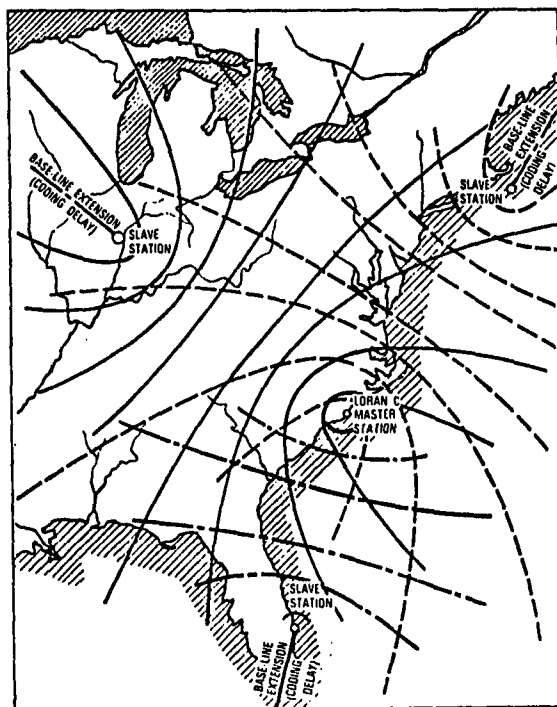
Figure 4-1. Generalized Loran-C navigation system (shown for half of U.S.)
utilizing hyperbola intersection to determine position-fix.
(Reproduced from Van Etten, p. 100 [64].)
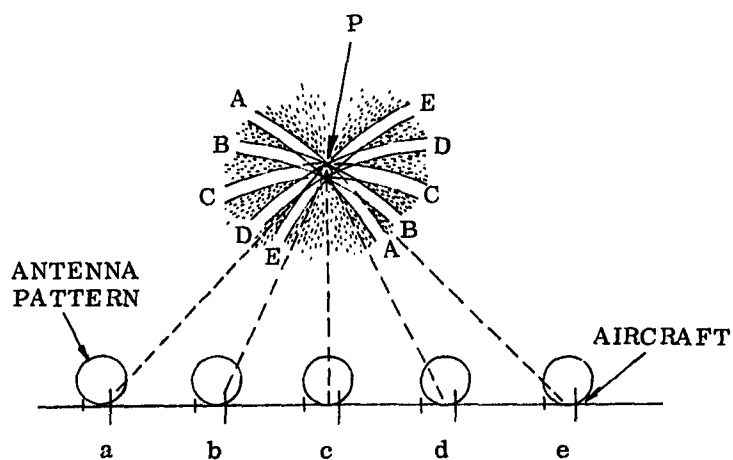
Figure 4-2. Multilateration radar image reconstruction of point "P"; plane
flies by the target emitting wide aperture pulses at locations a-e.
(Adapted from Kazel, p. 1239 [66].)

such points, with extraneous portions of the circular rings becoming background noise. It was reported that computer simulation produced the theoretical range resolution (15m for a pulse width of 0.1 μs on a carrier of 600 MHz) and an image dynamic range of 10 dB. It was suggested that echo signal processing and appropriate narrowing of the antenna pattern used could greatly enhance dynamic range. (Apparently only a simple binary echo detection scheme was used, thus eliminating any amplitude information from the image.) As a side note, it appeared that the processing schemes utilized (if any) to reduce artifactual effects such as "false intersections", might be applicable for incorporation into the PSI algorithm. However, upon investigating further, it appears that any such work beyond the basic concept presented in the reference cited is currently classified information.

The area of geophysics utilizes the technique of reflection seismology to map out underground terrain [67] . An explosive source is placed into the ground for the purpose of emitting compressional sound waves. Receivers, termed geophones, are symmetrically spaced in a linear array, away from the source in order to pick up the reflected shock waves. A hyperbolic relationship exists between time of flight and receiver location (multipath propagation and Snell's Law diffraction are neglected), thus allowing calculation of reflector locations. Furthermore, in order to obtain quantitative amplitude data, noise filtering and time-gain compensation are utilized.

The final process to be described is acoustic and is termed isochrone convergence imaging [68] . This method utilizes a single transmitter and multiple point-receivers located in one plane, to image an object in a parallel plane via the generation and superposition of circular loci, one per received echo, as illustrated in Figure 4-3(a). Utilizing a single transmitter, the object plane is insonified with a wide aperture acoustic pulse. Corresponding to the
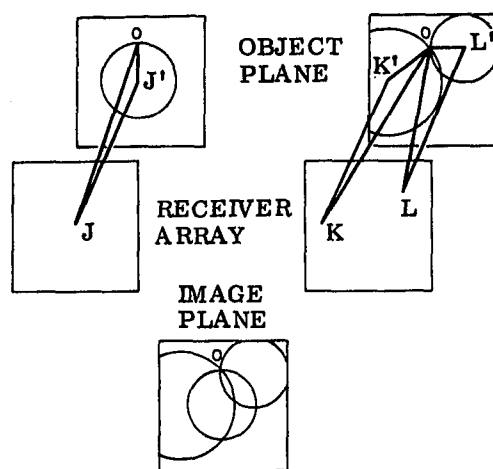
(a)
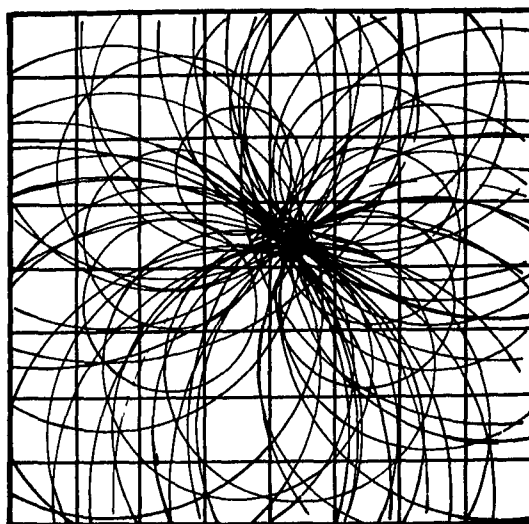
(b)

Figure 4-3. Isochrone convergence imaging.
(a) Reconstruction of point "o" utilizing three receivers.
(b) Reconstruction of a 7.5 mm ball bearing in water at 105 mm
from transducer array. Reconstruction is based on echo
peak amplitude timings. Spatial scale is 6 mm per division.
(Reproduced from Dow and Brown, pp. 130,134 [68] .)

time of each echo arrival, a circle may be drawn, centered about the given
receiver location (e.g. point J', corresponding to receiver J in Figure 4-3(a))
describing the locus of all points which could have echoed a signal at the given
time of arrival. Corresponding to each receiver location (J, K and L in the
illustration) circles are formed, which subsequently intersect and reinforce
at the reflector location (point O). As each receiver's output is examined,
a spiraling timebase is generated about the receiver location, starting at
time "2T", where "T" is the time required for the acoustic pulse to travel
from receiver location in transducer array to corresponding receiver co-
ordinate in the object focal plane, with the CRT beam intensity being modu-
lated at times of subsequent echo arrival, thus generating approximately cir-
cular loci. Figure 4-3 illustrates image reconstruction of a 7.5 mm ball
bearing. Methods of eliminating false intersections and other artifacts (e.g.
"smearing") in the reconstruction have not been reported. System resolution
was cited as being related to both the number of reflecting objects and number
of receivers.

Before proceeding with the PSI theory, since PSI is in effect a type of
tomography system, a brief reference should be made to computerized X-ray
tomography (CT) [9],[69],[70],[71]. Although the CT technique can be quite
closely compared with several ultrasonic imaging systems which have been devel-
oped, namely, time-of-flight [72],[73] and thru-transmission reconstruction-
based systems [74],[75] (see Section III(B)), PSI, as the concept has now been
modified, ignores thru-transmission signals, since they do not contain any
information with regard to scatterer location. In fact, such signals, when
processed by the PSI algorithm, actually obscure the image produced with
only scattered signals. CT involves X-raying a plane of tissue from many

angles via either rotating or rotating-and-translating a fan or rectangular X-ray beam. Since the X-rays travel essentially a non-deviated straight line path through the tissue, highly collimated receivers located directly opposite each transmitter location are used to detect straight line path attenuation through the tissue sample. The reconstruction algorithm, via a number of possible methods [76],[77], determines the attenuation attributable to each tissue image resolution element. The result is displayed as a gray-scale image, with a direct correspondence established between gray shade and attenuation coefficient. Useful with respect to PSI, are the gray scale image processing and windowing techniques, used to enhance or extract information from the reconstructed CT images. Some of these techniques may be applied to PSI either directly or after suitable modifications. Several of these techniques were applied to PSI and will be discussed in Chapter V.

C. ⸱ THEORETICAL FOUNDATIONS, ANALYSES AND HYPOTHESES

In the previous sections, some of the fundamental ideas of Pulse-Scatter Imaging have been mentioned. This section will present a formal description of PSI and discuss theoretical system limitations and considerations, as proposed by the author.

The investigation of PSI was pursued, intent on achieving the feasibility of an ultrasonic imaging system with six primary features --

    (i)   better image resolution than obtainable with B-scan

    (ii)   uniform scan procedure, independent of ultrasonographer variability

    (iii)   rapid scan time to minimize motion artifacts

    (iv)   minimal ultrasound dosage to patient

    (v)   system flexibility, such that once a complete set of data has been taken, arbitrary cross-sectional views may be observed in either standard or magnified perspective

(vi) ability to quantitatively analyze received data and provide a reliable

means of ultrasonic tissue characterization.

Three main assumptions regarding ultrasound interaction with biological

tissues were made at the outset and are consistent with current ultrasonic

research [78] -

(i) velocity of sound is constant; an average velocity of 1540 m/sec is

assumed.

(ii) most of the acoustic energy, upon reaching an interface is scattered

at other than 180° (i.e. backscatter) and will not be captured in the pulse echo

process.

(iii) multipath and multimode (i.e. non-longitudinal) signals may be

treated as system noise, e.g. after encountering more than one interface the

acoustic signal will be highly attenuated. (Although this assumption is generally

made, separate investigations should be conducted to determine its validity in

a more quantitative fashion.)

The basic PSI system is designed to be suitable for producing transverse

images of the body, such as are presently obtained for abdominal, pelvic and

breast examination. The acoustic portion of the system consists of a circular

array of "N_T" transducers, which is placed around the patient, as illustrated

in Figure 4-4. (For purposes of simplifying the illustrative figures, $N_T = 8$ will

be assumed.) Acoustic coupling between the transducers and patient may be

obtained in various ways, one of which would involve utilization of a water-filled

plastic bag. Proper sequencing of the transmission and reception functions of

this array will allow multidirectional modes of both insonification and scatter

reception. Assuming that "N_T" ideal, standard pulse-echo transducers were
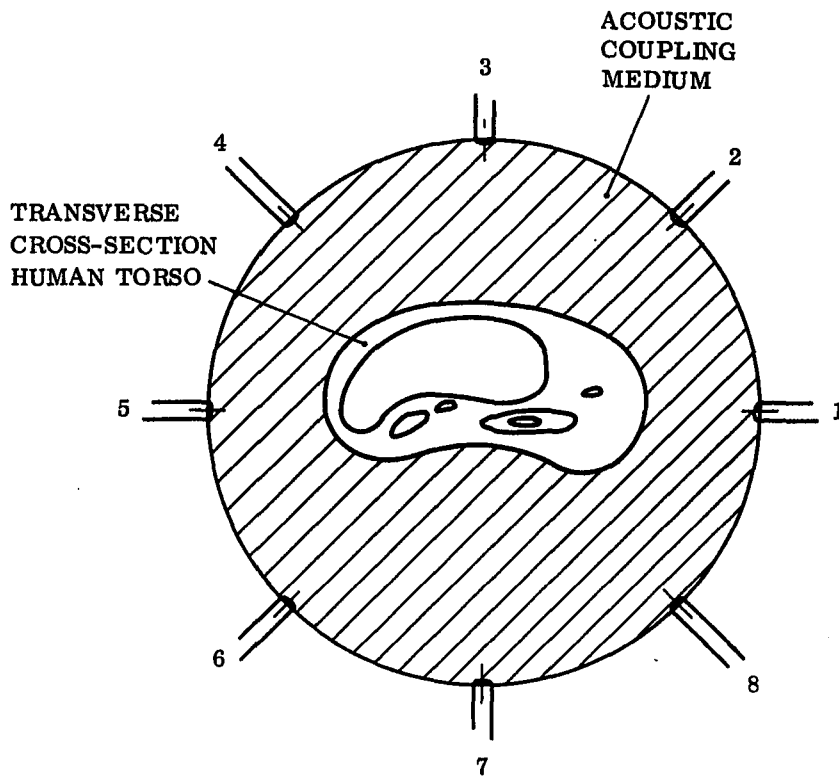
Figure 4-4. Orientation of PSI transducer array about patient

used in the specified array and directed at the center of the ring, although

insonification and reception would be from "N_T" directions, as a result of the

transducers' directional properties, illustrated in Figure 3-3, scattered echoes

will be received only if propagating radially with respect to the ring. In order

to overcome this problem, fan beam transducers, possessing an idealized beam

characteristic as shown in Figure 4-5(a), are utilized in place of the pulse-echo

probes. Assuming a given transducer has identical transmission and reception

characteristics, then a composite beam pattern, as illustrated in Figure 4-5(b),

will result, where there is a polygonal central area which is symmetrically

and equally insonified by each beam. Outside of this area, a given scatterer

FAN BEAM
TRANSDUCER

(a)

(b)

Figure 4-5. (a) Idealized fan beam pattern with beam angle, ϕ, and
beam thickness, t.
(b) Composite coverage of symmetric fan beam array.
Illustration is for eight transducers, each having a
beam angle of $\phi = 30^0$.

will be insonified by fewer than the total number of beams (N_T). Unless all

points are symmetrically insonified, scattering cannot be quantitatively charac-

terized. Thus, the object to be imaged must be placed within this area of sym-

metric insonification.

Figure 4-6 illustrates how to specify array diameter and beam angle in

order to achieve a desired imaging region. (Only four transducers are shown in

order to simplify the drawing.) Let "R" = radius of transducer array, "ϕ" = beam

angle and "r" = the radius of the largest circle that may be inscribed within the

$2N_T$-sided regular polygonal region which will result from a symmetric-array

of "N_T" transducers. Since the sides of a regular polygon are tangent to the

inscribed circle, such a circle represents a minimum area approximation for

Figure 4-5. (a) Idealized fan beam pattern with beam angle, ϕ, and beam thickness, t.
(b) Composite coverage of symmetric fan beam array. Illustration is for eight transducers, each having a beam angle of $\phi = 30^\circ$.

will be insonified by fewer than the total number of beams (N_T). Unless all points are symmetrically insonified, scattering cannot be quantitatively characterized. Thus, the object to be imaged must be placed within this area of symmetric insonification.

Figure 4-6 illustrates how to specify array diameter and beam angle in order to achieve a desired imaging region. (Only four transducers are shown in order to simplify the drawing.) Let "R" = radius of transducer array, "ϕ" = beam angle and "r" = the radius of the largest circle that may be inscribed within the $2N_T$-sided regular polygonal region which will result from a symmetric-array of "N_T" transducers. Since the sides of a regular polygon are tangent to the inscribed circle, such a circle represents a minimum area approximation for

R = RADIUS OF TRANSDUCER ARRAY

ϕ = FAN BEAM ANGLE

r = MINIMUM RADIUS OF
SYMMETRIC INSONIFICATION
$(N_T = \infty)$

$r = R \, SIN \, \phi/2$

Figure 4-6. Geometric layout for determining region of symmetric insonification from beam angle and array radius

the imaging region for $N_T < \infty$ and the limiting case for $N_T \to \infty$. As illustrated

$$r = R \sin \frac{\phi}{2} \qquad (4\text{-}1)$$

For completeness, the polygon, itself, is regular, contains "$2N_T$" sides and thus has interior angles

$$\theta = \frac{2\pi}{2N_T} = \frac{\pi}{N_T} \text{ radians} \qquad (4\text{-}2)$$

"N_T" determines "θ" while "ϕ" determines the size of the polygon (and radius, r, of inscribed circle). As a result, a given diameter imaging region may be obtained by varying either or both "N_T" and "ϕ". A compromise must be reached, however, since increasing "N_T" beyond the point where desired resolution has been obtained greatly increases hardware costs, data collection time, data storage requirements and image reconstruction time. Increasing "ϕ" to a very large value, aside from the possibility of fabrication difficulties, produces a beam whose energy density falls off very rapidly. Acoustic-intensity is inversely proportional to cross-sectional area. Therefore, using a plane wave approximation for Figure 4-5(a), as shown in Figure 4-7,

$$\frac{I}{I_o} = \frac{E_o/2 \,(d \tan \phi/2)\, t}{E_o/a_T} \qquad (4\text{-}3)$$

$$I = I_o \left(\frac{a_T}{2 \, t \, d \tan \frac{\phi}{2}} \right) \qquad (4\text{-}4)$$

where

I_o = acoustic-intensity at transducer face

I = acoustic intensity at approximately a distance "d" from transducer face, $d \gg d_T$

E_o = total acoustic energy output by transducer
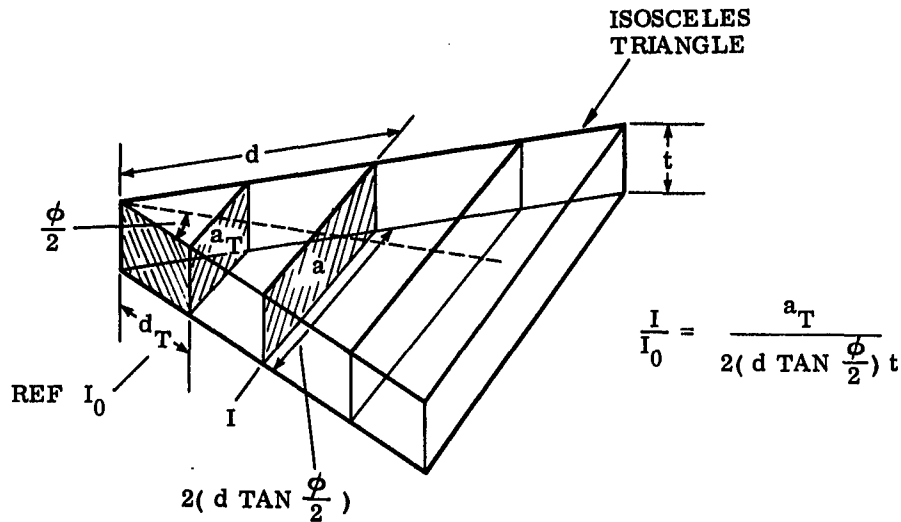
Figure 4-7. Plane wave approximation to Figure 4-5(a) for calculating decrease in fan beam intensity with increase in distance from transducer assuming a lossless medium

a_T = radiating area of transducer

ϕ = fan beam angle

t = fan beam thickness.

The above relationship has two implications. The first is that acoustic power will be greater in the outer portions of the imaging area. Power level must, therefore, be measured along the outer circumference of this region when considering safe dosage level. Secondly, quantitative interpretation of PSI data necessitates that the entire region be uniformly insonified. Both mathematical and physical proof of these requirements have been set aside for a separate study (this preliminary PSI investigation has concentrated on image detection rather than on quantitative aspects by necessity of limited funds (minimally calibrated hardware) and time requirements). The following hypothesis will be set forth, however, for proof at a later date. Assuming the plane wave approximation to the fan beam of Figure 4-7, a composite transmitted intensity may be calculated as shown in Figure 4-8, for a four transducer array and an imaging space of 8 × 8 elements (chosen for ease of calculation). The intensity
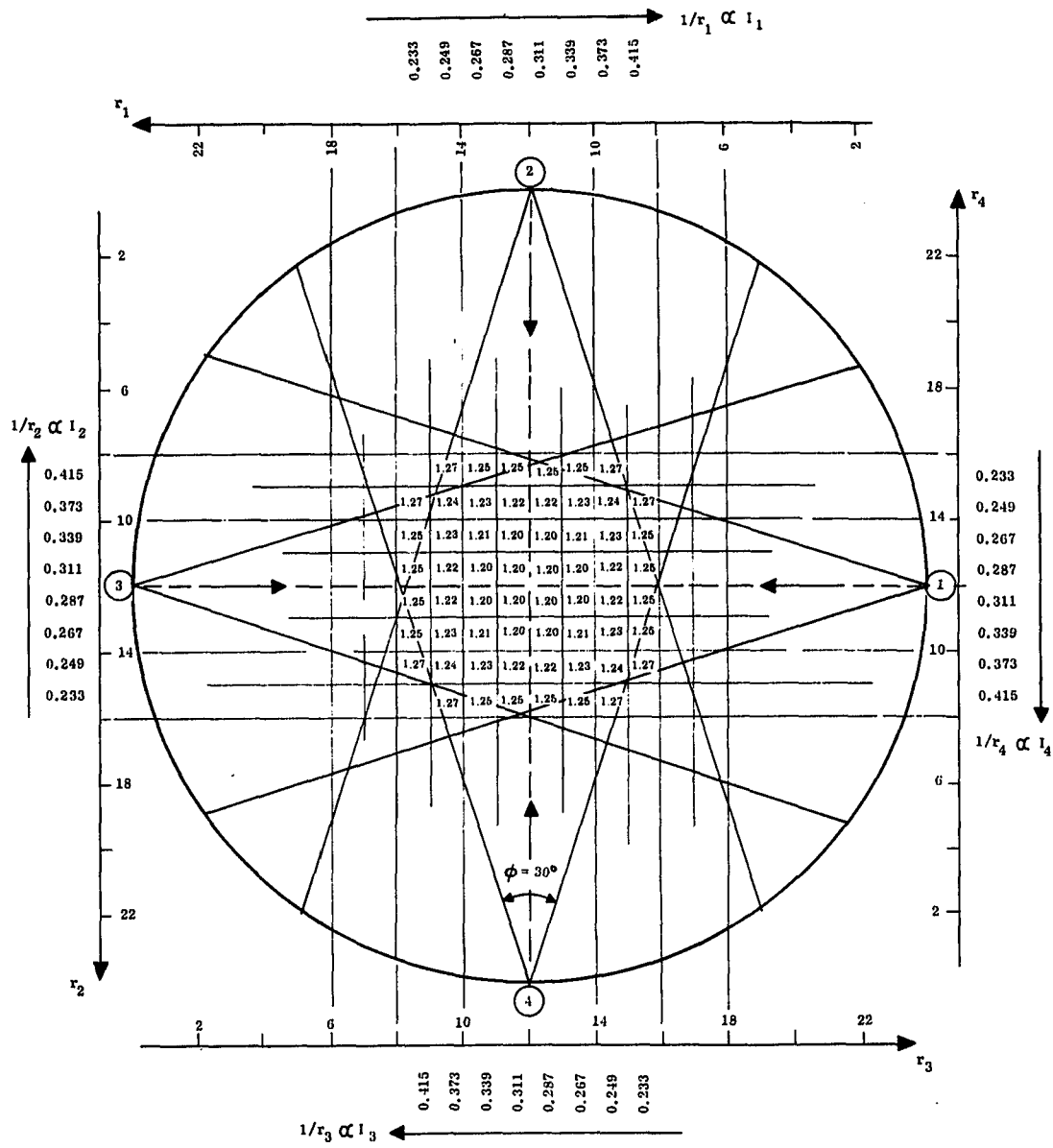
Figure 4-8. Relative acoustic intensities (I_0=1 at r=0) for composite fan beam profile (illustration for N_T=4)

values calculated along each transducer axis ($N_T = 4$ chosen to simplify the analysis) were normalized with respect to $I_0 = 1$ at $r = 0$, and were assumed to diminish as $1/r$, where r = distance from transducer face. Each of the relative intensities shown within the symmetric region of insonification were determined by simultaneously summing the contributions due to each of the individual trans-ducers, at the given location. Due to symmetric insonification, the composite intensity pattern increases radially outward, the radial uniformity improving with increasing "N_T". Thus, in addition to the standard time-gain compensa-tion, appropriate position-dependent weighting factors could be added to the PSI system to account for this spatially-dependent insonification.

With the specified array of "N_T" transducers surrounding the object to be imaged, each transducer is pulsed once in succession around the array. Imme-diately following each pulse, all transducers (including the transmitter) function as receivers to monitor the scattered signals. The output of each transducer is a conventional A-mode signal. In all, each of the "N_T" pulses generates "N_T" A-mode waveforms, producing a total number of transmitter/receiver pairs, N_{TP}, as

$$N_{TP} = N_T \times N_T = N_T^2 \text{ pairs} \qquad (4-5)$$

By reciprocity, for example, transmitting from transmitter one to receiver five is equivalent to transmitting from transmitter five to receiver one. Thus, the total number of "unique" transmitter/receiver pairs, N_{UP}, may be described as

$$N_{UP} = \frac{N_T \times (N_T + 1)}{2} \qquad (4-6)$$

"N_{UP}" is generally a little more than half of "N_{TP}". The use of a non-redundant data collection scheme, as illustrated in Figure 4-9, economizes on data storage space and processing time, as well as maintains proper data weighting. The cross-hatched designations represent the redundant data.

DATA COLLECTION FOR EIGHT TRANSDUCER RING

TRANSMITTER (Transducer Number)	RECEIVER (Transducer Number)							
1	1	2	3	4	5	6	7	8
2	2	3	4	5	6	7	8	1
3	3	4	5	6	7	8	1	2
4	4	5	6	7	8	1	2	3
5	5	6	7	8	1	2	3	4
6	6	7	8	1	2	3	4	5
7	7	8	1	2	3	4	5	6
8	8	1	2	3	4	5	6	7

Figure 4-9. Data collection for simulation of an eight transducer ring

As mentioned earlier, knowing the transmitter (T) and receiver (R) co-ordinates as well as echo time of flight, an ellipse with foci at the T/R coordinates and chord sum ((r+s), shown in Figure 4-10) corresponding to the total echo time-of-flight describes the locus of all points which could have been in-sonified by the transmitter prior to echoing a response to the given receiver in the measured amount of time. The echo amplitude is mapped into the particular ellipse's gray scale. Furthermore, the amplitude data undergoes time-gain compensation (TGC); echoes which have traveled a longer distance (longer time-of-flight) are multiplied by a value which is greater than for echoes which traveled shorter distances, in order to compensate for total signal attenuation, a factor which increases with time-of-flight. Additional gain weighting may be incorporated later in the processing route to overcome such situations as in-sonification non-uniformities due to fan beam divergence. Finally, geographic superposition and algebraic summation of the resultant ellipses will result in a
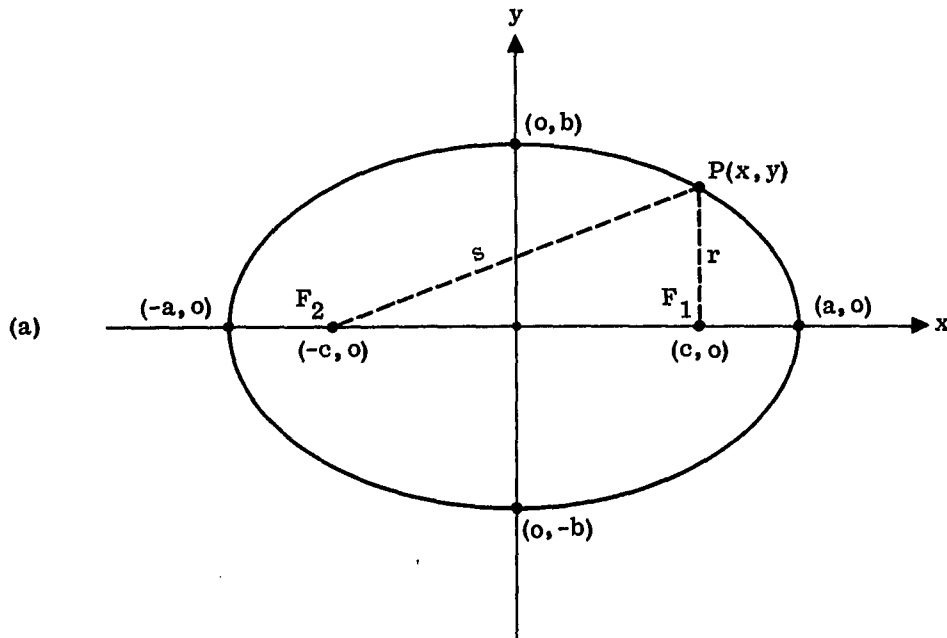
$$(b) \quad \frac{x^2}{a^2} + \frac{y^2}{b^2} = 1, \quad a > b > 0 \quad \text{FOR GEOMETRIC ORIENTATION SHOWN}$$

BASIC PROPERTY: $F_1 P(x, y) + F_2 P(x, y) = \text{CONSTANT}$

WHERE: F_1 AND F_2 ARE FOCI

P(x,y) IS AN ARBITRARY POINT ON THE CIRCUMFERENCE

Figure 4-10. Basic (a) elliptical geometry and (b) associated mathematics

gray scale image, where scatterer locations are displayed as ellipse intersec-tions and constructive reinforcement, while signals due to noise and artifact will exist as a relatively faint background construction. Figure 4-11(a) illustrates partial reconstruction of a point "x" by this process for a six transducer array, and the case where transducer number one has just been pulsed and utilized as a transmitter. Figure 4-11(b) illustrates reconstruction of a second point, "y", utilizing data from transmitter number four. Superposition of the reconstructions of "x" and "y" produces the composite image.
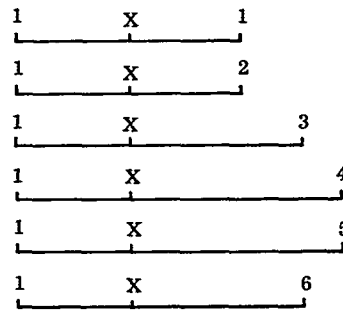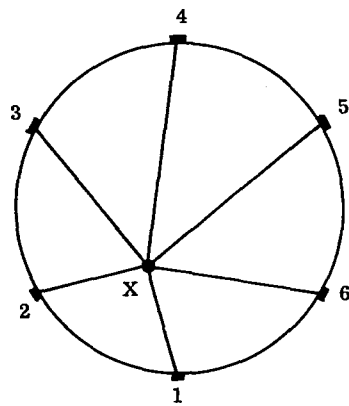
TRANSIT-TIME MEASUREMENTS
TO POINT "X" FOR
T/R PAIRS 1/1 - 1/6

(a)
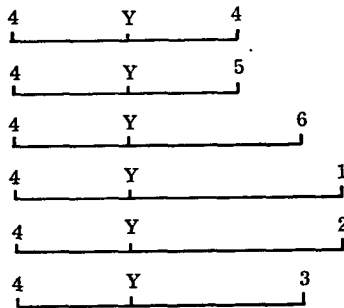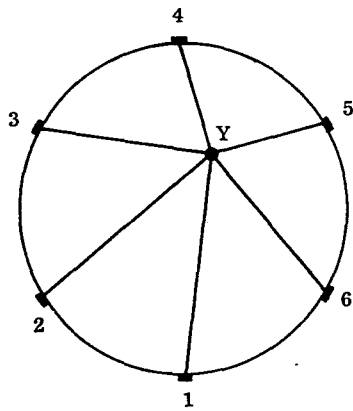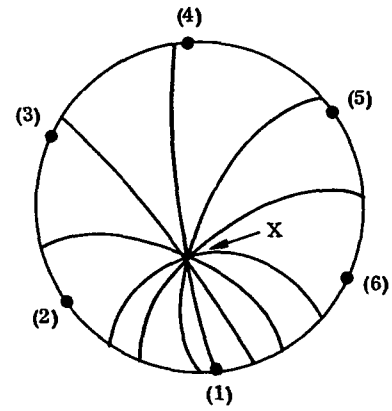
TRANSIT-TIME MEASUREMENTS
TO POINT "Y" FOR
T/R PAIRS 4/1 - 4/6

(b)
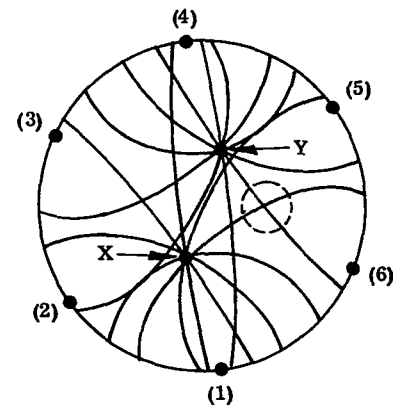
Figure 4-11. Demonstration of PSI reconstruction approach.
(a) Partial reconstruction of a single point, "X"
(b) Partial reconstruction of two points, "X" and "Y".
False intersection indicated in dotted circle.

Now, two problems become immediately evident. The first is that as sub-sequent data are gathered utilizing the remaining transducers as transmitters, ellipse superposition will generate some intersections where no scatterers are located. Such "false intersections" will be of low frequency and will simply fade into the background image. However, as more and more scatterers (i.e. echo producers) are placed in the field of view and more and more ellipses are superimposed, there is a greater chance, although still much less than for con-structive reinforcement at true scatterer locations, of having more than one false intersection occurring at a given set of coordinates. As alluded to when reviewing several other reinforcement imaging techniques in IV(B), this problem of false intersections (see Figure 4-11(b)) is spatially variant, de-pending on the transducer array geometry. Furthermore, analysis and modeling of this problem is particularly hampered by the fact that the frequency and degree of reinforcement of false intersections given a fixed transducer array geometry, is highly dependent on the number and spatial orientation of scatterers being imaged.

Mathematical descriptions of this problem could not be found in the (non-classified) literature and attempts at devising a suitable mathematical model and criteria for isolating false intersections, during the present investigation were not fruitful. Additional mathematics will be necessary to better handle this situation. A further complicating factor is the unpredictability of echo amplitudes which will be distributed between false intersections and true ones (i.e. ellipses corresponding to both strong and weak echoes may participate in false intersection). This overall problem must be solved in order to produce a truly quantitative image. Deferring this problem to a future study, the ap-proach to be taken will probably have to be a statistical one, where a complete range of various scattering patterns are analyzed for a given transducer array

geometry and an "average false intersection probability" will be determined. Such a factor should be spatially variant, although exhibiting a certain degree of symmetry, so that each pixel element will have a specific correction term. This factor will treat a portion of a given pixel's brightness as an unwanted dc signal which needs to be subtracted out.

During the PSI investigation, a combinatorial approach to this problem was attempted by assuming (for the case of all echoes being of unity amplitude) a maximum worst-case number of false intersections (m) occurring for reconstruction of a single scatterer (spatial variance must be kept in mind), of size equal to that of a single display pixel. Trying to image "T" targets will then result in a maximum false intersection amplitude of "mT", assuming an exact overlay each time, of those pixels containing worst-case ambiguities. True scatterers will reinforce $\frac{N_T(N_T+1)}{2}$ times (equal to the number of T/R pairs). A stylized signal (true scatterer) to noise (false intersections) ratio (SNR) could then be formed as

$$\text{SNR} = \frac{N_T(N_T+1)/2}{mT} = \frac{N_T(N_T+1)}{2mT} \tag{4-7}$$

Substitution of possible values into Equation (4-7) would suggest unsatisfactory results. However, the probability of worst-case false intersections occurring in exactly the same locations of the 320×320 pixel display used is intuitively quite small and otherwise, is dependent on target locations. Thus, it would appear that "mT" in Equation (4-7), is actually a gross exaggeration and not representative of "likely" worst-case occurrences.

The second of the two problems suggested earlier involves thru-transmissions. A thru-transmission signal is defined as one which travels directly from transmitter to receiver without being scattered. Thus, such a straight line path will reconstruct as a straight line joining the transmitter and receiver; more

practically speaking, such a signal would be reconstructed as a "narrow ellipse" due to distance uncertainties resulting from time quantization of signal sampling. This "narrow ellipse" contains no scattering information whatsoever, and if included in the reconstructed image would tend to write-over and obliterate the image from the truly scattered data. As a result, "N_{UP}" defined in Equation (4-6) will be reduced somewhat in order to disregard thru-transmission data. The number of T/R combinations disregarded will depend on array size and fan beam angle.

In determining the resolution of the PSI system, electronic and acoustic performance must be considered as well as the factors of image reconstruction and display. As was discussed back in Section III (B), in B-scan, axial resolution is dependent on excitation pulse width, whereas lateral resolution is limited by transducer beamwidth. The pulse-scatter imaging technique relies strictly on time differences of arrival in determining the positional relationships of the reconstruction ellipses. As a result, the primary limiting factor in determining resolution will be the pulse width, τ_{pw}, of transducer excitation. For the pulse-burst transducer excitation being used, τ_{pw} is generally no less than two cycles of the sinusoidal carrier [79], [80], [81] (frequency $= f_c$; period $= T_c = \dfrac{1}{f_c}$), for the highest quality, widest bandwidth transducers currently available. So, since two scatterers closer than a pulse width's spacing in time cannot be resolved, the maximum resolution attainable, $\mathcal{R}$, may be expressed as

$$\mathcal{R} = \frac{1}{c} \times \tau_{pw} \tag{4-8}$$

where: c = average acoustic velocity (μsec/mm)

τ_{pw} = transmitted pulse width (μsec)

Substituting some typical values into this equation, $f_c = 5$ MHz, $\tau_{pw} = 1$ μsec and c = 1540 m/sec results in $\mathcal{R} = 1.54$ mm. In general, pulse spreading will occur as the ultrasonic energy interacts with the propagating medium and object to be imaged. In order to minimize the degradation of such an effect, various detection and processing techniques may be used (e.g. leading-edge detection, correlation detection [82]). Due to the finite duration of each pulse, each ellipse drawn in the reconstruction process will really be an elliptical band whose spatial width corresponds to the originally transmitted pulse width. If leading-edge pulse detection were to be used, a thin-lined ellipse could be drawn, however, a region of uncertainty would still exist about the plotted ellipse, corresponding to the transmitted acoustic pulse width.

Since the data acquisition, processing and display approach to PSI has been digital, the initial A-mode-like signals obtained must be digitized. As a result, it must be certain that a high enough sampling frequency is used, otherwise, high frequency scattering may be missed. Additionally, sampling at too low a frequency (below at least 2 f_c, the Nyquist sampling frequency, where f_c = largest frequency component in signal) will cause loss of HF components, resulting in pulse-smearing and resolution degradation.

With respect to output display resolution, let the output display be "p" pixels square and "r" equal to the radius of the area of symmetric insonification. Thus, "p" pixels correspond to "2r" distance units or (2 × 2r/c) time units (round-trip echo travel). Display resolution, R_d, will then be

$$R_d = \frac{2r}{p} \text{ unit distance/pixel} \tag{4-9}$$

A display resolution, R_d, any greater than the acoustic resolution, $\mathcal{R}$, is of little practical value. Utilizing representative values from the PSI investigation,

and allowing the full display area to be comprised of only the symmetrically insonified region (optimized situation), typical maximum display resolution may be calculated as follows (see Figure 4-12).

(i) Display Device

p = 320 pixels (10 bit amplitude storage per pixel)

(ii) Array diameter, $D \approx 8" \rightarrow R = 4"$

Fan beam angle, $\phi \approx 30^o$

Radius of symmetric imaging region = $r = R \sin \frac{\phi}{2} = 1.04"$

.'. Diameter of symmetric imaging region = d = 2.08"

= 52.83 mm and so maximum round-trip distance

= 2 × 52.83 = 105.66 mm

(iii) Average acoustic velocity in tissue, c = 1540 m/sec

= 0.65 μsec/mm

320 pixels $\longleftrightarrow$ 68.69 μsec time window (r/t)

.'. 1 pixel = 0.21 μsec

or

320 pixels $\longleftrightarrow$ 105.66 mm

.'. 1 pixel = 0.165 mm (image scale)

= 0.33 mm (r/t acoustic travel)

Thus, based on the foregoing calculations, the transmitted pulse width is currently the determining factor for system resolution. (It should be noted that for the present PSI investigation, the full transducer array comprises the 320 × 320 pixel imaging region. Thus, the active imaging display is a centrally located circle of approximately two inches in diameter. For this situation, system resolution is that one pixel equals approximately 0.635 mm in distance or 0.826 μsec (r/t) in time. In this case as well, resolution is limited by the transmitted pulse width.)
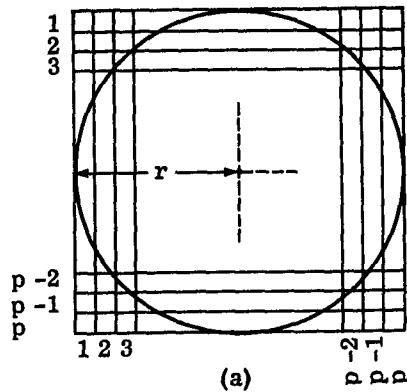
r = RADIUS OF SYMMETRICALLY
INSONIFIED REGION (mm)

DISPLAY RESOLUTION, $R_d = \frac{2r}{p}$ (mm)

(a)

ARRAY
CIRCUMFERENCE

REGION OF
SYMMETRIC
INSONIFICATION
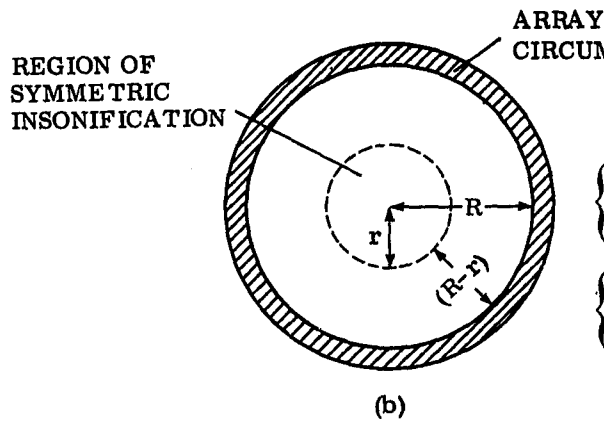
ACOUSTIC VELOCITY (SOFT TISSUE) = 0.65 μs/mm

$\begin{cases} \text{MAX. r/t DISTANCE} = 2(R+r) \text{ mm} \\ \text{MAX. r/t TIME} \longrightarrow 0.65(2)(R+r) = 1.3(R+r) \, \mu s \end{cases}$

$\begin{cases} \text{MIN. r/t DISTANCE} = 2(R-r) \text{ mm} \\ \text{MIN r/t TIME} \longrightarrow 0.65(2)(R-r) = 1.3(R-r) \, \mu s \end{cases}$

(b)

GATE

2.6r

t (μs)

$t_1 = 1.3(R-r)$ $t_2 = 1.3(R+r)$
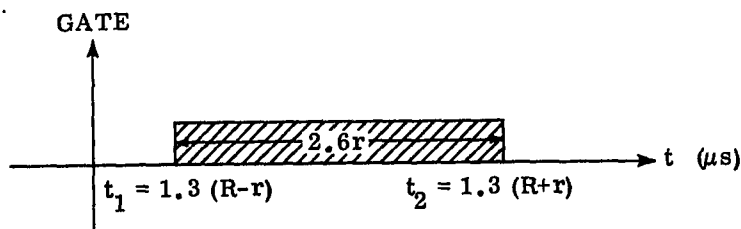
(c)

Figure 4-12. Time gating and data display for optimal image resolution
(a) Full field display
(b) Physical acoustic layout
(c) Gated data acquisition to enable display as in (a)

The final factor influencing image resolution relates directly to the re-construction process itself. Just as in computerized X-ray tomography (CT), the reconstruction process introduces a smearing of the resultant images. Such smearing results from the intersection of straight lines possessing a finite thickness. As will be illustrated via simulated and real data in the next chapter, when many lines cross at a single point, due to the finite line thickness, the point of intersection tends to bloom out and appear larger, the greater the number of intersecting lines [83], [84]. Mathematically, for a time invariant system, this phenomenon may be described as a convolution (*) relationship in the spatial domain (see Figure 4-13) -- -

$$f(x,y) * h(x,y) = g(x,y) \qquad (4\text{-}10)$$

where: $f(x,y)$ = original image in spatial domain

$h(x,y)$ = image transfer function

$g(x,y)$ = reconstructed image.

Ideally, $h(x,y)$ should be a representative unit impulse function, so that $f(x,y) = g(x,y)$. However, in particular for the straight line reconstruction techniques of CT, $h(x,y) \sim \frac{1}{r}$, where "r" equals distance away from the point being recon-structed [83], [84], [85], [86], [87]. This "$\frac{1}{r}$" relationship is actually the limiting case for an infinite number of straight lines intersecting at a point from all directions. As illustrated in Figure 4-14(a), the so-called "point-spread function" in the frequency domain is a triangularly shaped characteristic. Thus, in order to remove this smear artifact (providing a large enough number of rays have been used), either the function, $f_2(r)$, the reciprocal convolution function of "$\frac{1}{r}$", may be deconvolved with the image in the spatial domain, or $F_2(R) = 1/F_1(R)$, may be multiplied with the image in the spatial frequency domain (also see Figure 4-13).

ORIGINAL   IMAGE RECONSTRUCTION   RECONSTRUCTED
IMAGE   SYSTEM   IMAGE

$f(x, y)$ $h(x, y)$ $g(x, y) = f(x, y) * h(x, y)$

FOURIER
TRANSFORMATION
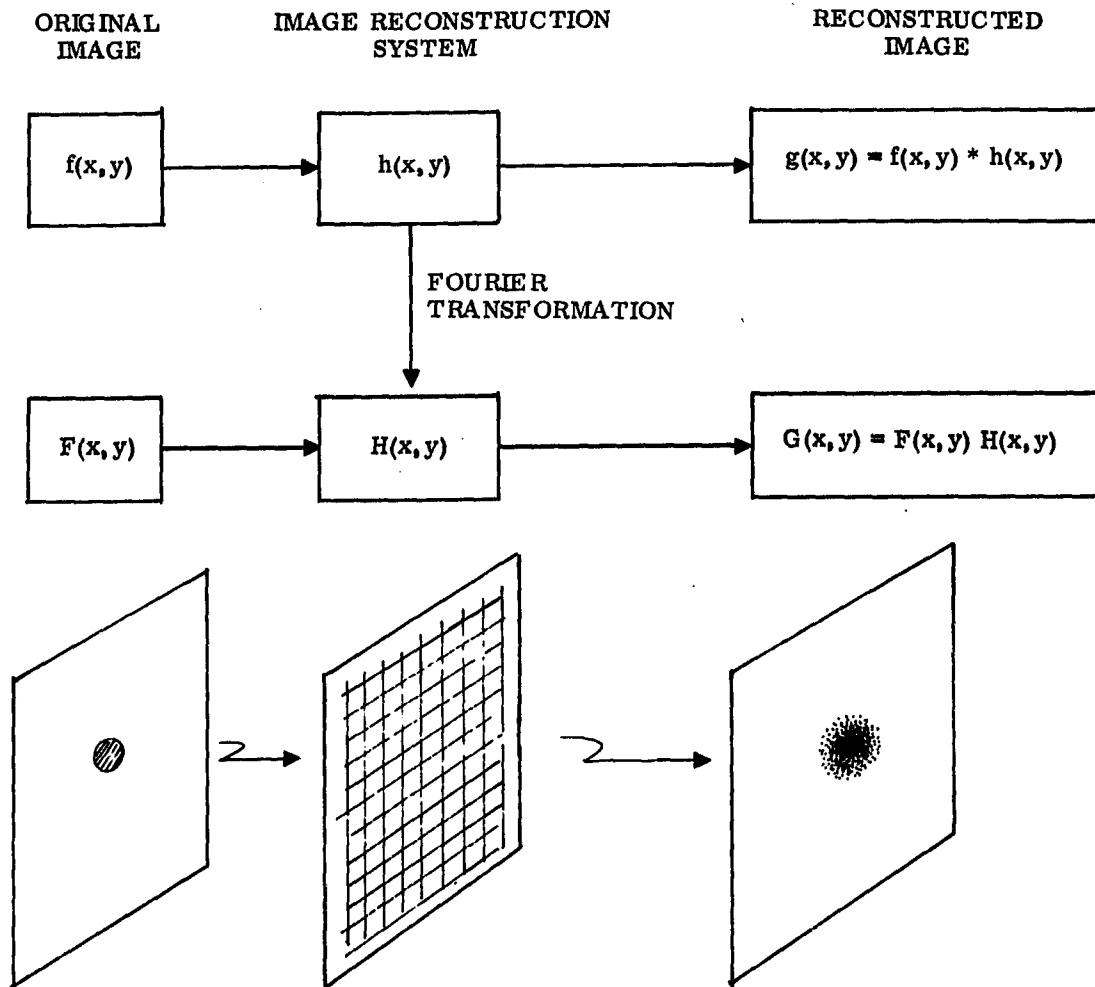
$F(x, y)$ $H(x, y)$ $G(x, y) = F(x, y) H(x, y)$

$$f(x, y) = g(x, y) * \frac{1}{h(x, y)}$$

$$F(x, y) = \frac{G(x, y)}{H(x, y)} \longrightarrow f(x, y) = F^{-1}(x, y)$$

Figure 4-13. Mathematical description of a generalized image reconstruction system

Unfortunately, the attempt that has been made thus far at applying CT deconvolution to PSI has indicated that the CT inverse functions are inappropriate for PSI, as discussed in the next chapter. Several possible reasons are that (i) the CT technique is based on straight line intersections, whereas PSI utilizes intersection of curves. Depending on the portions of the given ellipses involved in an intersection, the straight line approximation may or may not be valid. (ii) possibly not enough ellipses intersect at each pixel for the " $\frac{1}{r}$ " relation to be valid. (iii) both the physical acoustics and PSI reconstruction technique combine to produce characteristics of the reconstruction itself which vary spatially depending on scatterer orientation. Thus, extensive study is still necessary in order to determine a suitable deconvolution function for PSI. At this point, it appears reasonable to expect such a function to be similar to that of Figure 4-14.

Two final considerations, namely, number of transducers in array and fan beam angle, should be discussed before pursuing the details of the experimental procedure and results in the next two chapters. Thus far, it appears that substantially more testing of the PSI hardware and processing algorithm will be required before a complete theory as to the number of transducers and size of beam angle which produce an optimal system is developed. Although repeated analyses have been undertaken, an optimal transducer array size has yet to be determined. Factors which must be considered in this analysis include (i) transducer characteristics such as size, directional T/R performance and fan beam angle, (ii) array diameter, (iii) acoustical resolution of system (iv) display resolution, (v) scatterer characteristics and (vi) image reconstruction technique (e.g. amplitude of false intersections versus that of time scatterers for a given number of transducers). An ideal goal of PSI is to be
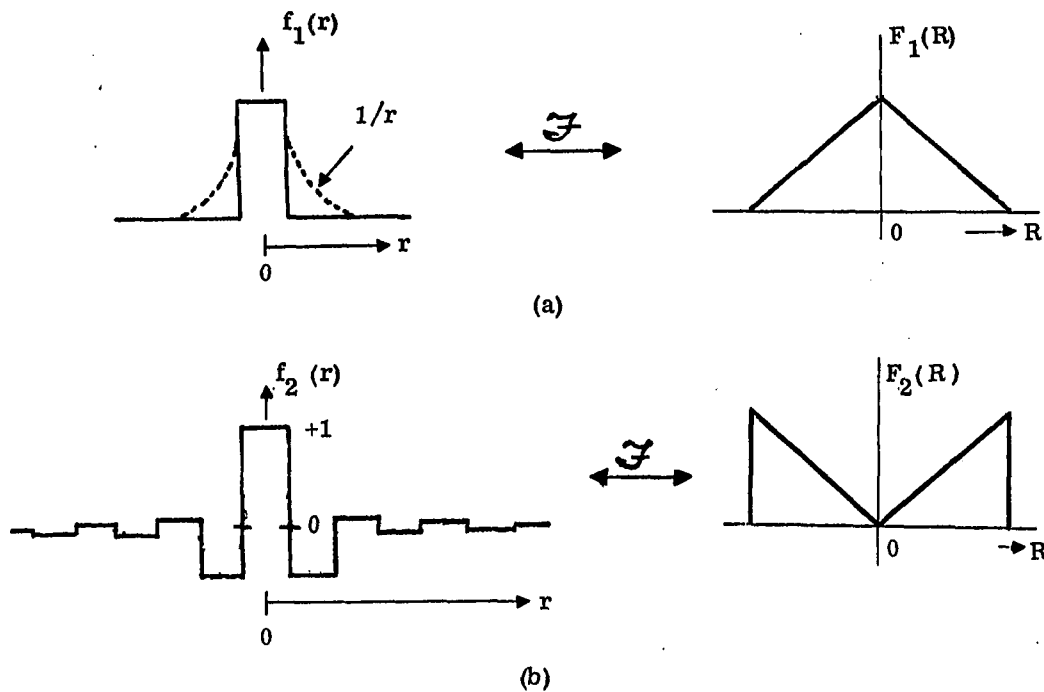
Figure 4-14. Reconstructed point-spread function, deconvolution and inverse
filtering
(a) Spatial and spatial frequency characteristics of reconstructed
point-spread function
(b) Reciprocal functions to either deconvolve (f_2) or inverse
filter (F_2) the reconstructed image in order to regain the
desired point impulse characteristic [87]

able to both insonify an object and detect its scatter omnidirectionally. How-
ever, neglecting the considerations of array construction, such omnidirectional
performance would require an infinite number of point-transducers in a contiguous
array, if every bit of scattered energy is to be received. Based on Equation
(4-6), if the number of transducers gets too great, then data acquisition and
image reconstruction tasks will get out of hand. A large number of tradeoffs
are possible, of which no "best" one appears obvious thus far. In the final
outcome, both monetary and physical hardware constraints will most likely
prove to be the determining factors.

Since, as discussed earlier, generation of image artifacts will be dependent on scatterer distribution, studies on biological scattering reported in the literature would seem to suggest use of a random scattering model for use in PSI system design. Thus, two different approaches have been attempted in order to get a "ball park" estimate of the number of transducers to use. More precise analysis will have to await further experience with the PSI approach. The first method determines "N_T" by equating positional information content of the image display with positional information contributed by an array of "N_T" transducers. Thus, a display "p" pixels square will contain $I_D = \log_2 (p)^2$ $= 2 \log_2 p$ bits of information. Since each array T/R pair receives a signal of "n" time samples, the total array contributes $I_A = \log_2 (N_T \times (N_T+1)/2 \times n)$ bits of information. Referring to Table 4-1, for the case of p = n = 320, $I_A \approx I_D$ for $N_T = 30$, suggesting an array of thirty transducers.

TABLE 4-1. POSITIONAL INFORMATION CONTENT OF "N_T" TRANSDUCER ARRAY FOR p = n = 320

N_T (Transducers)	$N_{UP} = \dfrac{N_T \times (N_T + 1)}{2}$ (Pairs)	$I_P = \log_2 \dfrac{320 \times N_T \times (N_T + 1)}{2}$ (Bits)
10	55	14.10
20	210	16.04
30	465	16.18
32	528	16.37
40	820	18.00
50	1275	18.64
60	1830	19.16

The second approach to this problem involves trying to insonify an object and detect its scatter "omnidirectionality". As discussed in Chapter II(C), for an object whose dimensions are much less than the acoustic wavelength, scattering will be omnidirectional. In cases where object dimensions are much greater than wavelength, scattering will be specular. This case being the most directional of all, is, therefore, the one which must be considered when determining the number of transducers required. Essentially, the more transducers, the finer the PSI angular insonification and reception characteristic.

When discussing the directional receiving characteristics of pulse-echo transducers earlier, it was mentioned that a transducer could receive back-scatter in the range $\pm 2^o$ off axis. (Note that this value will vary somewhat for the fan beam transducer.) This statement is equivalent to saying that a scatterer positioned normal to a transducer's axis may be rotated $\pm 2^o$ about its own axis without significantly affecting the pulse-echo response. Practically speaking, then, in order to "omnidirectionally" scan a given scatterer, it must be insonified every four degrees, for a total of $360^o/4^o = 90$ directions about the scatterer axis. As shown in Figure 4-15(a), the directional characteristics of the fan beam used may be determined by choosing a point, p, on any arc of the beam pattern sector, within the active imaging region. Draw both a tangent to the arc at the chosen point, and the perpendicular to the tangent. Following the perpendicular back to the transducer determines one of the "normal incidence" directions of the particular fan beam. Now, based on the previous discussion, if the tangent and its associated perpendicular are rotated about the point of tangency by $\pm 2^o$, the perpendicular will still map out the directions of scatter from the given point capable of being received by the particular transducer. Thus, as illustrated in Figure 4-15(b), the minimum number of transducers,

(a)

(b)

Figure 4-15. Determining number of transducers in PSI array

(a) Directionality characteristic for a single point in the PSI imaging region when insonified by a single beam, where $\pm q^\circ$ relates to transducer directionality

(b) Omnidirectional coverage of any scatterer in PSI imaging area for array containing 360/2q transducers

N_T, required to cover any point in the region of symmetric insonification to within $\pm q^O$ of any direction will be

$$N_T = \frac{360}{2q} \quad \text{transducers} \tag{4-11}$$

Using the directionality assumption previously mentioned of $\pm 2^O$ $(q = 2)$ for standard pulse-echo transducers, then $N_T = 90$. Based on Equation (4-6), $N_T = 90 \rightarrow 4095$ T/R pairs. Present computer data storage capability allows for a maximum of $N_T = 24$ to be simulated. (i.e. 1.2M 16-bit words on a PPP-11 RK-05 disc pack); simulation of $N_T = 90$ would require a storage capability of at least 16.38M 16-bit words, using the current data collection scheme.

The two exemplary approaches to array size determination presented indicate substantial differences $(N_T \approx 30$ and $N_T \approx 90)$ for the particular factors considered. Referring again to Table 4-1, until better quality experimental hardware is designed for further PSI development, $N_T = 32$ (for four quadrant symmetry) would appear to be a reasonable compromise.

The parameter of fan beam angle only serves to determine the size of the active imaging region for a given diameter transducer array, given the ideal transducer characteristics discussed earlier. However, two practical considerations must be taken into account. The first factor relates to the fact that a given transducer can only put out so much power. The larger the beam angle, the lower the power density, and consequently the lower the transducer's sensitivity. Secondly, the fan beam transducer presently being used derives its divergence from a piezoelectric ceramic in the form of a partial cylindrical shell. Whether or not a plane wave approximation is used for the

reflected wave, due to the receiver curvature, unless the pulse width is greater than the ceramic thickness, the receiver face will never experience complete excitation (see Figure 4-16). Unless compensated for in some fashion this effect will result in pulse-stretching and reduced sensitivity. For a given transducer size, the degree of transducer curvature will be directly proportional to beam angle. The remaining consideration with respect to beam angle simply relates to problems of physical construction. As will be discussed in the next chapter, the fan beam transducers used in this study were custom-made (K.B. Aerotech, Lewistown, Pa.) and, based on the literature reviewed, are the first of their kind for medical applications. Much work, therefore, needs to be done in the characterization and construction of fan beam transducers.

D. ADDITIONAL CAPABILITIES AND LIMITATIONS

The foregoing discussion describes the PSI system capable of imaging transverse cross-sections of the body. The transducers specified require a fan beam pattern. The next logical extension of the basic PSI geometry is to construct a cylindrical (3-D) rather than simply circular (2-D) transducer array. In this case, each transducer would require a cone beam characteristic in order for insonification and reception in three dimensions. Although image display would be cross-sectional (2-D), once a complete set of data has been collected, virtually any cross-sectional plane of data could be reconstructed and displayed. This 3-D concept is beyond the scope of the present investigation; future study, however, is recommended.

Aside from the consideration of image resolution already discussed, the remaining limitations of the basic PSI system are acoustic in nature and relate to the same factors plaguing B-scan systems. Two main points will be mentioned ---
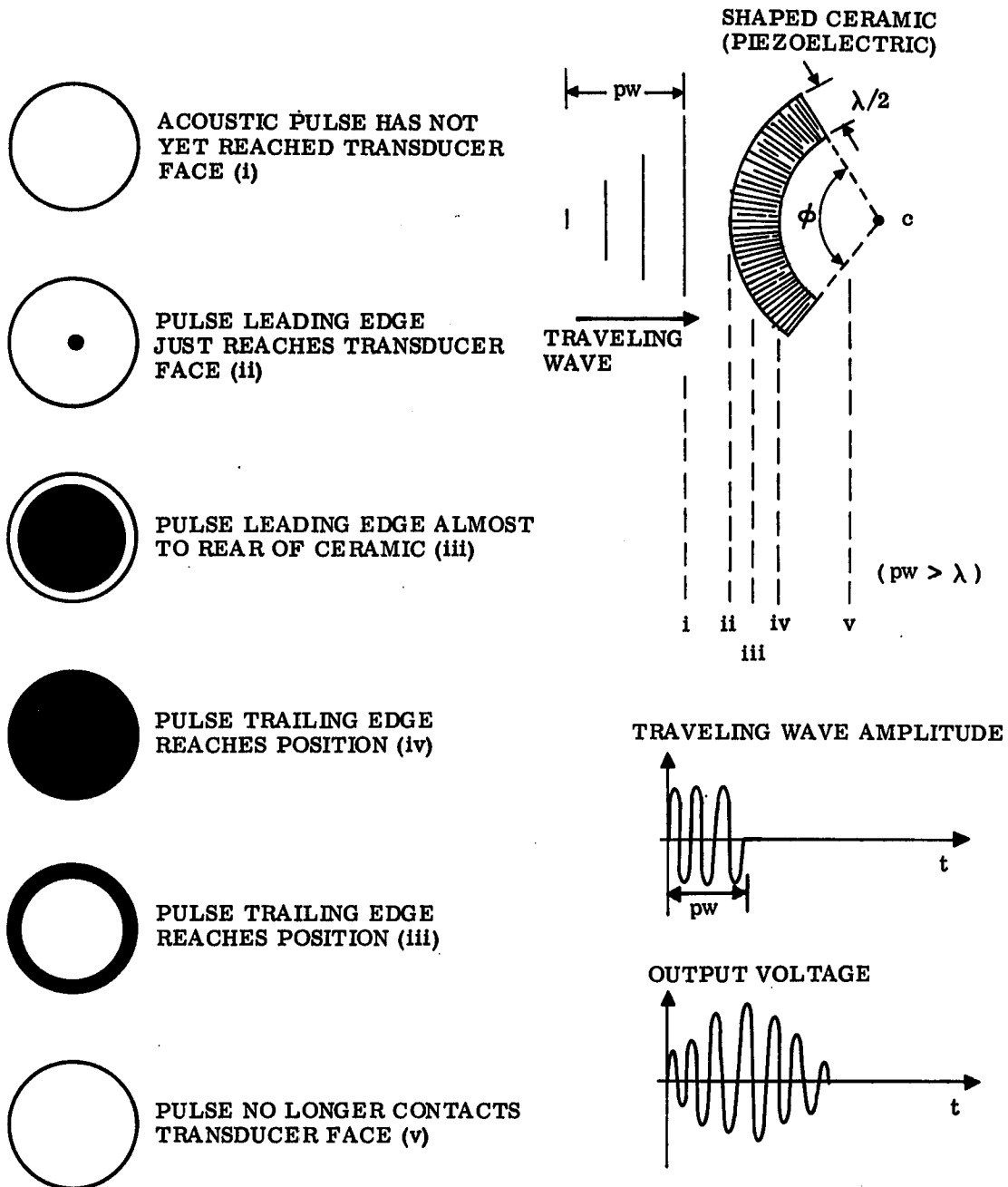
Figure 4-16. Insonification of a fan beam transducer (cylindrically-shaped piezoelectric ceramic) by a plane wave pulse

(i) Any sort of multipath propagation will produce erroneous results in a system based on time differences of arrival. B-scan systems, imaging with a single transducer assembly, tend to inherently "filter" out multipath reception by the single, highly directional receiving characteristic. When multipath is received, however, object placement error will exist in the B-scan displays. Although the PSI system will receive multipath propagation when such signals are at significant amplitudes, by nature of PSI's imaging by reinforcement, multipath will produce an insignificant contribution to the resultant image, since a particular multipath signal or even what has been termed a "creep" ray (i.e. an acoustic signal which travels into, around and back out of an object) will add to the image in a non-reinforcing mode.

(ii) When trying to perform a B-scan, gas and bone cause major difficulties. In the case of gas, reverberation of an acoustic pulse between the gas layer and transducer face will generally result in a streaked, obliterated image, since the B-scan interprets each succeeding (reverberated) pulse as a new reflector. For bone, the high acoustic attenuation (approximately 15 times that of soft tissue), limits sound penetration. Furthermore, if echoes could be received through bone, the difference in bone acoustic velocity would be great enough to cause misassignment of echo locations on the B-scan display, which assumes an average soft tissue velocity (velocity through bone is a little over 2.5 times that of soft tissue). Now, although the corresponding PSI signals would possess identical artifacts, PSI's multidirectional imaging would tend to make such an artifact less significant, due to its lesser degree of positional reinforcement. Finally, the digital image processing capability inherent of the PSI system further enables image enhancement or artifact removal.

CHAPTER V. EXPERIMENTAL TECHNIQUES UTILIZED IN INVESTIGATION
OF THE P.S.I. CONCEPT

A. INTRODUCTION AND PURPOSE

As mentioned in Chapter I(E), this investigation was undertaken, with
the intent of demonstrating the validity and feasibility of the Pulse-Scatter Im-
aging concept first via mathematical simulation and then through development
of a physical data acquisition capability and subsequent "real data" image re-
construction. Given the equipment, money and time available, the initial
protocol consisted of the following tasks ---

(i) mathematical simulation

(ii) develop reconstruction software suitable for real data insertion

(iii) build hardware to enable moderately accurate transducer positioning
(plus or minus a degree or so)

(iv) incorporation of appropriate electronics to transmit to and receive
data from the ultrasonic transducers

(v) image several simple objects and collect data directly from oscil-
loscope trace by hand digitization.

Thus, primarily due to financial considerations, it was decided that no at-
tempt in this investigation would be made at developing a "tuned" system.
Rather than devote a concentrated effort on developing the required transducers,
amplifiers and associated front-end electronics (e.g. 80 dB dynamic range log),

highly efficient reconstruction algorithm, optimized signal and image processing,

and the like, a task which would require several people at the minimum, the three

major areas of acoustics, signal processing and image reconstruction were to be

tackled more at a system level. Furthermore, this student was faced with achiev-

ing two inter-related goals. From the industrial standpoint, the final results must

conclude whether or not PSI shows enough promise to warrant investing upwards

of $100,000 and additional manpower for further research and prototype develop-

ment. Along academic lines, a more complete analysis is required, delving into

the student's understanding of the subject material as well as demonstration of

a logical rationale for investigation. It is intended that the material presented

thus far, in conjunction with the remaining description and discussion of the actual

experimentation itself, will meet the abovementioned goals. It should be noted

that the only major change in the protocol presented above, namely in part (v),

was the acquisition by General Electric of a high speed digital transient rec-

was the acquisition by General Electric of a high speed digital transient recorder

and PDP-11 computer interface, approximately mid-way through this study. As

a result, data could be automatically acquired via direct electronic digitization.

B.   IMAGE RECONSTRUCTION ALGORITHM DEVELOPMENT AND COMPUTER SIMULATION

As discussed in Chapter IV, the essence of the PSI scheme is to construct

and spatially sum gray-scaled ellipses, corresponding to amplitude-coded time-

of-arrival data. Various approaches may be utilized to perform this task de-

pending upon the equipment available. Parallel hardware processing methods

may be used in order to minimize reconstruction time.

For this investigation, although a convenience, high speed was not a requirement. The gray scale display used, was developed by GE Electronics Laboratory engineers several years ago for use as an X-ray CT display. This 320×320 pixel display unit has a self-contained 320×320 dynamic (non-random access) memory, 10 bits deep. Thus, each picture element can have associated with it one of 1024 values ranging from -512 to +511. A real time arithmetic processor internal to the display unit allows for manual "windowing" of the sixteen shades of gray displayed. As will be discussed at greater length later in this chapter, windowing involves assigning the sixteen gray shades to various regions of the -512 to +511 data. So, all in all, the reconstructed image is stored in $320 \times 320 = 102.4K$ memory locations.

The PDP-11 used for data processing contains only 24K of internal core memory as well as dual disc drives, each supporting a 1.2M 16-bit word capacity disc. Since the PPP-11, therefore, cannot maintain all 102.4K image cells in core memory during reconstruction, the image array must be stored on disc. Furthermore, this result necessitates processing the reconstruction data in memory chunks compatible with core storage. Since disc accesses (reads and writes) are so time consuming (relative to calculations time) it is desirable to minimize the number of disc accesses. However, for simplicity, it was elected to store data on the disc as 320 records, each record containing 320 elements. One record is therefore equivalent to one line of displayed data.

The straightforward way to view ellipse construction and superposition would be to "draw" into image memory one gray-coded, co-focal ellipse (through a memory random access process) corresponding to each point in a given T/R pair's received waveform. When a point being "drawn" coincides with a previously determined point, both numerical values are added and the sum put back

into memory. Disc data storage, however, precludes this method which requires random access to any of the 102.4K memory locations. Processing disc data requires reading or writing an entire data record. As a result, data will be processed one line at a time per received waveform. This method is obviously quite time consuming due to the huge number of disc accesses (i.e. a "read" or "write"), D, required.

$$D \approx \frac{N_T \times (N_T + 1)}{2} \times 320 \times 2 = 320 \, N_T \, (N_T + 1) \qquad (5\text{-}1)$$

(The value of "D" will be somewhat less than the value specified by Equation (5-1) as thru-transmission data is not utilized.) One PDP-11 RK-05 disc access takes an average of 70 msec. Thus, even an eight transducer reconstruction would require approximately $23,040 \times 70$ ms ≈ 27 minutes for disc accesses alone!

The methodology used in the PSI reconstruction algorithm will now be summarized. The actual Fortran program used is included under the name of "PSIV02.FOR" in Appendix B along with the rest of the software used in this study. (Note that the algorithm contains a number of options which are shown to be "commented out", to facilitate using these options under various test conditions without having to rewrite sections of source code each time. Thus, no attempt has been made to streamline the software at this point. Such streamlining and software optimization (particularly with respect to processing time) will begin the post-dissertation phase of this study.)

Now, let "N" equal T/R pair number, "N_{UP}" equal total number of data records recorded (including thru-transmissions) as defined in Equation (4-6), and "I" equal the image array record number. Figure 5-1 illustrates the matrix representation of the reconstructed image. As will be described, the

$$
\begin{array}{llll}
(1,1) & (1,2) & \cdots & (1,320) \\
(2,1) & (2,2) & \cdots & (2,320) \\
\vert & \vert & & \vert \\
\vert & \vert & & \vert \\
\vert & \vert & & \vert \\
(319,1) & (319,2) & \cdots & (319,320) \\
(320,1) & (320,2) & \cdots & (320,320)
\end{array}
$$
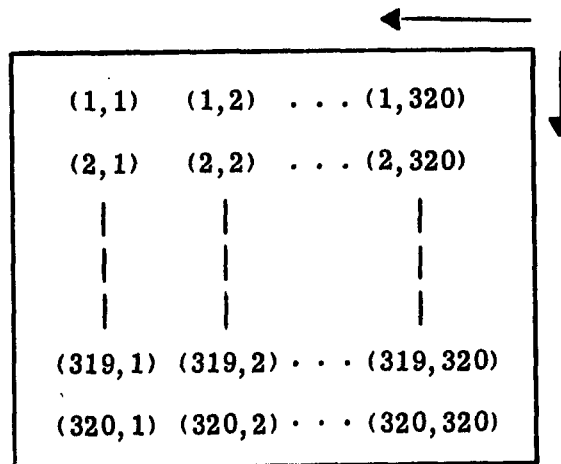
Figure 5-1. Representation of image matrix for PSI image reconstruction algorithm. As indicated by the two arrows shown, the PSI algorithm calculates the required ellipses by scanning the matrix from right to left in a row by row fashion beginning at element (1,320).

PSI algorithm calculates the required ellipses by scanning the entire matrix in a row by row fashion, to the left and down, beginning at element (1,320). The procedure goes as follows --

(i) Initialize image array to all zeroes

(ii) Read A-mode data record number one of N_{UP} (i.e. from T/R pair 1/1), which contains 320 integers indexed 1-320. The index value corresponds to distance (equals round-trip travel time divided by two) in pixels.

(iii) Read first row of image array into core memory.

(iv) Calculate distance, d, (in pixels) from transmitter one (T1) to image element (1,320) to receiver one (R1). Determine corresponding echo amplitude by reading the value of the dth element in (ii). Add this value to the value already stored in pixel (1,320).

(v) Calculate each of the distances from T1 to remaining pixel locations in first row [(1,J), J = 320,1,-1] to R1 and add the corresponding data values to the current pixel values.

(vi)   Return first row back to image array and read out the second row.

(vii)   Steps (iv) - (vi) are repeated until the entire image array has been scanned and modified.

(viii)   All co-focal ellipses have now been drawn for the data waveform corresponding to the T/R pair 1/1 (in this case a pulse-echo signal).

(ix)   The above procedure is now repeated beginning with (ii) for all the remaining $(N_{UP}-1)$ data waveforms.

(x)   Thus, the remaining sequence of data waveforms read in corresponds to T/R pairs 1/2, 1/3, $\cdots$ 1/N_T, 2/2, $\cdots$ 2/N_T, $\cdots$ $(N_{T-1})/(N_T-1)$, $(N_T-1)/N_T$, N_T/N_T as shown in Figure 4-9 for simulation of an eight transducer array.

As indicated, this algorithm (PSIV02.FOR) was programmed in Fortran on a PDP-11 computer. Data was then computer-generated to simulate three point scatterers, one located exactly in the center of the image array (5.15" diameter), and the other two, each spaced horizontally 5/8" from the center scatterer. Each simulated echo was assigned a unity amplitude. Figure 5-2 illustrates the resultant image displayed on the General Electric CT gray scale monitor, with various gray "window" settings. Windowing is a method of re-assigning (linearly, for the case of this particular gray scale monitor) the displayed shades of gray (see Figure 3-6, demonstrating linear and non-linear gray scale assignment) to the amplitude values (normalized by the reconstruction algorithm and stored in display memory) in the range -512 to +511 (10 bit resolution). Thus, the gray scale key displayed at the bottom of Figure 5-2(a), in particular, indicates that all data values $\leq$ -130 will be displayed as blackest black and all values $\geq$ +130 as whitest white. The centrally located integer is the value assigned to the gray shade immediately to the left of that number. (The CT display has a pushbutton to enable identification of this gray shade, G, by flashing the brightest shade of gray possible wherever "G" exists in the image.)

(a)   (b)

(c)   (d)
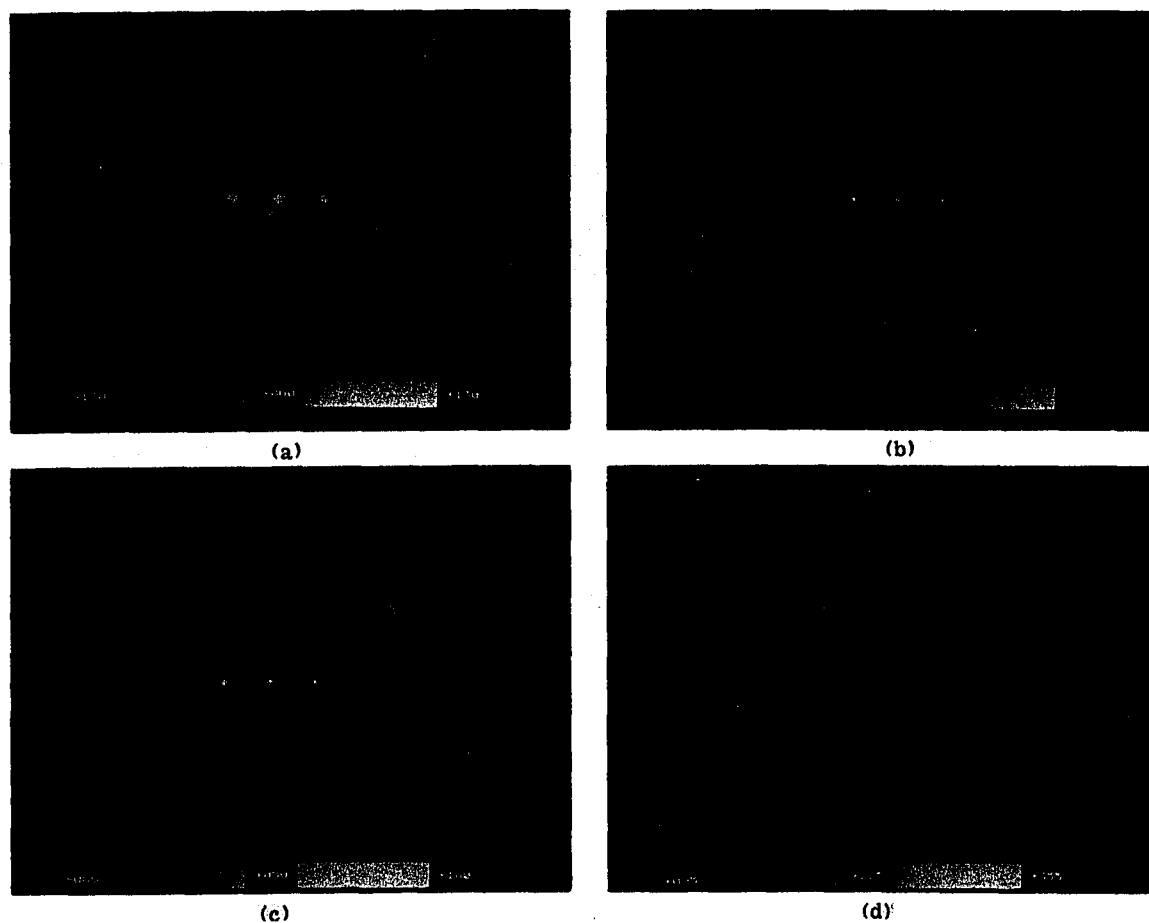
Figure 5-2. Eight transducer ring simulation of three point scatterers horizontally
separated 5/8" about center of 5.15" diameter array. Bright dots in
outer periphery represent transducer locations. Bright intersections
in center of image depict simulated targets. Gray scale assignment
within the -512 to +511 range shown at bottom of image.

(a) Display illustrating background reconstructions

(b) Same as (a) but with display brightness reduced

(c) Same as (a) but with gray scale "windowed" so as to remove
much of the background ellipse reconstruction

(d) Gray scale windowed even farther than in (c) to show only the
three point scatterers at center of image. (Note: any stray
"specks" are printing artifact and were not present in the
original image.)

Narrow windowing is particularly helpful for discriminating regions of similar intensity where wide windowing is beneficial for displaying widely separated image values.

As an aid to better understanding the geometry involved in PSI, a separate computer algorithm (TSTOK2.FOR in Appendix B) was written to compare this latter method of indirect ellipse generation, with the former one mentioned, of directly "drawing" each ellipse. A Tektronix graphics terminal was suitable for this task as the storage display was able to serve as the required 102.4K of "image memory". Being essentially an astable display, no gray scale could be truly depicted. Figure 5-3 illustrates the resultant Tektronix plot. Note how easily the ellipse geometry can be seen, for purposes of analysis (e.g. false intersections, etc.). In particular, straight lines corresponding to thru-transmission data can be seen passing through the center of display. Looking at plots such as the one in the figure made it apparent, after some thought, that such lines would have been present even had a scatter not been located at the center of the array, suggesting the concept of thru-transmission artifact.

A second simulation was performed to demonstrate the appearance of a uniform mass of scatterers. In a similar manner as for the three point scatterers, data was generated to simulate a square array of scatterers, uniformly encompassing an imaging region 40 pixels square, centered within the transducer array. Figure 5-4 shows the corresponding gray scale display, as expected. In the data generated, unity echo amplitudes were assigned.

As already mentioned, the PSI reconstruction algorithm, PSIV02.FOR. has been designed to facilitate various forms of data handling helpful in investigating PSI. In particular, program information such as data file names, data formats and reconstruction specifications may be entered at run-time by the

GENERAL ⬤ ELECTRIC

Simulated data: 3 point scatterers, 5/8'' separation   Date: 1/8/78

Data file: MOD3PT. DAT   Plot routine: TSTOK2. FOR

Transducer ring radius 5.15'' ; 8 transducer ring

36 ellipse families, 320 pts./ellipse, 3 ellipses per T/R pair, 108 ellipses total

Calibration: 175.58 μsec equals 320 picture units; 1 picture unit = 0.0818 cm
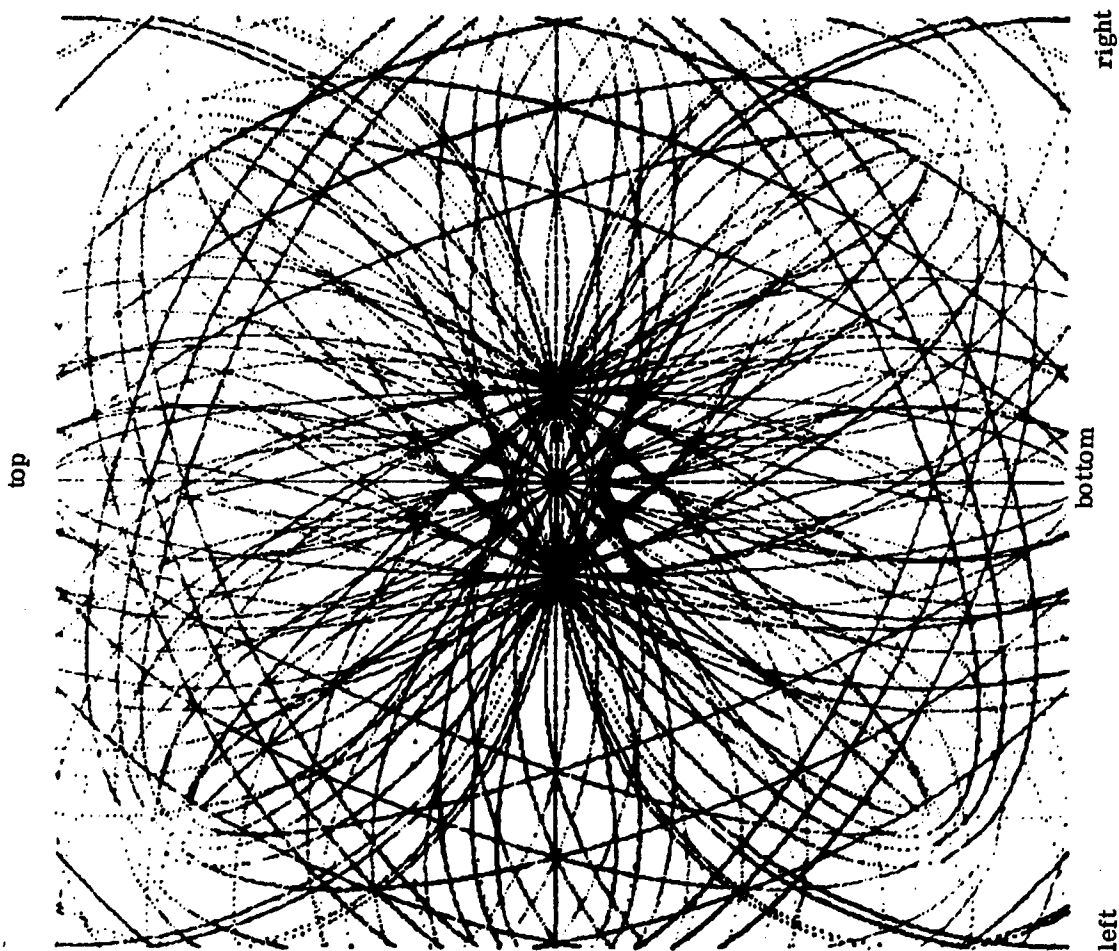
Figure 5-3. PSI reconstruction of three simulated point scatterers
horizontally separated 5/8" about center of 5.15" diameter
array, using "directly-drawn" ellipses on a Tektronix
CRT display terminal. Data used is identical to that of
Figure 5-2.

(a)
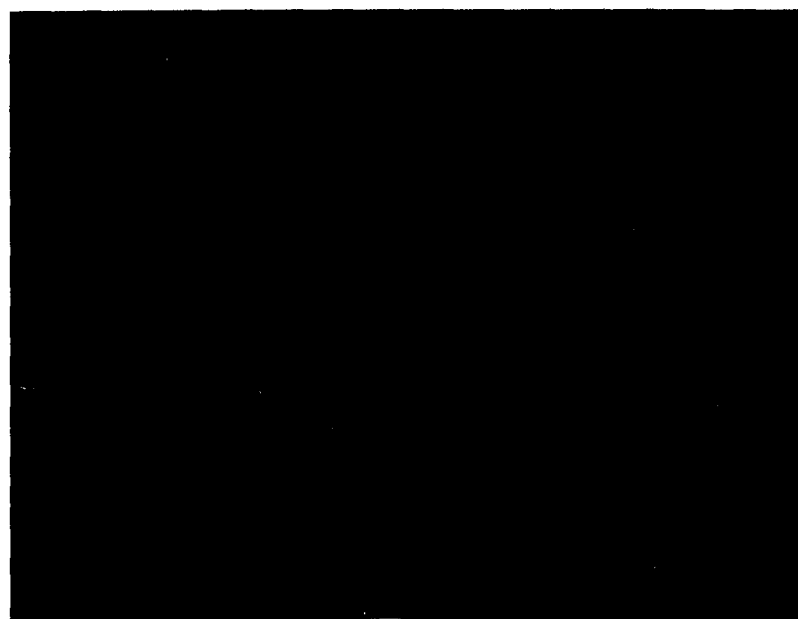
(b)

Figure 5-4. Simulation of a square uniform array of scatterers
(40 pixels square) located at the center of transducer
array
(a) Before gray-scale windowing
(b) After gray-scale windowing.

user via interactive questioning. Once the user has entered a given specification, this information is echoed back by the computer for user confirmation or modification. With respect to data formats presently used, in order to minimize disc storage, raw data is collected one byte (i.e. 8 bits) per data point, compatible with transient recorder output. After processing (e.g. peak detection, correlation detection, etc.), data is stored in integer format (16 bit word). In order to facilitate data scaling and interpolation, the calculations during reconstruction are performed in floating point format. Although the final reconstructed image is currently stored as floating point, it could just as easily be stored as integer data, since any floating point image data must be converted to integer format before being output to CT display. Floating point storage, however, lends slightly more accuracy for any post-reconstruction image processing that may be performed.

Two reconstruction program options which are presently "commented out" of PSIV02.FOR enable linear amplitude interpolation and input data deconvolution. It was mentioned that when assigning a gray value to an ellipse corresponding to a scatterer located a distance "d" from the T/R pair, the gray coding corresponds to the amplitude of the dth element of the 320 point processed received data waveform. In general this value "d" will be a non-integral value. Therefore, when being used, the interpolation routine assigns a gray value to the "d^{th} element" by performing a linear interpolation between the amplitudes of the elements with indicies immediately above and below the value "d". For the present investigation, it was found that the benefits achieved from interpolation were not worth the additional processing time, so that the interpolation routine has been temporarily commented out. Particularly when discussing CT and other PSI-related imaging techniques, it was pointed out that the reconstruction process convolves a "smear factor" into the reconstructed

image. Thus, supplying the proper data function required to "deconvolve" the smear artifacts from the input data, will enable the convolution routine to deconvolve the input data of the reconstruction smear prior to image reconstruction. Also mentioned earlier, a suitable deconvolution function compatible with PSI's elliptical geometry has yet to be determined. Thus, in the meantime, the convolution/deconvolution algorithm is not being used. (Although the convolution routine may be kept active by using an impulse convolution function, processing time is minimized by temporarily disabling the routine.)

Two options currently being used involve automatic reconstruction data scaling compatible with the -512 to +511 CT display data range, and the ability to watch the image as it is being reconstructed. Since reconstructed data will consist of positive numbers, $0 \to \infty$, the amplitudes must be reduced (normalized) and negative shifted in order to cover the CT display range -512 to +511. The subroutine called "SSWTCH.MAC" in Appendix B allows one to watch the reconstruction process in progress on a line by line basis if, on the PDP-11 console, switch register bit zero is set to zero. If bit zero is set to a one, the reconstruction output is deferred until after the entire image has been reconstructed. Not watching the reconstruction in progress speeds up reconstruction time as the image data does not have to be repeatedly output to the display monitor. Any remaining details of the reconstruction algorithm should be self-explanatory from the copy of PSIV02.FOR included in Appendix B.

C. EXPERIMENTAL DESIGN AND HARDWARE DEVELOPMENT

With the investigation of any new system, simulation is generally the cheapest and most flexible technique to use at the outset. As a result, the computer simulation discussed in the previous section was performed. Following the successful computer simulation, the next step in this investigation was hardware development for physical experimentation. Particularly in the

case of PSI, since the number and type of transducers in the array as well as the array diameter were unknown, the decision was made to design and utilize a technique which would allow for simulation of a circular array of "arbitrary diameter", containing a variable number of transducers.

In order to facilitate collection of data in the format of Figure 4-9, a scheme was developed which utilizes a fixed transmitter, rotating receiver and rotating platform on which the specimen to be imaged is fixed. The associated hardware to enable data collection via this scheme was designed and constructed with the assistance of Mr. Azad Minasian of the Electronics Laboratory's design group, and the GE Model Shop. Figure 5-5 depicts transmitter, receiver and specimen positioning for simulation of an eight-transducer ring. Simulation of "N_T" transducers requires that both the receiver and specimen be rotated in increments of $360/N_T$ degrees. Thus, as indicated in the figure, initially the transmitter, receiver and specimen are placed at 0°. (Note that transmitter and receiver at 0° is the pulse-echo condition requiring that the fixed transducer act as both the transmitter and receiver. In this investigation, since an electronic T/R switch was not available, to prevent saturation of the receiving amplifier by the high transmitted voltage, and thus obliterate the relatively minute signal received, the rotating receiver was placed as close to the transmitter as possible to simulate the pulse-echo mode.) Now, ideally the fixed transmitter (#1) would be pulsed and eight waveforms simultaneously received for T/R pairs 1/1 through 1/8. However, since available funds prevented use of simultaneous sample-and-hold multiplexing, the transmitter was pulsed once for each T/R pair, with the resultant A-mode waveform being recorded on magnetic disc via a digital transient recorder (to be discussed in greater detail in section D of this chapter). This procedure was permissible, since no movement existed between the transducers and specimen.

SPECIMEN ANGLE CLOCKWISE RELATIVE TO FIXED TRANSMITTER	TRANSMITTER (TRANSDUCER NUMBER)	RECEIVER (TRANSDUCER NUMBER)							
0°	1	1	2	3	4	5	6	7	8
45°	2	2	3	4	5	6	7	8	*1*
90°	3	3	4	5	6	7	8	*1*	*2*
135°	4	4	5	6	7	8	*1*	*2*	*3*
180°	5	5	6	7	8	*1*	*2*	*3*	*4*
225°	6	6	7	8	*1*	*2*	*3*	*4*	*5*
270°	7	7	8	*1*	*2*	*3*	*4*	*5*	*6*
315°	8	8	*1*	*2*	*3*	*4*	*5*	*6*	*7*
		0°	315°	270°	225°	180°	135°	90°	45°

RECEIVER ANGLE COUNTERCLOCKWISE RELATIVE TO FIXED TRANSMITTER (I.E. 0°)

NOTE: REDUNDANT T/R PAIRS ARE SHOWN CROSS-HATCHED

EIGHT TRANSDUCER RING BEING SIMULATED

RECEIVER POSITIONING

RECEIVER IS ROTATED IN A CLOCKWISE FASHION

POSITION OF FIXED TRANSMITTER (0°)

SPECIMEN POSITIONING

SPECIMEN IS ROTATED IN A COUNTER-CLOCKWISE FASHION

WATER TANK

Figure 5-5. Transmitter, receiver and specimen positioning for simulation of an eight transducer PSI array

Thus, as indicated above, the data corresponding to T/R pair 1/1 is obtained by recording the signal obtained from a single pulse of the transmitter with the receiver at approximately 350°. Then, referring to Figure 5-5, the receiver is placed at 315°, the transmitter is pulsed once, and signal 1/2 is obtained. The same procedure is followed in a counter-clockwise fashion until the receiver reaches 45° and signal 1/8 is recorded. Now, in order to simulate moving on to the next transmitter, the specimen is rotated clockwise $360/N_T$ degrees (or 45° for an eight transducer array), with the abovementioned procedure being followed until signals 2/2-2/8 are recorded. The same procedure of specimen and receiver rotation is then continued until all data corresponding to Figure 5-5 is obtained, $N_T \times (N_T + 1)/2$ signals in all.

Figure 5-6 indicates the overall equipment setup for PSI data collection (to be discussed in Section D). At the extreme right side of the photo is the water tank and hardware already described for PSI data collection. Figure 5-7 illustrates a more close-up view of the apparatus for transducer and specimen positioning. (Styrofoam liners on tank walls are utilized to minimize spurious echoes.) The aluminum bar suspended across the width of the tank supports the fixed transmitter and holder, whereas the rotating aluminum plate supports the rotating receiver and holder. An angular scale (circular protractor) mounted on the rotating plate enables calibrated transducer rotation. A similar but larger diameter scale mounted on the rotating specimen platform (Figures 5-7 and 5-8) enables calibrated rotation of the specimen. Several points should be mentioned regarding this apparatus. In order to simulate a circular array, both the receiving transducer and specimen should be rotated on the identical, perfectly circular path. Errors in this requirement will lead to errors in recorded time of echo arrival and transducer location. Similarly, all axes of rotation (i.e. those of the receiver and specimen) must be in exact alignment,
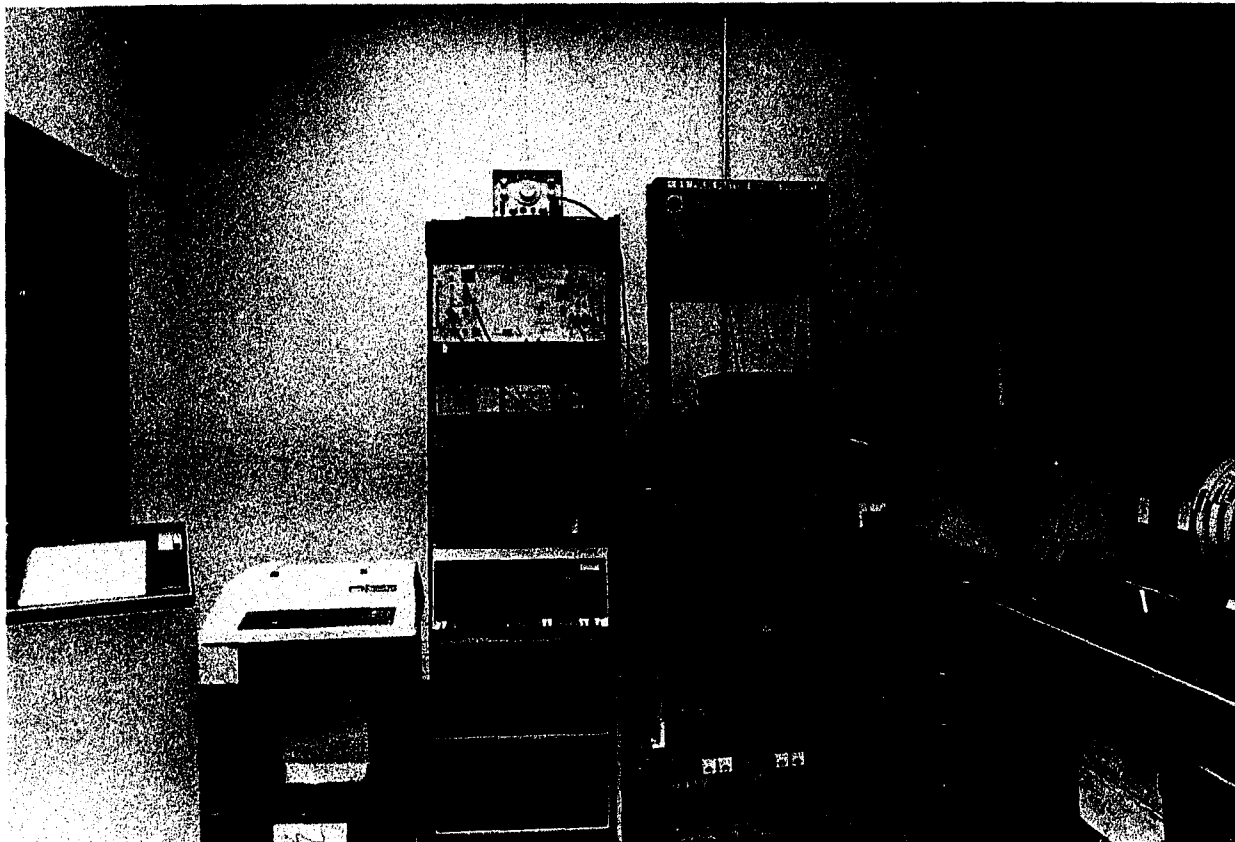
Figure 5-6. Equipment setup for collection of PSI data

otherwise positional and timing errors will result. Furthermore, the trans-

ducers should have their beam centers aimed at the exact center of the circular

array. Finally, the beams, themselves, should all be identically aligned in the

circular plane of the array.

Further examination of Figure 5-7 indicates a slit in the rotating alumi-

num disc to enable variation of the simulated array diameter by positioning the

receiving transducer closer to or further from the center of rotation. As shown

in close-up by Figure 5-8, each transducer is suspended in the water by a hollow

brass rod. Electrical connection to the transducer is made via a UHF connector

which, in turn is coupled to a right angle BNC connector combination, fixed to

the brass rod. A 50 ohm coaxial cable running through the brass rod ties the
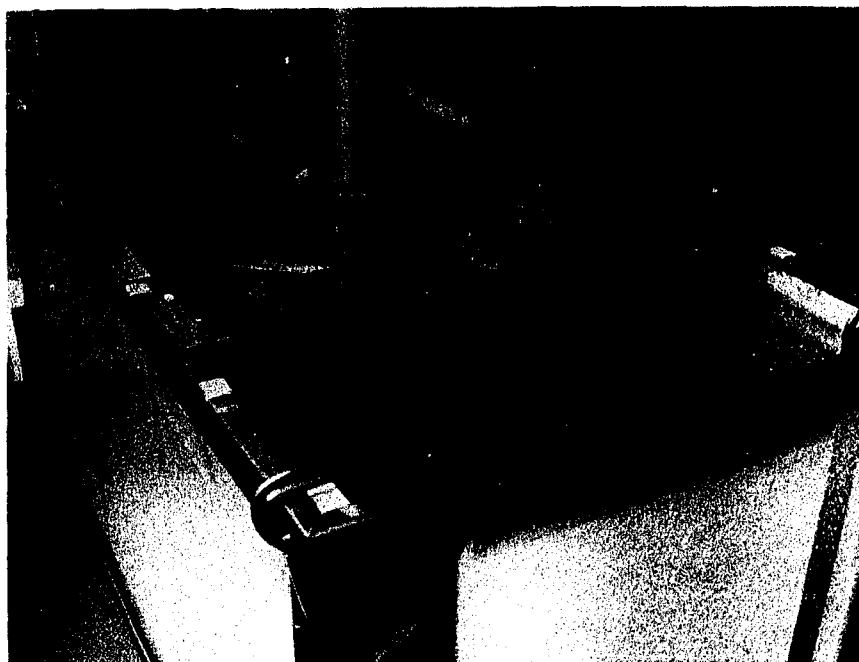
Figure 5-7. Close-up of PSI transducer positioning apparatus used in physical system simulation

Figure 5-8. Close-up of PSI specimen position platform and orientation of surrounding transducers for physical system simulation

connector assembly to the transmitting or receiving circuitry external to the

water tank (in the equipment rack shown in Figure 5-6). For proper impedance

matching and good electrical connection it is absolutely essential that all under-

water electrical connections be waterproof. Water leakage into a connection

will result in impedance variations and an improper matching between the 50

ohm transducer and 50 ohm coax assembly used. As was unfortunately demon-

strated on several occasions, such an impedance mismatch sets up antenna-

like behavior, resulting in all kinds of what appeared to be unpredictable elec-

trical pick-up (e.g. from the PDP-11, a nearby copying machine, etc.) through

the water into the receiving transducer. Such pick-up would obscure almost all

of the received echoes. For waterproofing, a combination of epoxy potting and

General Electric RTV (TM) compound were used. A waterproof seal between

the transducers used (guaranteed waterproof by the manufacturer) and the UHF

connector was made via a rubber O-ring. For the most part, once aligned,

the transducer assemblies were kept submersed in the water tank 24 hours a

day. Porosities in the epoxy potting developed periodically, as manifested by

spurious electrical transducer pickup, requiring periodic waterproofing. Design

of future apparatus of this type should provide a means for more efficient water-

proofing.

(Two transducer holders will be noted in the rotating aluminum plate.

Originally, it was felt that the use of two rotating transducers and one fixed

transducer might enable data collection with half as many transducer positionings.

However, after preliminary experimentation with a single rotating transducer,

such a scheme was found to be satisfactory, requiring that only a single ro-

tating fixture be used.) A close look at Figure 5-8 indicates a straight extender

attaching the fixed transducer to its holder. This extender was made from

several UHF and BNC mating connectors surrounded by waterproof epoxy potting, and enables the fixed transducer to reach the same diameter as the rotating receiver.

The specimen positioning platform is simply an 8" diameter, 3/8" thick aluminum disc mounted on an 8-1/2" square, 3/8" thick brass plate with rubber feet, so as to enable free rotation of the disc. The brass base was used to provide enough weight so that the platform assembly would not be moved unintentionally. As already mentioned, a circular protractor mounted on the disc provides an angular scale to enable calibrated rotation of the specimen. Several 0.064" diameter holes have been drilled in the top side of the rotating disc to enable specimen attachment via 0.064" diameter stainless steel pins, in order to keep the immediate and nearby area being imaged free of any extraneous material.

Returning to the alignment requirements mentioned earlier, the PSI simulating hardware possesses no accurate means for ensuring overall alignment, other than "eye-balling" the components and running a reconstruction of a scatterer (e.g. a metal rod) in the center of the imaging area. Prior to running a reconstruction, the equipment is aligned by examining the main pulse-echo from the rod as seen by the rotating transducer being used in the pulse-echo mode. For perfect hardware alignment, rotating the transducer and specimen to various positions should not influence the time of echo arrival. Subsequent reconstruction should then demonstrate the rod in the center of the image region. It must be kept in mind that positional errors are inevitable using this method of alignment and will contribute to a smeared image. Higher quality hardware which will eliminate both alignment and positional accuracies will be required to eliminate this smear factor. Such a system might be modeled after that currently in use at the University of Rochester, which utilizes digital stepper motors to control positional coordinates [28], [29], [30], [31], [34] .

Given the abovementioned hardware, the next factor which must be considered is transducer selection. As already discussed, two transducers with as identical characteristics as possible are required for a given simulation. In beginning the PSI investigation, since fan beam transducers were not commercially available, the decision was made to use readily available, non-focused transducers. In order to provide the future capability of frequency-sweeping, as wideband transducers as possible in the 1-10 MHz range were specified. A center frequency of 5 MHz was specified, compatible with the penetration and time resolution desired. Finally, the use of readily available half inch transducers would enable establishment of a relatively small although acceptable symmetric region of insonification one half inch in diameter. Given these considerations, two Panametrics, (Waltham, MA), 5 MHz, unfocused Videoscan Broadband Immersion transducers, Model #V309SU ($165.00 each), were used (see Figure 5-9). Appendix C-1 contains both data provided by the
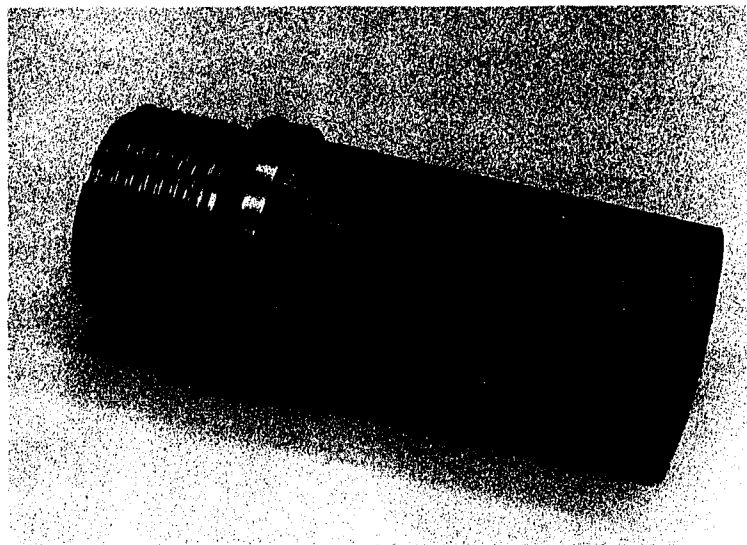
Figure 5-9. Photograph of one of the Panametrics 5 MHz, non-focused, 1/2" diameter ultrasonic transducers used

manufacturer as well as impedance profile data taken on a Hewlett-Packard #4815A RF vector impedance meter. The data presented indicate the variability that is common when trying to obtain two identical transducers. The impedance data show electrical resistances of 68 and 132 ohms for the two transducers. Thus, the 50 ohm impedance matching assumed throughout the PSI system is reasonably valid. Although position monitoring equipment was unavailable and so a beam pattern profile could not be accurately determined, a quarter-inch steel ball bearing was used to demonstrate an approximately half-inch beam width in the imaging area.

While preliminary data collection was begun with the Panametrics transducers, KB-Aerotech (Lewistown, PA) was contracted to manufacture a pair of prototype fan beam transducers, #83-114-000-150 ($450.00 each). All specifications were identical to that of the Panametrics transducers with the additional requirement of a 30° fan beam via a cylindrically-shaped piezoelectric ceramic (see Figure 5-10). It should be noted that both the Panametrics and Aerotech transducers were constructed of lead metaniobate, in order to achieve wideband characteristics. Manufacturer's specifications for the fan beam are presented in Appendix C-2. Preliminary monitoring of beam characteristics using the quarter-inch ball bearing indicated a fan beam of approximately 42°.

Due to the uniqueness of the fan beam probes, the transducers were sent to the U.S. Bureau of Radiological Health (BRH) in Rockville, MD, for beam profiling on their ultrasonovision system [88], [89]. Mr. Michael Haran, Research Physicist for the BRH Acoustics Branch, conducted the profiling. As will be indicated in the data presented in Appendix C-2, one of the two fan beam transducers (S/N 47264H) was found to possess a "half-fan" beam pattern. Examination of this transducer by the manufacturer indicated a de-lamination
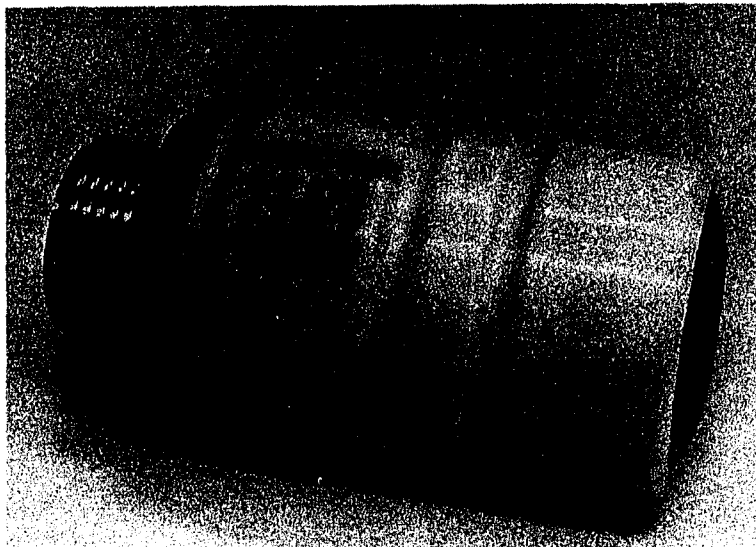
Figure 5-10. Photograph of 5 MHz KB-Aerotech fan beam ($\approx 42^{\circ}$ beam angle) transducer. Photo indicates the earliest version utilizing a $\lambda/4$ epoxy matching layer over the shaped ceramic (at right).

of the electrode plating on one half of the ceramic. Comparing this half-beam pattern with the complete pattern obtained for the other fan beam transducer (S/N 47265H) shown in Appendix C-2 is quite instructional. The half-beam pattern results from a transducer which has essentially half the diameter of the full-beam probe. As discussed in Chapter II, the smaller effective D/λ ratio of the half-beam probe results in a shorter near field than the full beam probe, a behavior which is illustrated quite nicely in the BRH profiles. On the full-beam profile, a beam angle of approximately 42° was also found, comparable with the ball-bearing profile performed earlier.

During preliminary testing of the fan beam probes, it was also found that the epoxy quarter-wave matching layer on the front of each transducer would, for a still unknown reason, blister and peel when immersed in the PSI water tank (the water was carefully analyzed and found to be identical to tap water).

As a result, the epoxy was finally removed (after repeated trials) and replaced

by a silver-lacquer coating. (It was felt that the impedance mismatch produced

by not having the quarter-wave layer would not be all that significant due to the

broadband pulse-burst excitation used. Quarter-wave matching is only at a

particular frequency and so is most significant in narrowband applications).

Although schedules could not permit re-profiling of the fan beams by the BRH,

the transducer manufacturer suggested that the original full-beam pattern

(S/N 47265H) should be representative of the present transducer performance.

One last fact concerning the fan beam probes is that each one has a small in-

ductor in parallel with the transducer input to null out capacitance and provide

a 50 ohm input impedance at 5 MHz.

D. DATA COLLECTION - HARDWARE AND SOFTWARE CONSIDERATIONS

The data scheme for collecting the "N_{UP}" A-mode waveforms required

to simulate an array of "N_T" transducers has already been described. This

section will predominantly concentrate on the hardware and software aspects

of data collection, and discuss the acquisition of a single A-mode waveform,

in particular.

Figure 5-11 illustrates a block diagram of the current data acquisition

and signal processing capability utilized in the PSI investigation. (As men-

tioned earlier, the only difference between the present and original system

configuration was the acquisition of the transient recorder.) All analog signals

are transmitted over 50 ohm coaxial cable. The transmitting transducer is ex-

cited by an Arenberg pulsed oscillator, #PG650-C, outputting an approximately

1.5 μs, 5 MHz burst with an 80V peak-to-peak (loaded by the transducer) amplitude

(see Figure 5-12). (Output amplitude, frequency and pulse-width are variable.)

The output of the receiving transducer is generally in the one millivolt

PULSE-SCATTER IMAGING SYSTEM (PSI)
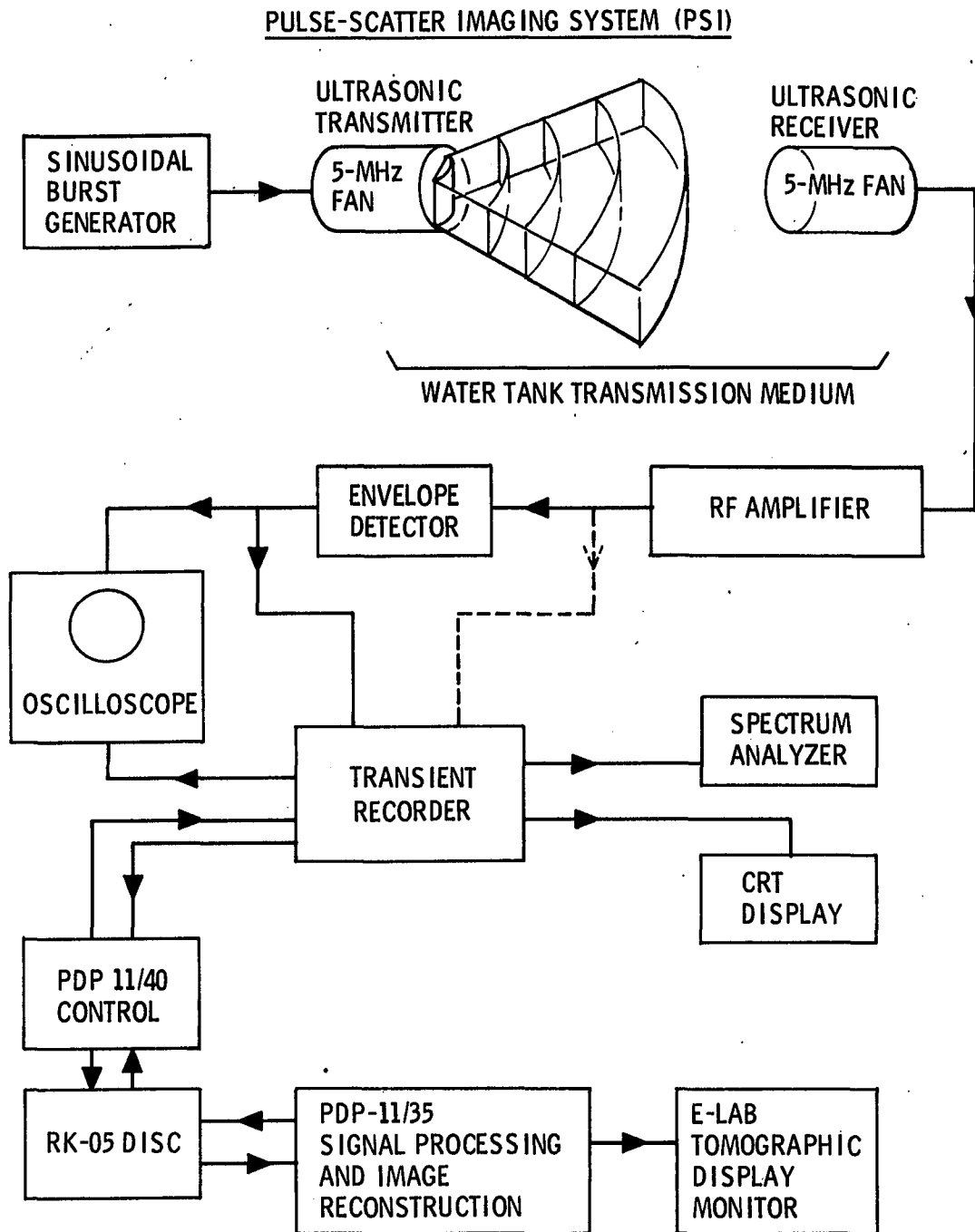
Figure 5-11. Pulse-Scatter Imaging System. Block diagram illustrating
possible signal flow pathways
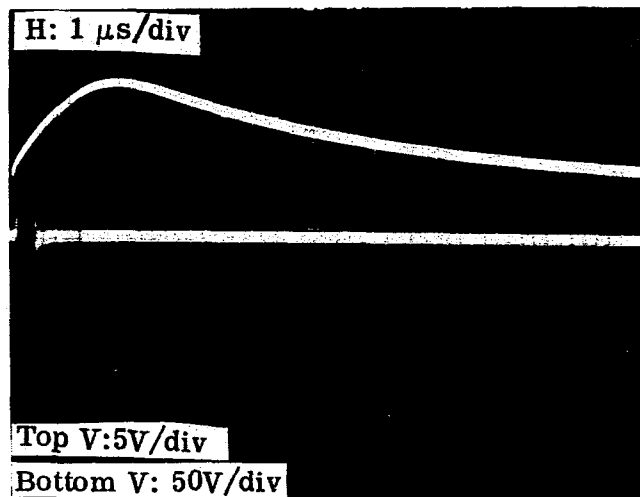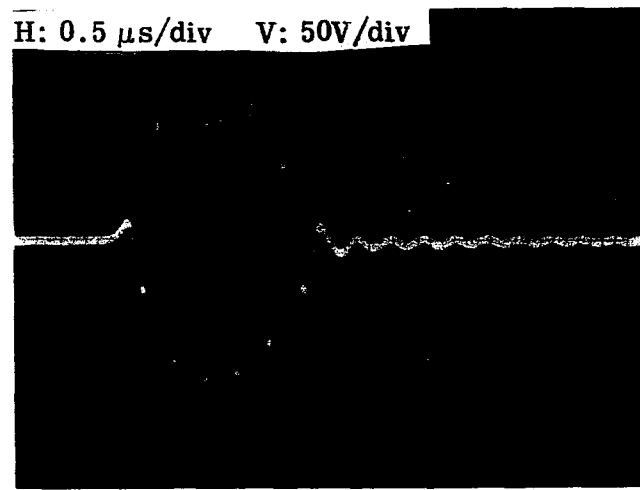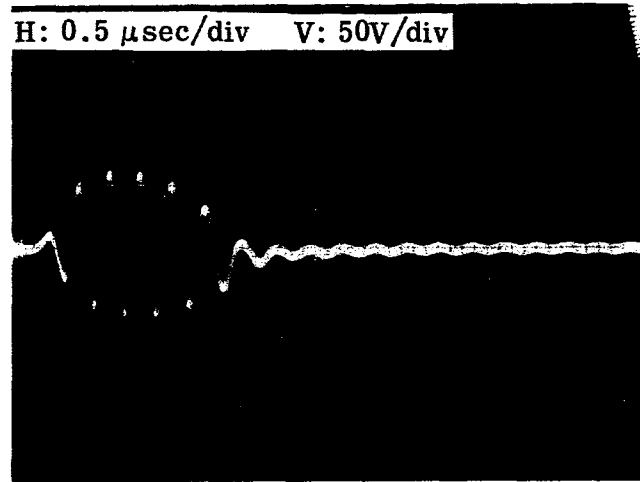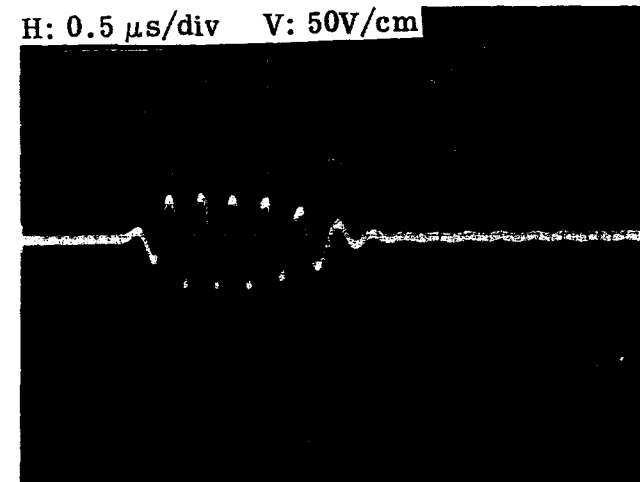
Figure 5-12. Outputs and timing from Arenberg pulsed oscillator (a) Trigger output (top) and pulse burst (~5 MHz), (b) Pulse burst shown with expanded sweep, (c) Output pulse burst when loaded by Panametrics transducer (#15289) and (d) Output pulse burst when loaded by KB Aerotech #4764 fan beam transducer

range (without inductive input tuning to increase input amplitude) and so is passed through an RF amplifier (RF Communications, Inc. #805) with 47 dB gain (0.1V rms max input) in series with a Hewlett Packard #461A RF amplifier, with gain settings of 20 dB and 40 dB for a 1V maximum input signal. Presently, the amplified output is passed through a simple diode-resistor-capacitor RF envelope detector (Telonic, #XD), which, in this case, passes the negative portion of the signal's envelope. The detector output is then input to an American Electronics Laboratories (AEL, Lansdale, PA) series 9000 pulse and transient recorder (PTR). The PTR, with the options ordered, has a wideband (4 Hz-50 MHz), variable gain (0-40 dB) front-end RF amplifier, followed by a high speed 8-bit A/D converter (100 MHz maximum sampling rate). Depending on how the trigger mechanism is adjusted (e.g. pre- or post-trigger delay), the input signal is sampled at the specified rate with the first 8192 samples being stored in memory. A PTR PDP-11 interface purchased from the manufacturer enables the digitized data to be output directly to the PDP-11 for storage and/or processing. Furthermore, the computer interface allows remote software control of all the PTR front panel controls from the PDP-11. When not outputting stored data to the computer, a captured waveform may be viewed on among other devices, an oscilloscope, as the stored data is constantly output to refresh the oscilloscope trace. Finally, the PTR may be operated in a dual timebase mode, enabling a given data waveform to be recorded using two different sampling frequencies, one rate for the first portion of the data and a different rate for the second portion.

Presently, the transient recorder is utilized in a predominantly manual fashion. The specified waveform is captured, after occurrence of the desired trigger signal, and observed in continuous refresh on an oscilloscope (the 8K of stored data is output once every 20 msec). Running the Fortran program

"READIN.FOR" (see Appendix B) on-line with the PTR, and transferring the PTR output from the scope mode to the digital mode, will enable automatic transfer of the stored PTR data to PDP-11 magnetic disc. Two factors must be kept in mind when choosing the PTR sampling frequency. First, the sampling frequency(s) chosen must be fast enough in accordance with the Shannon Sampling Theorem (i.e. sampling frequency must be at least twice the highest frequency in the signal to be recorded).The second point is that the time span of the stored waveform is inversely proportional to the sampling rate. Finally, proper adjustment of the sampling frequency (i.e. dual timebase), and pre- and post-trigger delays will enable efficient data storage by either recording at a very low sampling rate (thus storing fewer samples), or not recording at all, portions of a given waveform which are not of interest. As a result of these considerations, a 20 MHz sampling rate has been used, allowing 409.6 μsec of data storage in an 8K memory. This sampling rate is over twenty times the upper frequency component of the envelope detected signal, and allows for data storage well in excess of the 264 μsec required for simulation of an 8" diameter transducer array. Utilization of this high a sampling rate allows for excellent visualization of the sampled signal on an oscilloscope trace.

One slight variation in the present data collection process would be to have the PTR sample the raw RF signal, as indicated by the dotted line in Figure 5-11. Since the PSI reconstruction algorithm (as does the B-scan) requires magnitude data, rather than use the negative half wave analog envelope detector, digital envelope detection (e.g. full-wave) may be performed by software techniques. Furthermore other types of detection could be tried as well, such as correlation detection [90] , [91] . Although not yet tried, correlation detection would proceed as follows. A single pulse-burst is thru-transmitted, received and stored in computer memory in order to register a "typical" pulse. This typical pulse then contains the characteristics imposed by the transmitting transducer, re-

ceiving transducer and transmission medium. Performing mathematical cor-
relation between each A-mode waveform and this typical pulse should then result
in a new waveform, with narrow "spikes" occurring at points of strong correla-
tion, which could then be used to provide echo amplitude and time of arrival
information. The ideal signal for image reconstruction would consist of a series
of delta functions, each occurring at exactly the time when the beginning of an
echo is just first received in the usual A-mode signal. Furthermore, the delta
function should be weighted so as to correspond to the total scattered energy in
the given echo.

Once having been stored on magnetic disc, as will be discussed in the next
section (E), the data must be conditioned to be suitable for processing by the re-
construction algorithm "PSIV02.FOR". As already mentioned, the current
system is an "untuned" version of that which would comprise a working proto-
type. Also mentioned earlier, is the fact that one generally speaks of recording
at least an 80 dB dynamic range when trying to record standard pulse-echo sig-
nals. The required dynamic range is even greater when dealing with scattered
signals as well. One solution to this difficulty would be to replace the standard
RF amplifier used, with a logarithmic compression RF amplifier (presently un-
available at GE). Thus, the 48 dB (8 bits) dynamic range of the PTR could now
be effectively used over a much wider echo amplitude range. At present, without
the log amplifier, it is necessary to saturate the larger amplitude echoes in order
to differentiate between those of lesser amplitude. At this point, the lack of a
log amplifier is not all that critical since the present investigation is concentrating
simply on image detection and not quantitation.

Recording of the acoustic signal so as to obtain maximum dynamic range
from the PTR involves PTR and front-end reconstruction software adjustments
as indicated in Figure 5-13. Applying a positive full-scale offset (i.e. +128)
to the signal input to the PTR, followed by software inversion and addition of an

+128

−128

ENVELOPE − DETECTED
SIGNAL INPUT TO TRANSIENT
RECORDER

8192

+128

−128

+FS OFFSET AT
TRANSIENT RECORDER
INPUT

8192

+128

−128

INCREASE (DOUBLE)
TRANSIENT RECORDER
INPUT GAIN

8192

+128

−128

SOFTWARE INVERT
SIGNAL IN PDP-11

8192

+256

+128

ADD +128 TO
INSURE ONLY
POSITIVE VALUES
FOR IMAGE
RECONSTRUCTION

8192

+256

+128

"PEAK PROCESS"
DATA FROM 8192 −
POINT WAVEFORM
DOWN TO 320 PTS

320

ABSCISSA = TIME;   ORDINATE = DIGITAL SIGNAL AMPLITUDE

Figure 5-13. Basic conditioning of envelope detected signal prior to processing
by PSI reconstruction algorithm

additional positive full-scale offset results in an acoustic signal which occupies a fully-positive 8-bit range, 1-256.

E. DATA PROCESSING AND ANALYSIS TECHNIQUES

At present, storage of the raw PSI data is in the form of 8K, 8-bit bytes (i.e. 4K 16-bit words) per T/R pair waveform. As mentioned in Chapter IV, although far from the most efficient method, the data format presently accepted by the PSI reconstruction algorithm is a 320 point waveform, where each succeeding point in a given T/R pair's waveform corresponds to the ellipse echo amplitude to be "drawn" a unit pixel distance further from the given T/R coordinates. Thus, this 320th point in this echo envelope waveform corresponds to an echo time-of-flight equivalent to a round-trip distance of two transducer array diameters (i.e. "4R" as depicted in Figure 4-6, and discussed in V(B).) (The most efficient data acquisition scheme would be that depicted in Figure 4-12(c) where the 8K data points stored would correspond to 2.6 r μsec, where "r" equals radius of uniform region of insonification in mm. The resultant 8K data points would then be further processed down to 320 points such that the 320th point would now correspond to an echo time-of-flight equal to "4r" as depicted in Figure 4-12.)

Although various techniques are possible for reducing the 8K point waveform down to 320 points, the method presently used will be illustrated by example. Let us assume that the "exact" transducer array diameter being simulated is unknown. Now, if a 180° thru-transmission measurement, t, were made in water (acoustic velocity, c, equals 0.154 cm/μsec) the array diameter, D, would be determined as

$$D = t \times c \qquad\qquad (5\text{-}2)$$

Let's say t = 146 μsec. (This time would correspond to an array diameter of D = 22.46 cm.) In this case, the required 320 point PSI data waveform would

correspond to a maximum time-of-flight of "2t" or 292 μsec. Assuming that the PTR sampling period, T, was 50 ns (sampling frequency equals 20 MHz), then

$$S = \frac{2t}{T} \qquad (5\text{-}3)$$

where "S" equals the initial number of the total of 8K recorded samples required to exactly represent a maximum echo time-of-flight corresponding to two array diameters. Here, S = 292 μsec/50 nsec = 5840 samples. In order to convert these 5840 samples into a 320 point waveform, select the peak value from each of 320 uniform width data bins, each bin containing an integral number, "n", of original data points. For "n" to be an integer, "S " must be an integral multiple of 320. For our example, since 5840 is not an integral multiple of 320, select the next largest number, "S_I" which meets this criteria. In this case, $S_I = 6080$ (6080/320 = 19 = n). Therefore, only 6080 of the originally recorded 8192 data points are required to cover the time span of interest. Now, however, since we are working with 6080 rather than 5840 original points, reducing 6080 points down to 320 points by selecting the peak value for every 19 data points, results in a 320 point waveform corresponding to slightly more than a distance of one ring diameter. (This "peak processing" is performed by the program "PEAK.FOR", where the user must specify both "S_I" and "n"; see Appendix B.)

Thus, an additional calibration factor is required by which all distance calculations (equals round-trip travel time calculations divided by two) must be adjusted, since now, the 320 point waveform actually corresponds to S_I/S or 6080/5840 = 1.04 array diameters. Therefore, as part of the "PSIV02.FOR" algorithm, each distance calculation, d, must be multiplied by the calibration factor, "C",

$$C = S/S_I \qquad (5\text{-}4)$$

before looking up the amplitude of the "d" element in the 320 point waveform, as discussed in V(B).

The execution of "PEAK.FOR", therefore, produces "N_{UP}" 320 point, peak processed waveforms. "PEAK.FOR", is in effect, a crude form of digital filter. For looking at targets consisting of several individual points, this program is quite sufficient as the scattering frequency is relatively low. However, as was found when looking at some higher frequency scattering patterns as was obtained from the natural sponge (Chapter VI), several lower level high-frequency echoes were lost, thus demonstrating the need for more sophisticated digital filtering, preferably user interactive, in the "tuned" version of this system. In order to prevent the thru-transmission data (for example, for an eight transducer array of "straight beam", i.e. standard, transducers, T/R pairs 1/5, 2/6, 3/7, and 4/8) from appearing in the reconstruction, the program "ZERO.FOR" may be run to zero out all data records corresponding to thru-transmission. The most efficient way to achieve this goal, however, is to eliminate both recording and processing of thru-transmission data, thus reducing required data storage and processing time. It should be noted that, for example, an eight transducer array of fan beam probes will require omission of additional T/R pairs than listed above for a standard probe, with the number of thru-transmission pairs being directly proportional to fan beam angle.

Foregoing any additional acoustic data processing for the present investigation (logarithmic de-compression would have been required had a logarithmic amplifier been used in data recording), the data is processed by the image reconstruction algorithm "PSIV02.FOR" as described in V(B). The resultant gray-scale image of the patient or specimen may then either be examined directly or undergo further image processing. The fact that the reconstructed image is

stored on disc as a floating-point (could have been integer, instead) array 320 elements square, with a dynamic range in excess of 60 dB, facilitates image processing by any of the many techniques currently used in various fields (e.g. processing of moon pictures to remove noise and artifacts, establish structure patterns, etc.)[92],[93],[94],[95],[96],[97]. For ultra-high speed analysis, image processing techniques involving lasers and optics, surface acoustic wave (SAW) devices, etc. may be used. Such techniques may also find applicability for pre-reconstruction data processing.

The field of digital image processing is a highly technical field and for the most part is comprised of state of the art computer processing techniques. Although no major attempt has yet been made in this investigation to apply available digital processing techniques to enhance the reconstructed images, three simple schemes were tried quite briefly. The first technique tried was deconvolution, as discussed in Section IV(C).

Inverse filtering [92],[94] is a technique quite closely related to deconvolution, and may also be illustrated with the aid of Figure 4-13. To perform inverse filtering of an image, the two dimensional Fourier Transform must first be taken of the image (i.e. $G(x,y)$ as depicted in Figure 4-13). Now, taking the specific case discussed with respect to image de-smearing by deconvolution, as an example, a single image point is reconstructed in order to obtain the so-called point-spread function (PSF). Subsequent Fourier Transformation of the PSF results in $H(x,y)$ shown in Figure 4-13. Thus, dividing $G(x,y)$ by $H(x,y)$ in a pixel by pixel fashion will produce $F(x,y)$. Finally, taking the inverse two dimensional Fourier Transform of $F(x,y)$ should produce the desired image. As indicated in the discussion of deconvolution, except in the case where an exceedingly large number of ellipses intersect each and every point, each pixel will have its own, spatially-dependent PSF. Thus, for proper

inverse filtering, H(x, y) must reflect this spatial dependence as well. As an important practical consideration when dividing by H(x, y), special care must be taken to ensure that H(x, y) has no "zero terms" as well as a minimum of "small-valued" terms. Rather than the idealized representation of Figure 4-13, let's assume that a noise term, N(x, y), enters the reconstructed image. Thus,

$$G(x, y) = F(x, y) \, H(x, y) + N(x, y) \tag{5-5}$$

The result after inverse filtering (i.e. division by H(x, y)) is

$$G(x, y) = F(x, y) + \frac{N(x, y)}{H(x, y)} \tag{5-6}$$

Obviously, then, too many zeroes or small values present in the inverse filter function could produce a situation where the noise term is enhanced to the point where the desired image is obliterated. Much work and further experimentation needs to be done in order to determine the optimal inverse filter function for de-smearing, as no striking improvements were obtained using the PSF reconstructed at the center of a sixteen transducer array (see paragraph after next). Although discussed for the case of image de-smearing, inverse filtering finds widespread applicability in selectively enhancing or subduing various image characteristics. For example, low pass filtering will result in an image with rather non-discrete internal boundaries, whereas high-pass filtering emphasizes sharp lines and boundaries, somewhat of an alternative to edge detection via gray scale gradient thresholding [94] .

In so far as the de-smearing example is concerned, in general, deconvolution is preferred to inverse filtering due to the great computational savings. Deconvolution, in effect, is a one dimensional computation to bring about a two dimensional effect. Even though the two dimensional Fourier Transform is calculated via a 2-D FFT (see programs in Appendix B), inverse filtering is still quite time consuming.

Briefly, deconvolution for image de-smearing, using the CT deconvolution function produced a "washing out effect" (see Figure 6-8) when applied to a full 320 × 320 pixel image. When applied to the reconstruction of a single point scatterer located at the center of a sixteen transducer array, quite a reasonable improvement was obtained, as indicated in Figure 5-14 (central 20 × 20 pixel region is shown). Figure 5-15 shows the corresponding PSF perspective plot, but without the effect of gray scale windowing. This result is indicative of the fact that reconstruction at the center of the array is essentially by straight lines as in CT; secondly, although additional investigation is required by confirmation, PSI produces a spatially varying PSF.
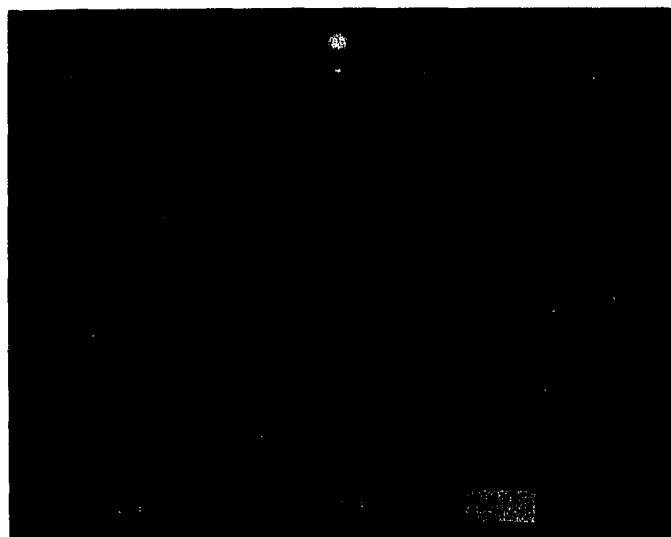
Figure 5-14. Reconstruction of a point scatterer (top of figure, central 20 pixel square portion of reconstruction shown) and result after deconvolution with CT function (lower spot)
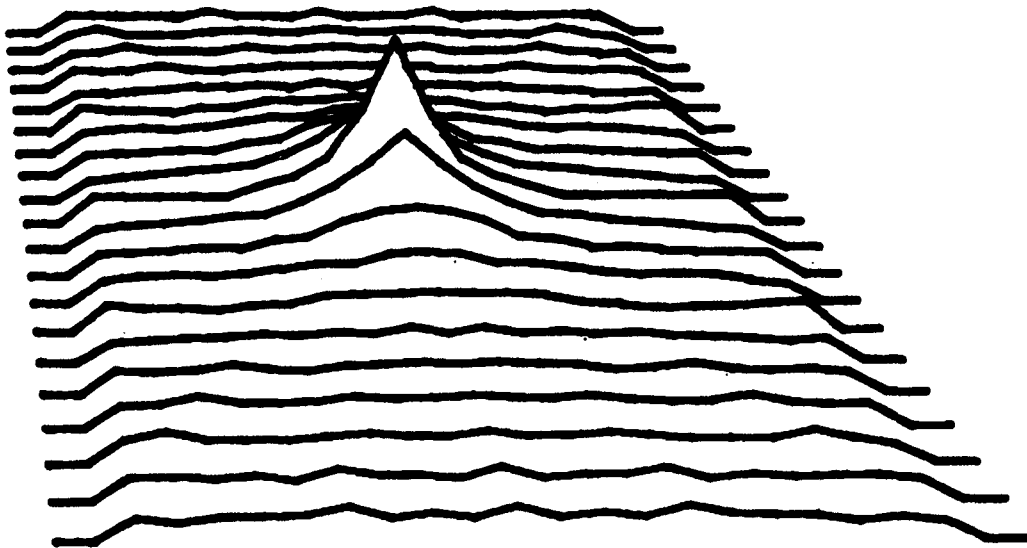
Figure 5-15. Perspective plot of point spread function (PSF). Reconstruction of centrally-located point scatterer within 16 transducer array. 20 × 20 pixel region shown.

Finally, the other image processing technique experimented with was histogram equalization [93],[94]. This technique involves creating a histogram of the gray scale values in the given image (e.g. see Figure 5-16). Such a histogram approximates the probability distribution for gray value occurrence in the given image. Integrating the histogram results in a cumulative distribution function (Figure 5-17) which is then used to reassign gray amplitudes by the transform relation where "new gray shades" are equally spaced along the ordinate of the CDF and "old gray amplitudes" maintain their original position on the abscissa. Since the CDF is a monotonically increasing function, a 1:1 mapping of original gray amplitude to new displayed gray shade results (Figure 5-18). In this way, each gray valve in the transformed image will occur with approximately equal likelihood, as indicated by an equalized CDF with slope approximately equal to one (Figure 5-19). Histogram equalization is most
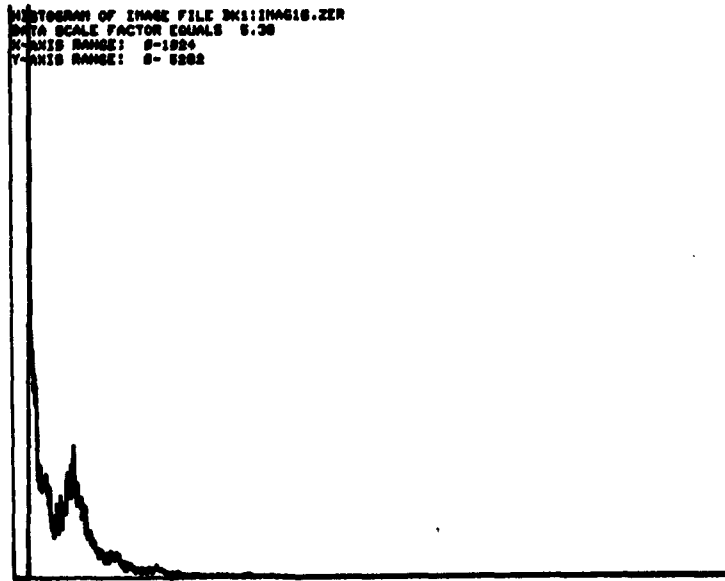
Figure 5-16. Histogram of gray scale values in a typical
PSI reconstructed image
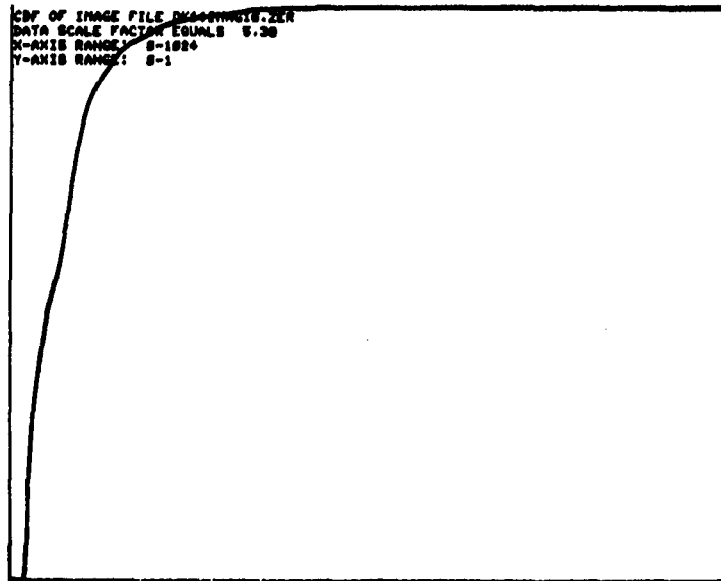
Figure 5-17. Integral of histogram in Figure 5-16 to produce a
cumulative distribution function (CDF)
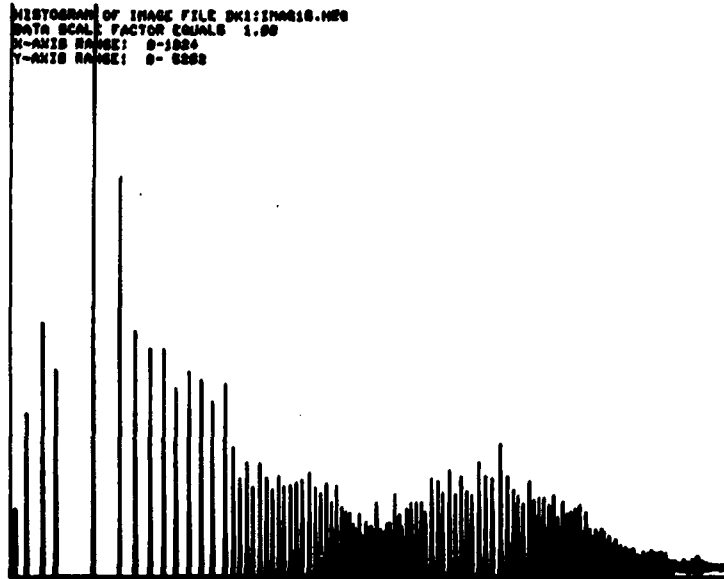
Figure 5-18. Histogram of gray values after reassignment of gray shades
shown in Figure 5-16 via CDF of Figure 5-17 and histogram
equalization technique
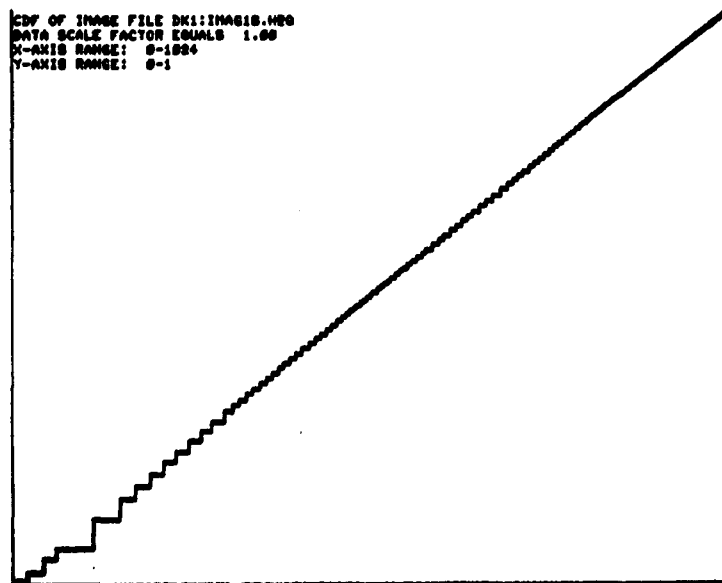
Figure 5-19. Integral of equalized histogram shown in Figure 5-18 to produce
unity slope CDF indicative of uniform gray shade distribution

appropriately applied to images where one expects a uniform distribution of gray shades. However, since this was not the case for the images examined (which include background reconstruction), the net result was enhancement of the background reconstruction and washout of the image region of interest. Although it has not yet been attempted, application of the histogram equalization technique only to the region of symmetric insonification, rather than to the entire image, should produce desired enhancement. The software used for this test is included in Appendix B (see "HISTOG.FOR").

CHAPTER VI. PSI RESULTS AND ANALYSES

A.   SIMULATED DATA

The basic ideas behind system simulation were presented in the last chapter. Simulated reconstructions utilizing the PSI technique were conducted for both solid plane and point scatterers. Two techniques were used to perform the reconstructions, namely one involving indirect ellipse generation on the PPP-11/35 and CT gray scale display (Figure 6-1) and the other involving direct ellipse generation and subsequent bi-level overlay on a Tektronix graphics terminal. As illustrated and discussed in the previous chapter, these simulated results, in conjunction with some of the early real data gathered suggested modification of the original PSI concept to exclude thru-transmission data. It should be noted that for convenience, the means of getting around the problem of thru-transmission data has been one of ignoring (i.e. zeroing out) all data records possessing a thru-transmission signal for a given transmitter. The proper technique to use, however, in future systems will be the use of time (or range) gating, to eliminate only the thru-transmission component and thus "zero out", in effect, only the thru-transmission component, and not the entire waveform.

A second major importance of simulation was to provide an appreciation for the problems associated with data calibration. It was readily observed

Figure 6-1. View of PSI reconstruction and processing hardware – PDP-11/35 and GE E-Lab CT display

through the use of a controlled (simulated) image that any miscalibration in the association of image distance (i.e. number of pixels in one array diameter) and travel time (i.e. thru-transmission time, or time for an acoustic pulse to travel a distance of one array diameter) resulted in erroneous reinforcement. Thus, even though the raw data collected would be of high quality, an erroneous calibration factor would result in an image looking like a "plate of spaghetti", since echo producing locations, as observed from various positions on the array circumference, would no longer coincide. Equation (5-4) discusses calculation of this calibration factor.

Finally, one other factor of importance determined from simulation is the existence of the "smear" factor already discussed. Although a suitable "de-smearing function" specifically tailored to the PSI technique has yet to be determined, the use of controlled images constructed with simulated data provides a tool for examining PSI smearing, particularly with respect to spatial variations.

B.   PSI RECONSTRUCTION OF REAL DATA

Having derived the initial PSI theory (Chapter IV) and performed preliminary simulations, the next step in this investigation was to reconstruct real images, obtaining data by hand from scope tracings, prior to acquisition and implementation of the transient recorder. The acoustic source consisted of the Arenberg pulsed oscillator exciting the Panametrics 5 MHz non-focused transducer. In order to get data comparable to simulated data, a test target (similar to that shown in Figure 6-2) was constructed. This object consists of three 0.064" diameter stainless steel rods, arranged in a straight line, separated by 5/8", with the middle pin being located as close to the center of rotation of the specimen platform as possible. Figure 6-3 illustrates the
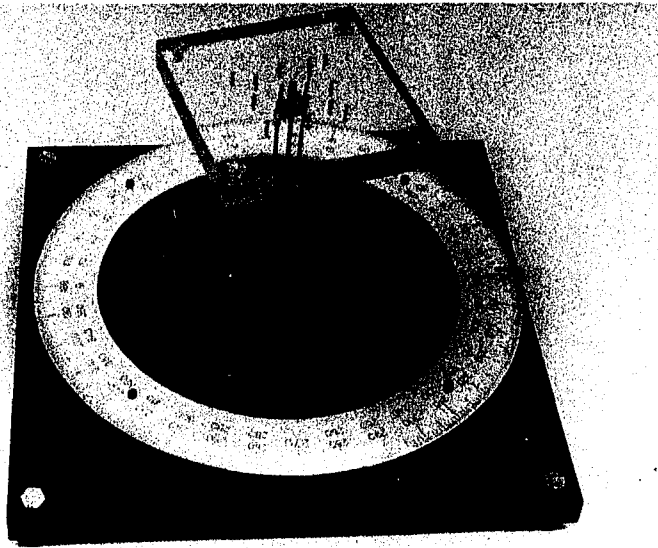
Figure 6-2. Test target comprised of three 0.064" diameter stainless steel rods shown on specimen platform
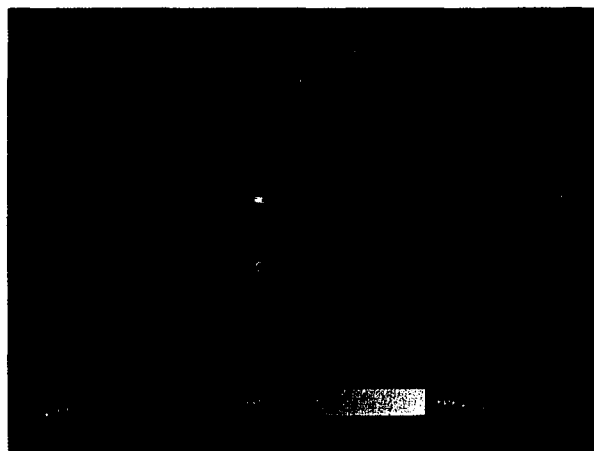
(a)
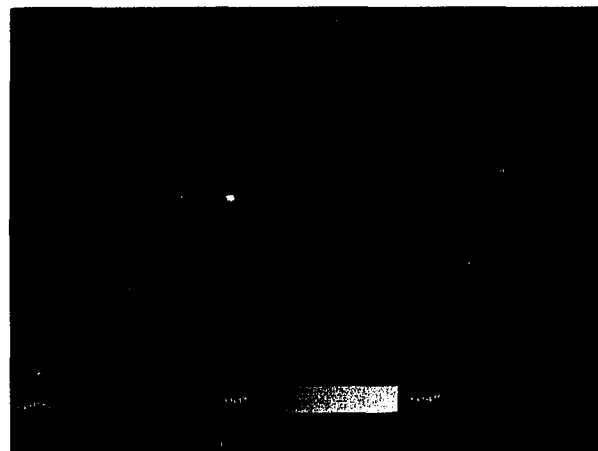
(b)
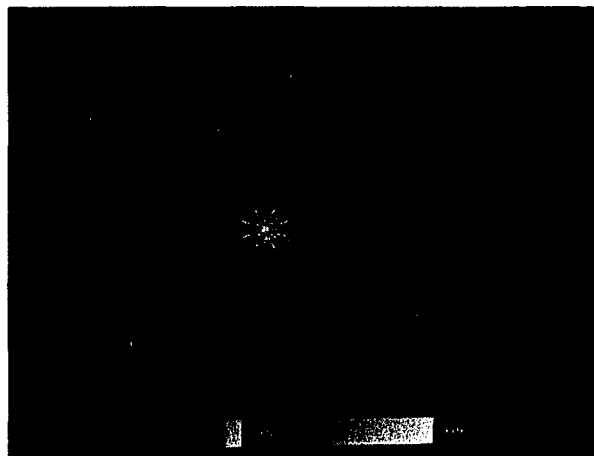
(c)
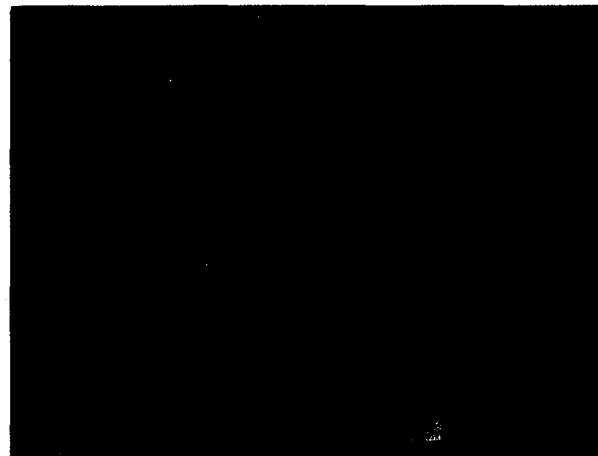
(d)

Figure 6-3. Image reconstructed from data recorded off oscilloscope traces, based on target similar to Figure 6-2. Rod separation is 5/8" each, about center

resultant image after PSI reconstruction on the CT display, whereas Figure

6-4 is the result of direct ellipse superposition on the Tektronix graphics ter-

minal. Both images are comparable in that the locations of the three rods can

be identified, as well as the fact that the center pin appears substantially

brighter than both adjacent pins. Based on the Panametric characterization

data of Appendix C, it is recalled that the output beam diameter is approxi-

mately one-half inch, resulting in an active imaging region of approximately

the same diameter. Thus, with 5/8" spacings about the center pin, this rod

target would require an active imaging diameter of no less than 1.25 inches.

So, the fact that both outer pins are beyond the uniform region of insonifica-

tion, results in their lesser acoustic coverage, as compared with that for the

center pin (which is insonified once for every transmitted pulse). Based on

this result, it was determined that the object to be imaged must lie with the

region of uniform insonification of the "straight beam" transducer (or region

of symmetric insonification for the fan beam probe) if quantitative results are

to be obtained. It is reiterated that this investigation is not designed to develop

a quantitative image, due to both hardware limitations (present inability to

adequately cover the required dynamic range) and the fact that a more exact

theory as to the phenomenon of false intersections must be developed. Figure

6-3 clearly illustrates the nature of the false intersection. It is noted that for

the symmetric transducer array and target, the ambiguous reinforcement ex-

hibits similar symmetry in addition to spatial variance. The imaging of the

single, centrally-located rod used in this target has been found to be a useful

object to image for purposes of equipment alignment and calibration. For such

a case, if an image does reconstruct as a small bright point or ring located at

the center of the imaged area, one immediately knows that a calibration or

GENERAL ⚙ ELECTRIC

<u>Real data:</u> 3 stainless steel rods, 0.064'' dia., 5/8'' separation   <u>Date:</u> 1/8/78

Transducer ring radius 5.15'';   8 transducer ring

36 ellipse families, 320 pts./ellipse, 3 ellipses per T/R pair, 108 ellipses total

Calibration: 176.0 μsec equals 320 picture units; 1 picture unit = 0.0820 cm
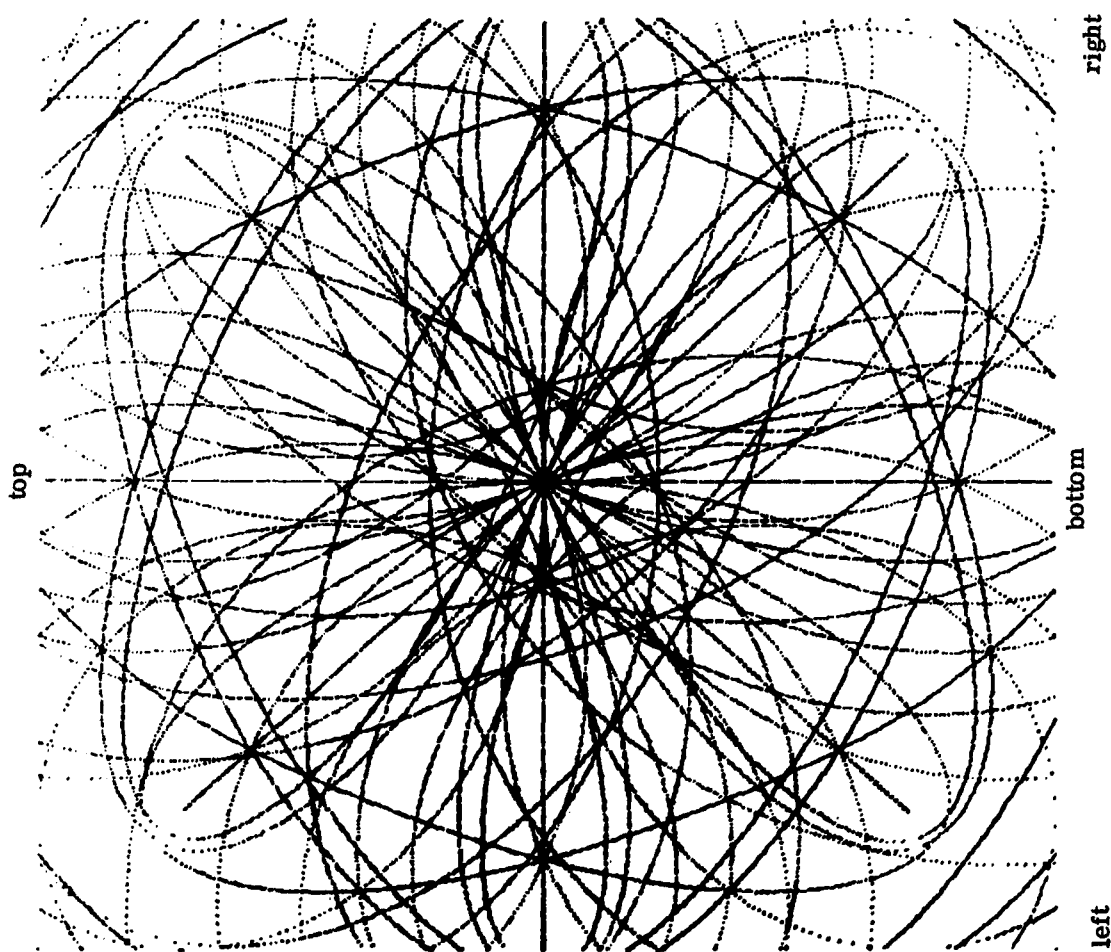
Figure 6-4.   Image reconstructed on Tektronix graphics display using same
data as Figure 6-3

alignment error exists. Relative target motion or an error in transducer placement will also result in a poorly reconstructed image.

In an attempt to image objects more like those encountered in medical systems, the Plexiglas triangle target shown in Figure 6-5 was constructed. Each leg of the triangular cross-section is approximately 1/2". Plexiglas was chosen as a preliminary target since its acoustic impedance $(3.1 \times 10^5 \text{g/cm}^2\text{-sec})$ is such that the echoes obtained are of relatively limited dynamic range. Plexiglas, however, is rather specular with respect to ultrasound and so results in "hit and miss" data when only a few receiving transducers are used. Figure 6-6 illustrates this point via the reconstructed images of the plexiglass triangle based on both eight and sixteen straight beam (i.e. Panametrics, 5 MHz) transducer array simulations. Referring especially to the narrow gray scale windowed version of each photo pair, it can readily be seen how much better coverage is obtained with the sixteen transducer array, as opposed to the eight transducer situation. The sixteen transducer array has the potential for observing scattering behavior for almost four times as many positions as for the eight transducer case. In addition to better object coverage is the fact that the more transmit/receive (T/R) pairs incorporated into a given image, the less will be the influence of background ellipse construction and false intersections in particular, on the final image. As discussed in Chapter IV, presumably each T/R pair will contribute information causing ellipses to intersect in a highly structured, predictable manner at points of true echo origin. On the other hand, depending on array and/or specimen symmetry, false intersections will tend to reinforce each other in a comparatively random fashion, as in general, one false intersection will not exactly overlay another. Although a rigorous mathematical proof has yet to be achieved, an intuitive
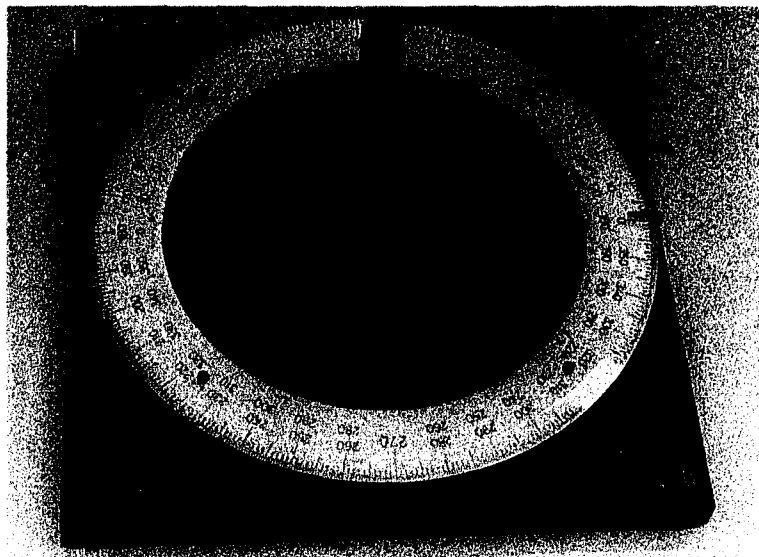
Figure 6-5. Plexiglass triangle target on specimen platform

BROAD
GRAY SCALE

NARROW
GRAY SCALE

16-TRANSDUCER
SCAN

8-TRANSDUCER
SCAN

PLEXIGLASS TRIANGLE TARGET
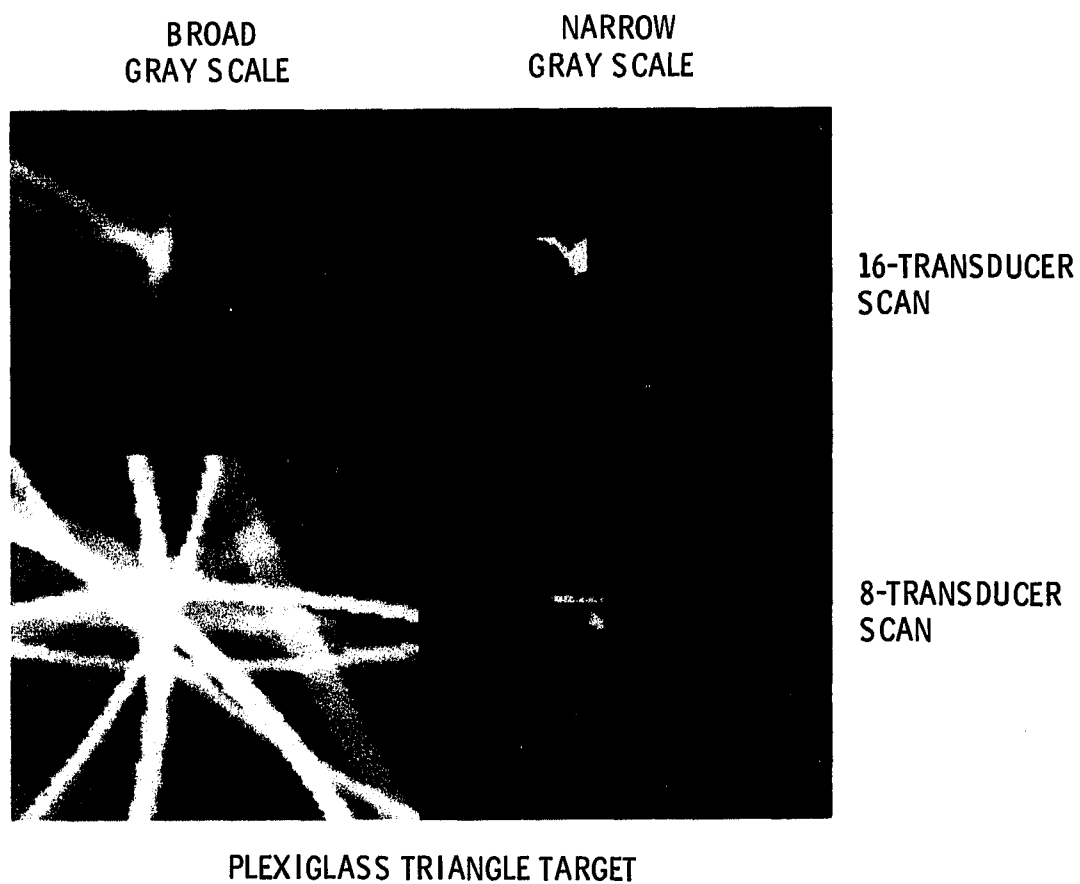
Figure 6-6. Plexiglass triangle image reconstruction for sixteen and eight
transducer scans. Central 80 × 80 pixel region shown in each
case

feel for this situation may be obtained from examination of the images reconstructed on the Tektronix graphics display (Figures 5-3 and 6-4).

In comparing the reconstructed image to the original object with respect to both Figures 6-5 and 6-6, as well as the remaining data to be presented in this paper, the geometric conventions of a standard Cartesian plane have been followed. Thus, the zero degree reference line in both the image and specimen is that line looking in from the right at the center of the array, and perpendicular to the vertical margin of the printed page. At this point it should be pointed out that most of the reconstructed images presented will only consist of the central eighty pixel square region of the full 320×320 pixel image. Since, as already mentioned, the 320×320 element image region corresponds to the entire array size and not just the symmetric imaging region (presently located within the 80 pixel square region), it has not been of value to perform any of the more recent reconstructions for much beyond the specified symmetric acoustic region. (Presently, reconstruction of the central eighty pixel square region takes one half hour and two hours for eight and sixteen transducer arrays, respectively. Disc storage required is 203 blocks (a full eighty lines of image are stored with those values outside of the central eighty pixels on a line being set equal to zero gray level). A full screen reconstruction, 320 pixels square, requires approximately four and fifteen hours to reconstruct images based on eight and sixteen transducer arrays, respectively. (Required disc storage for the image is 803 blocks.) For purposes of general illustration, Figure 6-7 shows one of the earlier full screen reconstructions (with broad gray scale windowing) of the plexiglass triangle target imaged with a sixteen transducer straight beam array. As described for the simulated images

Figure 6-7. Full 320 × 320 pixel reconstruction of plexiglass triangle illus-
trating background reconstruction and potential artifacts

presented earlier, the bright dots circularly disposed around the image periph-

ery represent transducer locations. (The transducer at 0° normally shows up

only very dimly due to raster timing as the electron beam jumps from the right

to the left hand side of the screen. The transducers at 180° and 270° fall off

the screen by one pixel. Both the "x" and "y" axes of the display are 320

elements long, while the reconstruction mathematics is based on axes ranging

from -160 to +160 (with the zero value in the middle, making a total of 321

points). Since the image scan begins at the top right of the screen, the 321st

point reached on both axes, falls off the display. As a result, only fourteen

transducers should be visible for the full screen display of a sixteen transducer

simulation. An eighty pixel square reconstruction should only indicate the

transducer number one, located at 0°. Figure 6-7 is instructive in that two

types of reconstruction artifact already discussed are clearly shown, namely

thru-transmission and noise reconstruction. Thru-transmissions, if not

removed from the data, reconstruct as the shaded elliptical regions beginning and ending on transducer vertices and passing over (degrading) the desired image. Noise, in this case, a relatively long duration burst inadvertently picked up during acoustic data acquisition by the transient recorder, is illustrated by the wide, relatively dark gray ellipse constructed in the upper right portion of the image. As this ellipse does not pass through the active imaging region, it can automatically be characterized as noise (based on simple range gating considerations).

In the early going, attempts were made at adapting X-ray CT de-smearing techniques to the similar smearing encountered with PSI reconstruction. Figure 6-8 illustrates the results obtained for application to the eight transducer scan of Figure 6-6. The top image pair demonstrates the validity of the deconvolution algorithm used by reacquiring the original image, after impulse convolution. The lower image pair demonstrates the result of deconvolution using a typical function (the spatial domain waveform of Figure 4-14(b)) used in X-ray CT. As discussed in Chapter IV, and now illustrated in Figure 6-8, the X-ray de-smearing function tends to wash out the PSI image. This occurrence is probably due to the fact that X-ray deconvolution is based on smearing due to an infinite number of straight line intersections. Such an assumption would be somewhat reasonable for a PSI array of on the order of one hundred transducers or more.

While on the topic of image de-smearing, attempts were also made to use the technique of inverse filtering, already discussed, via the FFT algorithms listed in Appendix B. The procedure involved formation of the inverse filter (i.e. de-smearing) function by dividing the two dimensional (2D) FFT of a

BROAD
GRAY SCALE

NARROW
GRAY SCALE

158
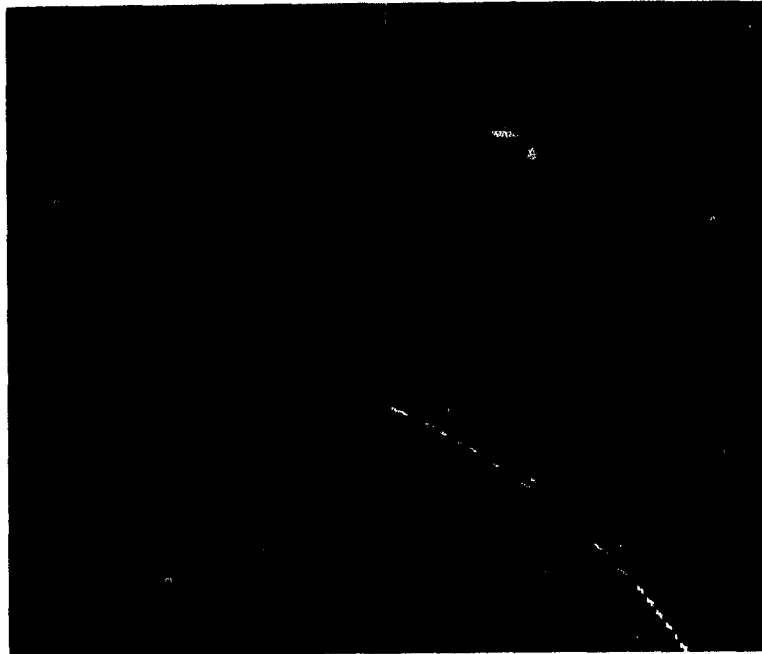
IMPULSE
DECONVOLUTION

DECONVOLUTION WITH CT
DE-SMEARING FUNCTION

PLEXIGLASS TRIANGLE TARGET

Figure 6-8. Deconvolution of eight transducer plexiglass triangle reconstruction

reconstructed single point (located at center of transducer array) image by

the 2D FFT of the original (i.e. non-reconstructed) image of the same point.

Dividing the resultant filter function into the 2D FFT of a given reconstructed

image, followed by taking the inverse transform, should produce the desired

sharp image. Such was not the case, however, most probably due to a require-

ment for a spatially varying inverse filter or deconvolution function. Although

a separate intensive study to determine the exact PSI de-smearing required is

beyond the scope of this investigation, the basic groundwork has now been laid

for such a study.

In order to image an object with presumably minimal dynamic range but

with substantially more scattering than the plexiglass triangle, a target con-

sisting of a transistor heat sink mounted on a 1/4" diameter nylon rod was

used (Figure 6-9). Figure 6-10 is the reconstructed image using only an eight
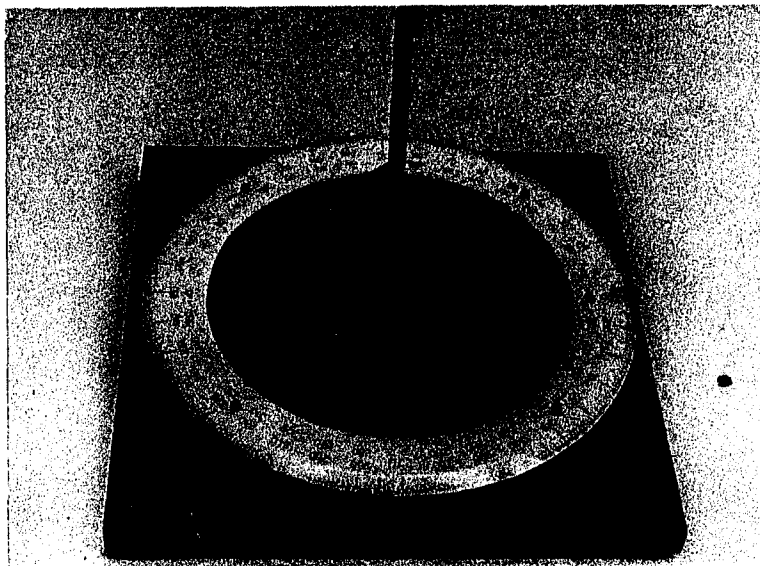
Figure 6-9. Target comprised of transistor heat sink mounted on 1/4"
diameter nylon rod
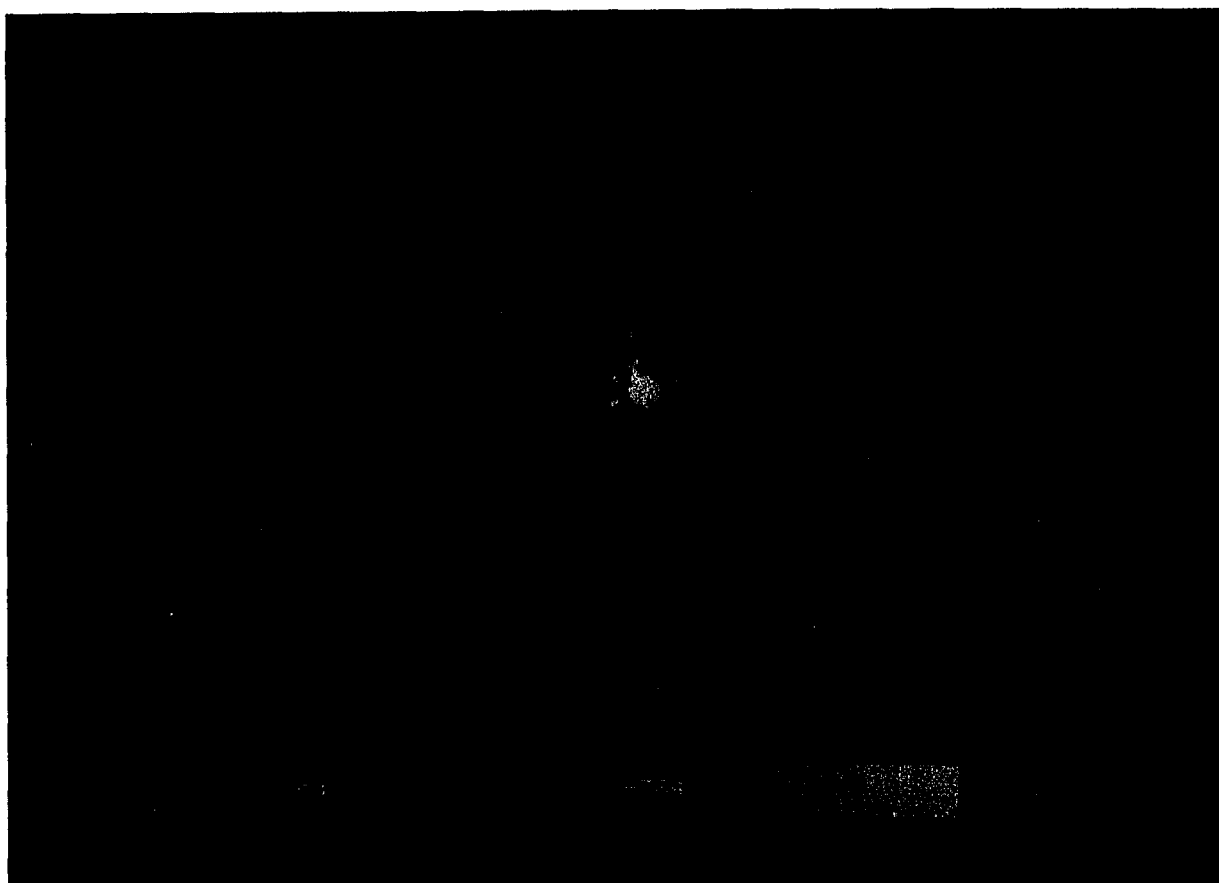
Figure 6-10. Reconstructed image of heat sink shown in Figure 6-9

transducer array simulation. All but three of the ten heat sink flanges are clearly visible (assuming good quality printed reproduction of the original image). As demonstrated with the plexiglass triangle target, an enlarged array is required to show the remaining flanges. However, it should be noted that in this case, the use of a sixteen transducer array produced an image quite comparable to that obtained with the eight transducer array. Apparently, the geometry of the heat sink in conjunction with other factors such as transducer radiation pattern, require that an even greater number of transducers is required to define the entire heat sink target.

The foregoing data provided strong encouragement (particularly since no attempt has been made to create a "tuned" system) as to the potential success of PSI as a general purpose imaging system. The two remaining tasks for this initial investigation were (i) the use of a fan beam probe and (ii) the demonstration of PSI on biological tissue. As discussed earlier, a pair of experimental 5 MHz, approximately 40° 3 dB fan beam transducers (fully waterproof) were built by KB Aerotech. Initial testing of the transducers demonstrated unsatisfactory acoustic performance, in addition to the fact that the front epoxy quarter-wave matching layer on each transducer softened, blistered and peeled on extended immersion in water. Furthermore, transducer characterization by the Bureau of Radiological Health (data presented in Appendix C) indicated electrode delamination from the ceramic on one of the transducers. After subsequent repair and replacement of the quarter-wave layer with a thin epoxy layer, blistering and peeling again resulted. Replacement of the epoxy with a silver lacquer coating also resulted in blistering and peeling. As all other transducers tested in a similar fashion failed to exhibit such deterioration, the present hypothesis is that some defect in the ceramic

material is preventing proper bonding and/or curing. In any case, an attempt was finally made to utilize the fan beam transducers,even with the blistered and peeled front silver lacquer coating,on both the objects previously imaged with the straight beam as well as some representative biological objects.

In short, some minimally recognizable results were obtained, as will be presented shortly. However, strong sidelobe interference was noted along with a somewhat irregular beam pattern. Although such performance might be directly a product of this new type of transducer design, the resultant irregularities on the transducer face are most likely highly contributory factors as well. As to be expected based on design considerations, the fan beam sensitivity and received output was quite a bit below the level of that achieved with standard transducers (e.g. the Panametrics pair first used). Furthermore, what mimicked as gross errors in hardware alignment was possibly due to range errors resulting from the potential problem of receiving a plane wavefront with a curved ceramic (see Figure 4-16 and associated discussion). As a result of the fan beam physical defects, an extended imaging program with them was not carried out. Rather, it was decided that some trial data be taken with the fan beams, followed by temporary use of the original straight beam transducers to complete the present investigation. A new fan beam design would then be attempted for future PSI investigation.

The following data were obtained using the fan beam transducers. Although some recognizable results were obtained, it appeared that, aside from the unpredictable influence of peeled and blistered silver lacquer on the face of the ceramic, the lower sensitivity, curved receiving face and strong sidelobes should all contribute to a degraded image. It should be mentioned that whenever possible, an eight transducer ring was simulated rather that, for example, a sixteen or more transducer ring, in order to accommodate the

amount of dedicated computer time available.

Figure 6-11 depicts the cross-sectional (transverse) reconstructed view of a single 0.064" diameter stainless steel rod as imaged by an eight fan beam array. It was noticed during data collection that the target exhibited a certain amount of play in its mounting hole and would exhibit slight positional shifting during specimen platform rotation. Also, it was noted that due to the thinness of the rod, it had a small degree of curvature, causing various echo times to be recorded throughout the beam's thickness. As a result, since this rod is being treated essentially as a point-scatterer located at the center of the array, rather than get a small point image as expected, the donut shape is obtained, shown in the lower portion of Figure 6-11. Due to the large acoustic impedance mismatch between the water ($\sim$1.5 g/cm^2 - sec $\times$ 10^5) and stainless steel (45.4 g/cm^2 - sec $\times$ 10^5), one would not expect to see appreciable internal echoes from the rod. An additional factor which should be pointed out is that a similar image appearance as obtained in Figure 6-11 may also be expected if the transducer array center and specimen platform center are not the same. Similarly, their centers of rotation must be true, a factor which does not exactly hold for the specimen table (primarily) due to the unavailability of funds to support a precisely machined apparatus. Much more precise scanning hardware must be obtained before any reasonable resolution determination can be made. Imaging of this single rod, however, aside from a visual check, has been the only means of determining whether or not the PSI apparatus is in reasonable alignment.

Figure 6-12 is an eight fan beam reconstruction of a 1/4" steel rod located at the center of the array, shown for broad and narrow gray scale assignments as indicated. This target was held firmly in place, and so far as
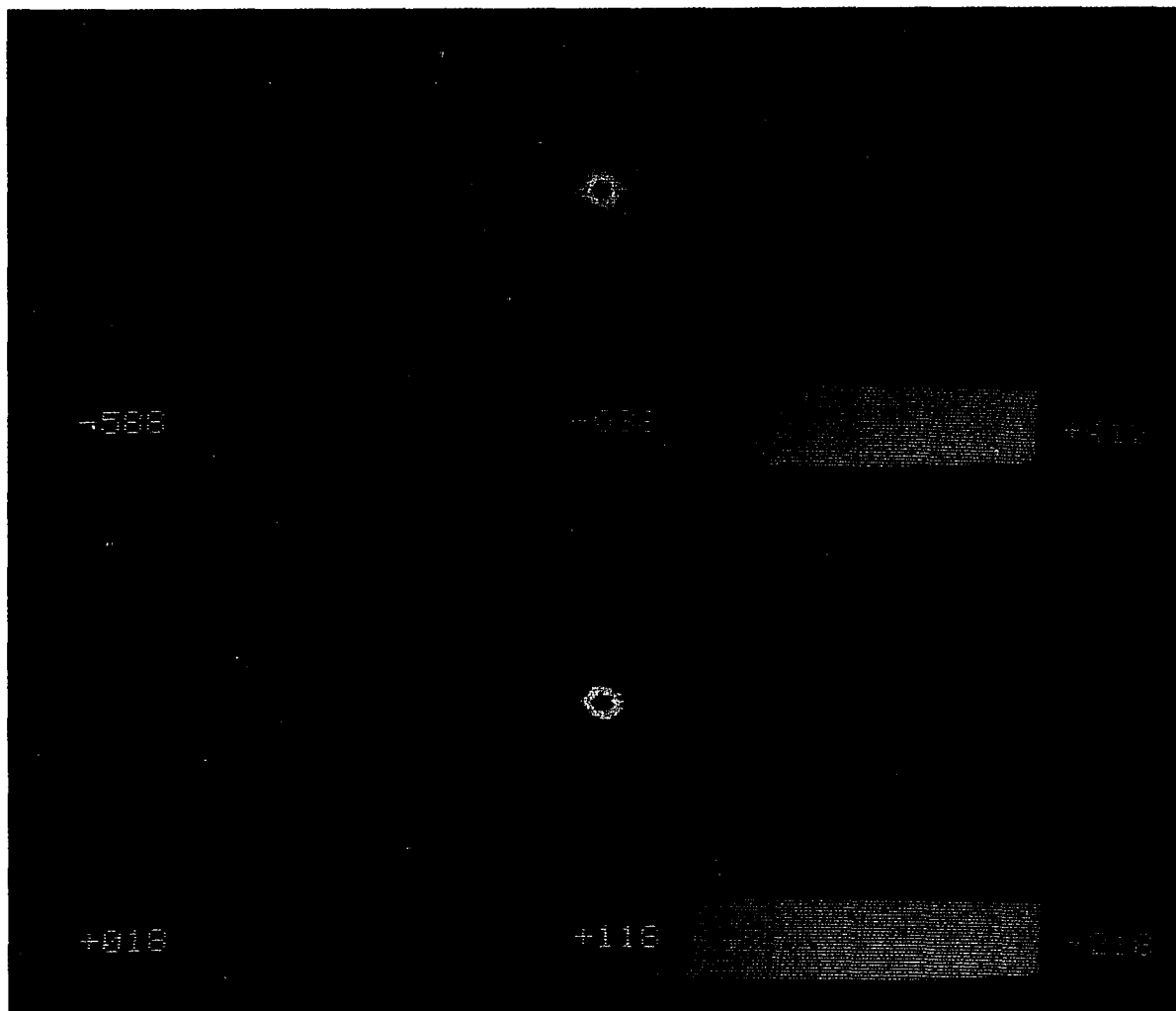
Figure 6-11. Eight fan beam reconstructed transverse image of a 0.064"
diameter stainless steel rod located at center of array
(top - broad gray scale, bottom - narrower gray scale)
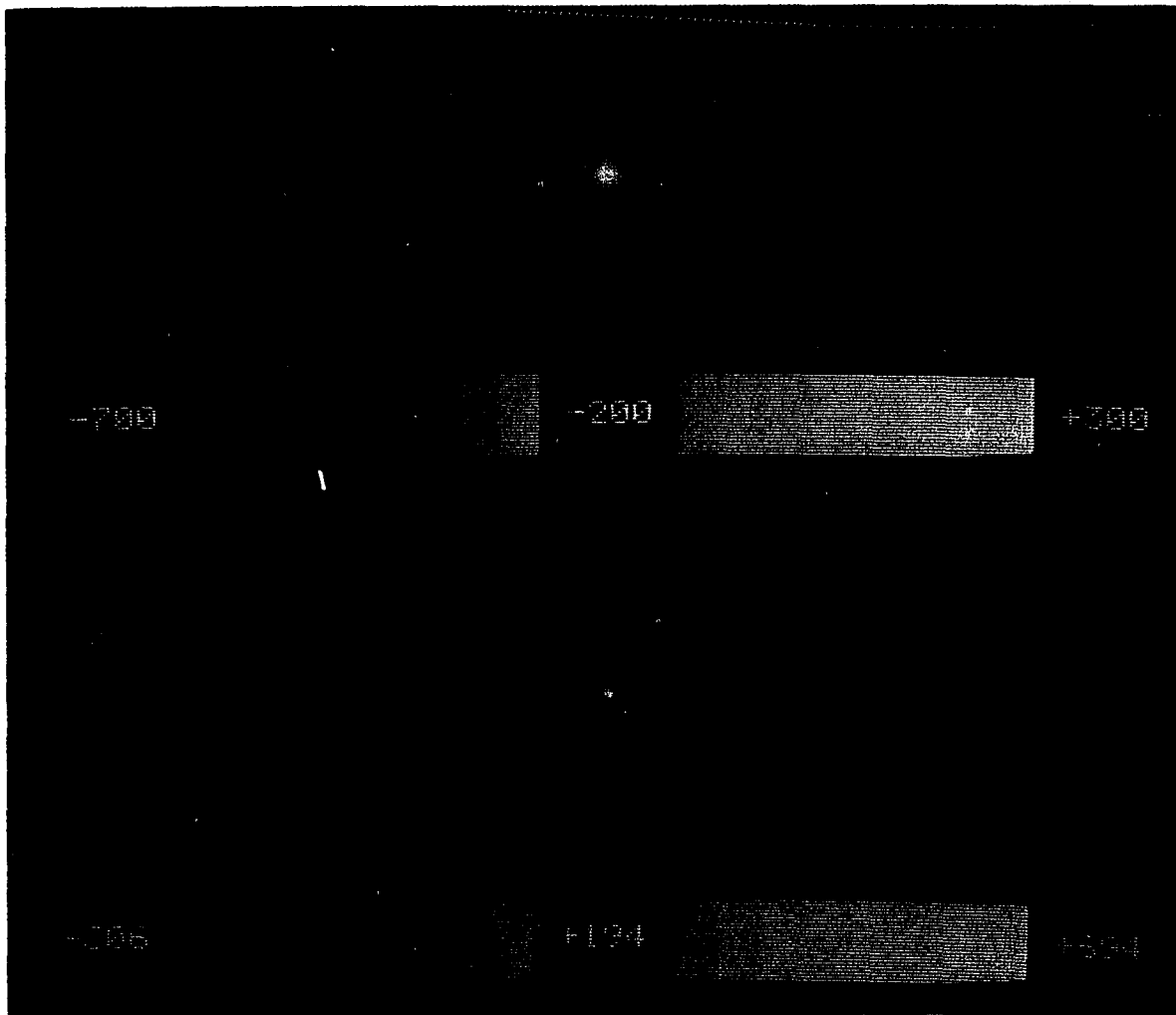
Figure 6-12. Eight fan beam reconstructed transverse image of a 1/4"
diameter steel rod located at center of array

could be determined was perfectly straight. This more controlled situation

resulted in an image more like that expected. Ideally, a 1/4" diameter in-

finitely thin ring would be expected. This situation presumes relatively little

acoustic transmission into the rod due to the large water/steel impedance

mismatch. However, the acoustic pulse width (and inadvertent pulse spreading)

will tend to change the infinitely thin outer contour of the rod to a contour band

extending towards the rod's center. This effect, in conjunction with the usual

reconstructing smearing will tend to fill in the rod's transverse outline as

shown in the figure. These "filling-in" effects are of greater significance for

objects this small.

Next, a target consisting of three 0.064" diameter stainless steel rods,

one rod at the center of the array and the other two rods 5/16" away from the

center. The rods are situated on a line passing through the center of the

array, making an angle of approximately twenty degrees with the horizontal.

The resultant image is shown in Figure 6-13. The actual locations of the three

rods compare with the three central dark areas of the image. Aside from the

likely causes of error mentioned earlier, a satisfactory explanation has yet to

be found for the oval appearance of each target location. However, whatever

the exact effect, such occurrence is apparently making the system 'see' an

effectively larger array diameter than was determined from direct thru-trans-

mission measurements. Figure 6-14 suggests this situation as the upper

portion of the figure was reconstructed with a PSIV02.FOR calibration factor

(CAL) of 0.985294 (as determined from direct water tank measurements)

while the lower reconstruction was performed with CAL=0.988971 (corres-

ponding to a thru-transmission time which is 0.5 μsec greater than that

measured). Using this modified calibration factor results in a somewhat

improved image. As for the foregoing images, an exact assessment of this
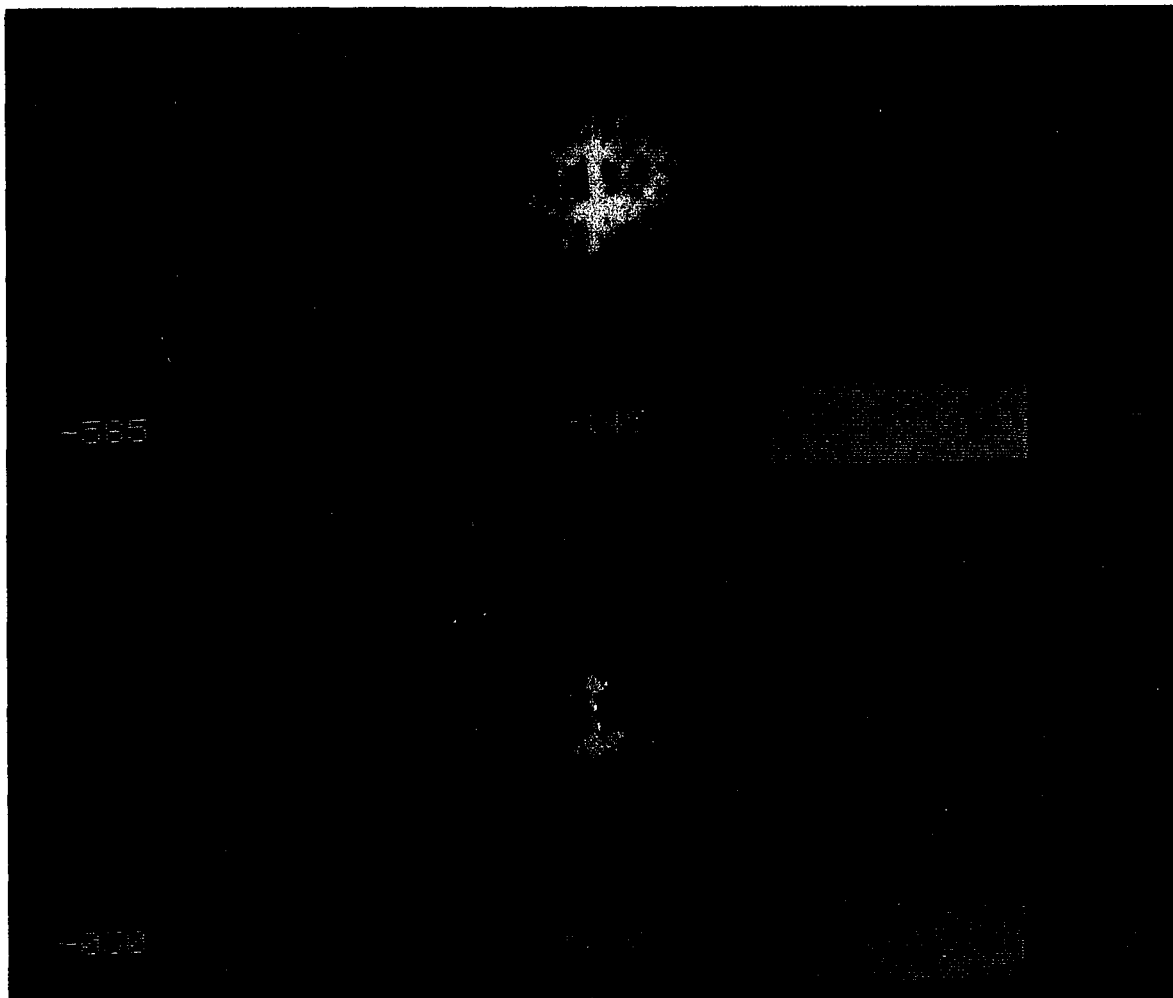
Figure 6-13. Eight fan beam scan of three co-linearly arranged 0.064"
diameter stainless steel rods separated by 5/16" about
middle pin located at center of transducer array
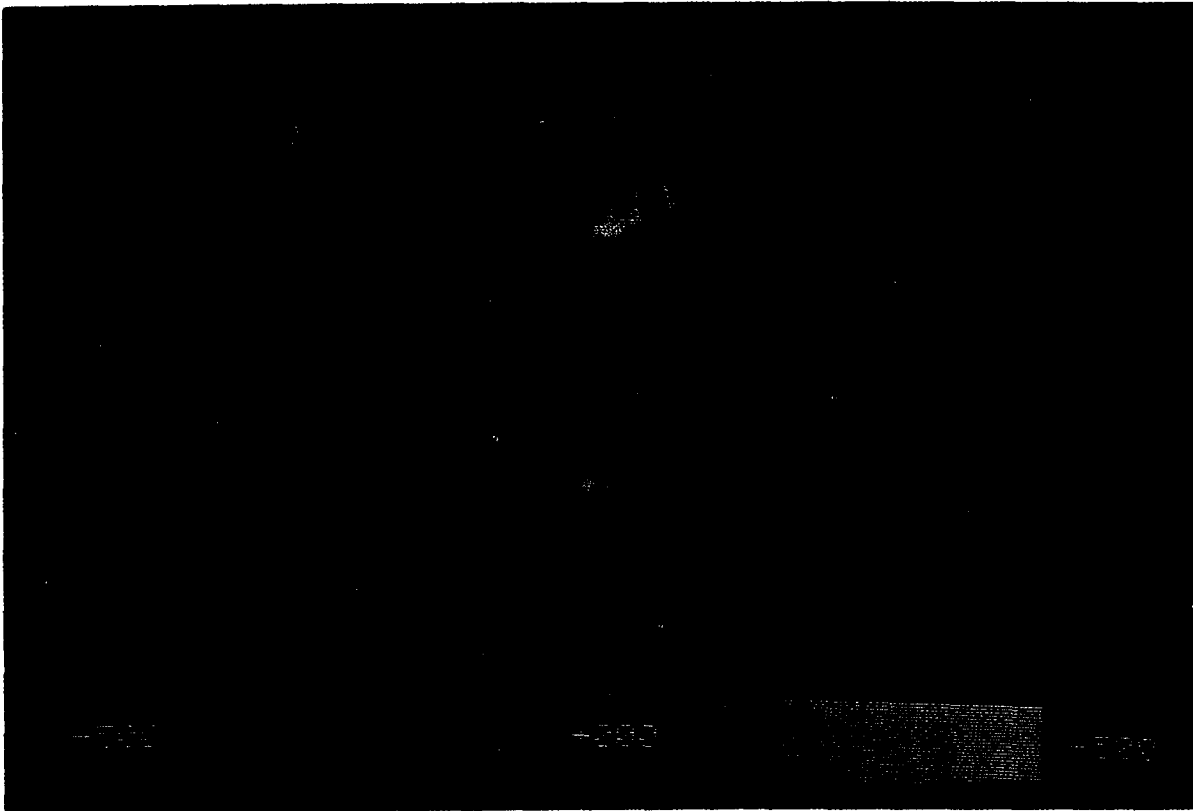
Figure 6-14. Reconstructed image obtained in Figure 6-13 (top - CAL = 0.985294) compared with image from an identical reconstruction except calibrated for a larger ring diameter (bottom - CAL = 0.987312)

problem must be deferred until a more physically sound fan beam and more precise scanning apparatus is obtained.

As a means of general illustration, Figure 6-15 shows the envelope detected transient recorder output obtained for sample scans with varying angles of reception for three stainless steel rods arranged as for Figure 6-14, except that rod spacings are now 3/16" (rod in upper right quadrant) and 9/16" (rod in lower left quadrant). When examining these waveforms, one must bear in mind that the transient recorder outputs all 8192 data samples stored in its memory (i.e. a single waveform) in twenty milliseconds. Knowing the sampling rate (in this case, 20 MHz) time intervals may be calculated accordingly. Note the quite extreme dependence of scattering angle seen by comparing the
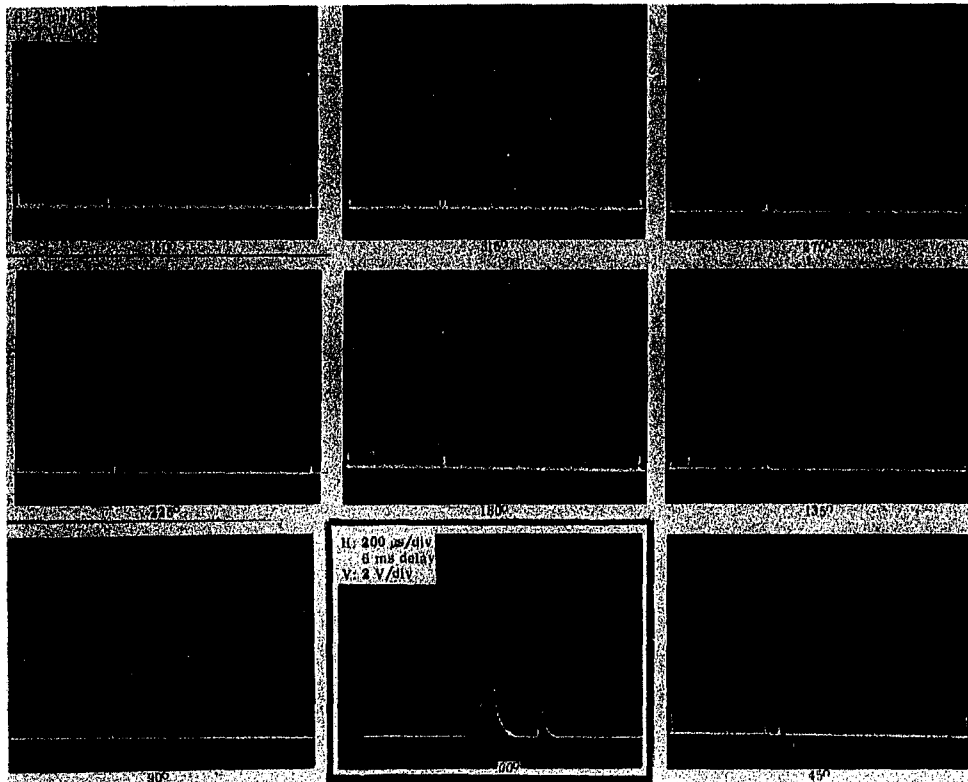
Figure 6-15. Sample envelope detected PTR output for various reception angles for fan beam scan of three 0.064" diameter rods with separations of 3/16" and 9/16"

waveforms with one another.

As a means for comparing the fan beam performance with that of the straight beam used, the Plexiglas triangle (Figure 6-16) and transistor heat sink (Figure 6-17) were scanned and can be compared with Figures 6-6 and 6-10, respectively. As far as the Plexiglas triangle is concerned, although the underlying reconstruction patterns appear to resemple one another, it appears that fan beam sensitivity may be insufficient to register the signal levels obtained with the straight beam. Whereas reconstruction from eight or sixteen Panametrics transducers did not drastically change the image (although, the greater array produced better specimen coverage), it appears
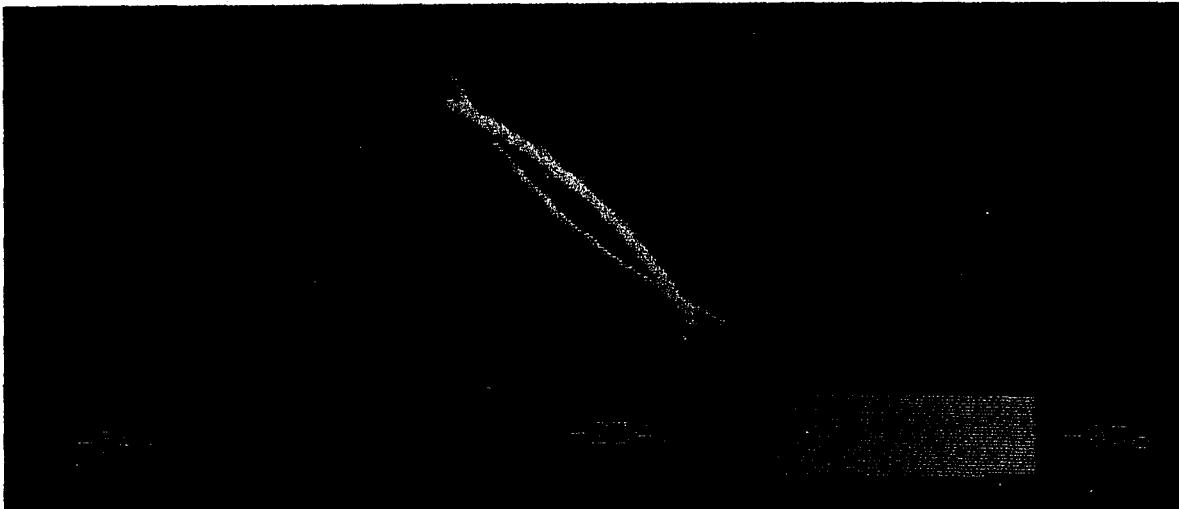
Figure 6-16. Reconstructed image of the Plexiglas triangle in Figure 6-5
using an eight fan beam array

that additional fan beam transducers might provide the additional image

reinforcement necessary. It is also possible that due to the high specularity

of the Plexiglas and different physical sizes of the fan beam and straight

beam transducers, the few fan beams used may have been situated so as to

just miss the generated schoes.

While still not as good as for the straight beam, the fan beam heat

sink reconstruction (Figure 6-17) bears some resemblance to the target

(Figure 6-9). The supporting 1/4" diameter nylon rod is brightly visible. The

heat sink flanges appear quite subdued and blurred. Again, this result, while

demonstrating a minimal performance of the fan beam suggests that the

relatively poor image is due to degraded transducer performance. Figure 6-18

shows various views of the RF scatter obtained from fan beam insonification

of the heat sink positioned at 0°, for a receiver position of 345°. Figure 6-19

depicts the PTR envelope detected signal from the heat sink for the same

specimen position but with various receiver angles.
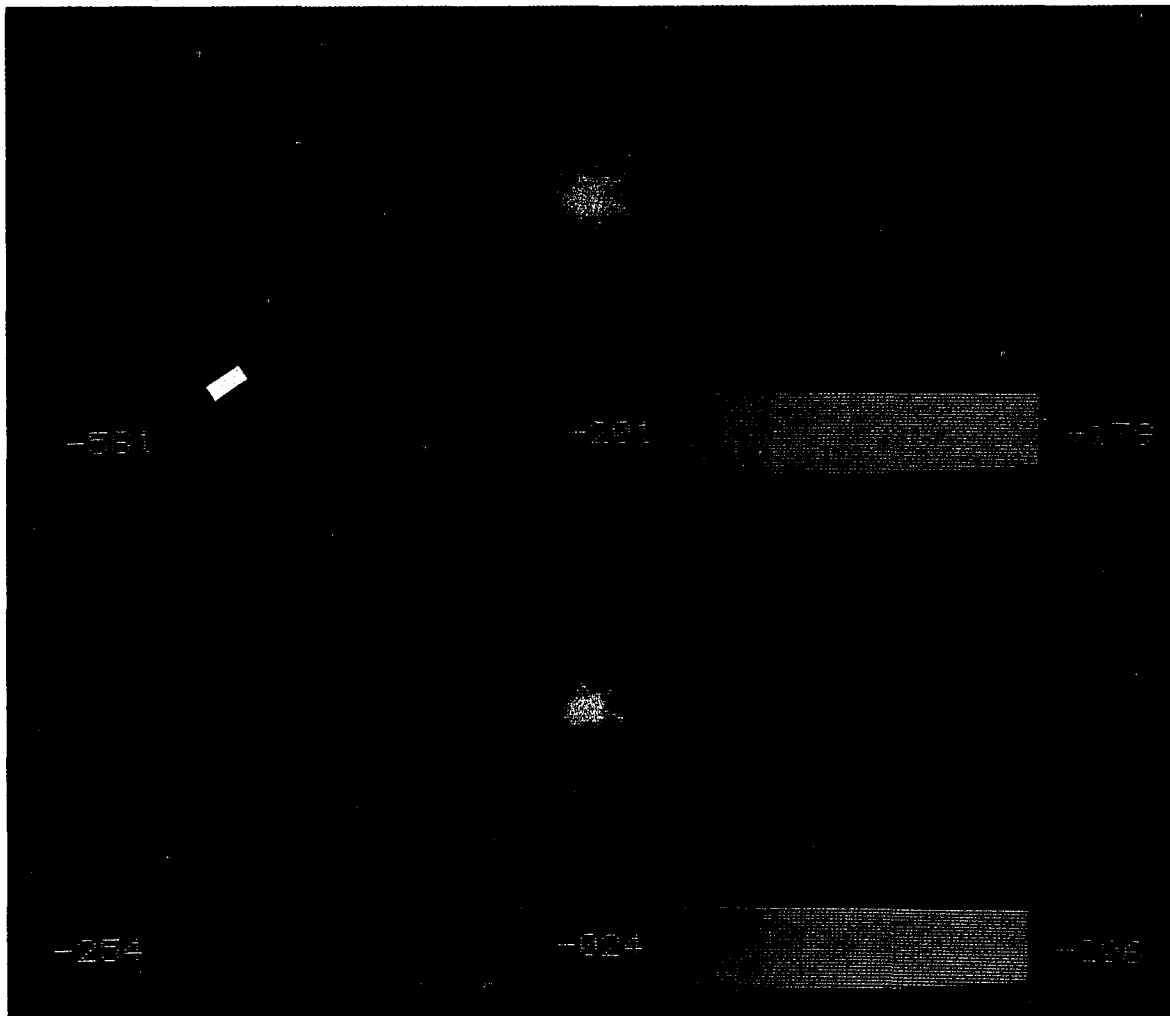
Figure 6-17. Eight fan beam transducer reconstruction of the transistor heat sink shown in Figure 6-9
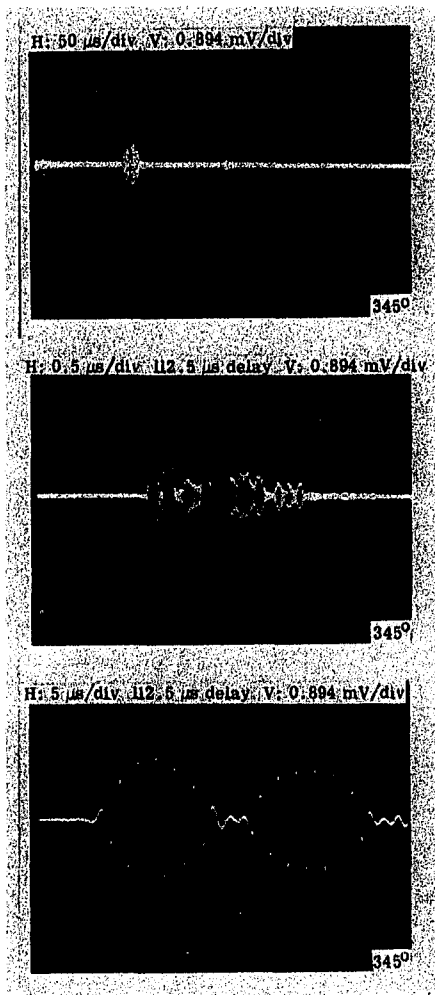
Figure 6-18. Expanded views of the RF acoustic scatter obtained from fan
beam insonification of transistor heat sink positioned at 0°.
Receiver angle is 345°.
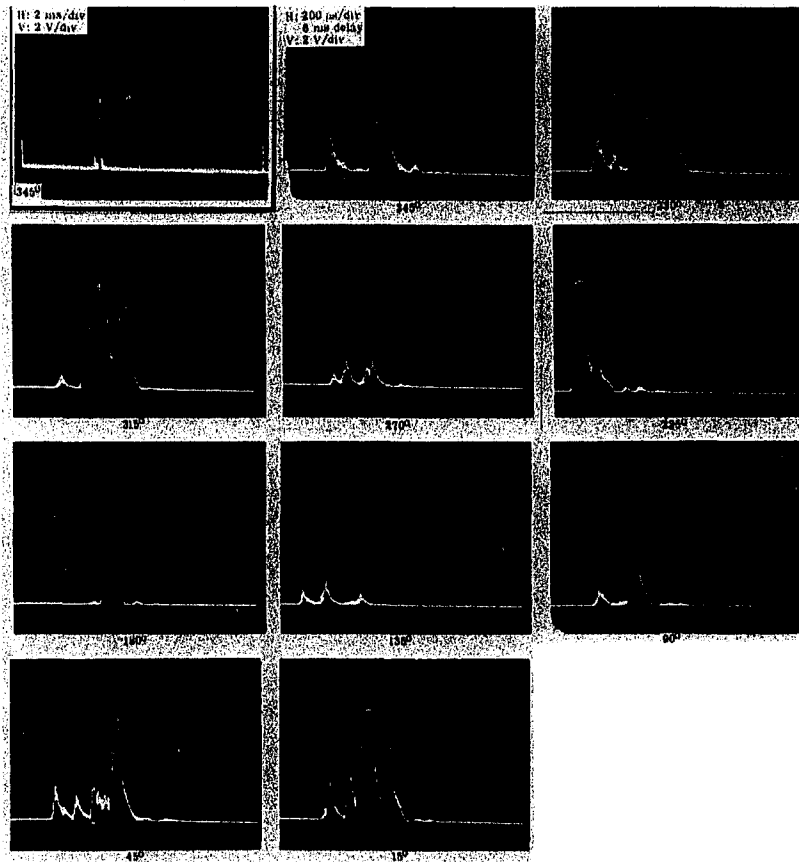
Figure 6-19. PTR envelope detected scatter obtained from fan beam
insonification of transistor heat sink positioned at 0°.
Data obtained at various receiver positions as indicated.

As a final test of the fan beam probes, two additional, more tissue-
like targets were used. The first specimen, shown in Figure 6-20 is a slab
of polyurethane gel (approximately $1.5" \times 1.75" \times 0.75"$) with six poly-
ethylene tubes (diameters ranging from about 1.5 - 4 thirty-seconds of an
inch) pushed into the polyurethane to create a cavity, such as a blood
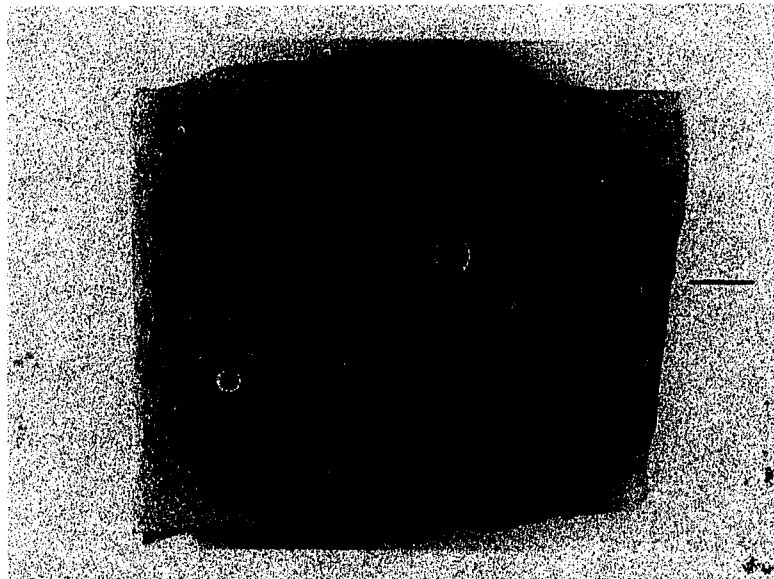
Figure 6-20. "Home-made" tissue phantom - polyurethane gel (1.5" ×
1.75" × 0.75") with six polyethylene tubes mounted on stainless
steel rod (0.064" diameter)

vessel. This target was held in place in the water tank by a 0.064" diameter

stainless steel rod located approximately at the center of the target. First,

an eight transducer scan was run, resulting in an apparently unrecognizable

image. However, in manipulating the transducers during the scanning process,

it appeared that echoes were originating off the tubes but falling between the

positions of measurement. Figure 6-21 shows the resultant sixteen transducer

image. As discussed earlier, polyerethane has an acoustic impedance similar

to that of water. Looking at the image, however, it appears that the relatively

low transmitted energy density and rather poor fan beam sensitivity combined

to permit little penetration to and/or reception from the metal rod supporting

the target at its center. Comparing the target's photograph and reconstructed

image quite carefully, the polyurethane outline is quite readily discernible.

Two of the polyethylene tubes (top left and bottom right) appear to be indicated

by the dark, outlined spots. Using some imaginative pattern recognition,
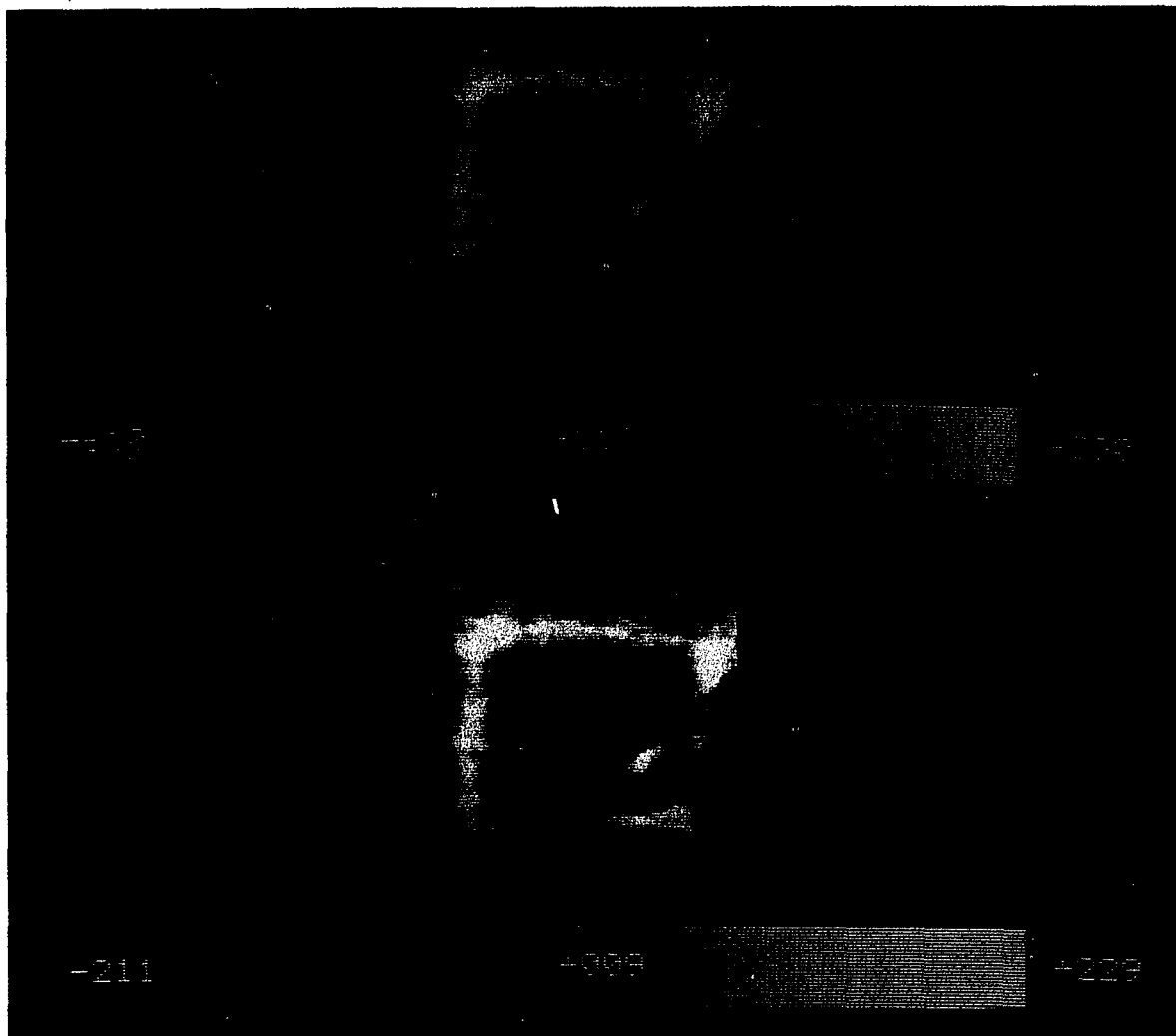
Figure 6-21. Sixteen fan beam reconstruction of target shown in
Figure 6-20 (top - broad gray scale, bottom -
narrow gray scale)

indications as to the other tubes' placement can be found. As discussed earlier, the fact that the beam possesses a finite thickness means that the image formed is the composite of all infinitely thin cross-sections encountered by the beam. As a result, unless, for this particular case, the tubes are perfectly vertical, the resultant image should indicate the tubular cross-sections as more of an elliptical region. Such appears to be the case here.

The final data attempted with the fan beam probe was an eight transducer scan of a chicken heart. The heart was oriented apex up, with a 0.064" diameter stainless steel rod passing through the heart's central vertical axis from base to apex. A full screen (320 × 320 pixel) image reconstruction was performed as shown in Figure 6-22. It appeared, however, that although echoes could be seen as originating from the outer surface of the heart, the echoes from the supporting rod were so large that they would, in general, saturate the receiving amplifier before enough gain could be obtained to view the small tissue echoes. The rod location is clearly seen in the image. An analagous circumstance exists in B-scan when one tries to image bone and tissue. As will be described towards the end of this chapter, when taking straight beam data of the chicken heart, a mounting fixture containing a horizontal pin was prepared so as to have only heart tissue in the imaging region.
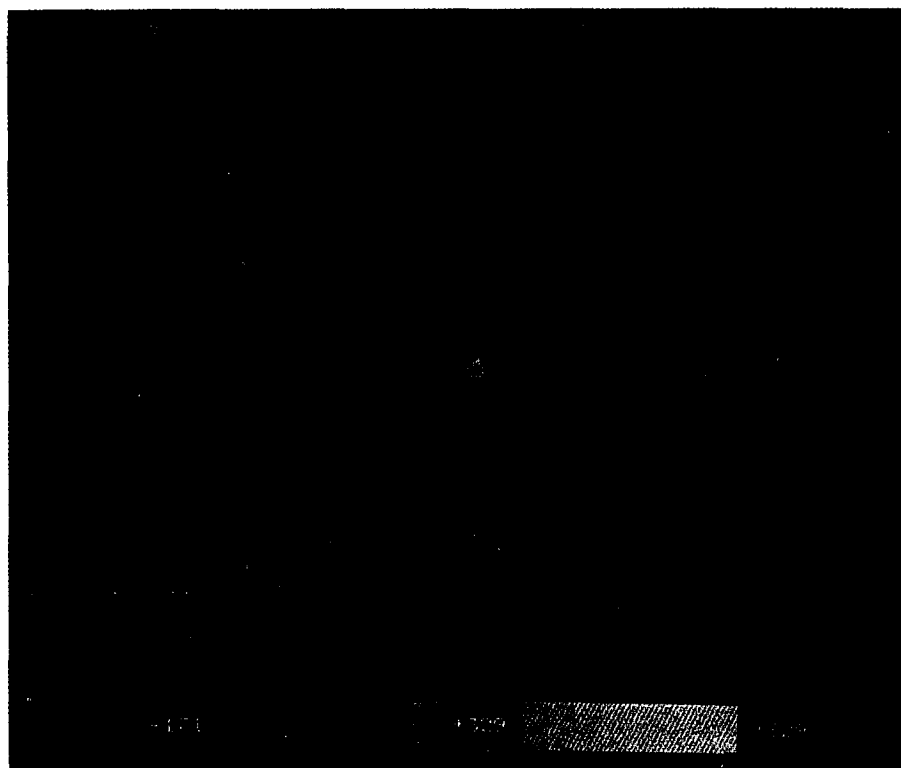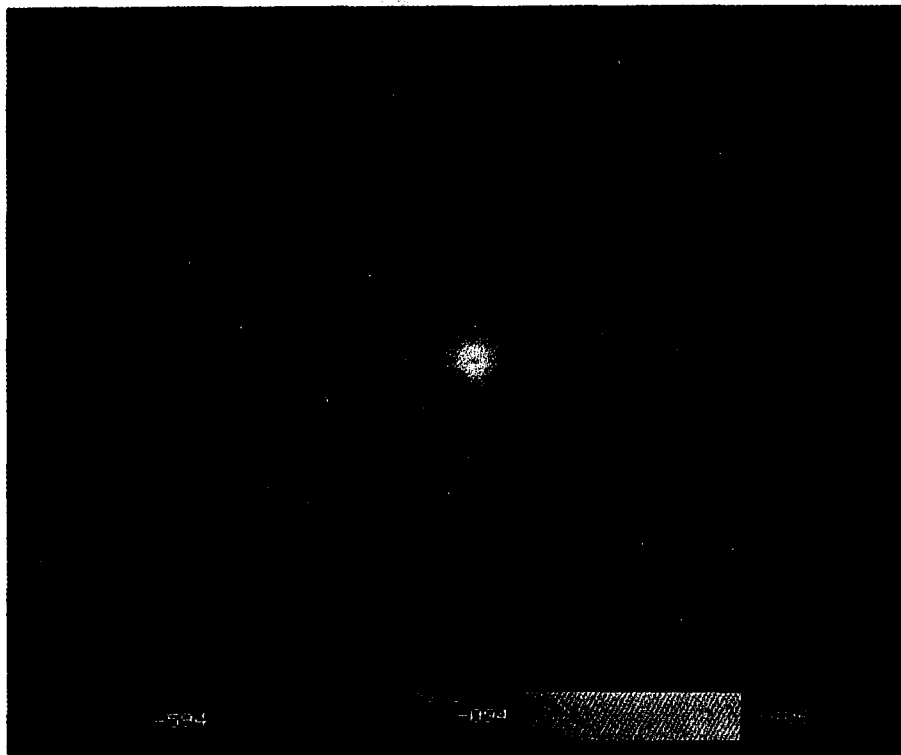
Figure 6-22. Reconstructed cross-sectional image of a chicken heart
vertically mounted on a stainless steel rod from data collected
with a simulated array of eight fan beams

As mentioned in the foregoing material, due to the difficulties experienced with the prototype fan beam transducer, only sample data was taken. The remaining data to be presented was taken using the pair of Panametrics 5 MHz, non-focused transducers described earlier. These transducers are sufficient for preliminary testing, as demonstrated at the beginning of this chapter. However, by not exhibiting a fan beam geometry, the two primary differences in imaging performance will be the resultant decreased area of uniform insonification as well as the more highly directional transducer receiving characteristic. Of course, the major advantage of the standard beam probe over the fan beam transducer, as already demonstrated, is increased sensitivity.

Thus, after placing the Panametrics transducers back into the PSI hardware, system alignment was checked by imaging the 0.064" stainless steel rod. Just as when using this target for checking fan beam alignment, the same problems of rod play and curvature, in addition to the non-true rotation of the specimen platform were present. The image of Figure 6-23 was obtained for an eight transducer scan, indicating reasonable system alignment. However, note how strong the left side of the image appears. This occurrence is probably due to asymmetric scatter from the specimen not being centered exactly in the beam.

As depicted in the upper left portion of Figure 6-24, the next object imaged was a segment of a natural sponge. The sponge, as shown, is approximately 2.25" long and 0.5" to 0.75" in diameter. The sponge was mounted on a base by a small segment of a 1/4" steel rod exposed to one end. A sixteen transducer scan was performed, insonifying the sponge approximately (as "eye-balled") through the transverse sections (1-5) indicated in the figure, with the resultant image as shown in Figures 6-25 and 6-26, for successive gray scale windowing and gray scale identification (lower portion of Figure 6-25). After imaging, the sponge was embedded in an epoxy resin (Norcast

Figure 6-23. Eight transducer Panametrics scan of 0.064" stainless steel rod located at center of simulated array used to check hardware alignment
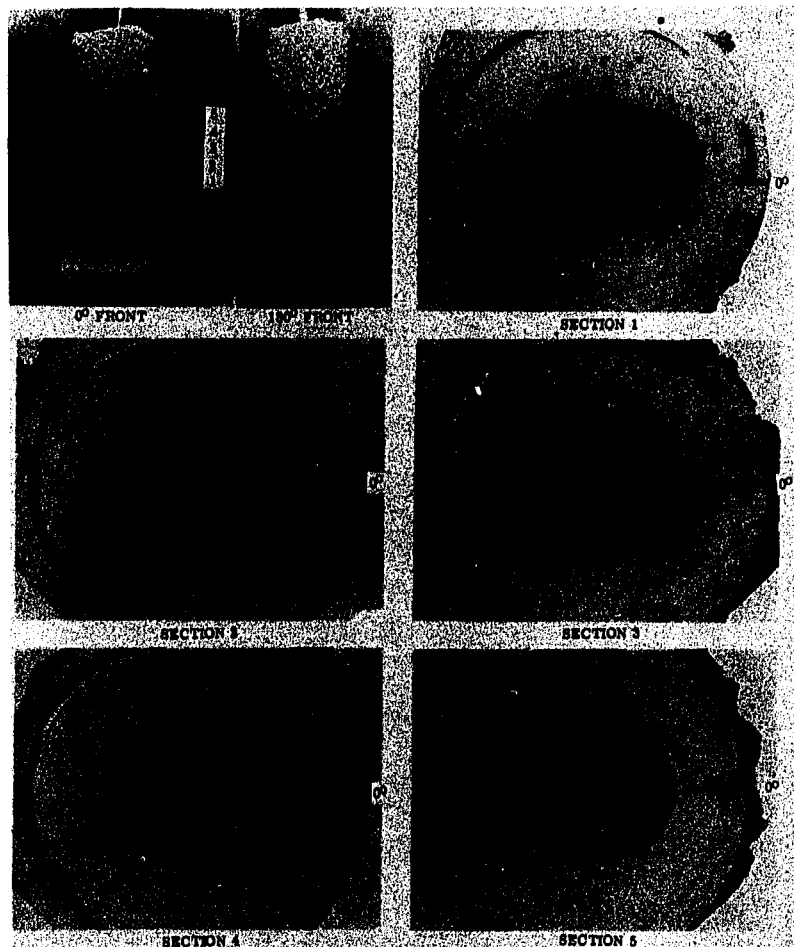
Figure 6-24. Natural sponge imaged by sixteen transducer Panametrics
array. Sponge segment shown (upper left) is approximately
2.25" long and 0.5" to 0.75" in diameter. Approximately 4 mm
thick cross-sectional views (looking from the bottom up) of
the sponge embedded in epoxy are shown. Scan orientation is
indicated.
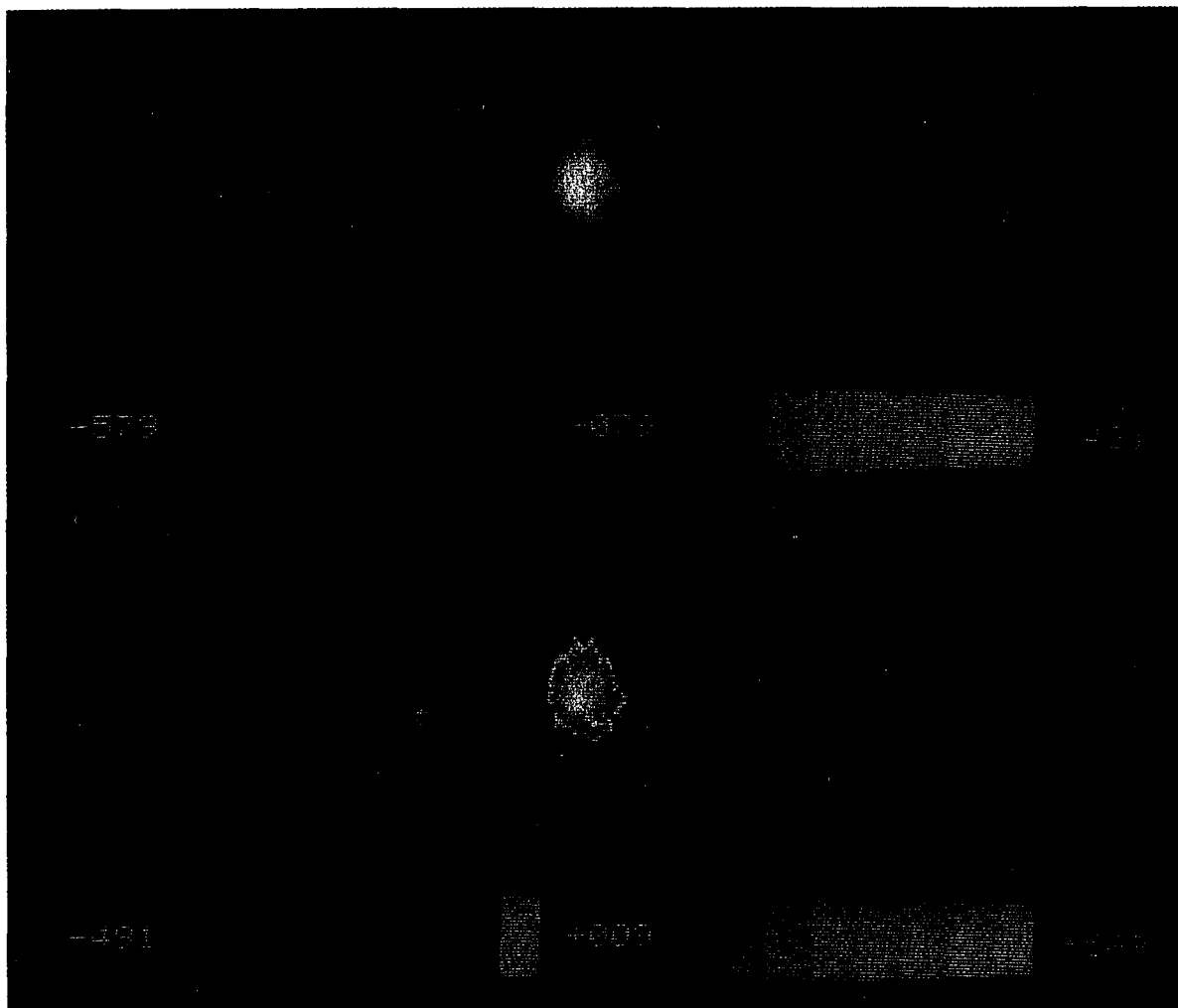
Figure 6-25. Sixteen transducer Panametrics scan of natural sponge shown
in Figure 6-24. Central 80×80 pixel region of image is shown.
Bottom image is gray scale identified to show external hole
structure of sponge
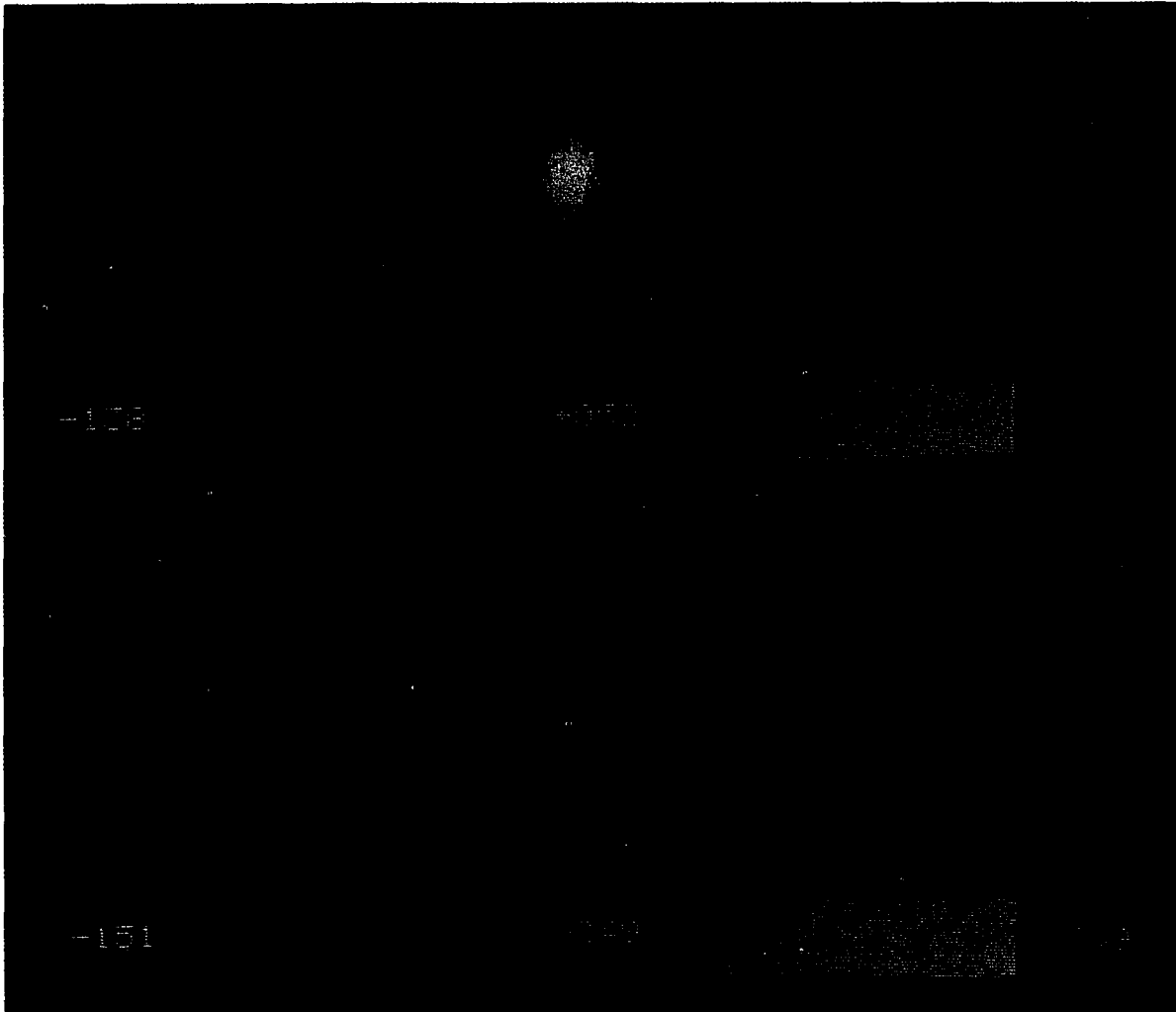
Figure 6-26. Sixteen transducer Panametrics scan of natural sponge shown
in Figure 6-24. Central 80 × 80 pixel region of image is shown.
Additional gray scale windowing from that of Figure 6-25

and Norcure) and then sectioned into approximately 4 mm thick segments as indicated in Figure 6-24. Now, in comparing the cross-sectional photos with the PSI scan, it must be emphasized that although it is tempting to compare the image with a single cross-section, the finite beam thickness (approximately 0.5") dictates that several of the sections shown will contribute to a composite image. Comparing the photographed cross-sections (view is looking up from bottom, 0° on right) with the resultant image (view is looking down from top, 0° on right), sections 2, 3 and 4 appear to be in view. In particular note the dark holes at the lower left and right corners (enhanced in the lower portion of Figure 6-25). They appear to correlate quite well, both in location and appearance, with the actual specimen. One particularly nice feature about the sponge is that its geometry and texture contribute to a rather uniform scattering pattern of reasonable amplitude. Figure 6-27 shows sample PTR output waveforms for the Panametrics sponge scan, with the specimen at 0° and receiver position as indicated. (The PTR voltage input range was set to ±0.1V. In conjunction with the PTR (+) full scale offset used, 0V-0.2V of envelope detected input maps into a 0-10V PTR output.) Note the much higher frequency scattering pattern as compared with that of the earlier objects scanned. Figure 6-28 shows the PTR envelope detected output for the same situation as in Figure 6-28, but over a narrow range of receiver angles, to demonstrate the wide scatter variability with only slight directional changes. Particularly from those results, one can readily see the large amount of additional information in off-normal scatter which is not monitored in B-scan.

As was done when imaging with the fan beam transducers, a "home-made" tissue phantom was constructed out of polyurethane gel and polyethylene tubing, as shown in Figure 6-29. Due to the smaller active imaging area of the straight
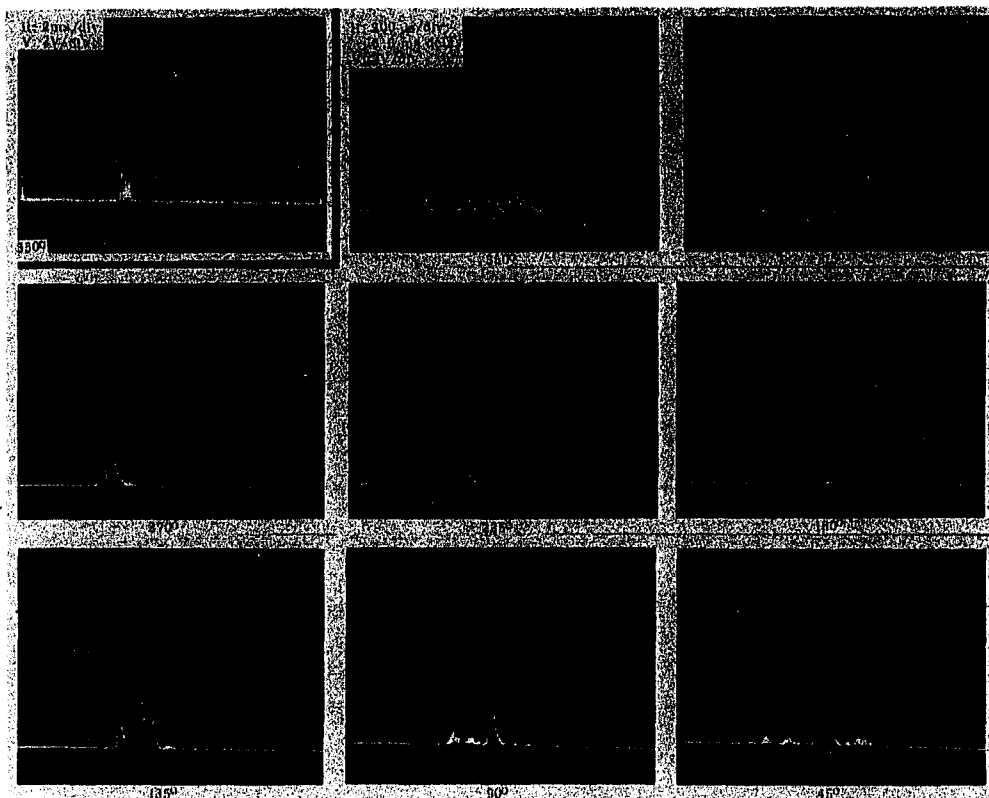
Figure 6-27. Panametrics scan of natural sponge. PTR envelope detected output signals for specimen at 0^0 and receiver position as indicated
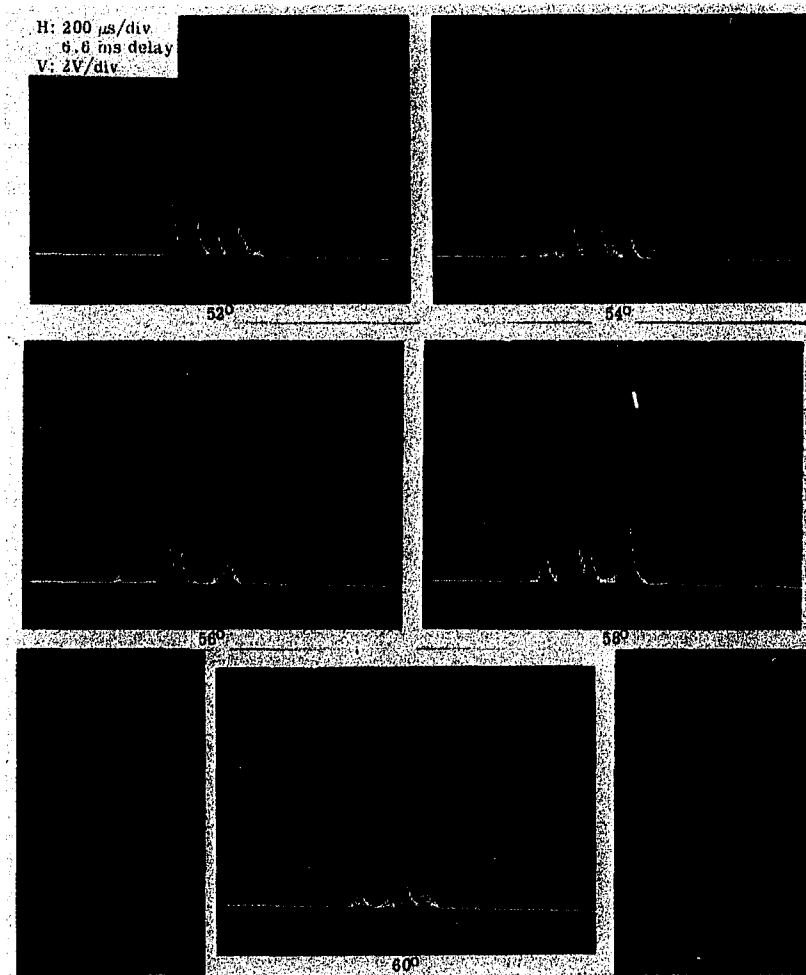
Figure 6-28. PTR envelope detected output for identical situation as in Figure 6-27 but for a narrow range of receiver angles to demonstrate the wide scattering variability with only slight changes in receiver position.
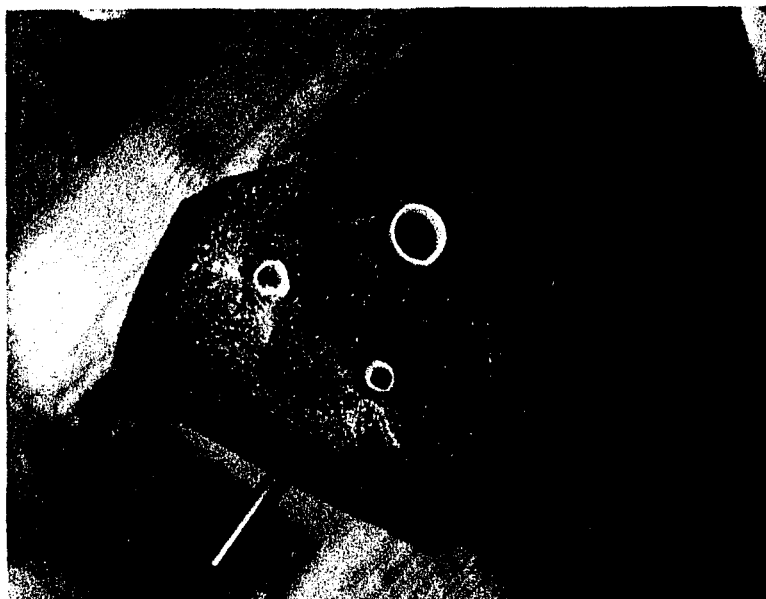
Figure 6-29. "Home-made" tissue phantom constructed from polyurethane
gel and three polyethylene tubes (approximately 0.5" on a side
by 0.75" thick) and mounted on a horizontal 0.064" diameter
stainless steel rod (located outside the imaging region).

beam array as compared with that of the fan beam, a smaller target (approxi-

mately 0.5" on a side by 0.75" thick) had to be constructed. Furthermore, as

indicated in the figure, the mounting hardware was kept outside the uniform

imaging region by using a horizontally oriented pin, mounted on the usual plastic

base. Figure 6-30 shows the corresponding image resulting from scanning with

a simulated sixteen transducer (Panametrics) array. Particularly in the last

level of windowing shown (bottom of figure), all three polyethylene tubes can

be seen. Note the relative correspondence between actual tube diameter and

corresponding "hole" diameter of image. However, based on the chopped up

appearance of each image (upper portion) it appears that part of the target ex-

tended outside the region of uniform insonification during the scanning process.

Again, it must be kept in mind that the finite beam thickness will determine the
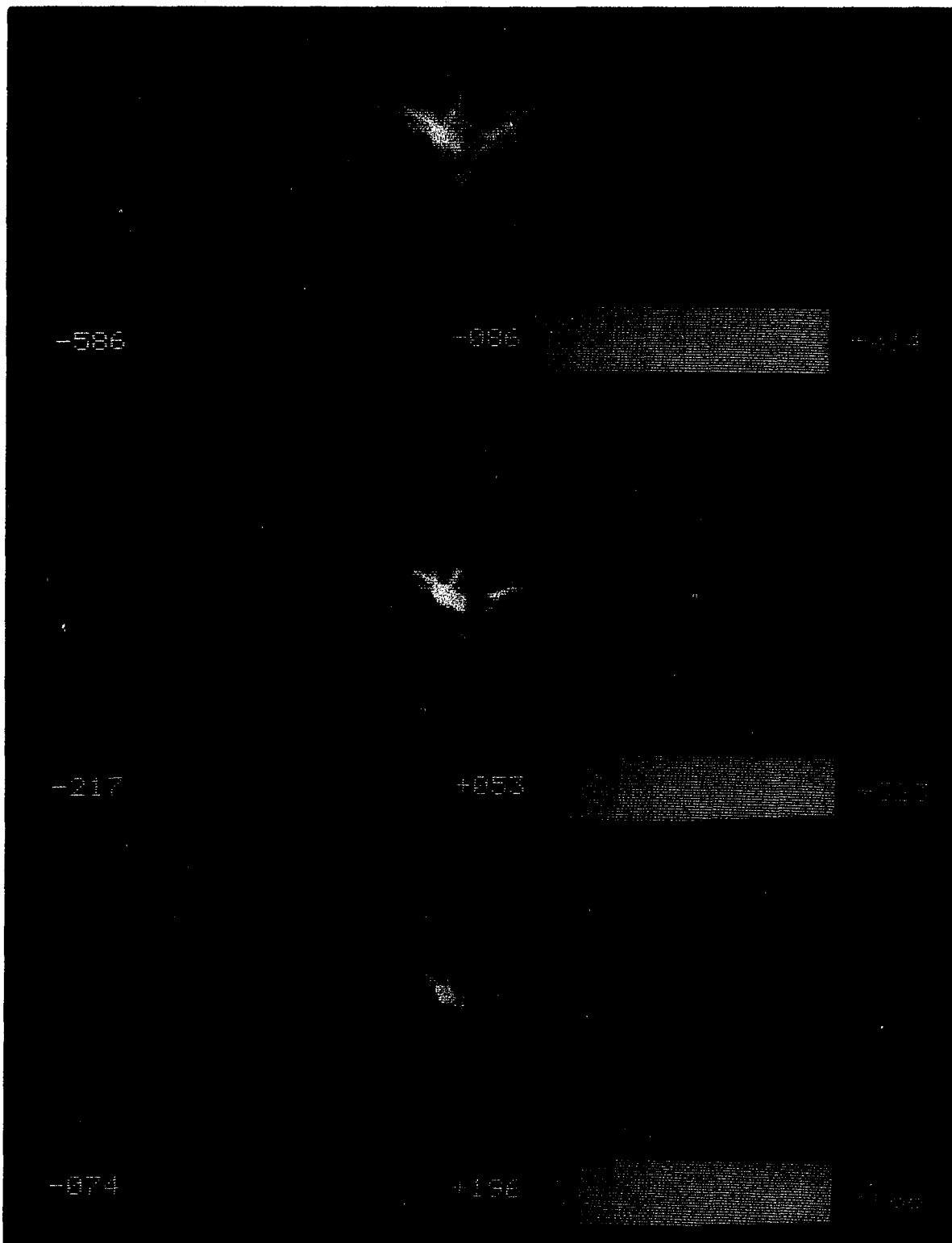
Figure 6-30. Reconstructed image from sixteen transducer (Panametrics - straight beam) scan of tissue phantom shown in Figure 6-29.

vertical resolution. The image shown is actually a vertical composite of many infinitely thin transverse planes throughout the specimen.

The final specimen was a chicken heart obtained from a local butcher and kept in saline solution for approximately one day under refrigeration. In all, it was estimated that the heart had been excised for approximately five days prior to imaging. The heart was mounted on the rotating specimen platform identically to the polyurethane target just discussed (Figure 6-31). Two sixteen transducer scans were performed. Following the scans, the heart was fixed in formalin solution for several days and then sectioned with a scalpel (Figure 6-32). Between the fixing and sectioning processes it appeared that the heart flattened in cross-section. Thus the exact outer shape should not correspond to that of the earlier formed image. As a further reference, Figure 6-33 shows, the base of the heart (section 1 of Figure 6-32), as viewed from base to apex.

For the first data set, the heart was oriented as pictured in the upper portion of Figure 6-31, with the zero degree scan reference indicated by the black line at the right of the figure. "Eye balling" the relative transducer and target positions, it appeared that the apex half of the heart was insonified. Figure 6-34 demonstrates the resultant image, for several levels of gray scale windowing and identification. The dark spot at the center of the image appears to be the left ventricle as in sections four through six (Figure 6-32).

The second data set was taken one day after the first (the heart refrigerated in saline in the interim). This time the heart was rotated 180° from its original position (as in the lower portion of Figure 6-31, zero degree reference being at the extreme right corner of the Plexiglas base). The heart was propped up slightly higher than for the first scan and so, again "eye-balling" the setup, it appeared that the base end of the heart was in the

main beam. Figure 6-35 contains the resultant image, which appears some-
what comparable to sections two through three (Figure 6-32). The dark spots
at the middle right and lower left portions of the image seem comparable to
parts of the right and left ventricle, respectively. The very bright section
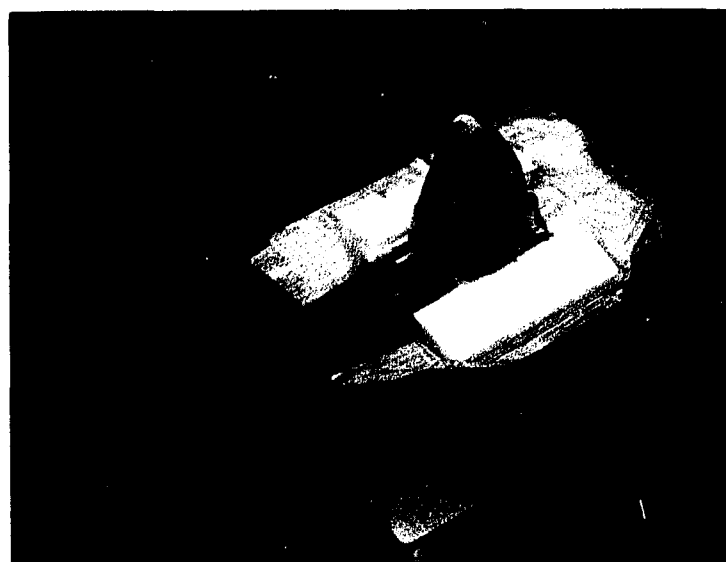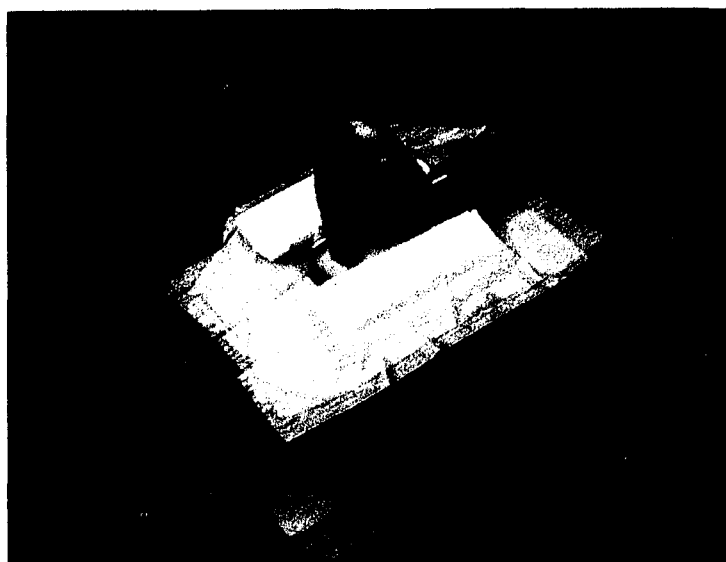
Figure 6-31. Front (upper photo) and rear (lower photo) of chicken heart
scanned with simulated sixteen transducer Panametrics array.
Black line at right of top photo indicates 0° scan reference
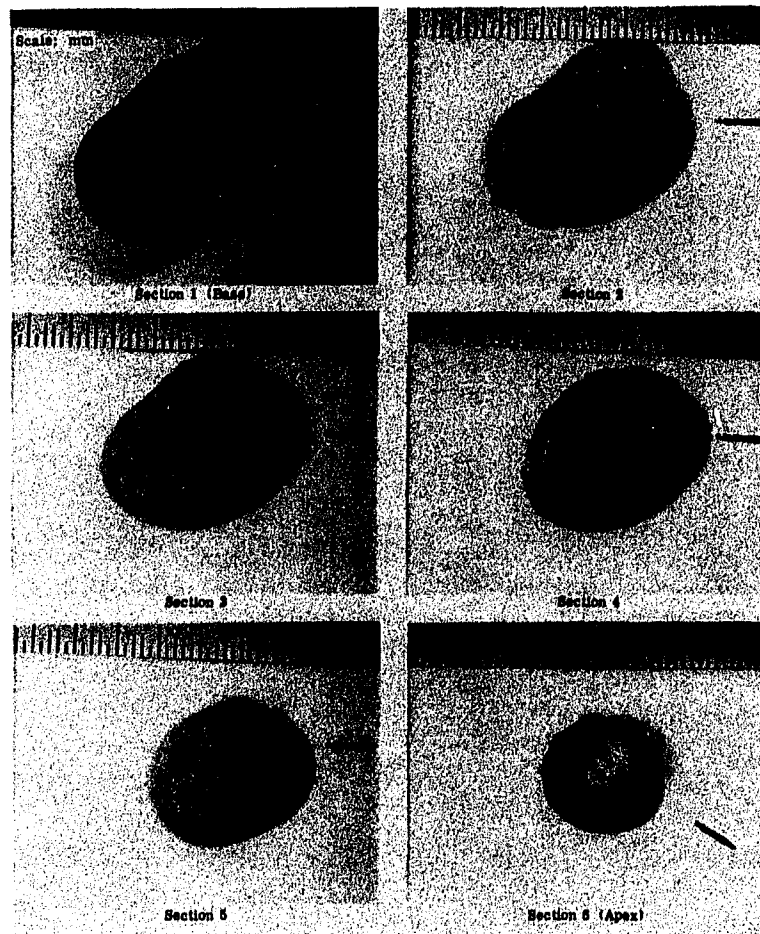
Figure 6-32. Cross-sectional views of heart shown in Figure 6-31 after fixing with formalin solution. Black line at right of each photo corresponds to the zero degree scan reference. Each section is approximately 5 mm thick. View is from apex to base (i.e. from the top down in Figure 6-31)
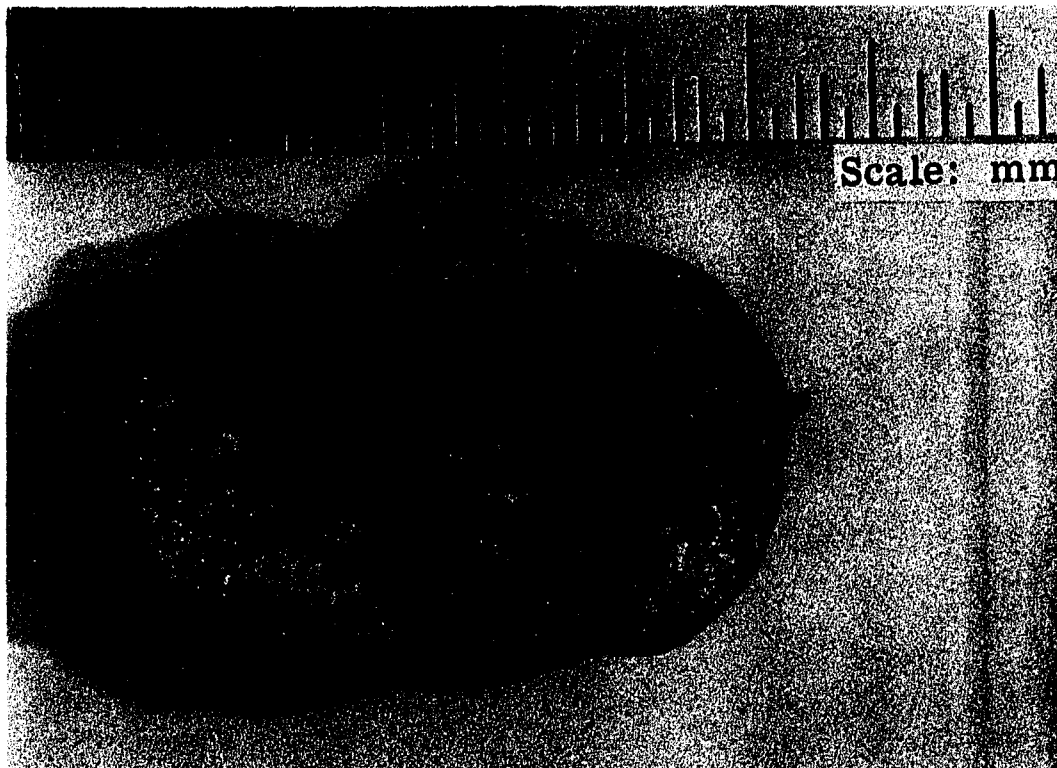
Figure 6-33. View of base of chicken heart cross-section (section 1 of
Figure 6-32) looking from base towards apex. Black line
indicates zero degree orientation.
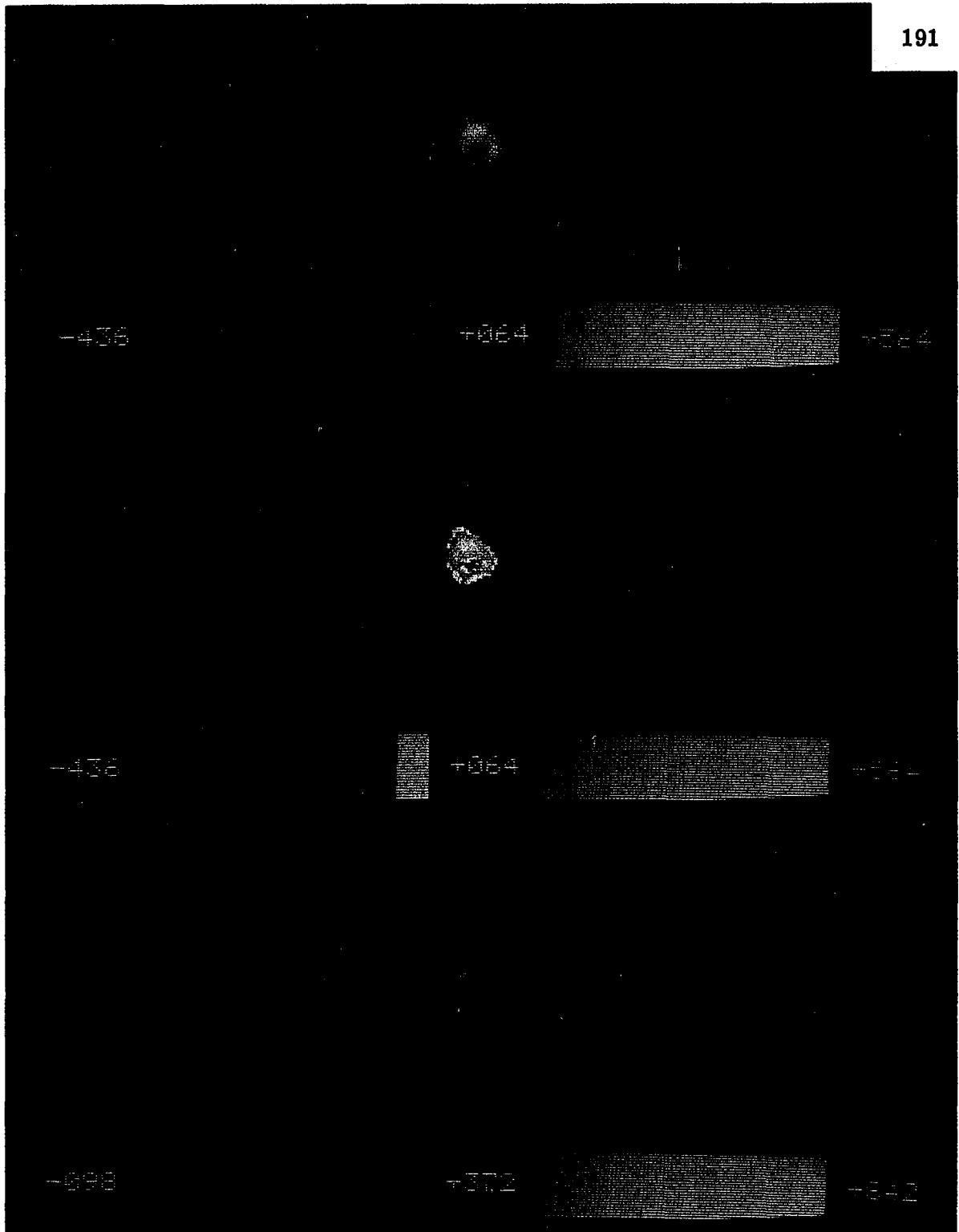
Figure 6-34. Sixteen transducer reconstruction of chicken heart shown in
Figures 6-31 thru 6-33 with various degrees of gray scale
windowing. Orientation is that shown in the upper portion of
Figure 6-31 (0⁰ on right). View is from apex to base (i.e. from
the top down). Middle image is gray scale identified to better
indicate outer tissue surface and what appears to be the left
ventricle
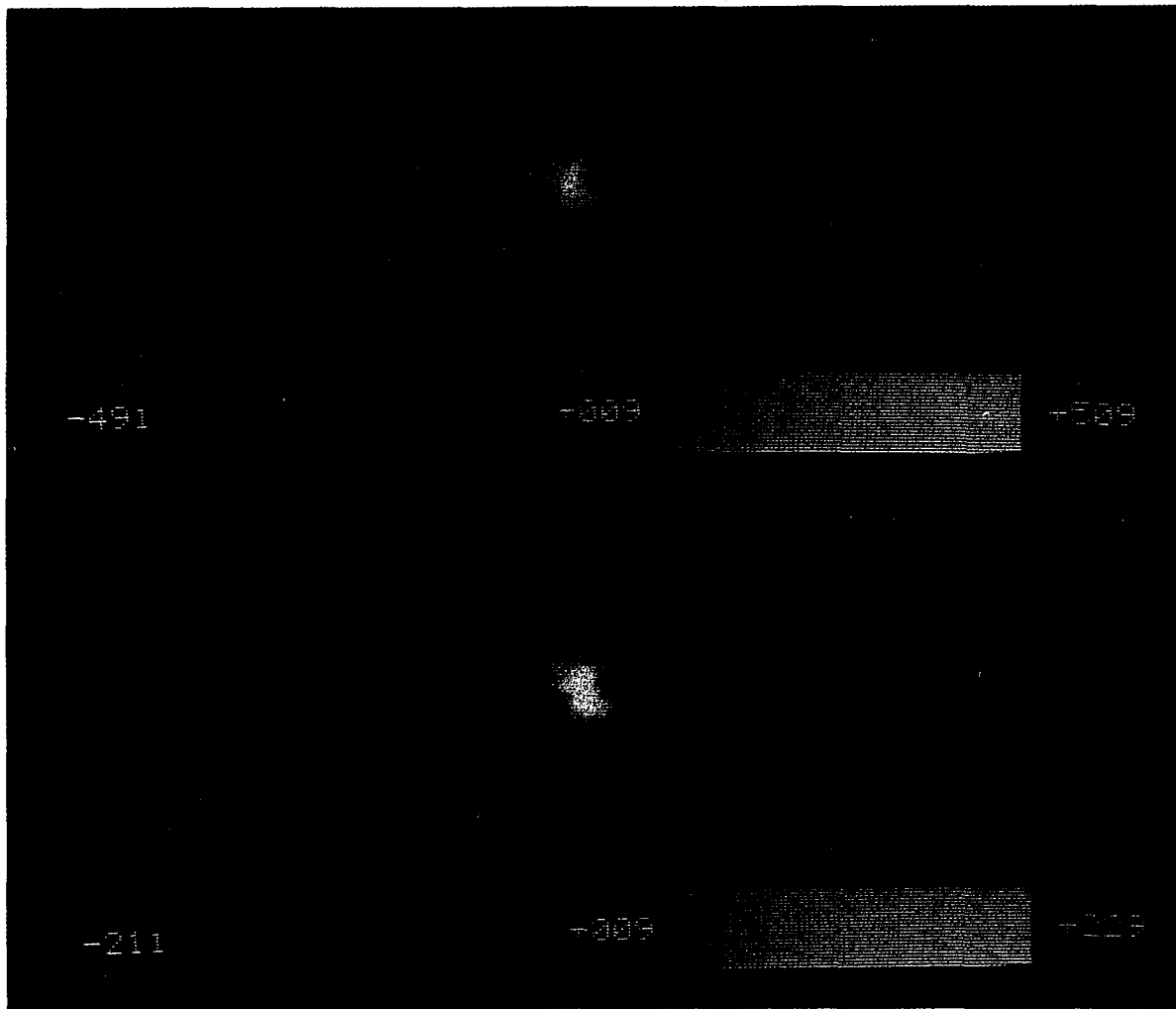
Figure 6-35. Similar scan to that of Figure 6-34 but with heart rotated 180°
(0° reference is on right lower portion of Figure 6-31) and a
slightly lower (towards base) portion of heart imaged. The two
dark circles appear to be the left and right ventricles with the
the central bright region being the interventricular septum.

would then represent the interventricular septum. However, a real definitive comparison is difficult, particularly since the lower portion has the chopped off appearance of Figure 6-30. This result suggests that the base region of the heart, being of larger diameter than the apical region, fell outside the uniformly insonified region. It becomes apparent that in order to make any reliable correlation between the reconstructed image and tissue specimen, precise positioning hardware is required in order to determine exact specimen and transducer positions. Secondly, a more precise sectioning technique would be helpful so as not to distort the specimen's geometry. Figures 6-36 and 6-37 present some reference RF and envelope detected waveforms, respectively, corresponding to the chicken heart scan with the specimen positioned as in the upper portion of Figure 6-34.

C.   ACHIEVEMENTS AND PROBLEMS

The data presented in this chapter pertaining to both biological and non-biological materials demonstrate the potential value of Pulse-Scatter Imaging as a technique for both high quality medical imaging and general materials imaging tasks. Compared with results obtained by current commercial techniques (e.g. B-scan), the images obtained in this investigation have been quite crude. However, it must be re-emphasized that no attempt was made at developing "tuned" hardware or software in this study, but rather the goal was to conduct an initial feasibility study by taking only a preliminary pencil-and-paper concept, analyzing and updating it and demonstrating its physical performance using real laboratory data. This latter task necessarily involved the design of an organized protocol in addition to the required hardware and software. In this respect, then, the results obtained may be termed "worst-case". Had encouraging data not been obtained, then the conclusion which might have been
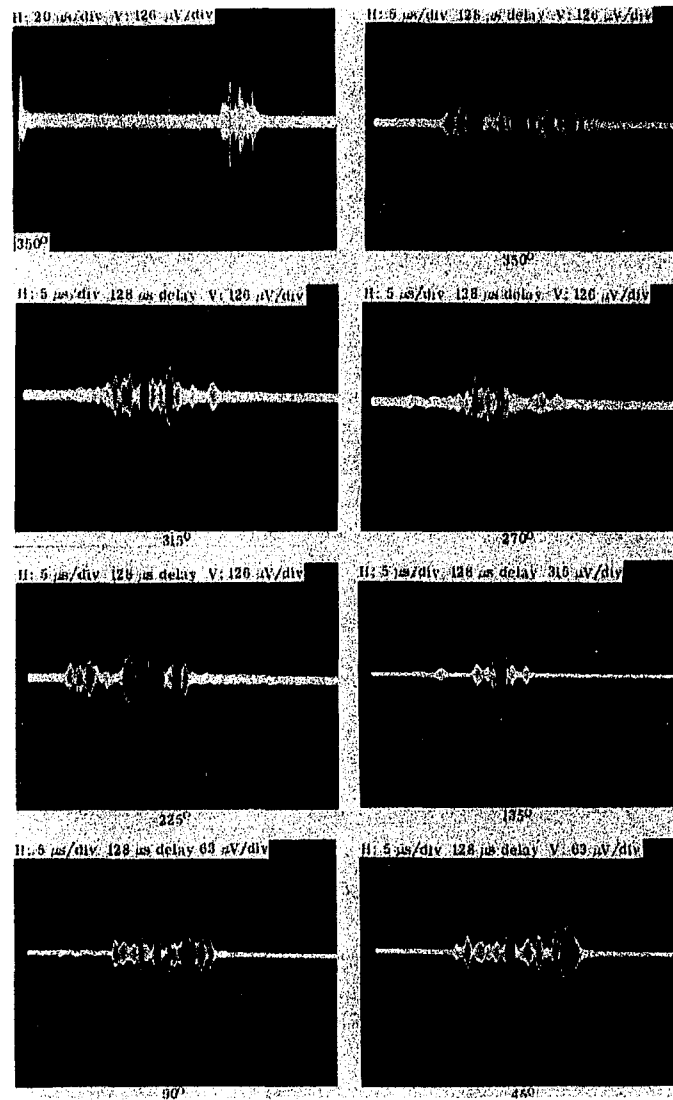
Figure 6-36. Sample RF waveforms for situation corresponding to Figure 6-34 with specimen at 0° and receiver positioning as indicated.
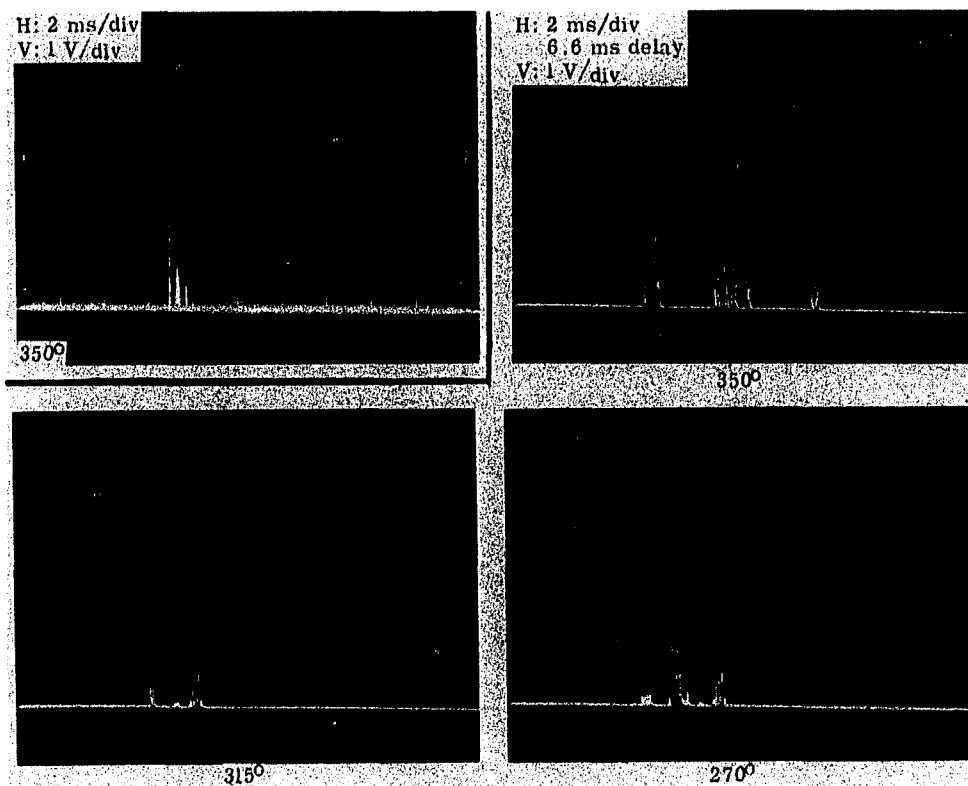
Figure 6-37. Sample PTR envelope detected output signals corresponding
to RF waveforms of Figure 6-36

drawn was that further system "tuning" or sophistication would be required before the basic concept could be truly disproved. Thus, bearing the above in mind in conjunction with the potential advantages of PSI, summarized in Section I(A), a dedicated effort should be launched aimed at developing a prototype system suitable for clinical use. Of course, such a task would encompass high level work in the areas of transducer design, electronic signal acquisition and processing, mathematical aspects of image reconstruction and digital image processing. As a reliable quantitative capability has not yet been achieved, obviously, tissue characterization could not be attempted. However, there is no doubt that once such a goal is attained, it is expected that in conjunction with the use of various signal and image processing techniques, greater tissue characterization than currently possible with B-scan techniques will come to pass by use of the additional scattered data.

The following brief discussion of some of the fundamental problems encountered in this investigation is intended as an aid to future development of PSI. The most logical place to begin this discussion is with the transducers used. Although the standard "straight beam" performed quite well for the purpose of this investigation, in order to get the acoustic coverage necessary to image objects with as large a diameter as the human body , a fan beam is required. Aside from what appeared to be a materials defect in the manufacturing of the prototype fan beam transducers, causing delamination of electrode material from the ceramic as well as blistering and peeling of the quarter wave front matching layer, the additional anticipated problems of excessive beam thickness, reduced sensitivity and sidelobe generation also contributed to deteriorated fan beam performance. Dedicated research and development is now required to produce a wide-angle, uniform fan beam with increased

sensitivity. As alluded to back in Section II(D), the three basic methods which may be utilized for fan beam generation are use of a lens and standard ceramic, use of a shaped ceramic, and mechanical sweeping of a "pencil beam" probe over the desired region of coverage. Separate transmitting on receiving transducers are also a possibility. Additionally, reduced beam thickness is necessary if better planar resolution is to be obtained. Finally, it would be advantageous for the transducer developed to possess as broadband a characteristic as possible (while still maintaining high sensitivity). Such a design would facilitate the use of multiple frequency techniques to be recommended in Section VII(C).

In so far as basic acoustics is concerned, multipath signals have thus far been treated as noise. For reasons discussed earlier, multipath signals have a greater chance of being received with PSI than for standard B-scan systems, since B-scan only utilizes pulse echo signals. Although multipath signal reinforcement did not appear present for the limited number of cases examined thus far, one must always be aware of such a possible influence.

As mentioned earlier, the PSI reconstruction algorithm (PSIV02.FOR), being far from streamlined in its present form, requires quite a considerable amount of time (two to fifteen hours for a sixteen transducer array) for image reconstruction. A major reason for such lengthy times is the limited core memory available for image storage in the computer during the reconstruction process, requiring round-about calculations, data swapping, and intermediate disc storage. Having an available random access memory equal in size to that used for image storage and display (320×320 memory locations, in this case) would considerably reduce reconstruction time. Modifications in the current Fortran algorithm for greater efficiency would also speed things up. Ultimately, a hardware processor would be required in order to approach real

time processing. One other aspect of the reconstruction algorithm which needs modification is the fact that at present, each transducer location is assigned a single pixel location. In fact, each transducer extends over many pixels and thus the times of flight measured and corresponding distances must be viewed accordingly. The smaller the transducer the lesser the effect of this situation.

The blurring and decreased image signal-to-noise ratio associated with image smearing (as in CT) and false intersections must also be dealt with. Both of these problems will probably involve some sort of a statistical solution as preliminary analysis thus far indicates spatial variations which relate to the actual object being imaged. The problem of image smearing can probably be handled by standard deconvolution techniques once a suitable set of deconvolution functions has been determined. Mathematical techniques, it has been suggested, do exist in the classified radar systems literature, which might be applicable to processing out "false intersections" occurring in the PSI image. The incorporation of thru-transmission data into the reconstructed image, as was demonstrated, degrades the reconstructed image and should not be used. Presently any data record which contains thru-transmission information is entirely ignored. However, since such data records contain valuable scattering data outside the specific thru-transmission time-window, a scheme should be developed to utilize the valid data.

The remaining difficulties to be noted at this time relate to the transducer mounting and electronics hardware. As already emphasized, proper alignment of the transducer rotating platform and specimen table is essential for proper image registration. A means must be incorporated into the hardware to enable monitoring and precise adjustment of this alignment. Furthermore, this hardware must be machined such that all centers of rotation are true. Such was not precisely the case for the rotating specimen platform used in this study.

Finally, two difficulties were encountered with system electronics. In trying to capture a pulse-echo signal, it is necessary to have a transmit/receive (T/R) switch in order to prevent the large excitation voltage from saturating the receiving amplifier and obliterating the low amplitude received echoes. Since such a T/R switch was not available (and a simple one made from diodes was not satisfactory), the pulse-echo data had to be simulated by placing the movable receiving transducer as close to the transmitter as possible. Obviously, such a signal will contribute some error, and so a T/R switch should be incorporated into any future system.

The remaining problem to be discussed here relates to system dynamic range. The dynamic range one generally hopes to achieve in pulse-echo systems is 80 dB. Intuitively, it would seem that an even wider range would be quite useful when dealing with scattered signals as well. In order to view both high and low level signals on the transient recorder (8 bit digitization) a logarithmic compression amplifier will be required prior to transient recorder input. Thus, when transferring the compressed data to the computer, under software control, the amplitude levels can be expanded back to cover the original range (the expanded signal will still only contain 256 bits of amplitude information, however). It is at this point in the data processing where time gain compensation may be applied as well.

CHAPTER VII. SUMMARY AND CONCLUSIONS

A. ACCOMPLISHMENTS

Some eighteen months ago, the concept of Pulse-Scatter imaging lay in the files of the General Electric Company's Electronics Laboratory, an untested concept, except for an initial preliminary computer simulation. With the present investigation now completed, the PSI concept has been worked up into a more complete theory and through both computer simulation and real data collected in the laboratory, has also been demonstrated to be an ultrasonic imaging technique of great potential value to the medical profession.

Prior to tackling the PSI concept itself, review of general ultrasonic theory and established ultrasonic imaging techniques, both medical and non-medical, were conducted. Time was spent both in the medical clinic and at case review sessions in order to get first line information as to ultrasonics as a modality for medical ultrasonic imaging as well as the associated difficulties. Hands-on clinical experience was also obtained.

Having gained a firm understanding as to the ultimate clinical application, this investigation was moved into the engineering laboratory, where the PSI concept was analyzed, a general protocol was established, and computer simul-lations were conducted. While these simulations pointed out many of the potential difficulties, including reconstruction smearing and ambiguous image

formation, nevertheless, the simulated targets were clearly reconstructed based on these results. Additions and corrections to the original theory were made.

Following the successful collection of some real data by hand with subsequent computer image reconstruction, a facility was designed to enable semi-automated data acquisition under computer control. Data could be acquired corresponding to a PSI array of up to and including twenty-four transducers, limited only by the disc memory capacity. Both inanimate (e.g. metal rods, Plexiglas triangle, transistor heat sink) and more biological-like (e.g. natural sponge, polyurethane/polyethylene tissue-phantom, excised chicken heart) structures were scanned, resulting in the reconstruction of rather crude but recognizable images. Although some data was collected using experimental prototype commercially obtained fan beam probes, most of the data was taken using standard non-focused transducers due to the fact that manufacturing defects in the fan probe produced unreliable results. In all, the general PSI feasibility has been demonstrated for medical ultrasonic imaging. Although widespread applications to tissue characterization were indicated, such a demonstration will have to wait until a more advanced (i.e. funded) PSI developmental effort is launched, whereby a more highly calibrated and quantitative (i.e. tuned) system can be built.

B. EVALUATION OF THE PSI TECHNIQUE

The data obtained in this investigation pertaining to both biological and non-biological materials demonstrate the potential value of pulse-scatter imaging as a technique for both high quality medical imaging and general materials imaging tasks. Although the images obtained in this investigation are quite crude compared with those obtained with commercially available apparatus, it must

be emphasized that no attempt in this study was made at developing optimized hardware or software. At the present time it appears that system resolution is comparable to B-scan, however, after final "tuning", the PSI image should possess more information than presently contained in a B-scan image. Digital image format allows for ready application of state-of-the-art image processing and feature extraction. PSI appears to be a feasible technique for medical imaging and should be pursued.

C. RECOMMENDATIONS FOR FURTHER INVESTIGATION

This study being only the very beginning of much hard work which lies ahead before PSI can be truly realized as a medical imaging modality, numerous recommendations for further investigation and development may be enumerated at this time. A brief list of the major points (in no particular order) is as follows:

(i) develop a reliable fan beam transducer possessing the somewhat mutually exclusive characteristics of wideband and high sensitivity

(ii) obtain a T/R switch to enable acquisition of the required pulse-echo data

(iii) design and implement a front-end logarithmic amplifier for capturing of the wide dynamic range required

(iv) design and build better transducer and specimen mounting hardware, where alignment can be assured and fine movements may be accurately controlled

(v) develop a more sophisticated mathematical theory (probably in conjunction with various simulations) to determine the required number and type of transducers in the PSI array

(vi)   determine the appropriate mathematics and modify the reconstruction algorithm to minimize the probability of a false intersection

(vii)   modify the PSI reconstruction algorithm to be able to magnify a reconstructed image or reconstruct it to a given display size

(viii)   develop the hardware (e.g. stepper motor control), and software to enable fully automated and monitored data acquisition by having computerized control of transducer position and data acquisition

(ix)   construct an actual array and image objects similar to those used in the present investigation

(x)   design a variable time-gain compensation (VTGC) scheme to correct for increased signal attenuation with increased time of travel

(xi)   improve image processing and signal processing software — think about hardware implementation

(xii)   design an aesthetic system to couple the imaging array to the patient. Probably some sort of water bag system will be required

(xiii)   apply radar techniques, such as chirping or pulse compression in order to minimize the effective transmitted pulse width and thus maximize resolution within the plane being imaged

(xiv)   incorporate techniques such as frequency sweeping and spectral analysis in an attempt to enhance tissue characterization capability through monitoring of frequency dependent scattering parameters

(xv)   perform preliminary prototype testing on anesthetized animals

(xvi)   in conjunction with the characteristics of the final array, design high speed switching, multiplexing and data acquisition circuitry to enable simultaneous data acquisition per transmitter from the PSI array

(xvii)   Once the final two-dimensional system has been completed, con-
struct a three dimensional array (i.e. a number of the two-dimensional arrays
stacked one above the other). Such an array, with proper electronic synchro-
nization would enable three-dimensional scatter detection, thus incorporating
even more scattering information into a given image. Furthermore, given a
single set of three-dimensional data, arbitrary two-dimensional cross-sections
situated within the array could be reconstructed.

APPENDIX A

PROPERTIES OF SOME PIEZOELECTRIC MATERIALS

TABLE A-1. TABLE OF CONSTANTS FOR SOME PIEZOELECTRIC MATERIALS [43]

Physical Property	Quartz 0^0 X-cut	Lithium Sulfate 0^0 Y-cut	Barium Titanate Type B	Lead Zirconate Titanate PZT-4	Lead Zirconate Titanate PZT-5	Lead Metaniobate	Units
Density, ρ	2.65	2.06	5.6	7.6	7.7	5.8	10^3 Kg/m^3
Acoustic impedance, ρ_c	15.2	11.2	24	30.0	28.0	16	10^6 Kg/m^{2}s
Max. operating temp.	550	75	70-90	250	290	500	^{0}C
Dielectric Constant	4.5	10.3	1,700	1,300	1,700	225	-
Electromechanical coupling factor for thickness mode, k_{33}	0.1	0.35	0.48	0.64	0.675	0.42	-
Electromechanical coupling factor for radial mode, Kp	0.1	-	0.33	0.58	0.60	0.07	-
Elastic quality factor, Q	10^6	-	400	500	75	11	-
Piezoelectric modulus for thickness mode, d_{33}	2.3	16	149	285	374	85	10^{-12} m/V
Curie temp.	575	-	115	320	365	550	^{0}C
Young's modulus, E	8.0	-	11.8	8.15	6.75	2.9	10^{10} N/m^2
Rated dynamic tensile strength	-	-	-	3,500	4,000	-	p.s.i.

APPENDIX B. PULSE-SCATTER IMAGING SYSTEM SOFTWARE

B-1. TITLE LISTINGS

SYSTEM SOFTWARE LISTING

File	Size	Date	File	Size	Date	File	Size	Date
1-NOV-78			PSICOP	17	12-JAN-78	HOLD .FOR	20	29-JAN-78
MONITR.SYS	46	5-DEC-77	OUT1 .FOR	2	13-JAN-78	INTCN2.FOR	1	1-FEB-78
RK .SYS	2	5-DEC-77	OUT2 .MAC	2	13-JAN-78	PSITRY.FOR	25	3-FEB-78
LPNONE.OLD	2	5-DEC-77	FLIB2 .MAC	8	13-JAN-78	INTERP.BAK	1	9-FEB-78
PR .SYS	2	5-DEC-77	ELIPS7.DAT	2	4-JAN-78	MOD3PT.DAT	2	8-FEB-78
PP .SYS	2	5-DEC-77	TSTOK2.SAV	69	8-JAN-78	NORMAL.FOR	4	8-FEB-78
FILL .SYS	2	5-DEC-77	ELIPS2.DAT	1	29-DEC-77	SQUARE.FOR	3	10-FEB-78
BA .SYS	7	5-DEC-77	FLIB .LLD	1	13-JAN-78	IMAG01.DAT	100	23-FEB-78
CBUILD.SYS	32	5-DEC-77	FLIB1 .FOR	5	13-JAN-78	ERASER.FOR	1	28-FEB-78
SYSMAC.SML	18	5-DEC-77	PSICP1	17	13-JAN-78	SWDPTR.MAC	2	1-MAR-78
CTNONE.SYS	5	5-DEC-77	OK1 .FOR	9	4-JAN-78	GTDATO.FOR	2	1-MAR-78
BATCH .SAV	25	5-DEC-77	ELIPS8.DAT	1	9-JAN-78	RDPTR .MAC	3	1-MAR-78
EDIT .SAV	19	5-DEC-77	TWRITE.MAC	2	20-DEC-77	PTRLST.MAC	84	1-MAR-78
MACRO .SAV	31	5-DEC-77	TCALL .FOR	2	20-DEC-77	DUALTB.MAC	51	1-MAR-78
ASEMBL.SAV	21	5-DEC-77	SIM5PT.DAT	3	2-JAN-78	GETDAT.SAV	49	8-MAR-78
EXPAND.SAV	12	5-DEC-77	GAUS .FOR	1	2-JAN-78	RDOUT .SAV	50	12-MAR-78
CREF .SAV	5	5-DEC-77	CNVOLV.FOR	2	2-JAN-78	TEKPLT.SAV	47	3-MAR-78
LINK .SAV	25	5-DEC-77	ELIPS .FOR	7	28-DEC-77	RDOUT .BAK	6	5-MAR-78
PIP .SAV	14	5-DEC-77	ELIPS6.DAT	2	3-JAN-77	TEKPLT.FOR	2	3-MAR-78
FILEX .SAV	11	5-DEC-77				PTRPLT.BAK	9	5-MAR-78
SRCCOM.SAV	11	5-DEC-77	ELIPS0.DAT	1	28-DEC-77	GETDAT.FOR	2	8-MAR-78
DUMP .SAV	5	5-DEC-77	GOOD .FOR	9	28-DEC-77	PEAK .BAK	5	9-MAR-78
PATCH .SAV	5	5-DEC-77	ELIPS3.DAT	1	29-DEC-77	PTRPLT.SAV	80	3-APR-78
PATCHO.SAV	33	5-DEC-77	OK3 .FOR	8	30-DEC-77	PKPLOT.FOR	9	21-MAR-78
VTMAC .MAC	7	5-DEC-77	ELIPS1.DAT	1	29-DEC-77	PSIGEN.OLD	28	11-MAR-78
SYSMAC.8K	25	5-DEC-77	ELIPS5.DAT	3	10-JAN-78	PSIGEN.INT	29	12-MAR-78
LIBR .SAV	15	5-DEC-77	DATGN3.FOR	2	2-JAN-78	PTRPLT.FOR	9	3-APR-78
FORTRA.HLP	2	5-DEC-77	DATGN5.FOR	2	2-JAN-78	RDOUT .FOR	6	12-MAR-78
ODT .OBJ	9	29-OCT-78	OK2 .FOR	9	3-JAN-77	CONV00.DAT	3	6-APR-78
VTHDLR.OBJ	8	29-OCT-78	OK .FOR	9	4-JAN-78	B .FOR	9	21-MAR-78
OTSCOM.OBJ	66	29-OCT-78	TSTOK2	10	8-JAN-78	E .FOR	7	21-MAR-78
FORLIB.V2S	132	5-DEC-77	CONV .DAT	6	2-JAN-78	PEAK .FOR	6	21-MAR-78
FORTRA.SAV	96	5-DEC-77	TSTOK2.SAV	10	8-JAN-78	PEAK .SAV	67	21-MAR-78
SYSLIB.LLD	4	5-DEC-77	SIMUL3.DAT	2	9-JAN-78	IMAGRD.DAT	203	23-MAR-78
LSRPIP.SAV	3	5-DEC-77	GRAYF .FOR	2	13-JAN-78	READ .SAV	19	24-MAY-78
LSRPIP.MAC	6	5-DEC-77	PSI .FOR	17	13-JAN-78	SINXX .FOR	2	23-MAR-78
ODT .SAV	8	5-DEC-77	SSWTCH.MAC	1	23-JAN-78	SEQ .FOR	8	27-MAR-78
KB .SYS	3	5-DEC-77	GRAYU .FOR	2	23-JAN-78	HSPRFL.FOR	3	26-APR-78
KB .MAC	34	5-DEC-77	PSICOP.FOR	17	23-JAN-78			
OUTPUT.MAC	2	7-DEC-77	ERASE .SAV	14	25-JAN-78	HSPRFL.SAV	47	26-APR-78
PIXOUT.FOR	2	7-DEC-77	INTCON.BAK	1	16-JAN-78	A .FOR	6	27-MAR-78
LBROWN.FOR	15	7-DEC-77	SAVE .FOR	19	27-JAN-78	SIMU00.DAT	90	27-MAR-78
KB1 .SYS	3	7-DEC-77	GRAYIU.FOR	2	27-JAN-78	PIXGEN.FOR	5	25-JAN-78
LP .SYS	2	7-DEC-77	SQUARE.SAV	20	10-FEB-78	CNVPLT.FOR	1	17-APR-78
CR .SYS	3	7-DEC-77	NORMAL.BAK	3	1-FEB-78	CONVOL.SAV	16	14-APR-78
MT .SYS	6	7-DEC-77	PSIBAK.FOR	18	25-JAN-78	READIN.BAK	6	5-APR-78
TT .SYS	2	7-DEC-77	ERASE .FOR	1	25-JAN-78	READIN.FOR	7	5-APR-78
DATA3 .FOR	3	9-JAN-78	OUT5 .MAC	2	25-JAN-78	READIN.SAV	53	5-APR-78
SEQPLT.FOR	8	23-MAR-78	SAVE	19	25-JAN-78	ZERO .SAV	65	6-APR-78
SEQPLT.SAV	79	23-MAR-78	CONV2U.FOR	1	1-FEB-78	ZERO .FOR	3	6-APR-78
COPBRN.FOR	16	15-DEC-77	CONV2F.FOR	1	1-FEB-78	INTCON.FOR	1	17-APR-78
PROC01.DAT	2	12-JAN-78	PSITRY.BAK	23	3-FEB-78	INTCON.SAV	19	17-APR-78
CONVF .FOR	1	12-JAN-78	OUT3 .FOR	1	17-JAN-78	UNFCON.FOR	1	17-APR-78
CONVU .FOR	1	12-JAN-78	OUT4 .FOR	1	25-JAN-78	UNFCON.SAV	19	17-APR-78

CONVOL.FOR	2	14-APR-78
INTERP.FOR	1	19-APR-78
TESTCN.FOR	2	17-APR-78
TESTCN.SAV	22	17-APR-78
PSICON.SAV	46	24-APR-78
CONVUU.DAT	3	24-APR-78
VSPRFL.FOR	3	26-APR-78
HPROFL.FOR	3	26-APR-78
VSPRFL.SAV	48	26-APR-78
FFT .FOR	2	28-APR-78
VPRINT.FOR	3	27-APR-78
HPRINT.FOR	3	27-APR-78
HPRINT.SAV	20	27-APR-78
VPRINT.SAV	21	27-APR-78
FORLIB.OBJ	131	29-OCT-78
SYSLIB.OBJ	37	29-OCT-78
OUT1 .OBJ	9	29-OCT-78
OUT2 .OBJ	1	29-OCT-78
TCALL .OBJ	9	29-OCT-78
OUTPUT.OBJ	1	29-OCT-78
SSWTCH.OBJ	1	29-OCT-78
OUT5 .OBJ	1	29-OCT-78
OUT3 .OBJ	6	29-OCT-78
OUT4 .OBJ	6	29-OCT-78
RDPTR .OBJ	1	29-OCT-78
GRAPH .OBJ	198	29-OCT-78
FLIB .OBJ	18	29-OCT-78
HPROFL.SAV	45	30-APR-78
PSPDGN.SAV	13	12-MAY-78
COMP2 .SAV	47	8-MAY-78
PSIGEN.SAV	48	14-MAY-78
PTSPRD.FOR	1	7-MAY-78
PTSPRD.SAV	68	7-MAY-78
PLOT3D.FOR	6	7-MAY-78
PSPDGN.FOR	1	12-MAY-78
COMP2 .FOR	33	8-MAY-78
INTERP.SAV	61	8-MAY-78
PSIGEN.LDN	33	8-MAY-78
PSIGEN.BAK	33	8-MAY-78
FFT .OBJ	10	29-OCT-78
FFT2D .FOR	5	13-MAY-78
FFT2D .BAK	5	12-MAY-78
FFRL32.FOR	5	13-MAY-78
FF3232.FOR	6	13-MAY-78
PSIGEN.FOR	33	13-MAY-78
FFTDIV.FOR	5	14-MAY-78
FFTDIV.SAV	56	14-MAY-78
FFT2D .RAI	6	15-MAY-78
RELIMA.FOR	6	15-MAY-78
RELIMA.SAV	62	15-MAY-78
INVERT.FOR	7	24-MAY-78
TWODIM.FOR	6	24-MAY-78
POINT .FOR	1	17-MAY-78
LDN .FOR	7	22-MAY-78

FFTVAL.FOR	2	22-MAY-78
MAGNIT.FOR	2	23-MAY-78
MAGNIT.SAV	20	23-MAY-78
COMPAR.FOR	30	23-MAY-78
COMPAR.SAV	46	23-MAY-78
READ .FOR	1	24-MAY-78
DIVIDE.FOR	7	24-MAY-78
DIVIDE.SAV	99	24-MAY-78
TWODIM.SAV	89	24-MAY-78
INVERT.SAV	92	24-MAY-78
PULOUT.SAV	14	24-MAY-78
PULOUT.FOR	1	24-MAY-78
PSIGEN.PHD	48	26-OCT-78
COMPAR.PHD	46	26-OCT-78
TEST .SAV	16	27-OCT-78
TEST .FOR	1	27-OCT-78
NEWPSI.BAK	33	28-OCT-78
PSIV02.BAK	35	28-OCT-78
PSIV02.FOR	37	29-OCT-78
PSIV02.SAV	49	29-OCT-78
PULL64.SAV	14	29-OCT-78
RDIMAG.FOR	1	29-OCT-78
RDIMAG.SAV	19	29-OCT-78
PULL64.FOR	1	29-OCT-78
HISTOG.FOR	12	29-OCT-78
HISTOG.SAV	63	29-OCT-78
HISTOG.BAK	10	29-OCT-78
TRY .FOR	1	30-OCT-78
TRY .SAV	19	30-OCT-78
SUBTR .SAV	20	30-OCT-78
CAL .SAV	15	31-OCT-78
SUBTR .FOR	2	30-OCT-78
CAL .FOR	1	31-OCT-78

246 FILES, 4638 BLOCKS
136 FREE BLOCKS

FORTRAN SOURCE LISTINGS

1-NOV-78

PIXOUT.FOR	2	7-DEC-77
LBROWN.FOR	15	7-DEC-77
DATA3 .FOR	3	9-JAN-78
SEQPLT.FOR	8	23-MAR-78
COPBRN.FOR	16	15-DEC-77
CONVF .FOR	1	12-JAN-78
CONVU .FOR	1	12-JAN-78
OUT1 .FOR	2	13-JAN-78
FLIB1 .FOR	5	13-JAN-78
OK1 .FOR	9	4-JAN-78
TCALL .FOR	2	20-DEC-77
GAUS .FOR	1	2-JAN-78
CNVOLV.FOR	2	2-JAN-78
ELIPS .FOR	7	28-DEC-77
GOOD .FOR	9	28-DEC-77
OK3 .FOR	8	30-DEC-77
DATGN3.FOR	2	2-JAN-78
DATGN5.FOR	2	2-JAN-78
OK2 .FOR	9	3-JAN-77
OK .FOR	9	4-JAN-78
TSTOK2.FOR	10	8-JAN-78
GRAYF .FOR	2	13-JAN-78
PSI .FOR	17	13-JAN-78
GRAYU .FOR	2	23-JAN-78
PSICOP.FOR	17	23-JAN-78
SAVE .FOR	19	27-JAN-78
GRAYIU.FOR	2	27-JAN-78
PSIBAK.FOR	18	25-JAN-78
ERASE .FOR	1	25-JAN-78
CONV2U.FOR	1	1-FEB-78
CONV2F.FOR	1	1-FEB-78
OUT3 .FOR	1	17-JAN-78
OUT4 .FOR	1	25-JAN-78
HOLD .FOR	20	29-JAN-78
INTCN2.FOR	1	1-FEB-78
PSITRY.FOR	25	3-FEB-78
NORMAL.FOR	4	8-FEB-78
SQUARE.FOR	3	10-FEB-78
ERASER.FOR	1	28-FEB-78
GTDATO.FOR	2	1-MAR-78
TEKPLT.FOR	2	3-MAR-78
GETDAT.FOR	2	8-MAR-78
PKPLOT.FOR	9	21-MAR-78
PTRPLT.FOR	9	3-APR-78
RDOUT .FOR	6	12-MAR-78
B .FOR	9	21-MAR-78
E .FOR	7	21-MAR-78
PEAK .FOR	6	21-MAR-78
SINXX .FOR	2	23-MAR-78
SEQ .FOR	8	27-MAR-78
HSPRFL.FOR	3	26-APR-78
A .FOR	6	27-MAR-78
PIXGEN.FOR	5	25-JAN-78

CNVPLT.FOR	1	17-APR-78
READIN.FOR	7	5-APR-78
ZERO .FOR	3	6-APR-78
INTCON.FOR	1	17-APR-78
UNFCON.FOR	1	17-APR-78
CONVOL.FOR	2	14-APR-78
INTERP.FOR	1	19-APR-78
TESTCN.FOR	2	17-APR-78
VSPRFL.FOR	3	26-APR-78
HPROFL.FOR	3	26-APR-78
FFT .FOR	2	28-APR-78
VPRINT.FOR	3	27-APR-78
HPRINT.FOR	3	27-APR-78
PTSPRD.FOR	1	7-MAY-78
PLOT3D.FOR	6	7-MAY-78
PSPDGN.FOR	1	12-MAY-78
COMP2 .FOR	33	8-MAY-78
FFT2D .FOR	5	13-MAY-78
FFRL32.FOR	5	13-MAY-78
FF3232.FOR	6	13-MAY-78
PSIGEN.FOR	33	13-MAY-78
FFTDIV.FOR	5	14-MAY-78
RELIMA.FOR	6	15-MAY-78
INVERT.FOR	7	24-MAY-78
TWODIM.FOR	6	24-MAY-78
POINT .FOR	1	17-MAY-78
LDN .FOR	7	22-MAY-78
FFTVAL.FOR	2	22-MAY-78
MAGNIT.FOR	2	23-MAY-78
COMPAR.FOR	30	23-MAY-78
READ .FOR	1	24-MAY-78
DIVIDE.FOR	7	24-MAY-78
PULOUT.FOR	1	24-MAY-78
TEST .FOR	1	27-OCT-78
PSIV02.FOR	37	29-OCT-78
RDIMAG.FOR	1	29-OCT-78
PULL64.FOR	1	29-OCT-78
HISTOG.FOR	12	29-OCT-78
TRY .FOR	1	30-OCT-78
SUBTR .FOR	2	30-OCT-78
CAL .FOR	1	31-OCT-78

94 FILES, 588 BLOCKS
136 FREE BLOCKS

MACRO SOURCE LISTINGS	OBJECT CODE LISTINGS	MACHINE CODE LISTINGS

```
1-NOV-78                    1-NOV-78                          1-NOV-78
VTMAC .MAC    7  5-DEC-77    ODT   .OBJ    9 29-OCT-78    BATCH .SAV   25  5-DEC-77
LSRPIP.MAC    6  5-DEC-77    VTHDLR.OBJ    8 29-OCT-78    EDIT  .SAV   19  5-DEC-77
KB    .MAC   34  5-DEC-77    OTSCOM.OBJ   66 29-OCT-78    MACRO .SAV   31  5-DEC-77
OUTPUT.MAC    2  7-DEC-77    FORLIB.OBJ  131 29-OCT-78    ASEMBL.SAV   21  5-DEC-77
OUT2  .MAC    2 13-JAN-78    SYSLIB.OBJ   37 29-OCT-78    EXPAND.SAV   12  5-DEC-77
FLIB2 .MAC    8 13-JAN-78    OUT1  .OBJ    9 29-OCT-78    CREF  .SAV    5  5-DEC-77
TWRITE.MAC    2 20-DEC-77    OUT2  .OBJ    1 29-OCT-78    LINK  .SAV   25  5-DEC-77
SSWTCH.MAC    1 23-JAN-78    TCALL .OBJ    9 29-OCT-78    PIP   .SAV.  14  5-DEC-77
OUT5  .MAC    2 25-JAN-78    OUTPUT.OBJ    1 29-OCT-78    FILEX .SAV   11  5-DEC-77
SWDPTR.MAC    2  1-MAR-78    SSWTCH.OBJ    1 29-OCT-78    SRCCOM.SAV   11  5-DEC-77
RDPTR .MAC   .3  1-MAR-78    OUT5  .OBJ    1 29-OCT-78    DUMP  .SAV    5  5-DEC-77
PTRLST.MAC   84  1-MAR-78    OUT3  .OBJ    6 29-OCT-78    PATCH .SAV    5  5-DEC-77
DUALTB.MAC   51  1-MAR-78    OUT4  .OBJ    6 29-OCT-78    PATCHO.SAV   33  5-DEC-77
13 FILES, 204 BLOCKS        RDPTR .OBJ    1 29-OCT-78    LIBR  .SAV   15  5-DEC-77
 136 FREE BLOCKS            GRAPH .OBJ  198 29-OCT-78    FORTRA.SAV   96  5-DEC-77
                            FLIB  .OBJ   18 29-OCT-78    LSRPIP.SAV    3  5-DEC-77
                            FFT   .OBJ   10 29-OCT-78    ODT   .SAV    8  5-DEC-77
                            17 FILES, 512 BLOCKS        SEQPLT.SAV   79 23-MAR-78
                             136 FREE BLOCKS            TSTOK2.SAV   69  8-JAN-78
                                                        ERASE .SAV   14 25-JAN-78
                                                        SQUARE.SAV   20 10-FEB-78
                                                        GETDAT.SAV   49  8-MAR-78
                                                        RDOUT .SAV   50 12-MAR-78
                                                        TEKPLT.SAV   47  3-MAR-78
                                                        PTRPLT.SAV   80  3-APR-78
                                                        PEAK  .SAV   67 21-MAR-78
                                                        READ  .SAV   19 24-MAY-78
                                                        HSPRFL.SAV   47 26-APR-78
                                                        CONVOL.SAV   16 14-APR-78
                                                        READIN.SAV   53  5-APR-78
                                                        ZERO  .SAV   65  6-APR-78
                                                        INTCON.SAV   19 17-APR-78
                                                        UNFCON.SAV   19 17-APR-78
                                                        TESTCN.SAV   22 17-APR-78
                                                        PSICON.SAV   46 24-APR-78
                                                        VSPRFL.SAV   48 26-APR-78
                                                        HPRINT.SAV   20 27-APR-78
                                                        VPRINT.SAV   21 27-APR-78
                                                        HPROFL.SAV   45 30-APR-78
                                                        PSPDGN.SAV   13 12-MAY-78
                                                        COMP2 .SAV   47  8-MAY-78
                                                        PSIGEN.SAV   48 14-MAY-78
                                                        PTSPRD.SAV   68  7-MAY-78
                                                        INTERP.SAV   61  8-MAY-78
                                                        FFTDIV.SAV   56 14-MAY-78
                                                        RELIMA.SAV   62 15-MAY-78
                                                        MAGNIT.SAV   20 23-MAY-78
                                                        COMPAR.SAV   46 23-MAY-78
                                                        DIVIDE.SAV   99 24-MAY-78
                                                        TWODIM.SAV   89 24-MAY-78
                                                        INVERT.SAV   92 24-MAY-78
                                                        PULOUT.SAV   14 24-MAY-78
                                                        TEST  .SAV   16 27-OCT-78
                                                        PSIV02.SAV   49 29-OCT-78
                                                        PULL64.SAV   14 29-OCT-78
                                                        RDIMAG.SAV   19 23-OCT-78
                                                        HISTOG.SAV   63 29-OCT-78
                                                        TRY   .SAV   19 30-OCT-78
                                                        SUBTR .SAV   20 30-OCT-78
                                                        CAL   .SAV   15 31-OCT-78
                                                        60 FILES, 2184 BLOCKS
                                                         136 FREE BLOCKS
```

B-2. RECONSTRUCTION ALGORITHM AND ASSOCIATED SOFTWARE

PSIV02.FOR
SSWTCH.MAC
OUT5.MAC
ERASE.FOR
TSTOK2.FOR

MAIN PSI RECONSTRUCTION PROGRAM. INTERPOLATION AND CONVOLUTION OPTIONS ARE
COMMENTED OUT; HOWEVER, A DUMMY CONVOLUTION FUNCTION MUST EXIST FOR PROGRAM
TO RUN (E.G. CONV00.DAT). USE THE FOLLOWING SEQUENCE TO 'LINK' THIS
PROGRAM . . .   .R LINK
                 *PSIV02=PSIV02,OUT5,SSWTCH,FLIB/F
THE COMPARISON MODE FOR THIS PROGRAM ALLOWS DISPLAYING OF SEVERAL IMAGES
ON THE SAME GRAY SCALE DISPLAY, I.E. AFTER OUTPUT OF AN IMAGE, THE DISPLAY
POINTER IS NOT AUTOMATICALLY RESET TO PIXEL (1,1). FOR EXAMPLE, FOUR IMAGES
EACH 80 PIXELS SQUARE, MAY BE SHOWN ONE BENEATH THE OTHER, ON THE SAME
DISPLAY FOR PURPOSES OF COMPARISON.

```
  1-NOV-78
PSIV02.FOR    37 29-OCT-78
C**********P.S.I.RECONSTRUCTION ALGORITHM VERSION 2 (10-29-78)**********
C         NO INTERPOLATION; NO CONVOLUTION; 'CAL' FACTOR ENTERED MANUALLY.
C*****GENERAL ELECTRIC CO.-----PULSE-SCATTER IMAGING*****
C*****IMAGE RECONSTRUCTION PROGRAM*****
C*****L. NADEL, L. BROWNING, R. GLUSICK*****
C*****FOR "TT" OUTPUT ON BASEMENT PDP-11 MUST <.ASS TT:LP>*****
C*****FOR "LP" OUTPUT ON FIRST FLOOR PDP-11 MUST <.ASS KB:LP>*****
C*****PROGRAM IS PRESENTLY INITIALIZED TO OUTPUT TO "LP" IN BASEMENT
C*********AND "TT" ON FIRST FLOOR.
C
C         =====NOTE:  IP IS NOW R (RADIUS OF RING) : F7.3 =====
C
C     C() IS THE ARRAY CONTAINING THE CONVOLVED DATA.
      DIMENSION C(320)
C     F() IS THE ARRAY CONTAINING THE DATA TO BE CONVOLVED.
      DIMENSION F(320)
C     G() IS THE ARRAY CONTAINING THE CONVOLUTION FUNCTION.
      DIMENSION G(320)
C     THEREFORE, C=F*G (WHERE "*" MEANS "CONVOLVED WITH").
      DIMENSION Z(320)
      DIMENSION IZ(320)
      DIMENSION IF(320)
      BYTE IBYTF(320)
      EQUIVALENCE (IBYTF(1),IF(1))
      DIMENSION IDATA(7)
      DIMENSION ICON(7)
      DIMENSION ITEMP(7)
      DIMENSION IDESCR(160)
      DATA IDESCR/160*2H /
      DATA NO/2HNO/
      DATA IDATA/2HDK,2H1:,2HPR,2HOC,2H00,2H.D,2HAT/
      DATA ICON/2HDK,2H1:,2HCO,2HNV,2H00,2H.D,2HAT/
      DATA ITEMP/2HDK,2H1:,2HIM,2HAG,2H00,2H.D,2HAT/
C         ----------SIGN ON-----------
      WRITE (6,88)
 88   FORMAT (' *****GENERAL ELECTRIC CO.-----PULSE-SCATTER IMAGING*****
     1',/,' ***************IMAGE RECONSTRUCTION ALGORITHM***************')
      CALL IDATE (MON,IDAY,IYR)
      WRITE (6,89) MON,IDAY,IYR
 89   FORMAT (/,' DATE:  ',I2,'-',I2,'-',I2)
      CALL TIME(SEC)
      DECHRS=SEC/3600.
      WRITE (6,87) DECHRS
 87   FORMAT (' TIME:  ',F6.3,' HOURS',///)
C     ----------------------------
      R=160.
C     <R> = TRANSDUCER CRCLE RADIUS IN # OF DATA BINS.
      DATA IMODE/2HNO/
C     IF IMODE='NO', THEN PROGRAM WILL NOT OPERATE IN MULTIPLE COMPARISON MODE.
      IREC=5
      ISEND=6
      LS=320
C       IFORM=0 FOR INTEGER WORD DATA INPUT .
C       IFORM=1 FOR BYTE DATA INPUT.
```

```
C        *****IFORM=2 FOR INTEGER DATA INPUT FROM A FLOATING
C             POINT SIZED FILE (AS IN THE ORIGINAL SIMULATIONS).*****
         IFORM=0
      NT=8
      PI2=6.2831853072
      XS=160.
      YS=160.
         CAL=0.985294
         RSCALE=1.0
C@@@@@@@@@@@@@@@@@@@@@@       TO PERMIT CHANGES     @@@@@@@@@@@@@@@@@@@@@@@@@
         WRITE (7,10)
  10     FORMAT(' BELOW CERTAIN VALUES "?" WILL APPEAR.'/,
     &' TYPE "NO" FOLLOWED BY A <CR> IF YOU DO NOT LIKE THOSE ',
     &'PARAMETERS---'/' THEN TYPE THE NEW VALUE ',
     &'FOLLOWED BY A <CR>. OTHERWISE, JUST TYPE <CR>.'/)
C        ALLOW FOR PROGRAM TO OUTPUT IMAGE FROM AN ALREADY
C              RECONSTRUCTED DATA FILE.
  13     WRITE(7,11)
  11     FORMAT (' DO YOU WANT PROGRAM TO EXECUTE THE OUTPUT ',
     1'MODE ONLY?',/,' ?')
         READ (IREC,98) IFUNCT
C98      FORMAT (A2)
         IF (IFUNCT.NE.NO) GO TO 30
         DATA IZ/320*0/
      DATA Z/320*0./
  14     WRITE(7,15) NT
  15     FORMAT(' THE NUMBER OF TRANSDUCERS (NT) = ',I2/' ?')
         READ(IREC,98) IANS
  98     FORMAT (A2)
         IF (IANS.NE.NO) GO TO 20
         READ(IREC,99) NT
  99     FORMAT (I2)
         GO TO 14
  20     WRITE(7,25) R
  25     FORMAT(' THE RADIUS OF THE RING OF TRANSDUCERS',
     &' (IN DATA BINS) =',F7.3/' ?')
         READ(IREC,98) IANS
C98      FORMAT (A2)
         IF (IANS.NE.NO) GO TO 30
         READ (IREC,59) R
  59     FORMAT (F7.3)
         GO TO 20
  30     WRITE(7,35) XS,YS,LS
  35     FORMAT (' THE SCAN BEGINS (W.R.T. THE CENTER OF
     & TRANSDUCERS) AT COORDINATES'/5X,' X=',F10.4,5X,'Y=',
     &F10.4/' AND EXTENDS TO THE LEFT & DOWN FOR ',I5,' BINS ',
     &'(CANNOT EXCEED 320).'/' ?')
         READ(IREC,98) IANS
C98      FORMAT (A2)
         IF ((IFUNCT.NE.NO).AND.(IANS.NE.NO)) GO TO 60
         IF (IANS.NE.NO) GO TO 40
         WRITE (7,58)
  58     FORMAT (' INSERT CHANGES AS:  XS<CR>YS<CR>LS<CR>',/)
         READ (IREC,97) XS,YS,LS
```

```
  97    FORMAT (F10.4,/,F10.4,/,I3)
        GO TO 30
C       <><><><><><><><><><><><><><><>
C       ALLOW FOR USER CAPABILITY TO SELECT IMAGE INPUT FILE.
C       <><><><><><><><><><><><><><><>
  40    WRITE (7,45) IDATA
  45    FORMAT(' THE DATA IS FROM THE FILE NAMED ',7A2/' ?')
        READ(IREC,98) IANS
C98     FORMAT (A2)
        IF (IANS.NE.NO) GO TO 665
        WRITE (7,1000)
1000    FORMAT (' ENTER FILE NAME IN FORM "DK1:PROC##.DAT"',/)
        READ(IREC,96) IDATA
  96    FORMAT (7A2)
        GO TO 40
 665    WRITE (7,663) IFORM
 663    FORMAT (' INPUT DATA FORMAT IS TYPE ',I1,'.     < WORD(0) OR ',
       1'BYTE(1)',/,33X,' OR ++SIMULATION TYPE(2)++ >',/,' ?')
C       ++SIMULATION TYPE++ --- WHEN INITIALLY FORMING SIMULATED SCAN DATA
C              FILES, THE SIMULATED DATA WAS INTEGER TYPE, BUT PLACED IN
C              FLOATING POINT SIZED ARRAYS (I.E. 640 WORDS RATHER THAN
C              320 WORDS). THUS, THE NEED FOR THE SPECIFICATION OF
C              'SIMULATION TYPE(2)' DURING SYSTEM DEVELOPMENT.
        READ (5,664) IANS
 664    FORMAT (A2)
        IF (IANS.NE.NO) GO TO 50
        READ (5,662) IFORM
 662    FORMAT (I1)
        GO TO 665
  50    WRITE(7,55) ICON
  55    FORMAT(' THE CONVOLVING FUNCTION IS FROM THE FILE',
       &' NAMED ',7A2/' ?')
        READ(IREC,98) IANS
C98     FORMAT (A2)
        IF (IANS.NE.NO) GO TO 60
        WRITE (7,1001)
1001    FORMAT (' ENTER FILE NAME IN FORM "DK1:CONV##.DAT"',/)
        READ(IREC,96) ICON
C96     FORMAT (7A2)
        GO TO 50
  60    WRITE(7,65) ITEMP
  65    FORMAT(' THE RECONSTRUCTED IMAGE WILL BE STORED IN THE FILE ',
       &'NAMED ',7A2/' ?')
        READ(IREC,98) IANS
C98     FORMAT (A2)
        IF (IANS.NE.NO) GO TO 71
        WRITE (7,1002)
1002    FORMAT (' ENTER FILE NAME IN FORM "DK1:IMAG##.DAT"',/)
        READ(IREC,96) ITEMP
C96     FORMAT (7A2)
        GO TO 60
  71    IF (IFUNCT.NE.NO) GO TO 777
1114    WRITE (7,1111) CAL
1111    FORMAT (' THE DATA CALIBRATION FACTOR IS ',F8.6,/,' ?')
```

```
C        'CAL' EQUALS THE NUMBER OF DATA SAMPLES FROM THE TRANSIENT RECORDER
C              REQUIRED TO COVER TRAVELING TWICE THE RING DIAMETER, DIVIDED
C              BY THE NEXT LARGEST NUMBER WHICH IS DIVISIBLE BY 320.
         READ (5,1112) IANS
  1112   FORMAT (A2)
         IF (IANS.NE.NO) GO TO 78
         WRITE (7,1119)
  1119   FORMAT (' ENTER CALIBRATION FACTOR.',/,' >')
         READ (5,1113) CAL
  1113   FORMAT (F8.6)
         GO TO 1114
    78   WRITE (7,67) RSCALE
    67   FORMAT (' THE DURING-RECONSTRUCTION SCALE FACTOR IS ',F9.4,/,' ?')
         READ (IREC,98) IANS
  C98    FORMAT (A2)
         IF (IANS.NE.NO) GO TO 72
         READ (IREC,73) RSCALE
    73   FORMAT (F9.4)
         GO TO 78
    72   DO 257 J=40,160,40
C        SUPPLY FOUR LINES OF 80 CHARACTERS EACH FOR IMAGE FILE COMMENTS.
C        STORE COMMENTS AT END OF RECONSTRUCTED IMAGE FILE.
   259   WRITE (7,258)
   258   FORMAT (' ENTER <= 80 CHARACTERS OF IMAGE FILE I.D.',/,
        1' TERMINATE LINE ENTRY WITH A <CR>. MAX. ENTRY = 4 LINES.')
         READ (5,256) (IDESCR(I),I=(J-39),J)
   256   FORMAT (40A2)
   257   CONTINUE
    70   WRITE(7,75)
    75   FORMAT(' WANT ANOTHER CHANCE?   (YES OR NO)')
         READ (IREC,98) IANS
  C98    FORMAT (A2)
         IF (IANS.NE.NO) GO TO 13
         IF (LS.GT.320) GO TO 30
C@@@@@@@@@@@@@@@@@@@@@@@@@@@@@@@@@@@@@@@@@@@@@@@@@@@@@@@@@@@@@@@@@@@@@@
         CALL TIME(SEC)
         DECHRS=SEC/3600.
         WRITE (6,17) DECHRS
    17   FORMAT (' START TIME:  ',F6.3,' HOURS',///)
C        LENGTH EQUALS THE NUMBER OF SAMPLES (I.E. INDICES) EACH IN
C              THE DATA AND CONVOLUTION FUNCTIONS.
         LENGTH=320
         IF (IFORM.EQ.0) IWIDTH=320
         IF (IFORM.EQ.0) LWIDTH=320
         IF (IFORM.EQ.1) IWIDTH=160
         IF (IFORM.EQ.1) LWIDTH=160
         IF (IFORM.EQ.2) IWIDTH=640
         IF (IFORM.EQ.2) LWIDTH=320
   777   LSP1=LS+1
         CALL ASSIGN (12,IDATA,14)
         CALL ASSIGN (14,ICON,14)
         CALL ASSIGN (18,ITEMP,14)
         NUMREC=NT*(NT+1)/2
C        THE PROCESSED DATA FILE WILL CONTAIN 320 SAMPLES PER RECORD.
```

```
C              FOR INTEGER DATA, THE RECORD LENGTH WILL BE 320 16-BIT WORDS.
C              FOR BYTE DATA, THE RECORD LENGTH WILL BE 160 16-BIT WORDS.
       DEFINE FILE 12 (NUMREC,IWIDTH,U,IVAR1)
       DEFINE FILE 14 (1,641,U,IVAR2)
         DEFINE FILE 18 (LSP1,640,U,IVAR3)
         IF (IFUNCT.NE.NO) GO TO 778
C      <><><><><><><><><><><><><><><><><><><><><>
C      USER CAN SPECIFY INDIVIDUAL INPUT AND OUTPUT FILE NAMES
C           VIA QUESTIONS AT BEGINNING OF PROGRAM.
C      <><><><><><><><><><><><><><><><><><><><><>
       READ (14'1) LG,(G(J),J=1,320)
       DO 100 I=1,LS
         WRITE (18'I) (Z(J),J=1,320)
C        INITIALIZE ITEMP TO (LS*(320*0.))
  100    CONTINUE
C      **********DESIGNATION OF T/R PAIRS***********
       IDXREC=0
       DO 200 M=1,NT
C      TRANSMITTER NUMBER DESIGNATION
       PSI=(M-1)*PI2/NT
       XT=R*COS(PSI)
       YT=R*SIN(PSI)
C      *****INDEX 'M' ALLOWS FOR ONLY UNIQUE T/R PAIRS*****
C      *****THERE ARE NT*(NT+1)/2 UNIQUE T/R PAIRS*****
C      *****CHANGING 'M' TO '1' WILL PRODUCE ALL N**2 T/R PAIRS*****
       DO 201 N=M,NT
C      RECEIVER NUMBER DESIGNATION
       PHI=(N-1)*PI2/NT
       XR=R*COS(PHI)
       YR=R*SIN(PHI)
       IDXREC=IDXREC+1
         READ (12'IDXREC) (IF(MN),MN=1,LWIDTH)
         DO 1 MN=1,LENGTH
         IF (IFORM.EQ.1) GO TO 660
C        *****FOR INTEGER INPUT DATA*****
C        INTEGER TO FLOATING POINT CONVERSION.
         F(MN)=FLOAT(IF(MN))
         GO TO 1
C        *****FOR BYTE INPUT DATA*****
C        BYTE TO FLOATING POINT CONVERSION.
  660    F(MN)=IBYTF(MN)
  1      CONTINUE
C      ***************************************************************
C      NOTE:   ALTHOUGH INPUT DATA IS IN INTEGER (I.E. 16 BITS) OR
C              BYTE (I.E. 8 BITS) FORMAT, ALL INTERNAL PROGRAM
C              CALCULATIONS ARE CARRIED OUT IN FLOATING POINT FORM.
C      ***************************************************************
       WRITE (6,666) M,N
  666  FORMAT (50X,'*****',I4,2X,I4,'*****')
       CALL CLOSE (ISEND)
      CALL CSCAN(XT,YT,XR,YR,XS,YS,LS,ITEMP,F,LENGTH,G,LG,C,ISEND,
     1IZ,Z,SCALE,CAL,RSCALE)
  201 CONTINUE
  200 CONTINUE
```

```
C          WRITE IMAGE IDENTIFICATION ON IMAGE FILE AFTER IMAGE.
           WRITE (18'(1+LS)) (IDESCR(I),I=1,160)
C----------PRINT TIME OF ALGORITHM COMPLETION----------
           CALL TIME(SEC)
           DECHRS=SEC/3600.
           WRITE (6,18) DECHRS
  18       FORMAT (' FINISH TIME:  ',F6.3,' HOURS',///)
C-------------------------------------------------------------
       WRITE (7,111)
 111   FORMAT(' WOULD YOU LIKE TO SEE THE TOTAL PICTURE?  (YES OR NO)')
       READ (IREC,98) IANS
C98  FORMAT(A2)
       IF (IANS.EQ.NO) GO TO 120
C          PRINT IMAGE FILE IDENTIFICATION.
 778   READ (18'LSP1) (IDESCR(I),I=1,160)
       WRITE (6,260) (IDESCR(I),I=1,160)
 260   FORMAT (1X,40A2)
       IF (IMODE.NE.NO) GO TO 942
     CALL OUTPUT(1,18432)
C    RESET DISPLAY MONITOR POINTER.
C    ****************************
 942   WRITE (7,920)
 920   FORMAT (' DO YOU WANT TO ENTER OUTPUT SCALE FACTOR MANUALLY?',
     1/,' YES OR NO ?',/,' >')
       READ (5,925) IANS
 925   FORMAT (A2)
       IF (IANS.EQ.NO) GO TO 930
       WRITE (7,1118)
 1118  FORMAT (' ENTER SCALE FACTOR (F7.3 FORMAT).',/,' >')
       READ (5,935) SCALE
 935   FORMAT (F7.3)
       WRITE (7,940) SCALE
 940   FORMAT (' MANUALLY ENTERED OUTPUT SCALE FACTOR IS ',F7.3,
     1/,' YES OR NO ?',/,' >')
       READ (5,941) IANS
 941   FORMAT (A2)
       IF (IANS.EQ.NO) GO TO 942
       GO TO 1117
C          CALCULATION OF OUTPUT DISPLAY SCALE FACTOR.
C          'SCALE' WILL CONVERT UNSCALED STORED IMAGE DATA INTO
C                THE RANGE 0-1023.
C          THIS CALCULATION OF 'SCALE' IS FOR DIRECT OUTPUT OF ENTIRE
C                IMAGE EITHER DIRECTLY FROM DISC FILE OR FROM DISC FILE
C                IMMEDIATELY AFTER RECONSTRUCTION.
C          THE VALUE 'RSCALE' IS ENTERED MANUALLY AND IS USED TO
C                TEMPORARILY SCALE DATA FOR DISPLAY DURING RECONSTRUCTION.
 930   RELMAX=0.
       DO 850 IMAX=1,LS
       READ (18'IMAX) (Z(J),J=1,320)
       DO 860 IMX=1,319,2
C          IN ORDER TO DISPLAY THE TRANSDUCER LOCATIONS AT THE BRIGHTEST GRAY SHADE,
C                THESE LOCATIONS ARE ASSIGNED A GRAY VALUE GREATER THAT THAT
C                EXPECTED FOR ANY POSSIBLE DATA POINT. THUS, THE USE OF THIS VALUE
C                FOR SCALING PURPOSES WILL PRODUCE AN ERRONEOUS SCALE FACTOR.
```

```
C                  THEREFORE, THE ASSUMPTION IS BEING MADE THAT ANY POINT ADJACENT TO
C                  A GIVEN TRANSDUCER LOCATION WILL NOT BE THE MAXIMUM VALUE BEING
C                  SOUGHT FOR PUSPOSES OF SCALING. SHOULD IT BE THAT POINT,
C                  ALL THAT WILL HAPPEN IS THAT THE BRIGHT POINT REPRESENTING THE
C                  TRANSDUCER LOCATION WILL BE TWO PIXELS WIDE RATHER THAN ONE.
C                  FOR THE TIME BEING, THIS METHOD SHOULD BE SATISFACTORY.  LDN
           IF ((Z(IMX)).GE.100000000000.) GO TO 860
           IF ((Z(IMX+1)).GE.100000000000.) GO TO 860
           RELMAX=AMAX1(Z(IMX),Z(IMX+1),RELMAX)
  860      CONTINUE
  850      CONTINUE
           SCALE=RELMAX/1023.
           WRITE (7,907) SCALE
  907      FORMAT (' THE CALCULATED OUTPUT SCALE FACTOR IS ',F7.3,/,' ?')
           READ (5,1115) IANS
 1115      FORMAT (A2)
           IF (IANS.EQ.NO) GO TO 942
 1117      WRITE (6,1116) SCALE
 1116      FORMAT (' THE FINAL OUTPUT SCALE FACTOR IS ',F7.3)
  943 DO 114 I=1,LS
           READ (18'I) (Z(J),J=1,320)
C          READ ONE LINE FROM RECONSTRUCTED DATA FILE PRIOR TO DISPLAY.
           DO 113 IJ=1,320
C       HARD LIMITER FOR DATA OUTPUT TO CT/T MONITOR.
C       SCALE DATA AMPLITUDE PRIOR TO DISPLAY.
           Z(IJ)=(SIGN(0.5,Z(IJ))+Z(IJ)/SCALE)-512.
C          IMAGE DISPLAY VALUES ARE NOW SCALED FROM -512. TO +511.
           IF (Z(IJ).GT.511.) Z(IJ)=511.
           IF (Z(IJ).LT.(-512.)) Z(IJ)=-512.
           IZ(IJ)=INT(Z(IJ))
  113      CONTINUE
      CALL OUTPUT(320,IZ)
  114 CONTINUE
      CALL CLOSE(18)
  120 WRITE(7,121)
  121 FORMAT(' WANT TO TRY IT AGAIN?  (YES OR NO)')
      READ (IREC,98) IANS
C98      FORMAT (A2)
           IF (IANS.EQ.NO) GO TO 122
           WRITE (7,1120)
 1120      FORMAT (' WANT IMAGE COMPARISON MODE? (YES OR NO)',/,' >')
           READ (IREC,98) IMODE
           GO TO 13
  122 WRITE(ISEND,125)
  125 FORMAT(//' DONE')
      STOP 'PULSE-SCATTER IMAGING---IMAGE RECONSTRUCTION ALGORITHM'
      END
      SUBROUTINE CSCAN(XT,YT,XR,YR,XS,YS,LS,ITEMP,F,LENGTH,G,LG,C,ISEND,
     1IZ,Z,SCALE,CAL,RSCALE)
      DIMENSION G(LG)
      DIMENSION IZ(320),Z(320),C(LENGTH),F(LENGTH)
C****************    CONVOLUTION    ****************************
      DO 1 III=1,LENGTH
      C(III)=F(III)
```

```
1       CONTINUE
        GO TO 2001
        MAX=LG
        DO 2000 J=1,LENGTH
C       +++4X RAD. = LARGEST T/R PATH WITHIN RING AREA+++
C       WRITE(6,2300) J
C2300   FORMAT(' *=',I5)
        C(J)=0
        J1=J+1
        IF (J.LE.LG) MIN=J
        DO 2100 I=1,MIN
 2100   C(J)=C(J)+F((J1-I))*G(I)
        IF (J.EQ.LENGTH.OR.MAX.LT.2) GO TO 2000
        JM=LENGTH-J+1
        IF(JM.LT.LG) MAX=JM
        DO 2200 I=2,MAX
 2200   C(J)=C(J)+F((J+I-1))*G(I)
 2000   CONTINUE
C*******************************************************************
 2001   CONTINUE
C2001   WRITE (6,5) (C(MN),MN=1,LENGTH)
 5      FORMAT (1X,10F6.1)
C...................      SCAN/BACKPROJECTION      ...................
        M1=(320-LS)/2
        M3=M1+1
        M4=M1+LS
        M5=M1+LS+1
C       USE SSWTCH ROUTINE TO BYPASS CALL OF "OUTPUT" WHEN OPERATING
C              WITHOUT CT/T MONITOR.
        CALL SSWTCH(1,LSS1)
        IF (LSS1.EQ.2) GO TO 138
        CALL OUTPUT(1,18432)
C       SUBROUTINE TO RESET DISPLAY MONITOR POINTER.
 138    DO 3000 J=1,LS
C       WRITE (ISEND,27) J
C27     FORMAT (' DISPLAY LINE ',I3,' IS BEING OUTPUT.')
C       CALL CLOSE(ISEND)
        Y=YS-J+1
        DTY=(YT-Y)*(YT-Y)
C       DTY = TRANSMIT DISTANCE (Y)
        DRY=(YR-Y)*(YR-Y)
C       DRY = RECEIVE DISTANCE (Y)
        READ (18'J) (Z(JJ),JJ=1,320)
        DO 3100 I=1,LS
        INDX=M1+LS-I+1
        X=XS-I+1
        DTX=(XT-X)*(XT-X)
C       DTX = TRANSMIT DISTANCE (X)
        DRX=(XR-X)*(XR-X)
C       DRX = RECEIVE DISTANCE (X)
C*****ONE UNIT DATA SAMPLE DISTANCE INDEX CORRESPONDS TO TWO
C       UNITS OF ACTUAL CALCULATED DISTANCE (DUE TO ROUND-
C       TRIP CALCULATION).*****
        TWOXD=SQRT(DTX+DTY)+SQRT(DRX+DRY)
```

```
        D=TWOXD/2.
C       SINCE THE 320 UNITS OF DATA WAVEFORM ACTUALLY CORRESPOND
C           TO 320 PIXEL UNITS OF DISTANCE, MULTIPLY BY 'CAL'
C           TO MAKE DISTANCE CALCULATION AND WAVEFORM INDEX UNIT
C           COMPARABLE.
C       ******************************************
C       EXAMPLE FOR DETERMINATION OF 'CAL' FACTOR.
C       ******************************************
C       FOR EXAMPLE, CAL=292./304.
C       ONE THRU TRANSMISSION EQUALS 292 USEC.
C       320 PTS. OF PROCESSED WAVEFORM CORRESPONDS TO 304 USEC.
C       'CAL' CAN BE MODIFIED FOR CALIBRATION IF 320 UNITS OF PROCESSED
C           DATA DOES NOT EXACTLY CORRESPOND TO 320 PIXEL ELEMENTS.
C       ******************************************
        D=D*CAL
C       ID=D
C       ROUND OFF DISTANCE TO NEAREST INTEGER.
        ID=INT(D+0.5)
        IF (((ID+1).GT.LENGTH).OR.(ID.LT.1)) GO TO 3100
        FR=D-ID
C       Z(INDX)=0.5+Z(INDX)+(1.-FR)*C(ID)+FR*C((ID+1))
C******LINEAR INTERPOLATION BETWEEN DATA POINTS.*****
C       Z(INDX)=Z(INDX)+(1.-FR)*C(ID)+FR*C((ID+1))
C       <><><><><>CALCULATION WITHOUT INTERPOLATION<><><><><>
        Z(INDX)=Z(INDX)+C(ID)
 3100 CONTINUE
        GO TO 1015
C***THE FOLLOWING STATEMENTS WERE ORIGINALLY USED TO BLACKEN AREA
C    SURROUNDING PARTIAL RECONSTRUCTION. SINCE THIS PROCEDURE
C    ELIMINATED SEVERAL TRANSDUCERS FROM DISPLAY, METHOD USED IS
C    TO INITIALIZE IMAGE ARRAY TO -512 PRIOR TO RECONSTRUCTION.***
C       IF (M1.LE.0) GO TO 1010
C       DO 3200 I=1,M1
C3200 Z(I)=-512.
C1010   IF (M5.GT.320) GO TO 1015
C       DO 3400 I=M5,320
C3400 Z(I)=-512.
C&&&&&&&&&&&&&&&&&&&&&       TRANSDUCER LOCATOR       &&&&&&&&&&&&&&&&&&&&&&&&
 1015 IXS=INT(SIGN(0.5,XS)+XS)
        IY=INT(SIGN(0.5,Y)+Y)
        IYTR=INT(SIGN(0.5,YT)+YT)
        IF (IY.NE.IYTR) GO TO 4100
        IXTR=INT(SIGN(0.5,XT)+XT)
        IND=M1+LS-IXS+IXTR
        IF (IND.LT.1.OR.IND.GT.320) GO TO 4100
        Z(IND)=999999999999.
 4100 IYREC=INT(SIGN(0.5,YR)+YR)
        IF (IY.NE.IYREC) GO TO 4300
        IXREC=INT(SIGN(0.5,XR)+XR)
        IND=M1+LS-IXS+IXREC
        IF (IND.LT.1.OR.IND.GT.320) GO TO 4300
        Z(IND)=999999999999.
 4300 CONTINUE
C&&&&&&&&&&&&&&&&&&&&&&&&&&&&&&&&&&&&&&&&&&&&&&&&&&&&&&&&&&&&&&&&&&&&&&&&&&&&&
```

```
C        STORE RECONSTRUCTED IMAGE VALUES AS UNSCALED QUANTITIES.
C        'RSCALE' IS SCALE FACTOR ON DISC OUTPUT TO DISPLAY.
C        THIS FACTOR SHOULD BE MANUALLY ENTERED AT BEGINNING OF PROGRAM
C            SO AS TO PRODUCE GRAY SHADES IN THE RANGE 0-1023, FOR
C            DISPLAY DURING IMAGE RECONSTRUCTION. THE SCALE FACTOR
C            'SCALE', COMPUTED EARLIER, AUTOMATICALLY SCALES FINAL
C            IMAGE PRIOR TO DISPLAY IN ORDER TO ACHIEVE A DATA
C            RANGE FROM 0-1023. SUBSEQUENT SUBTRACTION
C            OF 512 RESULTS IN A FINAL DISPLAYED DATA
C            RANGE OF -512 TO +511.
        WRITE (18'J) (Z(JJ),JJ=1,320)
C***"SSWTCH" IS USED TO INHIBIT DISPLAY DURING IMAGE
C    RECONSTRUCTION VIA BIT 0 (LSB) BEING EITHER A '0' OR '1'.
C    THIS ROUTINE IS OF MOST VALUE WHEN USING THE LOW SPEED DATA LINK.
C    LSB=0 DISPLAYS RECONSTRUCTION IN PROGRESS; LSB=1 INHIBITS DISPLAY.***
        CALL SSWTCH(1,LSS1)
        IF (LSS1.EQ.2) GO TO 3000
        DO 3300 I=1,320
        Z(I)=SIGN(0.5,Z(I))+(Z(I)/RSCALE)-512.
C        HARD LIMITER TO LIMIT RANGE OF VALUES OUTPUT TO CT/T DISPLAY.
        IF (Z(I).GT.511.) Z(I)=511.
        IF (Z(I).LT.(-512.)) Z(I)=-512.
        IZ(I)=INT(Z(I))
 3300   CONTINUE
        CALL OUTPUT(320,IZ)
C       WRITE (ISEND,25)
C25    FORMAT(' RETURN FROM OUTPUT')
        CALL CLOSE(ISEND)
 3000 CONTINUE
C.........................................................
        RETURN
        END
```

SUBROUTINE CALLED BY PSIV02 TO ENABLE OPTIONAL VIEWING OF IMAGE DURING
RECONSTRUCTION.

.

```
 6-OCT-78
SSWTCH.MAC     1 23-JAN-78


                          ;P.S.I. SUBROUTINE
            .GLOBL SSWTCH  ;FOR VIEWING RECONSTRUCTION IN PROGRESS
            R3=%3          ;DEFINE R3
            R5=%5          ;DEFINE R5
            PC=%7          ;DEFINE PROGRAM COUNTER REGISTER
SSWTCH: TST (R5)+          ;VALUE IN R5 PTS. TO NO. OF SUBROUTINE ARGUMENTS
        MOV @(R5)+,R3      ;VALUE IN R5 PTS. TO THE VALUE (1)
        BIT R3,@#177570    ;SWITCH REGISTER ADDRESS = 177570
        BEQ 1$
        MOV #2,@(R5)       ;IF LSB=1, DO NOT DISPLAY RECONSTRUCTING IMAGE
        RTS PC
1$:     MOV #1,@(R5)       ;IF LSB=0, DISPLAY RECONSTRUCTING IMAGE
        RTS PC
        .END
```

USED TO OUTPUT DATA TO CT DISPLAY. THE EXPECTED FORTRAN CALLING SEQUENCE
FOR THIS ROUTINE IS: CALL OUTPUT (N,I)
WHERE: N= NO. OF DATA POINTS (LAST SIGNIFICANT 10 BITS OF 16 BIT
DATA WORD IS ACCEPTED BY DISPLAY MEMORY) AND I= NAME OF ARRAY (INTEGER) IN
WHICH DATA IS STORED. NOTE THAT 'CALL OUTPUT (1,18432) PLACES CT DISPLAY
POINTER AT TOP LEFT CORNER OF SCREEN. I.E. PIXEL (1,1). EACH DATA VALUE
ENTERED AFTER EXECUTION OF THIS STATEMENT WILL CAUSE THE DISPLAY POINTER
TO MOVE ONE LOCATION TO THE RIGHT, UNTIL THE END OF A 320 POINT LINE HAS
BEEN REACHED, AT WHICH TIME POINTER JUMPS TO NEXT LINE. DISPLAY MEMORY IS NOT
RANDOM ACCESS.

```
 2-NOV-78
OUTS  .MAC    2 27-OCT-78



            .TITLE   CT/T DISPLAY GENERATOR INTERFACE
  ;
  ;         EXPECTED FORTRAN CALLING SEQUENCE
  ;
  ;         CALL OUTPUT(ISIZE,IARRAY)
  ;
  ;         R.E.GLUSICK              17-FEB-76
  ;
            .GLOBL   OUTPUT
            OUT      =167772        ;AT DR11-C
            STATUS   =167774        ;AT DR11-C
            SIZE     =%3
            ARRAY    =%4
            R5       =%5
OUTPUT:     TST      (R5)+          ;NUMBER OF ARGS
            MOV      @(R5)+,SIZE    ;SET UP LOOP COUNT
            MOV      (R5),ARRAY     ;GET ADDRESS OF ARRAY
1$:         BIT      STATUS,OK      ;CHECK DR11-C READY
            BNE      1$             ;GO BACK IF NOT READY
            MOV      (ARRAY)+,OUT   ;MOV DATA TO DR11-C
            DEC      SIZE           ;STEP LOOP COUNT
            BGT      1$             ;REPEAT IF NOT DONE
            RTS      %7             ;NORMAL RETURN
OK:         .WORD    1              ;INTERFACE READY MASK
            .END
```

PROGRAM TO COMPLETELY ERASE CT DISPLAY. TO ACTIVATE WHILE IN MONITOR,
TYPE: .R ERASE

 6-OCT-78
ERASE .FOR   1 25-JAN-78

```
        TYPE 10
10      FORMAT (' ERASE CT/T SCREEN')
        CALL OUTPUT(1,"120000)
        CALL OUTPUT(1,"060000)
        STOP
        END
```

THIS ROUTINE USED TO PERFORM PSI RECONSTRUCTION ON TEKTRONIX 4002A
GRAPHIC CRT STORAGE TERMINAL VIA DIRECT ELLIPSE DRAWING AND SUBSEQUENT
OVERLAY ON THE STORAGE SCREEN TO FORM ESSENTIALLY A BISTABLE IMAGE.

6-OCT-78
TSTOK2.FOR   10 8-JAN-78

```
        DIMENSION DATA(8,8,5),X(8),Y(8),YOLD(320,2)
        DIMENSION YNEW(320,2),XNEW(320,2)
      CALL INIT
        ICOUNT=0
        IXP=1
        IXM=2
        WRITE (7,15)
15      FORMAT (' ENTER NUMBER OF MICROSECONDS IN ONE THRU-TRANSMISSION',
     1' <F6.2 FORMAT>.',/)
        READ (5,16) CAL
16      FORMAT (F6.2)
        WRITE (7,202)
202     FORMAT (' AFTER "*" ENTER DATA FILE NAME IN FORM "ELIPS*.DAT".',/)
        CALL ASSIGN (11,'ELIPS*.DAT',-1,'OLD','CC')
        WRITE (7,408)
408     FORMAT (' ENTER NUMBER OF TRANSDUCERS IN RING.')
        READ (5,409) NT
409     FORMAT (I2)
        NPTS=320
        WRITE (7,410)
410     FORMAT (' ENTER NO. OF DATA POINTS PER RECEIVED SIGNAL.')
        READ (5,411) NUMDAT
411     FORMAT (I4)
        IPOUT=320
        PI2=6.2831853072
        WRITE (7,301)
301     FORMAT (' TYPE IN RADIUS OF TRANSDUCER RING
     1 <F5.2 --- IN INCHES>.')
        READ (5,300) R
300     FORMAT (F5.2)
      CALL INIT
        WRITE (6,320) NT,R
320     FORMAT (' THERE ARE ',I2,' TRANSDUCERS IN THE RING.',
     1/,' TRANSDUCER RING RADIUS IS ',F5.2,' INCHES.')
        NELIPS=(NT*(NT+1))/2
        WRITE (6,406) NELIPS,NPTS
406     FORMAT (' THERE WILL BE ',I4,' ELLIPSE FAMILIES.',/,
     1' EACH ELLIPSE WILL CONTAIN ',I3,' POINTS.')
        WRITE (6,412) NUMDAT
412     FORMAT (' THERE WILL BE ',I4,' ELLIPSES PER T/R PAIR.')
        WRITE (6,17) CAL
17      FORMAT (' CALIBRATION IS ',F6.2,' MICROSECONDS EQUALS 320',
     1' PICTURE UNITS (I.E. TRANSDUCER RING DIAMETER).')
      CALL CLOSE(6)
C     HAVE PRINTER OUTPUT CURRENT CONTENTS OF BUFFER
C     VELOCITY OF SOUND IN WATER IS 1490 METERS/SECOND.
        VELOC=1490.
        EQUIV=(VELOC*CAL)/(10000.*320.)
        WRITE (6,18) EQUIV
18      FORMAT (' ONE PICURE UNIT CORRESPONDS TO ',F7.4,' CENTIMETERS.',
     1/,' THE IMAGE DIMENSIONS ARE 320 X 320 PICTURE UNITS.')
      CALL CLOSE(6)
        CONVER=320./CAL
        IYPASS=160
```

```
        DO 778 IXPASS=1,321,160
        IXPASS=IXPASS-1
        REWIND 11
        CALL AMODE
        WRITE (6,666) IXPASS,IYPASS
  666   FORMAT (' ELIPSE CONSTRUCTION PASS NUMBER (',I3,',',I3,').')
        CALL CLOSE(6)
C       HAVE PRINTER OUTPUT CURRENT CONTENTS OF BUFFER
        DO 310 M=1,NT
        X(M)=R*COS((PI2*(M-1))/NT)
        Y(M)=R*SIN((PI2*(M-1))/NT)
        X(M)=(X(M)*(160./R))+IXPASS
        Y(M)=(Y(M)*(160./R))+IYPASS
C       TRANDSUCER COORDINATES CENTERED AT (IXPASS,IYPASS) FOR CALCULATION
  310   CONTINUE
        DO 200 I=1,NT
        DO 210 J=1,NT
        READ (11,205,END=570) (DATA(I,J,K),K=1,NUMDAT)
  205   FORMAT (F6.2)
        DO 707 K=1,NUMDAT
        DATA(I,J,K)=CONVER*DATA(I,J,K)
  707   CONTINUE
        XT=X(I)
        YT=Y(I)
        XR=X(J)
        YR=Y(J)
        XM=(XT+XR)/2
        YM=(YT+YR)/2
        THETA=ATAN2((YT-YR),(XT-XR))
        ANGLE=THETA*360./PI2
        DO 220 K=1,NUMDAT
        INDEX=320/NPTS
        DO 230 IXOLD=1,320,INDEX
        D=DATA(I,J,K)
        IF (DATA(I,J,K).EQ.0.) GO TO 229
        A=(D/2.)**2.
        B=(XT-XM)**2.
        C=(YT-YM)**2.
        E=(IXOLD-XM)**2.
        IF ((1.-E/A).LT.-.01) GO TO 229
        IF (((1.-E/A).GT.-.01).AND.((1-E/A).LT.0.)) E=A
        F=A-B-C
        IF (F.LT.-.01) GO TO 229
        IF (((F).LT.0.).AND.((F).GE.-.01)) F=0
        YOLD(IXOLD,IXP)=YM+SQRT((F)*(1.-E/A))
        YOLD(IXOLD,IXM)=YM-SQRT((F)*(1.-E/A))
        XOLD=FLOAT(IXOLD)
        XOLD=XOLD-XM
        YOLD(IXOLD,IXP)=YOLD(IXOLD,IXP)-YM
        YOLD(IXOLD,IXM)=YOLD(IXOLD,IXM)-YM
        YNEW(IXOLD,IXP)=XOLD*SIN(THETA)+YOLD(IXOLD,IXP)*COS(THETA)
        YNEW(IXOLD,IXM)=XOLD*SIN(THETA)+YOLD(IXOLD,IXM)*COS(THETA)
        XNEW(IXOLD,IXP)=XOLD*COS(THETA)-YOLD(IXOLD,IXP)*SIN(THETA)
        XNEW(IXOLD,IXM)=XOLD*COS(THETA)-YOLD(IXOLD,IXM)*SIN(THETA)
```

```
        YNEW(IXOLD,IXP)=YNEW(IXOLD,IXP)+YM
        YNEW(IXOLD,IXM)=YNEW(IXOLD,IXM)+YM
        XNEW(IXOLD,IXP)=XNEW(IXOLD,IXP)+XM
        XNEW(IXOLD,IXM)=XNEW(IXOLD,IXM)+XM
      YNEW(IXOLD,IXP)=YNEW(IXOLD,IXP)-(IYPASS-160.)
      YNEW(IXOLD,IXM)=YNEW(IXOLD,IXM)-(IYPASS-160.)
      XNEW(IXOLD,IXP)=XNEW(IXOLD,IXP)-(IXPASS-160.)
      XNEW(IXOLD,IXM)=XNEW(IXOLD,IXM)-(IXPASS-160.)
        GO TO 230
229     YOLD(IXOLD,IXP)=0.
        YOLD(IXOLD,IXM)=0.
        YNEW(IXOLD,IXP)=0.
        XNEW(IXOLD,IXP)=0.
        YNEW(IXOLD,IXM)=0.
        XNEW(IXOLD,IXM)=0.
230     CONTINUE
      CALL IWIND(20,720,20,720)
      CALL RWIND(0.,320.,0.,320.)
      CALL CWIND(20,720,20,720)
      CALL MOVE(XNEW(1,1),YNEW(1,1))
      YPREV=0.
      DO 500 IXD=2,320
      IF(ABS(YNEW(IXD,1)).GT.1.E-18.AND.ABS(YPREV).LE.1.E-18)
     &CALL MOVE(XNEW(IXD,1),YNEW(IXD,1))
      IF(ABS(YPREV).GT.1.E-18.AND.ABS(YNEW(IXD,1)).GT.1.E-18)
     &CALL DRAW(XNEW(IXD,1),YNEW(IXD,1))
      YPREV=YNEW(IXD,1)
500 CONTINUE
C     CALL MOVE(XNEW(1,1),YNEW(1,1))
C     CALL DRAW(XNEW(1,2),YNEW(1,2))
      YPREV=0.
      DO 510 IXD=1,320
      IF(ABS(YNEW(IXD,2)).GT.1.E-18.AND.ABS(YPREV).LE.1.E-18)
     &CALL MOVE(XNEW(IXD,2),YNEW(IXD,2))
      IF(ABS(YPREV).GT.1.E-18.AND.ABS(YNEW(IXD,2)).GT.1.E-18)
     &CALL DRAW(XNEW(IXD,2),YNEW(IXD,2))
      YPREV=YNEW(IXD,2)
510 CONTINUE
        CALL AMODE
        ICOUNT=ICOUNT+1
220     CONTINUE
210     CONTINUE
200     CONTINUE
      IXPASS=IXPASS+1
770 CONTINUE
      GO TO 520
570 CALL AMODE
      WRITE (6,571)
571 FORMAT (' #####ERROR---INSUFFICIENT DATA---#####')
520 CALL AMODE
        XCOUNT=ICOUNT/3.
        WRITE (6,7) XCOUNT
7       FORMAT (' THERE WERE A TOTAL OF ',F6.1,' ELLIPSES DRAWN.')
        STOP '---P.S.I. FOR MANUAL DATA ACQUISITION TRIALS-----'
        END
```

B-3. TRANSIENT RECORDER SOFTWARE AND ASSOCIATED ROUTINES

READIN.FOR
RDPTR.MAC
SWDPTR.MAC
GETDAT.FOR
GTDATO.FOR
RDOUT.FOR

USED TO READ PSI DATA FROM AEL PTR-9000 TRANSIENT RECORDER DIGITAL OUTPUT
INTERFACE, ONE WAVEFORM AT A TIME. SUBROUTINE RDPTR.MAC IS CALLED, AN ASSEMBLY
LANGUAGE ROUTINE TO DIRECT THE ACTUAL DATA TRANSFER. THIS PROGRAM
IS THE ROUTINE USED FOR DATA COLLECTION. TO 'LINK' THIS PROGRAM USE THE FOLLOWING
SEQUENCE . . .   .R LINK
                 *READIN=READIN,RDPTR/F

 6-OCT-78
 READIN.FOR   ? 5-APR-78


```
C        READING OF DATA FROM TRANSIENT RECORDER.
         DIMENSION IDATA(7),IBUF(9000)
         BYTE LBUF(9000)
         EQUIVALENCE (LBUF(1),IBUF(1))
C        EQUIVALENCE STATEMENT TO ALLIGN FIRST VALUES OF EACH ARRAY.
         DATA N/1HN/
C        SET UP FILE FOR DATA STORAGE.
 50      WRITE (7,10)
 10      FORMAT (' ENTER NAME OF FILE FOR DATA STORAGE IN FORM',
        1' DK1:DATA##.DAT',/,' >')
         READ (5,20) IDATA
 20      FORMAT (7A2)
         WRITE (7,30) IDATA
 30      FORMAT (' THE RAW INPUT DATA WILL BE STORED IN THE FILE',
        1' NAMED ',7A2,/,' Y OR N ?',/,' >')
         READ (5,40) IANS
 40      FORMAT (A1)
         IF (IANS.EQ.N) GO TO 50
 150     WRITE (7,110)
 110     FORMAT (' ENTER DATA OUTPUT FORMAT --- WORD(0) OR BYTE(1)',
        1/,' >')
         READ (5,120) IFORM
 120     FORMAT (I1)
         WRITE (7,130) IFORM
 130     FORMAT (' DATA OUTPUT FORMAT WILL BE TYPE ',I1,/,
        1' Y OR N ?',/,' >')
         READ (5,140) IANS
 140     FORMAT (A1)
         IF (IANS.EQ.N) GO TO 150
         IF (IFORM.EQ.0) ISIZE=8192
         IF (IFORM.EQ.1) ISIZE=4096
 100     WRITE (7,60)
 60      FORMAT (' ENTER NUMBER OF TRANSDUCERS IN RING.',/,' >')
         READ (5,70) NT
 70      FORMAT (I2)
         WRITE (7,80) NT
 80      FORMAT (' THERE ARE ',I2,' TRANSDUCERS IN THE RING.',
        1/,' Y OR N ?',/,' >')
         READ (5,90) IANS
 90      FORMAT (A1)
         IF (IANS.EQ.N) GO TO 100
         NUMREC = NT*(NT+1)/2
         CALL ASSIGN (12,IDATA,14)
         DEFINE FILE 12 (NUMREC,ISIZE,U,IVAR1)
C        "NPTS" EQUALS NUMBER OF POINTS TO BE READ FROM PTR.
         NPTS=9000
C        READ 9000 PTS. RATHER THAN 8192 PTS. TO ENSURE THAT PTR
C            MEMORY IS CLEARED (IE. DATA READY BIT IS NOT SET).
C        NOTE: FOR SOME REASON, THE PTR WILL OUTPUT DATA WORDS
C            CORRESPONDING TO INDICES 8193-8200. THESE ADDITIONAL
C            VALUES ARE EQUAL TO THE FIRST EIGHT VALUES OUTPUT FROM MEMORY.
C            THIS SHOULD NOT HAPPEN, BUT DOES ANYWAY.
         DO 500 I=1,NUMREC
         CALL RDPTR (IBUF,NPTS,IFORM)
```

```
C         "IBUF" IS DIMENSIONED FOR 9000.
C         FOR WORD FORMAT. 8K DATA POINTS WILL OCCUPY 1ST 8192 WORDS OF IBUF.
C         FOR BYTE FORMAT. 8K DATA POINTS WILL OCCUPY 1ST 4096 WORDS OF IBUF.
          WRITE (12'I) (IBUF(J),J=1,ISIZE)
D         IF (IFORM.EQ.0) GO TO 999
D         WRITE (6,998) (LBUF(M),M=1,8200)
D998      FORMAT (1X,10I8,'*****BYTES*****')
D         GO TO 997
D999      WRITE (6,996) (IBUF(IN),IN=1,8200)
D996      FORMAT (1X,10I8,'*****WORDS*****')
 997      WRITE (7,160) I,NUMREC
 160      FORMAT (' RECORD NUMBER',I4,' OF ',I4,' WAS JUST',
     1'  ENTERED INTO DISC FILE.')
          IF (I.EQ.NUMREC) GO TO 500
          WRITE (7,190)
 190      FORMAT (' COMPUTER IS AWAITING NEXT RECORD.')
 500      CONTINUE
 580      WRITE (7,170)
 170      FORMAT (' ****************************',/,' DATA ENTRY IS NOW',
     1'  COMPLETE.',/,' ****************************',//,
     1'  WANT TO MAKE ANY CHANGES?',/,' Y OR N ?',/,' >')
          READ (5,180) IANS
 180      FORMAT (A1)
          IF (IANS.EQ.N) GO TO 510
 560      WRITE (7,520)
 520      FORMAT (' ENTER RECORD NUMBER TO BE RE-RECORDED.',/,' >')
          READ (5,530) IAGAIN
 530      FORMAT (I4)
          WRITE (7,540) IAGAIN
 540      FORMAT (' RECORD NUMBER ',I4,' WILL BE RE-RECORDED OVER.',
     1/,' Y OR N ?',/,' >')
          READ (5,550) IANS
 550      FORMAT (A1)
          IF (IANS.EQ.N) GO TO 560
          CALL RDPTR (IBUF,NPTS,IFORM)
          WRITE (12'IAGAIN) (IBUF(J),J=1,ISIZE)
          WRITE (7,570) IAGAIN
 570      FORMAT (' RECORD NUMBER ',I4,' WAS JUST RE-RECORDED.')
          GO TO 580
 510      STOP 'COLLECTION OF P.S.I. DATA VIA TRANSIENT RECORDER'
          END
```

THIS FORTRAN CALLABLE SUBROUTINE IS USED TO TRANSFER A SPECIFIED NUMBER OF
8 BIT WORDS (NPTS) FROM AEL PTR-9000 TRANSIENT RECORDER MEMORY TO SPECIFIED
INTEGER ARRAY (IARRAY) IN CALLING PROGRAM. PTR DATA (8 BITS=1 BYTE PER DATA
POINT) MAY EITHER BE PACKED TWO POINTS PER STORED WORD (16 BITS) OR ONE POINT
PER STORED WORD, IN WHICH CASE DATA VALUE WILL OCCUPY THE EIGHT LEAST
SIGNIFICANT BITS OF THE STORED WORD.

```
    6-OCT-78
    RDPTR .MAC    3  1-MAR-78


    ;        R D P T R
    ;
    ;        READS DATA FROM PULSE AND TRANSIENT RECORDER
    ;
    ;        FORTRAN ENTRY:
    ;            CALL RDPTR(IARRAY,NPTS,IPK)
    ;                 WHERE   IARRAY IS START ADDR OF ARRAY IN WHICH TO STORE DATA
    ;                         NPTS IS NO. OF POINTS TO READ
    ;                         IPK = 1 TO PACK DATA IN BYTE FORMAT (2 POINTS/WORD)
    ;                             = 0 TO STORE 1 POINT PER WORD
    ;
    ;FOLLOWING ARE DEVICE ADDRESSES:
    STATUS=164015
    INPUT=164010
    ;
            .GLOBL RDPTR
            .MCALL ..V2...,.REGDEF
            ..V2..
            .REGDEF
    RDPTR:  MOV 2(R5),R0              ;PUT START ADDR INTO R0
            MOV @4(R5),R1             ;AND NO. OF POINTS TO READ INTO R1
            BLE RTN                   ;SHOULD BE GREATER THAN 0
    ;
    ;       NOTE.  WILL ONLY WAIT FOR READY FLAG BEFORE STARTING TRANSFER.
    ;              ONCE TRANSFER STARTED, ASSUME DATA ALWAYS READY.
    ;
    WAIT:   TSTB @#STATUS
            BEQ WAIT                  ;IF BYTE = 0, DATA NOT READY
            TST @6(R5)                ;CHECK WHETHER TO PACK
            BNE BFMT
    WFMT:   MOV @#INPUT,R2            ;STORING IN WORD FORMAT
            ADD #200,R2               ;CHANGING FROM OFFSET BINARY TO 2'S COMPL
            COM R2                    ;DATA MUST BE INVERTED
            MOVB R2,R3                ;QUICK AND DIRTY SIGN EXTEND
            MOV R3,(R0)+
            SOB R1,WFMT
            BR RTN
    BFMT:   MOV @#INPUT,R2            ;STORING IN BYTE FORMAT
            ADD #200,R2               ;CHANGING FROM OFFSET BINARY TO 2'S COMPL
            COM R2
            MOVB R2,(R0)+
            SOB R1,BFMT
    RTN:    RTS PC
            .END
```

THE AEL PTR-9000 TRANSIENT RECORDER IS CAPABLE OF REMOTE SOFTWARE CONTROL
VIA THE INTERFACE BOARD PROVIDED BY THE MANUFACTURER, WHICH IS CONNECTED
VIA THE DEC DR-11B. THE CONTROL SIGNALS ARE CABELED VIA TWISTED
PAIR, WHEREAS DIGITAL DATA TRANSFER BETWEEN THE PTR AND PDP-11 IS VIA 40
CONDUCTOR, SHIELDED FLAT RIBBON.

```
    6-OCT-78
  SWDPTR.MAC    2  1-MAR-78


  ;      S W D P T R
  ;
  ;      SETS WORDS IN PULSE AND TRANSIENT RECORDER
  ;
  ;      FORTRAN ENTRY:
  ;          CALL SWDPTR(CODE,IVAL)
  ;              WHERE    CODE IS 2 CHAR MNEUMONIC CODE FOR DEVICE ADDR
  ;                       IVAL IS VALUE TO BE SENT
  ;
         .GLOBL SWDPTR
         .MCALL ..V2....REGDEF
         ..V2..
         .REGDEF
  ;
  ;ALLOWABLE MNEUMONICS ARE:
  W1="W1
  W2="W2
  W3="W3
  W4="W4
  SR="SR
  MR="MR
  ;
  SWDPTR: MOV @2(R5),R0          ;PUT CODE FOR ADDR INTO R0
          MOV @4(R5),R1          ;STORE VALUE IN R1
  ;
  ;      NOW CHECK CODE AGAINST ALLOWABLE MNEUMONICS
  ;      IF MATCH, SET APPROPRIATE ADDRESS
  ;
          CMP R0,#W1
          BNE 1$
          MOV R1,@#164000
          RTS PC
  1$:     CMP R0,#W2
          BNE 2$
          MOV R1,@#164002
          RTS PC
  2$:     CMP R0,#W3
          BNE 3$
          MOV R1,@#164004
          RTS PC
  3$:     CMP R0,#SR
          BNE 4$
          CLR @#164006
          RTS PC
  4$:     CMP R0,#MR
          BNE 5$
          CLR @#164012
          RTS PC
  5$:     CMP R0,#W4
          BNE RTN
          MOV R1,@#164016
  RTN:    RTS PC
          .END
```

234

ROUTINE TO OUTPUT PSI DATA FROM DISC STORAGE: FILE, RECORD AND PORTION OF
RECORD FOR OUTPUT TO PRINTER MUST BE SPECIFIED.


```
        6-OCT-78
        GETDAT.FOR    2  8-MAR-78

              DIMENSION IBUF(9000)
              BYTE LBUF(8192)
              EQUIVALENCE (LBUF(1),IBUF(1))
              DATA N/1HN/
              WRITE (7,10)
      10      FORMAT (' ENTER NUMBER OF WORDS TO BE READ INTO MEMORY',/,
             1' >')
              READ (5,20) NWDS
      20      FORMAT (I4)
              WRITE (7,100)
      100     FORMAT (' ENTER NUMBER OF POINTS TO BE OUTPUT TO PRINTER',
             1' >')
              READ (5,90) NUM
      90      FORMAT (I4)
              WRITE (7,30)
      30      FORMAT (' ENTER DATA OUTPUT FORMAT <"0"=WORD,"1"=BYTE>'
             1,/,' >')
              READ (5,40) IFORM
      40      FORMAT (I1)
      80      CALL RDPTR (IBUF,NWDS,IFORM)
              IF (IFORM.EQ.1) GO TO 999
              WRITE (6,50) (IBUF(I),I=1,NUM)
      50      FORMAT (1X,10I10)
              GO TO 998
      999     WRITE (6,51) (LBUF(J),J=1,NUM)
      51      FORMAT (1X,10I10)
      998     WRITE (7,60)
      60      FORMAT (' DONE? <YES OR NO>',/,' >')
              READ (5,70) IANS
      70      FORMAT (A1)
              IF (IANS.EQ.N) GO TO 80
              STOP 'READING OF DATA FROM PTR'
              END
```

OUTPUTS DATA FROM PTR ONTO PRINTER IN OCTAL FORMAT.

6-OCT-78
GTDATO.FOR   2   1-MAR-78

```
        DIMENSION IBUF(9000)
        DATA N/1HN/
        WRITE (7,10)
10      FORMAT (' ENTER NUMBER OF WORDS TO BE READ INTO MEMORY',/,
       1' >')
        READ (5,20) NWDS
20      FORMAT (I4)
        WRITE (7,100)
100     FORMAT (' ENTER NUMBER OF POINTS TO BE OUTPUT TO PRINTER',
       1' >')
        READ (5,90) NUM
90      FORMAT (I4)
        WRITE (7,30)
30      FORMAT (' ENTER DATA OUTPUT FORMAT <"0"=WORD,"1"=BYTE>'
       1,/,' >')
        READ (5,40) IFORM
40      FORMAT (I1)
80      CALL RDPTR (IBUF,NWDS,IFORM)
        WRITE (6,50) (IBUF(I),I=1,NUM)
50      FORMAT (1X,10O8)
        WRITE (7,60)
60      FORMAT (' DONE? <YES OR NO>',/,' >')
        READ (5,70) IANS
70      FORMAT (A1)
        IF (IANS.EQ.N) GO TO 80
        STOP 'READING OF DATA FROM PTR'
        END
```

THIS ROUTINE IS A UTILITY PROGRAM TO EXAMINE DATA STORED IN PTR
VIA OUTPUT TO PRINTER.

6-OCT-78
RDOUT .FOR   6 12-MAR-78

```
C         OUTPUT OF PTR DATA FROM DISC FILE TO PRINTER.
          DIMENSION IDATA(7),IBUF(8192)
          BYTE LBUF(8192)
          EQUIVALENCE (LBUF(1),IBUF(1))
          DATA N/1HN/
50        WRITE (7,10)
10        FORMAT (' ENTER THE NAME OF DATA FILE TO BE READ IN FORM',
     1' DK1:DATA##.DAT',/,' >')
          READ (5,20) IDATA
20        FORMAT (7A2)
          WRITE (7,30) IDATA
30        FORMAT (' DATA WILL BE READ FROM THE FILE NAMED ',
     17A2,/,' Y OR N ?',/,' >')
          READ (5,40) IANS
40        FORMAT (A1)
          IF (IANS.EQ.N) GO TO 50
150       WRITE (7,110)
110       FORMAT (' ENTER DATA STORAGE FORMAT - WORD(0) OR BYTE(1)',
     1'-ORIGINAL DATA (8192 PTS.)',/,' OR WORD(2) OR BYTE(3)-',
     1'PROCESSED DATA (320 PTS.)',/,' >')
          READ (5,120) IFORM
120       FORMAT (I1)
          WRITE (7,130) IFORM
130       FORMAT (' DATA STORAGE FORMAT IS TYPE ',I1,/,' Y OR N ?',/,' >')
          READ (5,140) IANS
140       FORMAT (A1)
          IF (IANS.EQ.N) GO TO 150
          IF (IFORM.EQ.0) ISIZE=8192
          IF (IFORM.EQ.1) ISIZE=4096
          IF (IFORM.EQ.2) ISIZE=320
          IF (IFORM.EQ.3) ISIZE=160
440       WRITE (7,400)
400       FORMAT (' ENTER NUMBER OF RECORDS IN FILE.',/,' >')
          READ (5,410) NUMBER
410       FORMAT (I4)
          WRITE (7,420) NUMBER
420       FORMAT (' THE DATA FILE CONTAINS ',I4,' RECORDS.',/,' Y OR N ?',
     1/,' >')
          READ (5,430) IANS
430       FORMAT (A1)
          IF (IANS.EQ.N) GO TO 440
300       WRITE (7,310)
310       FORMAT (' ENTER RECORD NUMBER TO BE OUTPUT.',/,' >')
          READ (5,320) NUMREC
320       FORMAT (I4)
          WRITE (7,330) NUMREC
330       FORMAT (' RECORD NUMBER ',I4,' WILL BE OUTPUT.',/,' Y OR N ?',
     1/,' >')
          READ (5,340) IANS
340       FORMAT (A1)
          IF (IANS.EQ.N) GO TO 300
350       WRITE (7,360)
360       FORMAT (' ENTER STARTING AND ENDING POINTS OF RECORD TO BE',
     1' OUTPUT IN FORM',/,10X,' <STARTING,ENDING>',/,' >')
```

```
      READ (5,370) ISTART,IEND
370   FORMAT (2I8)
      WRITE (7,380) ISTART,IEND
380   FORMAT (' THE RECORD OUTPUT WILL EXTEND FROM THE INDICES ',
     1I4,' TO ',I4,'.',/,' Y OR N ?',/,' >')
      READ (5,390) IANS
390   FORMAT (A1)
      IF (IANS.EQ.N) GO TO 350
      CALL ASSIGN (12,IDATA,14)
      DEFINE FILE 12 (NUMBER,ISIZE,U,IVAR1)
      READ (12'NUMREC) (IBUF(I),I=1,ISIZE)
      IF ((IFORM.EQ.0).OR.(IFORM.EQ.2)) GO TO 999
      WRITE (6,998) (LBUF(M),M=ISTART,IEND)
998   FORMAT (1X,10I6,'     *BYTES*')
      GO TO 995
999   WRITE (6,996) (IBUF(IN),IN=ISTART,IEND)
996   FORMAT (1X,10I6,'     *WORDS*')
995   WRITE (6,160) NUMREC,IDATA,ISTART,IEND
160   FORMAT (' RECORD NUMBER ',I4,' OF DATA FILE ',7A2,' WAS JUST',
     1/,10X,' READ FROM THE DISC.',/,' LOCATIONS ',I4,' THRU ',I4,
     1' WERE OUTPUT TO PRINTER.')
      CALL CLOSE (12)
C     EMPTY TERMINET BUFFER (FOR WHEN TERMINET IS USED).
      CALL CLOSE (6)
      WRITE (7,750)
750   FORMAT (' DO YOU WANT TO EXAMINE ANYMORE DATA? (Y OR N)',
     1/,' >')
      READ (5,760) IANS
760   FORMAT (A1)
      IF (IANS.NE.N) GO TO 50
      STOP 'PRINTOUT OF P.S.I. DATA FROM DISC FILE.'
      END
```

B-4. ROUTINES FOR PROCESSING PTR DATA PRIOR TO IMAGE

RECONSTRUCTION

PEAK.FOR
ZERO.FOR

```
USED TO 'PEAK PROCESS' EACH 8K POINT WAVEFORM RECORDED FROM TRANSIENT
RECORDER DOWN TO 320 POINTS PER WAVEFORM. THIS IS A TEMPORARY ROUTINE UNTIL
A MORE SOPHISTICATED DIGITAL FILTERING ALGORITHM IS DESIGNED.


     6-OCT-78
     PEAK  .FOR    6 21-MAR-78


     C       PTR DATA PROCESSING.
     C       SELECTION OF MAXIMUM VALUE FROM A GIVEN (BEGINNING) INTERVAL
     C    .     OF THE 8192 PTR DATA POINTS SO AS TO FORM A 320 DATA POINT ARRAY.
     C       DATA WILL BE OUTPUT IN INTEGER FORMAT.
             DIMENSION IDATA(7),IBUF(4096),JBUF(8192),IOUTP(7),MAX(320)
             BYTE LBUF(8192)
             EQUIVALENCE (LBUF(1),IBUF(1))
             DATA N/1HN/
     50      WRITE (7,10)
     10      FORMAT (' ENTER THE NAME OF DATA FILE TO BE READ IN FORM',
            1' DK1:DATA##.DAT',/,' >')
             READ (5,20) IDATA
     20      FORMAT (7A2)
             WRITE (7,30) IDATA
     30      FORMAT (' DATA WILL BE READ FROM THE FILE NAMED ',
            17A2,/,' Y OR N ?',/,' >')
             READ (5,40) IANS
     40      FORMAT (A1)
             IF (IANS.EQ.N) GO TO 50
     60      WRITE (7,70)
     70      FORMAT (' ENTER NAME OF FILE TO CONTAIN OUTPUT DATA IN FORM ',
            1'DK1:PROC##.DAT',/,' >')
             READ (5,80) IOUTP
     80      FORMAT (7A2)
             WRITE (7,90) IOUTP
     90      FORMAT (' DATA WILL BE OUTPUT TO THE FILE NAMED ',7A2,
            1/,' Y OR N ?',/,' >')
             READ (5,100) IANS
     100     FORMAT (A1)
             IF (IANS.EQ.N) GO TO 60
     150     WRITE (7,110)
     110     FORMAT (' ENTER RANGE OF INDICES OF INTEREST (SHOULD BE A ',
            1'MULTIPLE OF 320).',/,' >')
             READ (5,120) IRANGE
     120     FORMAT (I4)
             WRITE (7,130) IRANGE
     130     FORMAT (' THE FIRST ',I4,' DATA POINTS WILL BE CONVERTED',
            1' TO 320 DATA POINTS.',/,' Y OR N ?',/,' >')
             READ (5,140) IANS
     140     FORMAT (A1)
             IF (IANS.EQ.N) GO TO 150
     440     WRITE (7,400)
     400     FORMAT (' ENTER NUMBER OF TRANSDUCERS IN RING.',/,' >')
             READ (5,410) NT
     410     FORMAT (I4)
             WRITE (7,420) NT
     420     FORMAT (' THERE ARE ',I2,' TRANSDUCERS IN RING.',/,' Y OR N ?',
            1/,' >')
             READ (5,430) IANS
     430     FORMAT (A1)
             IF (IANS.EQ.N) GO TO 440
             NUMREC=NT*(NT+1)/2
             ISTART=1
             IEND=IRANGE
```

```
        CALL ASSIGN (12,IDATA,14)
        DEFINE FILE 12 (NUMREC,4096,U,IVAR1)
        CALL ASSIGN (13,IOUTP,14)
        DEFINE FILE 13 (NUMREC,320,U,IVAR2)
C       BREAK ORIGINAL DATA INTO EQUAL SEGMENTS OF IRANGE/320=NPEAK.
C           THEN RECORD MAXIMUM VALUE OF INTERVAL SEQUENTIALLY IN A
C           320 POINT ARRAY.
        NPEAK=IRANGE/320
        DO 200 K=1,NUMREC
        READ (12'K) (IBUF(I),I=1,4096)
C       ORIGINAL DATA IS INVERTED BY ENVELOPE DETECTOR. REINVERT DATA.
C       ****************************
C       BYTE TO INTEGER CONVERSION.
C       ****************************
        DO 887 IJK=1,8192
        JBUF(IJK)=LBUF(IJK)
887     CONTINUE
        DO 888 NEG=1,8192
C       ADD +128 TO DATA VALUES SO THAT DATA WILL NOW RANGE
C           BETWEEN 0 AND 256. THUS, ADDING ONE VALUE TO ANOTHER
C           WILL RESULT IN REINFORCEMENT (I.E. INCREASED BRIGHTNESS).
C           IF (-) NUMBERS WERE ADDED TOGETHER, A VISUAL DE-EMPHASIS
C           WOULD RESULT RATHER THAN A REINFORCEMENT.
        JBUF(NEG)=-JBUF(NEG)+128
888     CONTINUE
        INDEX=0
        IEND=IRANGE-NPEAK+1
        DO 210 L=ISTART,IEND,NPEAK
        INDEX=INDEX+1
        MAX(INDEX)=JBUF(L)
        DO 220 M=1,NPEAK
        IF (JBUF(L-1+M).GT.MAX(INDEX)) MAX(INDEX)=JBUF(L-1+M)
220     CONTINUE
210     CONTINUE
        WRITE (13'K) (MAX(N),N=1,320)
200     CONTINUE
        STOP 'PSI PEAK DATA PROCESSING DOWN TO 320 POINTS PER RECORD.'
        END
```

USED TO ZERO OUT A GIVEN RECORD OR GROUP OF RECORDS ON DISC FILE (I.E. ONE
RECORD CORRESPONDS TO ONE A-MODE WAVEFORM) IN A GIVEN PSI SCAN
AND RESULTANT DATA SET. NOTE: ALL STATEMENTS (E.G. EQUIVALENCE) AND
VARIABLES (E.G. IBUF,JBUF,IOUTP) CORRESPONDING TO READING DATA FROM DISC ARE
REMNANTS OF AN EARLIER PROGRAM AND MAY BE REMOVED FROM THIS VERSION.

```
   6-OCT-78
   ZERO  .FOR    3  6-APR-78

   C        PTR DATA PROCESSING.
   C        ****************************
   C        PROGRAM TO ZERO OUT GIVEN RECORDS IN THE PEAK-PROCESSED DATA.
   C        ****************************
   C        DATA WILL BE OUTPUT IN INTEGER FORMAT.
            DIMENSION IDATA(7),IBUF(4096),JBUF(8192),IOUTP(7),MAX(320)
            BYTE LBUF(8192)
            EQUIVALENCE (LBUF(1),IBUF(1))
            DATA N/1HN/
   50       WRITE (7,10)
   10       FORMAT (' ENTER THE NAME OF DATA FILE TO BE READ IN FORM',
          1' DK1:DATA##.DAT',/,' >')
            READ (5,20) IDATA
   20       FORMAT (7A2)
            WRITE (7,30) IDATA
   30       FORMAT (' DATA WILL BE READ FROM THE FILE NAMED ',
          17A2,/,' Y OR N ?',/,' >')
            READ (5,40) IANS
   40       FORMAT (A1)
            IF (IANS.EQ.N) GO TO 50
            NT=8
            NUMREC=NT*(NT+1)/2
            CALL ASSIGN (13,IDATA,14,'OLD')
            DEFINE FILE 13 (NUMREC,320,U,IVAR2)
            WRITE (7,8)
   8        FORMAT (' M A K E  S U R E  A  B A C K - U P  D A T A ',
          1'F I L E',/,' H A S  B E E N  C R E A T E D',
          1' ! ! ! ! ! ! ! ! ! ! ! !',//)
   7        WRITE (7,1)
   1        FORMAT (' ENTER RECORD TO BE ZEROED',/,' >')
            READ (5,2) IZERO
   2        FORMAT (I4)
            DO 3 LZERO=1,320
            MAX(LZERO)=0
   3        CONTINUE
            WRITE (13'IZERO) (MAX(IN),IN=1,320)
            WRITE (7,4) IZERO
   4        FORMAT (' RECORD NUMBER ',I4,' WAS JUST ZEROED.')
            WRITE (7,5)
   5        FORMAT (' ARE YOU DONE?',/,' Y OR N',/,' >')
            READ (5,6) IANS
   6        FORMAT (A1)
            IF (IANS.EQ.N) GO TO 7
            STOP 'PSI PEAK DATA PROCESSING DOWN TO 320 POINTS PER RECORD.'
            END
```

B-5. GRAPHIC DISPLAY SOFTWARE

PTRPLT.FOR
SEQPLT.FOR
PKPLOT.FOR
TEKPLT.FOR
PTSPRD.FOR
PLOT3D.FOR

PROGRAM TO READ ORIGINAL PTR DATA FROM DISC AND PLOT ON TEKTRONIX 4002A
GRAPHICS TERMINAL. NUMBER OF POINTS PLOTTED WILL BE EQUALLY SPACED ACROSS
ENTIRE X-AXIS. Y-AXIX RANGE IS -128 TO +137. NOTE: <u>ALL</u> PSI GRAPHICS MUST
LINK WITH GRAPH.OBJ (TEKTRONIX GRAPHICS PACKAGE FROM JIM FAWCETT).

```
       6-OCT-78
       PTRPLT.FOR    9  3-APR-78


       C        PLOT OF PTR DATA FROM DISC FILE ON TEKTRONIX GRAPHICS TERMINAL.
       C
       C        THERE IS A BUG IN THIS PROGRAM, SUCH THAT THE ALPHANUMERICS
       C            ·WHICH ARE PRINTED ON TOP OF THE PLOT WHEN THE STARTING
       C             INDEX=1, DOES NOT ALWAYS APPEAR AT THE TOP OF THE SCREEN
       C       `     WHEN THE STARTING INDEX DOES NOT =1.
       C
                DIMENSION IDATA(7),IBUF(8192)
                BYTE LBUF(8192)
                EQUIVALENCE (LBUF(1),IBUF(1))
                DATA N/1HN/
                CALL INIT
                CALL WAIT(6)
         50     WRITE (7,10)
         10     FORMAT (' ENTER THE NAME OF DATA FILE TO BE READ IN FORM',
              1' DK1:DATA##.DAT',/,' >')
                READ (5,20) IDATA
         20     FORMAT (7A2)
                WRITE (7,30) IDATA
         30     FORMAT (' DATA WILL BE READ FROM THE FILE NAMED ',
              17A2,/,' Y OR N ?',/,' >')
                READ (5,40) IANS
         40     FORMAT (A1)
                IF (IANS.EQ.N) GO TO 50
        150     WRITE (7,110)
        110     FORMAT (' ENTER DATA STORAGE FORMAT --- WORD(0) OR BYTE(1)',
              1/,' >')
                READ (5,120) IFORM
        120     FORMAT (I1)
                WRITE (7,130) IFORM
        130     FORMAT (' DATA STORAGE FORMAT IS TYPE ',I1,/,' Y OR N ?',/,' >')
                READ (5,140) IANS
        140     FORMAT (A1)
                IF (IANS.EQ.N) GO TO 150
                IF (IFORM.EQ.0) ISIZE=8192
                IF (IFORM.EQ.1) ISIZE=4096
        440     WRITE (7,400)
        400     FORMAT (' ENTER NUMBER OF RECORDS IN FILE.',/,' >') .
                READ (5,410) NUMBER
        410     FORMAT (I4)
                WRITE (7,420) NUMBER
        420     FORMAT (' THE DATA FILE CONTAINS ',I4,' RECORDS.',/,' Y OR N ?',
              1/,' >')
                READ (5,430) IANS
        430     FORMAT (A1)
                IF (IANS.EQ.N) GO TO 440
        300     WRITE (7,310)
        310     FORMAT (' ENTER RECORD NUMBER TO BE OUTPUT.',/,' >')
                READ (5,320) NUMREC
        320     FORMAT (I4)
                WRITE (7,330) NUMREC
        330     FORMAT (' RECORD NUMBER ',I4,' WILL BE OUTPUT.',/,' Y OR N ?',
              1/,' >')
                READ (5,340) IANS
```

```
340      FORMAT (A1)
         IF (IANS.EQ.N) GO TO 300
350      WRITE (7,360)
360      FORMAT (' ENTER STARTING AND ENDING POINTS OF RECORD TO BE',
        1' PLOTTED IN FORM',/,10X,' <STARTING,ENDING>',/,' >')
         READ (5,370) ISTART,IEND
370      FORMAT (2I8)
         WRITE (7,380) ISTART,IEND
380      FORMAT (' THE DATA PLOTTED WILL EXTEND FROM THE INDICES ',
        1I4,' TO ',I4,'.',/,' Y OR N ?',/,' >')
         READ (5,390) IANS
390      FORMAT (A1)
         IF (IANS.EQ.N) GO TO 350
         CALL ASSIGN (12,IDATA,14)
         DEFINE FILE 12 (NUMBER,ISIZE,U,IVAR1)
         READ (12'NUMREC) (IBUF(I),I=1,ISIZE)
         CALL INIT
         NUM=IEND-ISTART+1
         XNUM=FLOAT(NUM)
C        IWIND IS THE SCREEN COORDINATE RANGE IN INTEGERS.
C            MAXIMUM VALUES ARE (X1,X2,Y1,Y2) --- (0,1024,0,760).
         CALL IWIND(20,1004,20,740)
C        RWIND DEFINES THE REAL NUMBER RANGE (I.E. PROGRAM DATA)
C            WHICH IS MAPPED INTO THE SCREEN COORDINATE RANGE SPECIFIED
C            IN IWIND. THESE NUMBERS MUST BE FLOATING POINT.
         CALL RWIND(FLOAT(ISTART),FLOAT(IEND),-128.,137.)
C        CWIND DEFINES A CLIPPING WINDOW. THE VALUES SPECIFIED ARE IN
C            INTEGER FORMAT AND RELATE TO THE SCREEN COORDINATE RANGE
C            AS SPECIFIED IN THE IWIND DEFINITION.
C            TRANSFORMED DATA VALUES OUTSIDE THE CLIPPING WINDOW WILL
C            NOT BE PLOTTED ON THE SCREEN.
         CALL CWIND(20,1004,20,740)
         IF (IFORM.EQ.0) GO TO 999
C        PLOT ROUTINE FOR CASE WHERE DATA IS IN BYTE FORMAT.
         BUF=LBUF(ISTART)
         CALL MOVE(FLOAT(ISTART),BUF)
         DO 100 K=ISTART+1,IEND
         BUF=LBUF(K)
         CALL DRAW(FLOAT(K),BUF)
100      CONTINUE
         GO TO 995
C        PLOT ROUTINE FOR CASE WHERE DATA IS IN INTEGER FORMAT.
999      CALL MOVE(FLOAT(ISTART),FLOAT(IBUF(ISTART)))
         DO 101 L=ISTART+1,IEND
         CALL DRAW(FLOAT(L),FLOAT(IBUF(L)))
101      CONTINUE
C        PLOT HORIZONTAL SCALE MARKINGS AT 128,96,64,32,0,
C            -32,-64,-96, AND -128.
995      DO 800 I1=1,129,32
         A=FLOAT(I1-1)
         CALL MOVE(FLOAT(ISTART),A)
         DO 820 I3=1,2
         CALL DRAW(FLOAT(IEND),A)
         A=-A
```

```
C         IF VERTICAL COORDINATE = 0, DON'T BOTHER REPLOTTING.
          IF ((I1-1).EQ.0) I3=2
          CALL MOVE(0.,A)
  820     CONTINUE
  800     CONTINUE
          CALL CLOSE (12)
          CALL MOVE(FLOAT(ISTART),137.)
          CALL AMODE
C         BEFORE PRINTING PLOT I.D. ON SCREEN, TYPE <CR>.
          READ (5,760) ICHAR
  760     FORMAT (A1)
          WRITE (7,160) IDATA,NUMREC,ISTART,IEND
  160     FORMAT ('+DATA FILE ',7A2,5X,'RECORD NO. ',I4,5X,'INDICES ',
         1I4,' THRU ',I4)
C         IN ORDER NOT TO PRINT "STOP" ON SCREEN BEFORE COPY HAS BEEN MADE,
C             LET PROGRAM WAIT TO READ ONE CHARACTER FROM KEYBOARD BEFORE
C             PROCEEDING FURTHER.
          READ (5,761) ICHAR
  761     FORMAT (A1)
          WRITE (7,888)
  888     FORMAT (' WANT TO PLOT MORE DATA FROM THE SAME FILE? (Y OR N)',/,
         1' >')
          READ (5,889) IANS
  889     FORMAT (A1)
          IF (IANS.NE.N) GO TO 300
          STOP
          END
```

THIS ROUTINE SEQUENTIALLY PLOTS EACH PEAK PROCESSED RECORD FROM A GIVEN DATA
FILE, WITH THE PREVIOUS PLOT BEING ERASED BEFORE PROCEEDING TO THE NEXT PLOT.
A <CR> MUST BE TYPED FOLLOWING A GIVEN PLOT IN ORDER TO DISPLAY I.D. INFORMATION
TO BE PRINTED AT TOP OF PLOT. A SECOND <CR> MUST BE TYPED FOR ERASURE OF
SCREEN PRIOR TO AUTOMATIC PLOTTING OF NEXT RECORD OF FILE. AS WITH ALL GRAPHICS
ROUTINES USED IN THIS SYSTEM, THEY MUST BE LINKED WITH 'GRAPH.OBJ' .
THIS ROUTINE IS THE PRIMARY METHOD OF EXAMINING THE DATA GOING INTO THE
RECONSTRUCTION ALGORITHM POST-PTR DATA COLLECTION AND PROCESSING.

```
     6-OCT-78
     SEQPLT.FOR    8 23-MAR-78


     C          PLOT OF PTR DATA FROM DISC FILE ON TEKTRONIX GRAPHICS TERMINAL.
                DIMENSION IDATA(7),IBUF(8192)
                BYTE LBUF(8192)
                EQUIVALENCE (LBUF(1),IBUF(1))
                DATA N/1HN/
                CALL INIT
     50         WRITE (7,10)
     10         FORMAT (' ENTER THE NAME OF DATA FILE TO BE READ IN FORM',
               1' DK1:DATA##.DAT',/,' >')
                READ (5,20) IDATA
     20         FORMAT (7A2)
                WRITE (7,30) IDATA
     30         FORMAT (' DATA WILL BE READ FROM THE FILE NAMED ',
               17A2,/,' Y OR N ?',/,' >')
                READ (5,40) IANS
     40         FORMAT (A1)
                IF (IANS.EQ.N) GO TO 50
     150        WRITE (7,110)
     110        FORMAT (' ENTER DATA STORAGE FORMAT --- WORD(0) OR BYTE(1)',
               1/,' >')
                READ (5,120) IFORM
     120        FORMAT (I1)
                WRITE (7,130) IFORM
     130        FORMAT (' DATA STORAGE FORMAT IS TYPE ',I1,/,' Y OR N ?',/,' >')
                READ (5,140) IANS
     140        FORMAT (A1)
                IF (IANS.EQ.N) GO TO 150
                IF (IFORM.EQ.0) ISIZE=320
                IF (IFORM.EQ.1) ISIZE=160
     440        WRITE (7,400)
     400        FORMAT (' ENTER NUMBER OF RECORDS IN FILE.',/,' >')
                READ (5,410) NUMBER
     410        FORMAT (I4)
                WRITE (7,420) NUMBER
     420        FORMAT (' THE DATA FILE CONTAINS ',I4,' RECORDS.',/,' Y OR N ?',
               1/,' >')
                READ (5,430) IANS
     430        FORMAT (A1)
                IF (IANS.EQ.N) GO TO 440
     350        WRITE (7,360)
     360        FORMAT (' ENTER STARTING AND ENDING POINTS OF RECORD TO BE',
               1' PLOTTED IN FORM',/,10X,' <STARTING,ENDING>',/,' >')
                READ (5,370) ISTART,IEND
     370        FORMAT (2I8)
                WRITE (7,380) ISTART,IEND
     380        FORMAT (' THE DATA PLOTTED WILL EXTEND FROM THE INDICES ',
               1I4,' TO ',I4,'.',/,' Y OR N ?',/,' >')
                READ (5,390) IANS
     390        FORMAT (A1)
                IF (IANS.EQ.N) GO TO 350
                CALL ASSIGN (12,IDATA,14)
                DEFINE FILE 12 (NUMBER,ISIZE,U,IVAR1)
     C          ##########FOR PLOTTING OF ALL RECORDS SEQUENTIALLY##########
                DO 8888 NUMREC=1,NUMBER
```

```
        READ (12'NUMREC) (IBUF(I),I=1,ISIZE)
        CALL INIT
        NUM=IEND-ISTART+1
        XNUM=FLOAT(NUM)
C       IWIND IS THE SCREEN COORDINATE RANGE IN INTEGERS.
C           MAXIMUM VALUES ARE (X1,X2,Y1,Y2) --- (0,1024,0,760).
        CALL IWIND(20,1004,20,740)
C       RWIND DEFINES THE REAL NUMBER RANGE (I.E. PROGRAM DATA)
C           WHICH IS MAPPED INTO THE SCREEN COORDINATE RANGE SPECIFIED
C           IN IWIND. THESE NUMBERS MUST BE FLOATING POINT.
        CALL RWIND(FLOAT(ISTART),FLOAT(IEND),0.,267.)
C       CWIND DEFINES A CLIPPING WINDOW. THE VALUES SPECIFIED ARE IN
C           INTEGER FORMAT AND RELATE TO THE SCREEN COORDINATE RANGE
C           AS SPECIFIED IN THE IWIND DEFINITION.
C           TRANSFORMED DATA VALUES OUTSIDE THE CLIPPING WINDOW WILL
C           NOT BE PLOTTED ON THE SCREEN.
        CALL CWIND(20,1004,20,740)
        IF (IFORM.EQ.0) GO TO 999
C       PLOT ROUTINE FOR CASE WHERE DATA IS IN BYTE FORMAT.
        BUF=LBUF(ISTART)
        CALL MOVE(FLOAT(ISTART),BUF)
        DO 100 K=ISTART+1,IEND
        BUF=LBUF(K)
        CALL DRAW(FLOAT(K),BUF)
 100    CONTINUE
        GO TO 995
C       PLOT ROUTINE FOR CASE WHERE DATA IS IN INTEGER FORMAT.
 999    CALL MOVE(FLOAT(ISTART),FLOAT(IBUF(ISTART)))
        DO 101 L=ISTART+1,IEND
        CALL DRAW(FLOAT(L),FLOAT(IBUF(L)))
 101    CONTINUE
C       PLOT HORIZONTAL SCALE MARKINGS AT 0,64,128,192,256
 995    DO 800 I1=1,257,64
        A=FLOAT(I1-1)
        CALL MOVE(FLOAT(ISTART),A)
        CALL DRAW (FLOAT(IEND),A)
 800    CONTINUE
        CALL MOVE(FLOAT(ISTART),267.)
        CALL AMODE
C       BEFORE PRINTING PLOT I.D. ON SCREEN, TYPE <CR>.
C       READ (5,760) ICHAR
C760    FORMAT (A1)
        WRITE (7,160) IDATA,NUMREC,ISTART,IEND
 160    FORMAT ('+DATA FILE ',7A2,5X,'RECORD NO. ',I4,5X,'INDICES ',
       1I4,' THRU ',I4)
C       IN ORDER NOT TO PRINT "STOP" ON SCREEN BEFORE COPY HAS BEEN MADE,
C           LET PROGRAM WAIT TO READ ONE CHARACTER FROM KEYBOARD BEFORE
C           PROCEEDING FURTHER. TYPE <CR> TO PLOT NEXT RECORD OF FILE.
        READ (5,761) ICHAR
 761    FORMAT (A1)
 8888   CONTINUE
        CALL CLOSE (12)
        WRITE (7,888)
 888    FORMAT (' WANT TO PLOT MORE DATA FROM ANOTHER FILE? (Y OR N)',/,
       1' >')
        READ (5,889) IANS
 889    FORMAT (A1)
        IF (IANS.NE.N) GO TO 50
        STOP
        END
```

THIS ROUTINE PLOTS PEAK-PROCESSED DATA (FROM PEAK.FOR) ON THE TEKTRONIX
4002A GRAPHICS DISPLAY. USER SPECIFIES DATA WAVEFORM TO BE PLOTTED.

6-OCT-78
PKPLOT.FOR   9 21-MAR-78

```
C       PLOT OF PTR DATA FROM DISC FILE ON TEKTRONIX GRAPHICS TERMINAL.
C
C       THERE IS A BUG IN THIS PROGRAM, SUCH THAT THE ALPHANUMERICS
C          .WHICH ARE PRINTED ON TOP OF THE PLOT WHEN THE STARTING
C           INDEX=1, DOES NOT ALWAYS APPEAR AT THE TOP OF THE SCREEN
C           WHEN THE STARTING INDEX DOES NOT =1.
C
        DIMENSION IDATA(7),IBUF(8192)
        BYTE LBUF(8192)
        EQUIVALENCE (LBUF(1),IBUF(1))
        DATA N/1HN/
        CALL INIT
50      WRITE (7,10)
10      FORMAT (' ENTER THE NAME OF DATA FILE TO BE READ IN FORM',
     1' DK1:DATA##.DAT',/,' >')
        READ (5,20) IDATA
20      FORMAT (7A2)
        WRITE (7,30) IDATA
30      FORMAT (' DATA WILL BE READ FROM THE FILE NAMED ',
     17A2,/,' Y OR N ?',/,' >')
        READ (5,40) IANS
40      FORMAT (A1)
        IF (IANS.EQ.N) GO TO 50
150     WRITE (7,110)
110     FORMAT (' ENTER DATA STORAGE FORMAT --- WORD(0) OR BYTE(1)',
     1/,' >')
        READ (5,120) IFORM
120     FORMAT (I1)
        WRITE (7,130) IFORM
130     FORMAT (' DATA STORAGE FORMAT IS TYPE ',I1,/,' Y OR N ?',/,' >')
        READ (5,140) IANS
140     FORMAT (A1)
        IF (IANS.EQ.N) GO TO 150
        IF (IFORM.EQ.0) ISIZE=320
        IF (IFORM.EQ.1) ISIZE=160
440     WRITE (7,400)
400     FORMAT (' ENTER NUMBER OF RECORDS IN FILE.',/,' >')
        READ (5,410) NUMBER
410     FORMAT (I4)
        WRITE (7,420) NUMBER
420     FORMAT (' THE DATA FILE CONTAINS ',I4,' RECORDS.',/,' Y OR N ?',
     1/,' >')
        READ (5,430) IANS
430     FORMAT (A1)
        IF (IANS.EQ.N) GO TO 440
300     WRITE (7,310)
310     FORMAT (' ENTER RECORD NUMBER TO BE OUTPUT.',/,' >')
        READ (5,320) NUMREC
320     FORMAT (I4)
        WRITE (7,330) NUMREC
330     FORMAT (' RECORD NUMBER ',I4,' WILL BE OUTPUT.',/,' Y OR N ?',
     1/,' >')
        READ (5,340) IANS
340     FORMAT (A1)
```

```
        IF (IANS.EQ.N) GO TO 300
350     WRITE (7,360)
360     FORMAT (' ENTER STARTING AND ENDING POINTS OF RECORD TO BE',
       1' PLOTTED IN FORM',/,10X,' <STARTING,ENDING>',/,' >')
        READ (5,370) ISTART,IEND
370     FORMAT (2I8)
        WRITE (7,380) ISTART,IEND
380     FORMAT (' THE DATA PLOTTED WILL EXTEND FROM THE INDICES ',
       1I4,' TO ',I4,'.',/,' Y OR N ?',/,' >')
        READ (5,390) IANS
390     FORMAT (A1)
        IF (IANS.EQ.N) GO TO 350
        CALL ASSIGN (12,IDATA,14)
        DEFINE FILE 12 (NUMBER,ISIZE,U,IVAR1)
        READ (12'NUMREC) (IBUF(I),I=1,ISIZE)
        CALL INIT
        NUM=IEND-ISTART+1
        XNUM=FLOAT(NUM)
C       IWIND IS THE SCREEN COORDINATE RANGE IN INTEGERS.
C          MAXIMUM VALUES ARE (X1,X2,Y1,Y2) --- (0,1024,0,760).
        CALL IWIND(20,1004,20,740)
C       RWIND DEFINES THE REAL NUMBER RANGE (I.E. PROGRAM DATA)
C          WHICH IS MAPPED INTO THE SCREEN COORDINATE RANGE SPECIFIED
C          IN IWIND. THESE NUMBERS MUST BE FLOATING POINT.
        CALL RWIND(FLOAT(ISTART),FLOAT(IEND),0.,267.)
C       CWIND DEFINES A CLIPPING WINDOW. THE VALUES SPECIFIED ARE IN
C          INTEGER FORMAT AND RELATE TO THE SCREEN COORDINATE RANGE
C          AS SPECIFIED IN THE IWIND DEFINITION.
C          TRANSFORMED DATA VALUES OUTSIDE THE CLIPPING WINDOW WILL
C          NOT BE PLOTTED ON THE SCREEN.
        CALL CWIND(20,1004,20,740)
        IF (IFORM.EQ.0) GO TO 999
C       PLOT ROUTINE FOR CASE WHERE DATA IS IN BYTE FORMAT.
        BUF=LBUF(ISTART)
        CALL MOVE(FLOAT(ISTART),BUF)
        DO 100 K=ISTART+1,IEND
        BUF=LBUF(K)
        CALL DRAW(FLOAT(K),BUF)
100     CONTINUE
        GO TO 995
C       PLOT ROUTINE FOR CASE WHERE DATA IS IN INTEGER FORMAT.
999     CALL MOVE(FLOAT(ISTART),FLOAT(IBUF(ISTART)))
        DO 101 L=ISTART+1,IEND
        CALL DRAW(FLOAT(L),FLOAT(IBUF(L)))
101     CONTINUE
C       PLOT HORIZONTAL SCALE MARKINGS AT 0,64,128,192,256
995     DO 800 I1=1,257,64
        A=FLOAT(I1-1)
        CALL MOVE(FLOAT(ISTART),A)
        CALL DRAW (FLOAT(IEND),A)
800     CONTINUE
        CALL CLOSE (12)
        CALL MOVE(FLOAT(ISTART),267.)
        CALL AMODE
```

```
C        BEFORE PRINTING PLOT I.D. ON SCREEN, TYPE <CR>.
C        READ (5,760) ICHAR
C760     FORMAT (A1)
         WRITE (7,160) IDATA,NUMREC,ISTART,IEND
  160    FORMAT ('+DATA FILE ',7A2,5X,'RECORD NO. ',I4,5X,'INDICES ',
        1I4,' THRU ',I4)
C        IN ORDER NOT TO PRINT "STOP" ON SCREEN BEFORE COPY HAS BEEN MADE,
C           LET PROGRAM WAIT TO READ ONE CHARACTER FROM KEYBOARD BEFORE
C           PROCEEDING FURTHER.
         READ (5,761) ICHAR
  761    FORMAT (A1)
         WRITE (7,888)
  888    FORMAT (' WANT TO PLOT MORE DATA FROM THE SAME FILE? (Y OR N)',/,
        1' >')
         READ (5,889) IANS
  889    FORMAT (A1)
         IF (IANS.NE.N) GO TO 300
         STOP
         END
```

PLOTS A VARIABLE NUMBER (NUM<=500) OF MANUALLY ENTERED 8 BIT VALUES
ON THE TEKTRONIX GRAPHICS TERMINAL.


```
      6-OCT-78
      TEKPLT.FOR    2  3-MAR-78


             DIMENSION VAL(500)
             CALL INIT
             WRITE (7,10)
   10        FORMAT ('TYPE IN NUMBER OF VALUES TO BE PLOTTED.',/,' >')
             READ (5,20) NUM
   20        FORMAT (I4)
             XNUM=FLOAT(NUM)
             CALL IWIND (20,1004,20,740)
             CALL RWIND (1.,XNUM,-128.,128.)
             CALL CWIND (20,1004,20,740)
             WRITE (7,50)
   50        FORMAT (' ENTER VALUES TO BE PLOTTED ONE PER LINE.',/,' >')
             READ (5,60) (VAL(J),J=1,NUM)
   60        FORMAT (F5.0)
   C         INSERT WAIT COMMAND TO ALLOW 'PAGE' TO ERASE SCREEN.
             CALL WAIT(6)
             CALL PAGE
             I=1
             CALL MOVE (FLOAT(I),VAL(I))
             DO 100 I=2,NUM
             CALL DRAW (FLOAT(I),VAL(I))
   100       CONTINUE
             CALL AMODE
             STOP 'PLOT OF PTR DATA - DATA ENTERED BY HAND.'
             END
```

```
C       PROGRAM TO FORMAT POINT SPREAD DATA SO AS TO BE COMPATIBLE
C            WITH JIM FAWCETT'S PERSPECTIVE PLOT ROUTINE. (PLOT3D.FOR)
        DIMENSION A(20,320)
        CALL ASSIGN (11,'DK1:PTSPRD.DAT',14,'NEW','CC')
        CALL ASSIGN (10,'DK1:PTNC16.DAT',14)
        DEFINE FILE 10 (20,640,U,IVAR1)
        DO 500 I=1,20
        READ (10'I) (A(I,J),J=1,320)
500     CONTINUE
        I=10
        WRITE (11,100) I,I
100     FORMAT (1X,I3,1X,I3)
        DO 200 L=1,20
        WRITE (11,300) (A(L,N),N=151,170)
300     FORMAT (5G12.4)
200     CONTINUE
        STOP
        END
```

PLOT ROUTINE BORROWED FROM JIM FAWCETT (GE E-LAB) TO ISOMETRICALLY PLOT
PSI POINT-SPREAD FUNCTION ON TEKTRONIX GRAPHICS DISPLAY.


```
    6-OCT-78
    PLOT3D.FOR    6  7-MAY-78

           COMMON/COMARE/T(50),K(50)
           DIMENSION A(36,36),B(36,36),NAME(3)
           REAL NAME
           WRITE(7,40)
        40 FORMAT(1H ,'ENTER SOURCE FILENAME')
           READ(5,50) NAME
        50 FORMAT(3A4)
           CALL ASSIGN(10,NAME,0,'OLD')
           REWIND 10
           CALL INITT(120,T,K)
           READ(10,30) IA,JA
        30 FORMAT(I3,1X,I3)
           DO 10 I=1,IA
           READ(10,20,END=60) (A(I,J),J=1,JA)
        20 FORMAT(5G12.4)
        10 CONTINUE
           IB=IA+4
           JB=JA+4
           DO 70 I=1,IB
           DO 70 J=1,JB
           IF(I.LE.2.OR.IA+2.LT.I) GOTO 90
           IF(J.GT.2.AND.J.LE.JA+2) GOTO 80
        90 B(I,J)=0.
           GOTO 70
        80 B(I,J)=A(I-2,J-2)
        70 CONTINUE
        60 CALL PLOT3D(B,IB,JB,T,K)
           CALL FINITT(20,20,T,K)
           STOP
           END
           SUBROUTINE PLOT3D(AR,IA,JA)
           COMMON/COMARE/T(50),K(50)
           DIMENSION AR(36,36)
           DATA XH,X0,XF,ZH,Z0,ZF/1.5,.2,.7,.1,.2,.7/
           DATA ASAT,AS/1.E+10,.2/
           CALL AMAX(AR,IA,JA,ASAT,AMX)
           XD=FLOAT(IA-1)*(XH-XF)/(XF-X0)
           ZD=ZF*XD/FLOAT(JA-1)
           A=(ZH-Z0)/(XH-X0)
           B=Z0-A*X0
           CALL HIDLIN(A*X0+B,X0,1,T,K)
           DO 10 I=1,IA
           X=X0+(XH-X0)*FLOAT(I-1)/(XD+FLOAT(I-1))
           CALL MOVER(A*X+B,X)
           DO 10 J=2,JA
           Z=A*X+B+ZD*FLOAT(J-1)/(XD+FLOAT(I-1))
           Y=AS*XD*AR(I,J)/(AMX*(XD+FLOAT(I)))+X
           CALL HIDLIN(Z,Y,0,T,K)
        10 CONTINUE
           RETURN
           END
           SUBROUTINE AMAX(A,IA,JA,ASAT,AMX)
           DIMENSION A(36,36)
           AMX=-1.E+18
```

```
      AMN=1.E+18
      DO 10 I=1,IA
      DO 10 J=1,JA
      IF(A(I,J).GT.AMX) AMX=A(I,J)
      IF(A(I,J).LT.AMN) AMN=A(I,J)
   10 CONTINUE
      DO 20 I=1,IA
      DO 20 J=1,JA
      IF(A(I,J).GT.ASAT) A(I,J)=ASAT
   20 CONTINUE
      RETURN
      END
      SUBROUTINE HIDLIN(X,Y,IFLG)
      DIMENSION S(1024)
      COMMON/COMARE/T(50),K(50)
      DATA FN/1024./
      DATA FTEST/1.E-10/
      IF(IFLG.EQ.0) GOTO 40
      A=(FN-1.)/(T(2)-T(1))
      B=1.-A*T(1)
      DO 30 I=1,1024
   30 S(I)=0.
      RETURN
   40 IF(ABS(X-T(5)).LT.FTEST) GOTO 10
      C=(Y-T(6))/(X-T(5))
      D=Y-C*X
      XMIN=AMIN1(X,T(5))
      XMAX=AMAX1(X,T(5))
      FIMIN=A*XMIN+B
      FIMAX=A*XMAX+B+1
      DX=ABS(X-T(5))/(FIMAX-FIMIN)
      IMIN=IFIX(FIMIN)
      IMAX=IFIX(FIMAX)-1
      XT=XMIN-DX
      DO 50 I=IMIN,IMAX
      XT=XT+DX
      YT=C*XT+D
      IF(YT.LT.S(I)) CALL MOVER(XT,YT)
      XTP=XT+DX
      YTP=C*XTP+D
      IF(YT.GE.S(I).AND.YTP.LT.S(I+1)) CALL DRAWR(XT,YT)
      IF(YT.GT.S(I)) S(I)=YT
   50 CONTINUE
      IF(YT.GE.S(IMAX)) CALL DRAWR(X,Y)
      IF(YT.LT.S(IMAX)) CALL MOVER(X,Y)
      RETURN
   10 I=IFIX(A*X+B)
      YMAX=AMAX1(Y,T(6))
      IF(S(I).GE.YMAX) RETURN
      YMIN=AMIN1(Y,T(6))
      YMIN=AMAX1(YMIN,S(I))
      CALL MOVER(X,YMIN)
      CALL DRAWR(X,YMAX)
      RETURN
      END
```

B-6. POINT SPREAD FUNCTION PROFILING

RDIMAG.FOR
HPROFL.FOR
HSPRFL.FOR
VSPRFL.FOR

ROUTINE (NON-GENERAL AS WRITTEN) TO OUTPUT THE VALUES STORED IN AN IMAGE
DATA FILE TO PRINTER FOR EXAMINATION.

2-NOV-79
RDIMAG.FOR   1 29-OCT-78

```
C       PROGRAM TO PRINTOUT UNFORMATTED DATA IN FORMATTED FORM.
        CALL ASSIGN (13,'DK1:FILE01.IMA',0,'OLD')
        DEFINE FILE 13 (64,640,U,IVAR3)
        DIMENSION VALUE(320)
        DO 500 I=1,64
        READ (13'I) (VALUE(J),J=1,320)
500     WRITE (6,100) (VALUE(J),J=1,320)
100     FORMAT (1X,10F8.2,1X)
        STOP 'UNFORMATTED TO FORMATTED CONVERSION.'
        END
```

PLOTS HORIZONTAL BRIGHTNESS PROFILE FOR A SINGLE LINE.

6-OCT-78
HPROFL.FOR   3 26-APR-78

```
C         PROGRAM TO PLOT HORIZONTAL BRIGHTNESS PROFILE FOR DETERMINATION
C              OF DECONVOLUTION FUNCTION.
          DIMENSION IMAGE(7), VAL(320)
          DATA N/1HN/
          CALL INIT
140       WRITE (7,100)
100       FORMAT (' ENTER IMAGE FILE NAME',/,' >')
          READ (5,110) IMAGE
110       FORMAT (7A2)
          WRITE (7,120) IMAGE
120       FORMAT (' IMAGE DATA IS FROM FILE ',7A2,/,' Y OR N ?',/,' >')
          READ (5,130) IANS
130       FORMAT (A1)
          IF (IANS.EQ.N) GO TO 140
          CALL ASSIGN (20,IMAGE,14)
          DEFINE FILE 20 (321,640,U,IVAR1)
340       WRITE (7,300)
300       FORMAT (' ENTER SCALE FACTOR [XX.XX]',/,' >')
          READ (5,310) SCALE
310       FORMAT (F5.2)
          WRITE (7,320) SCALE
320       FORMAT (' THE SCALE FACTOR IS ',F5.2,/,' Y OR N ?',/,' >')
          READ (5,330) IANS
330       FORMAT (I1)
          IF (IANS.EQ.N) GO TO 340
190       WRITE (7,150)
150       FORMAT (' ENTER HORIZONTAL LINE NUMBER TO BE PROFILED',/,' >')
          READ (5,160) LINE
160       FORMAT (I3)
          WRITE (7,170) LINE
170       FORMAT (' LINE NUMBER ',I3,' WILL BE PROFILED.'
     1,/,' Y OR N ?',/,' >')
          READ (5,180) IANS
180       FORMAT (A1)
          IF (IANS.EQ.N) GO TO 190
          READ (20'LINE) (VAL(J),J=1,320)
C         *****GRAPHICS*****
          CALL IWIND (20,1004,20,740)
          CALL RWIND (150.,171.,0.,512.)
          CALL CWIND (20,1004,20,740)
          CALL WAIT(6)
          CALL PAGE
          CALL MOVE (1.,(VAL(1))/SCALE)
          DO 500 K=2,320
          CALL DRAW (FLOAT(K),(VAL(K))/SCALE)
500       CONTINUE
          CALL AMODE
700       CONTINUE
          STOP
          END
```

PLOTS HORIZONTAL BRIGHTNESS PROFILES IN A CONTOUR FASHHION, BUT
WITHOUT A HIDDEN LINE ALGORITHM.

6-OCT-78
HSPRFL.FOR   3 26-APR-78


```
C       PROGRAM TO PLOT HORIZONTAL BRIGHTNESS PROFILE FOR DETERMINATION
C          OF DECONVOLUTION FUNCTION.
        DIMENSION IMAGE(7), VAL(320)
        DATA N/1HN/
140     WRITE (7,100)
100     FORMAT (' ENTER IMAGE FILE NAME',/,' >')
        READ (5,110) IMAGE
110     FORMAT (7A2)
        WRITE (7,120) IMAGE
120     FORMAT (' IMAGE DATA IS FROM FILE ',7A2,/,' Y OR N ?',/,' >')
        READ (5,130) IANS
130     FORMAT (A1)
        IF (IANS.EQ.N) GO TO 140
        CALL ASSIGN (20,IMAGE,14)
        DEFINE FILE 20 (321,640,U,IVAR1)
340     WRITE (7,300)
300     FORMAT (' ENTER SCALE FACTOR [XX.XX]',/,' >')
        READ (5,310) SCALE
310     FORMAT (F5.2)
        WRITE (7,320) SCALE
320     FORMAT (' THE SCALE FACTOR IS ',F5.2,/,' Y OR N ?',/,' >')
        READ (5,330) IANS
330     FORMAT (I1)
        IF (IANS.EQ.N) GO TO 340
        CALL INIT
C       ****GRAPHICS****
        DO 700 N=15,300,15
        LINE=N/15
        READ (20'LINE) (VAL(J),J=1,320)
        CALL IWIND (10+N,704+N,10+N,440+N)
        CALL RWIND (151.,170.,0.,512.)
        CALL CWIND (20,1004,20,740)
        CALL MOVE (1.,(VAL(1))/SCALE)
        DO 500 K=2,320
        CALL DRAW (FLOAT(K),(VAL(K))/SCALE)
        CALL AMODE
700     CONTINUE
        STOP
        END
```

PLOTS VERTICAL BRIGHTNESS PROFILE WITHIN THE CENTRAL (20X20) PIXEL REGION
OF THE (320X320) DISPLAYED IMAGE USED TO EXAMINE THE POINT-SPREAD FUNCTION.

6-OCT-78
VSPRFL.FOR   3 26-APR-78

```
C          PROGRAM TO PLOT VERTICAL BRIGHTNESS PROFILE FOR DETERMINATION
C               OF DECONVOLUTION FUNCTION.
           DIMENSION IMAGE(7), VAL(20),XVAL(320)
           DATA N/1HN/
140        WRITE (7,100)
100        FORMAT (' ENTER IMAGE FILE NAME',/,' >')
           READ (5,110) IMAGE
110        FORMAT (7A2)
           WRITE (7,120) IMAGE
120        FORMAT (' IMAGE DATA IS FROM FILE ',7A2,/,' Y OR N ?',/,' >')
           READ (5,130) IANS
130        FORMAT (A1)
           IF (IANS.EQ.N) GO TO 140
           CALL ASSIGN (20,IMAGE,14)
           DEFINE FILE 20 (31,640,U,IVAR1)
340        WRITE (7,300)
300        FORMAT (' ENTER SCALE FACTOR [XX.XX]',/,' >')
           READ (5,310) SCALE
310        FORMAT (F5.2)
           WRITE (7,320) SCALE
320        FORMAT (' THE SCALE FACTOR IS ',F5.2,/,' Y OR N ?',/,' >')
           READ (5,330) IANS
330        FORMAT (I1)
           IF (IANS.EQ.N) GO TO 340
           CALL INIT
C          *****GRAPHICS*****
           DO 700 N=15,300,15
           LINE=(N/15)+149
           DO 888 MN=1,20
           READ (20'MN) (XVAL(J),J=1,320)
           VAL(MN)=XVAL(LINE)
888        CONTINUE
           CALL IWIND (10+N,704+N,10+N,440+N)
           CALL RWIND (1.,20.,0.,512.)
           CALL CWIND (20,1004,20,740)
           CALL MOVE (1.,(VAL(1))/SCALE)
           DO 500 K=2,20
           CALL DRAW (FLOAT(K),(VAL(K))/SCALE)
500        CONTINUE
           CALL AMODE
700        CONTINUE
           STOP
           END
```

B-7. IMAGE PROCESSING

FFT.FOR
FFT2D.FOR
FFTDIV.FOR
TWODIM.FOR
RELIMA.FOR
DIVIDE.FOR
INVERT.FOR
MAGNIT.FOR
PULL64.FOR
HISTOG.FOR

SUBROUTINE TO CALCULATE <=1024 POINT FFT (ONE DIMENSIONAL)
OF A GIVEN SIGNAL. NUMBER OF POINTS IN FFT MUST BE A POWER OF TWO.

6-OCT-78
FFT   .FOR   2 28-APR-78

```
        SUBROUTINE FFT(A,M)
        COMPLEX A(1024),U,W,T
        PI=3.14159265
        N=2**M
        NV2=N/2
        NM1=N-1
        J=1
        DO 10 I=1,NM1
        IF(I.GE.J) GOTO 20
        T=A(J)
        A(J)=A(I)
        A(I)=T
   20 K=NV2
   30 IF(K.GE.J) GOTO 10
        J=J-K
        K=K/2
        GOTO 30
   10 J=J+K
        DO 40 L=1,M
        LE=2**L
        LE1=LE/2
        U=CMPLX(1.,0.)
        W=CMPLX(COS(PI/LE1),-SIN(PI/LE1))
        DO 40 J=1,LE1
        DO 50 I=J,N,LE
        IP=I+LE1
        T=A(IP)*U
        A(IP)=A(I)-T
   50 A(I)=A(I)+T
   40 U=U*W
        RETURN
        END
```

ROUTINE TO CALCULATE TWO DIMENSIONAL FFT OF THE 64X64 ARRAY LOCATED AT THE
CENTER OF THE PSI IMAGING ARRAY. INTERMEDIATE CALCULATIONS
STORED IN CORE MEMORY.


```
      6-OCT-78
      FFT2D .FOR    5 13-MAY-78


C         PROGRAM TO COMPUTE 2-D FFT OF POINT-SPREAD FUNCTION.
C         INITIAL APPLICATION TO A 64X64 POINT SPREAD FUNCTION R(64,64)
          DIMENSION IPTSPD(7),IOUT(7),R(64,64),Z(320),IDESCR(24),XIM(64,64)

          COMPLEX A(64)
          DATA N/1HN/
          DATA IDESCR/2HFF,2HT ,2HOF,2H P,2HOI,2HNT,2H S,2HPR,2HEA,2HD ,
      12HFU,2HNC,2HCT,2HIO,2HN ,2H--,2H 1,2H6 ,2HTR,2HAN,
      12HSD,2HUC,2HER,2HS./
  140     WRITE (7,100)
  100     FORMAT (' ENTER NAMES OF POINT-SPREAD ARRAY AND OUTPUT ',
      1'FFT FILES ',/,'         IN FORM:  <DK1:IPTSPD.DAT,
      1DK1:OUTPUT.DAT>',/,' >')
          READ (5,110) IPTSPD,IOUT
  110     FORMAT (7A2,1X,7A2)
          WRITE (7,120) IPTSPD,IOUT
  120     FORMAT (' THE POINT-SPREAD FUNCTION IS IN THE FILE ',
      1'NAMED ',7A2,/,' THE FFT OF THE POINT-SPREAD FUNCTION WILL BE ',
      1'STORED IN THE FILE ',/,'       NAMED ',7A2,/,' Y OR N ?',/,' >')
          READ (5,130) IANS
  130     FORMAT (A1)
          IF (IANS.EQ.N) GO TO 140
          CALL ASSIGN (11,IPTSPD,14)
          CALL ASSIGN (12,IOUT,14)
          DEFINE FILE 11 (64,640,U,IVAR1)
          DEFINE FILE 12 (65,640,U,IVAR2)
C         READ IN POINT-SPREAD IMAGE ARRAY.
          DO 150 I=1,64
          READ (11'I) (Z(J),J=1,320)
C         STRIP OFF FIRST AND LAST 128 POINTS PER LINE OF IMAGE ARRAY.
          DO 700 J=1,64
  700     R(I,J)=Z(J+128)
  150     CONTINUE
C         ***********************************
C         COMPUTE FFT AND STORE ON DISC FILE.
C         ***********************************
C         FORM COMPLEX ARRAY FOR FFT.
C         ***ROW CALCULATIONS***
          DO 200 K=1,64
          DO 210 L=1,64
          A(L)=CMPLX(R(K,L),0.)
  210     CONTINUE
          CALL FFT(A,6)
C         FFT OF ROW REPLACED INTO ARRAY 'A'.
C         PLACE FFT OF ROW BACK INTO POINT-SPREAD ARRAY.
          DO 220 M=1,64
          R(K,M)=REAL(A(M))
          XIM(K,M)=AIMAG(A(M))
  220     CONTINUE
  200     CONTINUE
C         ***COLUMN CALCULATIONS***
          DO 300 KK=1,64
          DO 310 LL=1,64
          A(LL)=CMPLX(R(LL,KK),XIM(LL,KK))
```

```
  310     CONTINUE
          CALL FFT(A,6)
C         FFT OF COLUMN REPLACED INTO ARRAY 'A'.
C         PLACE FFT OF COLUMN BACK INTO POINT-SPREAD ARRAY.
          DO 320 MM=1,64
          R(MM,KK)=REAL(A(MM))
  320     CONTINUE
  300     CONTINUE
C         WRITE TRANSFORMED ARRAY, R(64,64), ONTO DISC FILE.
          DO 710 I=1,320
  710     Z(I)=0.
          DO 400 I=1,64
C         RESTORE LEADING AND TRAILING 128 PIXELS FOR COMPATIBILITY
C             WITH PSIGEN DISPLAY ALGORITHM.
          DO 720 JJ=1,64
  720     Z(JJ+128)=R(I,JJ)
          WRITE (12'I) (Z(J),J=1,320)
  400     CONTINUE
          WRITE (12'65) (IDESCR(I),I=1,24)
          STOP 'TWO DIMENSIONAL FFT OF PSI POINT SPREAD FUNCTION.'
          END
```

PROGRAM TO DIVIDE ONE REAL (64X64) FFT ARRAY BY ANOTHER.

6-OCT-78
FFTDIV.FOR   5 14-MAY-78

```
C         TWO-DIMENSIONAL 64 POINT FFT.
C         PROGRAM TO DIVIDE TWO-DIMENSIONAL FFT OF IMAGE ARRAY BY
C              TWO-DIMENSIONAL FFT OF POINT-SPREAD FUNCTION.
          DIMENSION AFFT(64,64),BFFT(64),TEMP(320),IMAGE(7),ISPRED(7),
         1IQUOT(7),IDESCR(13)
          DATA IDESCR/2H64,2H X,2H 6,2H4 ,2HFF,2HT ,2HQU,2HOT,2HIE,2HNT,
         12H A,2HRR,2HAY/
          DATA N/1HN/
  140     WRITE (7,100)
  100     FORMAT (' ENTER NAMES OF IMAGE FFT ARRAY, POINT-SPREAD ',
         1'FFT ARRAY, AND',/,'     QUOTIENT FFT ARRAY FILES IN FORM:  ',
         1/,'     <DK1:FIMAGE.DAT,DK1:FSPRED.DAT,DK1:FFQUOT.DAT>',/,' >')
          READ (5,110) IMAGE,ISPRED,IQUOT
  110     FORMAT (7A2,1X,7A2,1X,7A2)
          WRITE (7,120) IMAGE,ISPRED,IQUOT
  120     FORMAT (' THE IMAGE FFT IS FROM THE FILE NAMED:  ',7A2,/,
         1' THE POINT-SPREAD FFT IS FROM THE FILE NAMED:  ',7A2,/,
         1' THE QUOTIENT FFT WILL BE STORED IN THE FILE NAMED:  ',7A2,/,
         1' Y OR N ?',/,' >')
          READ (5,130) IANS
  130     FORMAT (A1)
          IF (IANS.EQ.N) GO TO 140
          CALL ASSIGN (11,IMAGE,14)
          CALL ASSIGN (12,ISPRED,14)
          CALL ASSIGN (13,IQUOT,14)
          DEFINE FILE 11 (65,640,U,IVAR1)
          DEFINE FILE 12 (65,640,U,IVAR2)
          DEFINE FILE 13 (65,640,U,IVAR3)
C         FFT FILES ARE COMPATIBLE WITH PSIGEN.FOR DISPLAY.
C         MUST STRIP OFF FIRST AND LAST 128 WORDS OF EACH LINE.
          DO 200 I=1,64
          READ (11'I) (TEMP(J),J=1,320)
          DO 210 K=1,64
  210     AFFT(I,K)=TEMP(K+128)
  200     CONTINUE
          DO 600 M=1,64
          READ (12'M) (TEMP(J),J=1,320)
C         DUE TO LIMITED MEMORY, READ OUT BFFT() ONE LINE AT A TIME.
C         MUST STRIP OFF FIRST AND LAST 128 WORDS OF LINE.
          DO 610 K=1,64
  610     BFFT(K)=TEMP(K+128)
C         DIVIDE AFFT() BY BFFT() AND PLACE RESULT IN AFFT().
          DO 310 N=1,64
C         IN ORDER TO GUARD AGAINST DIVISION BY ZERO, SHOULD BFFT(N)=0.,
C              THEN SET AUTOMATICALLY SET QUOTIENT TO ZERO.
          IF (BFFT(N).NE.0.) GO TO 310
          AFFT(M,N)=0.
          GO TO 600
  310     AFFT(M,N)=AFFT(M,N)/BFFT(N)
  600     CONTINUE
C         RESTORE LEADING AND TRAILING 128 PIXELS FOR COMPATIBILITY
C              WITH PSIGEN DISPLAY ALGORITHM.
          DO 400 I=1,320
  400     TEMP(I)=0.
```

```
      DO 500 I=1,64
      DO 510 J=1,64
510   TEMP(J+128)=AFFT(I,J)
      WRITE (13'I) (TEMP(K),K=1,320)
500   CONTINUE
      WRITE (13'65) (IDESCR(I),I=1,13)
      STOP 'QUOTIENT OF FFT[IMAGE]/FFT[POINT-SPREAD].'
      END
```

ROUTINE TO TAKE 2-D FFT OF THE CENTRAL PORTION OF A 64X320 DATA ARRAY.
INTERMEDIATE CALCULATIONS ARE STORED IN CORE MEMORY.


```
 6-OCT-78
TWODIM.FOR     6 24-MAY-78


C        PROGRAM TO COMPUTE 2-D FFT OF A 64X64 REAL DATA ARRAY.
C        DUE TO MEMORY LIMITATIONS OF THE PDP-11/35, THIS PROGRAM
C            WILL ONLY RUN ON THE PDP 11/40 IN BASEMENT.
C        REAL AND IMAGINARY PARTS WILL BE KEPT IN SEPARATE FILES
C            TO FACILITATE ANALYSIS.
         DIMENSION INPUT(7),R(64,64),Z(320),IDREAL(9),IDIMAG(11)
         DIMENSION XIM(64,64),IOUTR(7),IOUTI(7)
         COMPLEX A(64)
         DATA N/1HN/
         DATA IDREAL/2HRE,2HAL,2H F,2HFT,2H O,2HF ,2HFI,2HLE,2H  /
         DATA IDIMAG/2HIM,2HAG,2HIN,2HAR,2HY ,2HFF,2HT ,2HOF,2H F,
       12HIL,2HE /
 140     WRITE (7,100)
 100     FORMAT (' ENTER NAMES OF INPUT ARRAY AND [RE] AND [IM] OUTPUT ',
       1'FFT FILES ',/,'        IN FORM:  <DK1:INPUTX.DAT,
       1DK1:REALXX.DAT,DK1:IMAGXX.DAT>',/,' >')
         READ (5,110) INPUT,IOUTR,IOUTI
 110     FORMAT (7A2,1X,7A2,1X,7A2)
         WRITE (7,120) INPUT,IOUTR,IOUTI
 120     FORMAT (' THE INPUT ARRAY IS IN FILE ',7A2,/,' THE REAL ',
       1'FFT PART OF THE INPUT ARRAY WILL BE STORED IN FILE ',
       17A2,/,' THE IMAGINARY FFT PART OF THE INPUT ARRAY WILL ',
       1'BE STORED IN FILE ',7A2,/,' Y OR N ?',/,' >')
         READ (5,130) IANS
 130     FORMAT (A1)
         IF (IANS.EQ.N) GO TO 140
         CALL ASSIGN (11,INPUT,14)
         CALL ASSIGN (12,IOUTR,14)
         CALL ASSIGN (13,IOUTI,14)
         DEFINE FILE 11 (64,640,U,IVAR1)
         DEFINE FILE 12 (65,640,U,IVAR2)
         DEFINE FILE 13 (65,640,U,IVAR3)
C        READ IN INPUT IMAGE ARRAY.
         DO 150 I=1,64
         READ (11'I) (Z(J),J=1,320)
C        STRIP OFF FIRST AND LAST 128 POINTS PER LINE OF IMAGE ARRAY.
         DO 700 J=1,64
 700     R(I,J)=Z(J+128)
 150     CONTINUE
C        **********************************
C        COMPUTE FFT AND STORE ON DISC FILE.
C        **********************************
C        FORM COMPLEX ARRAY FOR FFT.
C        ***ROW CALCULATIONS***
         DO 200 K=1,64
         DO 210 L=1,64
C        FORM ROW ARRAY.
         A(L)=CMPLX(R(K,L),0.)
 210     CONTINUE
         CALL FFT(A,6)
C .      FFT OF ROW REPLACED INTO ARRAY 'A'.
C        PLACE FFT OF ROW BACK INTO POINT-SPREAD ARRAY.
         DO 220 M=1,64
         R(K,M)=REAL(A(M))
```

THIS VERSION OF 2-D FFT STORES
ALL INTERMEDIATE CALCULATIONS
IN CORE MEMORY. (MAY BE USED ON
PDP 11/40 IN BASEMENT.)

```
         XIM(K,M)=AIMAG(A(M))
  220    CONTINUE
  200    CONTINUE
C        ***COLUMN CALCULATIONS***
         DO 300 KK=1,64
         DO 310 LL=1,64
         A(LL)=CMPLX(R(LL,KK),XIM(LL,KK))
  310    CONTINUE
         CALL FFT(A,6)
.C       FFT OF COLUMN REPLACED INTO ARRAY 'A'.
C        PLACE FFT OF COLUMN BACK INTO POINT-SPREAD ARRAY.
         DO 320 MM=1,64
         R(MM,KK)=REAL(A(MM))
         XIM(MM,KK)=AIMAG(A(MM))
  320    CONTINUE
  300    CONTINUE
C        WRITE TRANSFORMED ARRAY [RE], R(64,64), ONTO DISC FILE.
C        WRITE TRANSFORMED ARRAY [IM], XIM(64,64), ONTO DISC FILE.
         DO 710 I=1,320
  710    Z(I)=0.
         DO 400 I=1,64
C        RESTORE LEADING AND TRAILING 128 PIXELS FOR COMPATIBILITY
C            WITH PSIGEN DISPLAY ALGORITHM.
         DO 720 JJ=1,64
  720    Z(JJ+128)=R(I,JJ)
         WRITE (12'I) (Z(J),J=1,320)
         DO 730 JJ=1,64
  730    Z(JJ+128)=XIM(I,JJ)
         WRITE (13'I) (Z(J),J=1,320)
  400  . CONTINUE
         WRITE (12'65) (IDREAL(I),I=1,9),(INPUT(J),J=1,7)
         WRITE (13'65) (IDIMAG(I),I=1,11),(INPUT(J),J=1,7)
         STOP 'TWO DIMENSIONAL FFT OF A (64 X 64) DATA ARRAY.'
         END
```

SAME AS 'TWODIM.FOR' EXCEPT THAT INTERMEDIATE VALUES ARE STORED ON DISC
DUE TO LIMITED CORE MEMORY.


```
 6-OCT-78
 RELIMA.FOR    6 15-MAY-78


C        PROGRAM TO COMPUTE 2-D FFT OF INPUT FUNCTION.
C        INITIAL APPLICATION TO A 64X64 INPUT FUNCTION R(64,64)
         DIMENSION INPUT(7),IOUTR(7),IOUTI(7),R(64,64),Z(320),
        1IDREAL(14),IDIMAG(16),XIM(320),ZERO(320)
         COMPLEX A(64)
         DATA N/1HN/
         DATA ZERO/320*0./
         DATA IDREAL/2HRE,2HAL,2H F,2HFT,2H O,2HF ,2HIN,2HPU,2HT ,2HFU,
        12HNC,2HTI,2HON,2H--/
         DATA IDIMAG/2HIM,2HAG,2HIN,2HAR,2HY ,2HFF,2HT ,2HOF,2H I,2HNP,
        12HUT,2H F,2HUN,2HCT,2HIO,2HN-/
 140     WRITE (7,100)
 100     FORMAT (' ENTER NAMES OF INPUT ARRAY, OUTPUT REAL FFT, AND ',
        1'OUTPUT IMAGINARY FFT FILES ',/,'     IN FORM:  <DK1:INPUTX.DAT,'
        1'DK1:OUREAL.DAT,DK1:OUTIMAG.DAT>',/,' >')
         READ (5,110) INPUT,IOUTR,IOUTI
 110     FORMAT (7A2,1X,7A2,1X,7A2)
         WRITE (7,120) INPUT,IOUTR,IOUTI
 120     FORMAT (' THE INPUT FUNCTION IS IN THE FILE ',7A2,/,
        1' THE REAL FFT OF INPUT FUNCTION WILL BE IN FILE ',7A2,/,
        1' THE IMAGINARY FFT OF INPUT FUNCTION WILL BE IN FILE ',7A2,/,
        1' Y OR N ?',/,' >')
         READ (5,130) IANS
 130     FORMAT (A1)
         IF (IANS.EQ.N) GO TO 140
         CALL ASSIGN (11,INPUT,14)
         CALL ASSIGN (12,IOUTR,14)
         CALL ASSIGN (13,IOUTI,14)
         DEFINE FILE 11 (64,640,U,IVAR1)
         DEFINE FILE 12 (65,640,U,IVAR2)
         DEFINE FILE 13 (65,640,U,IVAR3)
C        READ IN POINT-SPREAD IMAGE ARRAY.
         DO 150 I=1,64
         READ (11'I) (Z(J),J=1,320)
C        STRIP OFF FIRST AND LAST 128 POINTS PER LINE OF IMAGE ARRAY.
         DO 700 J=1,64
 700     R(I,J)=Z(J+128)
 150     CONTINUE
C        ***********************************
C        COMPUTE FFT AND STORE ON DISC FILE.
C        ***********************************
C        FORM COMPLEX ARRAY FOR FFT.
C        ***ROW CALCULATIONS***
         DO 200 K=1,64
         DO 210 L=1,64
         A(L)=CMPLX(R(K,L),0.)
 210     CONTINUE
         CALL FFT(A,6)
C        FFT OF ROW REPLACED INTO ARRAY 'A'.
C        PLACE FFT OF ROW BACK INTO POINT-SPREAD ARRAY.
         DO 220 M=1,64
         R(K,M)=REAL(A(M))
         XIM(M)=AIMAG(A(M))
 220     CONTINUE
```

THIS VERSION FOR 2-D FFT USES INTERMEDIATE DISC DATA STORAGE DUE TO LIMITED CORE MEMORY. (FOR USE ON 1st FLOOR PDP 11/355

```
C          PLACE IMAGINARY PART OF ROW FFT IN DISC FILE.
           WRITE (13'K) (XIM(M),M=1,64)
  200      CONTINUE
           DO 510 I=1,65
  510      WRITE (13'I) (ZERO(J),J=1,320)
C          ***COLUMN CALCULATIONS***
           DO 300 KK=1,64
           DO 310 LL=1,64
C          READ ENTIRE IMAGINARY PART ROW FROM DISC FILE AND PULL OUT
C              ELEMENT (KK).
           READ (13'LL) (XIM(III),III=1,64)
           A(LL)=CMPLX(R(LL,KK),XIM(KK))
  310      CONTINUE
C          COLUMN (KK) MATRIX IS NOW COMPLETE.
           CALL FFT(A,6)
C          FFT OF COLUMN REPLACED INTO ARRAY 'A'.
C          PLACE FFT OF COLUMN BACK INTO POINT-SPREAD ARRAY.
           DO 320 MM=1,64
           R(MM,KK)=REAL(A(MM))
           READ (13'MM) (XIM(N),N=1,320)
           XIM(KK+128)=AIMAG(A(MM))
           WRITE (13'MM) (XIM(N),N=1,320)
  320      CONTINUE
  300      CONTINUE
C          WRITE TRANSFORMED ARRAY, R(64,64), ONTO DISC FILE.
           DO 710 I=1,320
  710      Z(I)=0.
           DO 400 I=1,64
C          RESTORE LEADING AND TRAILING 128 PIXELS FOR COMPATIBILITY
C              WITH PSIGEN DISPLAY ALGORITHM.
           DO 720 JJ=1,64
  720      Z(JJ+128)=R(I,JJ)
           WRITE (12'I) (Z(J),J=1,320)
  400      CONTINUE
           WRITE (12'65) IDESCR,IOUTR
           WRITE (13'65) IDESCR,IOUTI
           STOP 'TWO DIMENSIONAL FFT OF PSI POINT SPREAD FUNCTION.'
           END
```

THIS ROUTINE WILL DIVIDE ONE (64X64) FFT ARRAY BY ANOTHER, GIVEN, THE REAL
AND IMAGINARY PARTS OF EACH FROM SEPARATE FILES.

6-OCT-78
DIVIDE.FOR   7 24-MAY-78

```
C        PROGRAM TO DIVIDE TWO (64X64) FFT ARRAYS.
         DIMENSION AAREAL(64),AAIMAG(64),BREAL(64),BIMAG(64),
1Y(320),Z(320),FFTRL(64,64),FFTIM(64,64),IDREAL(14),IDIMAG(17),
1IAREAL(7),IAIMAG(7),IBREAL(7),IBIMAG(7),IQREAL(7),IQIMAG(7)
         COMPLEX A(64),B(64),C
         DATA IDREAL/2HRE,2HAL,2H Q,2HUO,2HTI,2HEN,2HT ,2HOF,2H F,2HFT,
12H A,2HRR,2HAY,2HS /
         DATA IDIMAG/2HIM,2HAG,2HIN,2HAR,2HY ,2HQU,2HOT,2HIE,2HNT,2H O,
12HF ,2HFF,2HT ,2HAR,2HRA,2HYS,2H  /
         DATA N/1HN/
140      WRITE (7,100)
100      FORMAT (' ENTER NAMES OF [RE] DIVIDEND, [IM] DIVIDEND,',
1'[RE] DIVISOR, [IM] DIVISOR,',/,'     [RE] QUOTIENT, AND',
1' [IM] QUOTIENT FILES IN FORM:',/,' <DK1:DIVIDR.DAT,',
1'DK1:DIVIDI.DAT<CR>DK1:DIVISR.DAT,DK1:DIVISI.DAT<CR>',/,
1'      DK1:QUOTR.DAT,DK1:QUOTI.DAT<CR>>')
         READ (5,110) IAREAL,IAIMAG,IBREAL,IBIMAG,IQREAL,IQIMAG
110      FORMAT (7A2,1X,7A2)
         WRITE (5,120) IAREAL,IAIMAG,IBREAL,IBIMAG,IQREAL,IQIMAG
120      FORMAT (' RE[A]= ',7A2,5X,' IM[A]= ',7A2,/,
1' RE[B]= ',7A2,5X,' IM[B]= ',7A2,/,' RE[QUOT]= ',7A2,5X,
1'IM[QUOT]= ',7A2,/,' Y OR N ?',/,' >')
         READ (5,130) IANS
130      FORMAT (A1)
         IF (IANS.EQ.N) GO TO 140
200      WRITE (7,210)
210      FORMAT (' ENTER FFT DIVISOR THRESHOLD VALUE <F5.2>.',/,' >')
         READ (5,220) THRESH
220      FORMAT (F5.2)
         WRITE (7,230) THRESH
230      FORMAT (' FFT DIVISOR THRESHOLD VALUE = ',F5.2,/,
1' Y OR N ?',/,' >')
         READ (5,240) IANS
240      FORMAT (A1)
         IF (IANS.EQ.N) GO TO 200
         CALL ASSIGN (11,IAREAL,14)
         CALL ASSIGN (12,IAIMAG,14)
         CALL ASSIGN (13,IBREAL,14)
         CALL ASSIGN (14,IBIMAG,14)
         CALL ASSIGN (15,IQREAL,14)
         CALL ASSIGN (16,IQIMAG,14)
         DEFINE FILE 11 (65,640,U,IVAR1)
         DEFINE FILE 12 (65,640,U,IVAR2)
         DEFINE FILE 13 (65,640,U,IVAR3)
         DEFINE FILE 14 (65,640,U,IVAR4)
         DEFINE FILE 15 (65,640,U,IVAR5)
         DEFINE FILE 16 (65,640,U,IVAR6)
C        FFT FILES ARE COMPATIBLE WITH PSIGEN DISPLAY.
C        MUST STRIP OFF FIRST AND LAST 128 WORDS OF EACH LINE.
C        COMPLEX DIVIDE POINT BY POINT, ROW BY ROW.
         DO 500 I=1,64
         READ (11'I) (Y(J),J=1,320)
         READ (12'I) (Z(J),J=1,320)
C        STRIP OFF LEADING AND TRAILING 128 WORDS.
```

```
        DO 510 K=1,64
        AAREAL(K)=Y(K+128)
 510    AAIMAG(K)=Z(K+128)
        READ (13'I) (Y(J),J=1,320)
        READ (14'I) (Z(J),J=1,320)
C       STRIP OFF LEADING AND TRAILING 128 WORDS.
        DO 520 K=1,64
        BREAL(K)=Y(K+128)
 520    BIMAG(K)=Z(K+128)
C       FORM COMPLEX ROWS FOR DIVIDEND AND DIVISOR.
C       DIVIDE OUT POINT BY POINT ACROSS ROW.
        DO 530 K=1,64
        A(K)=CMPLX(AAREAL(K),AAIMAG(K))
        B(K)=CMPLX(BREAL(K),BIMAG(K))
C       CHECK FOR AN ARBITRARILY VANISHING DIVISOR.
C       IF MAGNITUDE OF DIVISOR IS NOT GREATER THAN THRESHOLD VALUE
C            ENTERED AT BEGINNING OF PROGRAM, THEN LEAVE DIVIDEND
C            UNCHANGED.
        IF (SQRT((BREAL(K))**2.+(BIMAG(K))**2.).GT.THRESH) GO TO 700
        C=A(K)
        GO TO 710
 700    C=A(K)/B(K)
 710    FFTRL(I,K)=REAL(C)
 530    FFTIM(I,K)=AIMAG(C)
 500    CONTINUE
C       ADD BACK LEADING AND TRAILING 128 WORDS FOR PSIGEN COMPATIBILITY.
C       INITIALIZE TEMPORARY OUTPUT ARRAY.
        DO 800 N=1,320
        Y(N)=0.
 800    Z(N)=0.
C       WRITE OUTPUT TO DISC FILE.
        DO 600 I=1,64
        DO 610 J=1,64
        Y(128+J)=FFTRL(I,J)
 610    Z(128+J)=FFTIM(I,J)
        WRITE (15'I) (Y(K),K=1,320)
        WRITE (16'I) (Z(K),K=1,320)
 600    CONTINUE
        WRITE (15'65) (IDREAL(I),I=1,14),(IQREAL(J),J=1,7)
        WRITE (16'65) (IDIMAG(I),I=1,17),(IQIMAG(J),J=1,7)
        STOP 'COMPLEX DIVISION OF TWO (64X64) FFT ARRAYS.'
        END
```

PROGRAM TO COMPUTE INVERSE FFT OF A 64X64 IMAGE TRANSFORM SPECIFIED BY ITS
REAL AND IMAGINARY PARTS. REAL AND IMAGINARY PARTS OF OUTPUT ARE STORED IN
SEPARATE FILES. THE INVERTED IMAGE WILL BE EQUIVALENT TO THE FFT INVERSE
EXCEPT FOR THE FACT THAT DIAGONALLY OPPOSITE QUADRANTS OF THE RESULTANT
IMAGE MUST BE INTERCHANGED.

```
      6-OCT-78
      INVERT.FOR   7 24-MAY-78


      C        PROGRAM TO COMPUTE 2-D FFT OF A 64X64 REAL DATA ARRAY.
      C        DUE TO MEMORY LIMITATIONS OF THE PDP-11/35, THIS PROGRAM
      C            WILL ONLY RUN ON THE PDP 11/40 IN BASEMENT.
      C        REAL AND IMAGINARY PARTS WILL BE KEPT IN SEPARATE FILES
      C            TO FACILITATE ANALYSIS.
               DIMENSION INPUTR(7),R(64,64),Z(320),IDREAL(9),IDIMAG(11)
               DIMENSION XIM(64,64),IOUTR(7),IOUTI(7),Y(320),INPUTI(7)

               COMPLEX A(64)
               DATA N/1HN/
               DATA IDREAL/2HRE,2HAL,2H F,2HFT,2H O,2HF ,2HFI,2HLE,2H  /
               DATA IDIMAG/2HIM,2HAG,2HIN,2HAR,2HY ,2HFF,2HT ,2HOF,2H F,
              12HIL,2HE /
      140      WRITE (7,100)
      100      FORMAT (' ENTER NAMES OF [RE] AND [IM] INPUT ARRAY AND ',
              1'[RE] AND [IM] OUTPUT FFT FILES ',/,'        IN FORM:  ',
              1'<DK1:INPUTR.DAT,DK1:INPUTI.DAT,DK1:REALXX.DAT,',
              1'DK1:IMAGXX.DAT>',/,' >')
               READ (5,110) INPUTR,INPUTI,IOUTR,IOUTI
      110      FORMAT (7A2,1X,7A2,1X,7A2,1X,7A2)
               WRITE (7,120) INPUTR,INPUTI,IOUTR,IOUTI
      120      FORMAT (' THE REAL PART OF THE INPUT ARRAY IS IN FILE ',7A2,/,
              1' THE IMAGINARY PART OF THE INPUT ARRAY IS IN FILE ',7A2,/,
              1' THE REAL FFT PART OF THE INPUT ARRAY WILL BE STORED IN FILE ',
              17A2,/,' THE IMAGINARY FFT PART OF THE INPUT ARRAY WILL BE ',
              1'STORED IN FILE ',7A2,' Y OR N ?',/,' >')
               READ (5,130) IANS
      130      FORMAT (A1)
               IF (IANS.EQ.N) GO TO 140
               CALL ASSIGN (10,INPUTR,14)
               CALL ASSIGN (11,INPUTI,14)
               CALL ASSIGN (12,IOUTR,14)
               CALL ASSIGN (13,IOUTI,14)
               DEFINE FILE 10 (64,640,U,IVAR4)
               DEFINE FILE 11 (64,640,U,IVAR1)
               DEFINE FILE 12 (65,640,U,IVAR2)
              ·DEFINE FILE 13 (65,640,U,IVAR3)
      C        READ IN INPUT IMAGE ARRAY.
               DO 150 I=1,64
               READ (10'I) (Y(J),J=1,320)
               READ (11'I) (Z(J),J=1,320)
      C        STRIP OFF FIRST AND LAST 128 POINTS PER LINE OF IMAGE ARRAY.
               DO 700 J=1,64
               XIM(I,J)=Z(J+128)
      700      R(I,J)=Y(J+128)
      150      CONTINUE
      C        ********************************
      C        COMPUTE FFT AND STORE ON DISC FILE.
      C        ********************************
      C        FORM COMPLEX ARRAY FOR FFT.
      C        ***ROW CALCULATIONS***
               DO 200 K=1,64
               DO 210 L=1,64
      C        FORM ROW ARRAY.
```

```
        A(L)=CMPLX(R(K,L),XIM(K,L))
 210    CONTINUE
        CALL FFT(A,6)
C       FFT OF ROW REPLACED INTO ARRAY 'A'.
C       PLACE FFT OF ROW BACK INTO POINT-SPREAD ARRAY.
        DO 220 M=1,64
        R(K,M)=REAL(A(M))
        XIM(K,M)=AIMAG(A(M))
 220    CONTINUE
 200    CONTINUE
C       ***COLUMN CALCULATIONS***
        DO 300 KK=1,64
        DO 310 LL=1,64
        A(LL)=CMPLX(R(LL,KK),XIM(LL,KK))
 310    CONTINUE
        CALL FFT(A,6)
C       FFT OF COLUMN REPLACED INTO ARRAY 'A'.
C       PLACE FFT OF COLUMN BACK INTO POINT-SPREAD ARRAY.
        DO 320 MM=1,64
        R(MM,KK)=REAL(A(MM))
        XIM(MM,KK)=AIMAG(A(MM))
 320    CONTINUE
 300    CONTINUE
C       WRITE TRANSFORMED ARRAY [RE], R(64,64), ONTO DISC FILE.
C       WRITE TRANSFORMED ARRAY [IM], XIM(64,64), ONTO DISC FILE.
        DO 710 I=1,320
 710    Z(I)=0.
        DO 400 I=1,64
C       RESTORE LEADING AND TRAILING 128 PIXELS FOR COMPATIBILITY
C           WITH PSIGEN DISPLAY ALGORITHM.
        DO 720 JJ=1,64
 720    Z(JJ+128)=R(I,JJ)
        WRITE (12'I) (Z(J),J=1,320)
        DO 730 JJ=1,64
 730    Z(JJ+128)=XIM(I,JJ)
        WRITE (13'I) (Z(J),J=1,320)
 400    CONTINUE
        WRITE (12'65) (IDREAL(I),I=1,9),(INPUTR(I),I=1,7)
        WRITE (13'65) (IDIMAG(I),I=1,11),(INPUTI(I),I=1,7)
        STOP 'TWO DIMENSIONAL FFT OF A (64 X 64) DATA ARRAY.'
        END
```

CALCULATED THE MAGNITUDE ARRAY OF A GIVEN (64X64) FFT ARRAY.

6-OCT-78
MAGNIT.FOR   2 23-MAY-78

```
C       PROGRAM TO FORM MAGNITUDE ARRAY (64X64) FROM REAL AND
C            IMAGINARY PARTS OF INVERTED FFT ARRAY.
        DIMENSION A(320),B(320),C(320),IDESCR(5)
        DATA IDESCR/2HMA,2HGN,2HIT,2HUD,2HE /
        DATA C/320*0./
        CALL ASSIGN (11,'DK1:TROUTR.INV',14)
        CALL ASSIGN (12,'DK1:TROUTI.INV',14)
        CALL ASSIGN (13,'DK1:MAGNIT.INV',14)
        DEFINE FILE 11 (65,640,U,IVAR1)
        DEFINE FILE 12 (65,640,U,IVAR2)
        DEFINE FILE 13 (65,640,U,IVAR3)
        DO 500 I=1,64
        READ (11'I) (A(J),J=1,320)
        READ (12'I) (B(J),J=1,320)
        DO 600 M=129,192
600     C(M)=SQRT((A(M))**2.+(B(M))*2.)
500     WRITE (13'I) (C(M),M=1,320)
        WRITE (13'65) (IDESCR(I),I=1,5)
        STOP 'FORMATION OF MAGNITUDE ARRAY FROM INVERTED RE & IM FFT.'
        END
```

```
C          PROGRAM TO PULL OUT MIDDLE 64 LINES FROM 800 BLOCK IMAGE FILE.
C          VALUES TO EITHER SIDE OF THE 64X64 SQUARE WILL BE ZEROED.
           DIMENSION Z(320)
           CALL ASSIGN (11,'DK1:FILE01.IMA',14)
           DEFINE FILE 11 (320,640,U,IVAR1)
           CALL ASSIGN (12,'DK1:FILE02.IMA',14)
           DEFINE FILE 12 (64,640,U,IVAR2)
           DO 500 I=129,192
           READ (11'I) (Z(J),J=1,320)
           DO 600 IZERO=1,128
           Z(IZERO)=0.
600        Z(IZERO+192)=0.
           K=I-128
500        WRITE (12'K) (Z(J),J=1,320)
           STOP 'PULL OUT OF MIDDLE 64 IMAGE LINES.'
           END
```

PROGRAM TO TAKE A GIVEN DATA FILE, AND REASSIGN ALL GRAY SHADES FOR
EQUAL PROBABILITY OF OCCURRENCE IN THE IMAGE (HISTOGRAM EQUALIZATION)
AND FORM A NEW FILE WITH THE TRANSFORMED IMAGE.


```
       1-NOV-78
      HISTOG.FOR    12 29-OCT-78
       136 FREE BLOCKS


              DIMENSION IMAGE(7),IHIST(1024),Z(320),CDF(1024),IOUT(7),
            1IDESCR(160)
              DATA N/1HN/
              DATA IHIST/1024*0/
              DATA CDF/1024*0./
              RELMAX=0.
              CALL INIT
              CALL WAIT (6)
      140     WRITE (7,100)
      100     FORMAT (' ENTER IMAGE FILE NAME',/,' >')
              READ (5,110) IMAGE
      110     FORMAT (7A2)
              WRITE (7,120) IMAGE
      120     FORMAT (' IMAGE DATA IS FROM FILE ',7A2,/,' Y OR N ?',/,' >')
              READ (5,130) IANS
      130     FORMAT (A1)
              IF (IANS.EQ.N) GO TO 140
      800     WRITE (7,810)
      810     FORMAT (' ENTER NUMBER OF LINES IN IMAGE FILE',/,' >')
              READ (5,820) NLINE
      820     FORMAT (I3)
              WRITE (7,830) NLINE
      830     FORMAT (' THE IMAGE FILE CONTAINS ',I3,' LINES.',/,/,
            1' Y OR N ?',/,' >')
              READ (5,840) IANS
      840     FORMAT (A1)
              IF (IANS.EQ.N) GO TO 800
      2299    WRITE (7,2255)
      2255    FORMAT (' ENTER NUMBER OF CENTRALLY-LOCATED POINTS ',
            1'PER IMAGE LINE.',/,' >')
              READ (5,2266) NPTS
      2266    FORMAT (I3)
              WRITE (7,2277) NPTS
      2277 FORMAT (' THERE ARE ',I3,' CENTRALLY-LOCATED POINTS ',
            1'PER IMAGE LINE.',/,' Y OR N ?',/,' >')
              READ (5,2288) IANS
      2288    FORMAT (A2)
              IF (IANS.EQ.N) GO TO 2299
      145     WRITE (7,105)
      105     FORMAT (' ENTER OUTPUT FILE NAME',/,' >')
              READ (5,115) IOUT
      115     FORMAT (7A2)
              WRITE (7,125) IOUT
      125     FORMAT (' OUTPUT DATA IS FROM FILE ',7A2,/,' Y OR N ?',/,' >')
              READ (5,135) IANS
      135     FORMAT (A1)
              IF (IANS.EQ.N) GO TO 145
              WRITE (7,905)
      905     FORMAT (' ENTER UP TO FOUR LINES (80 CHAR. EACH) OF FILE ',
            1'I.D. DATA.',/,' >')
              READ (5,906) (IDESCR(ICHAR), ICHAR=1,160)
      906     FORMAT (40A2)
              CALL ASSIGN (20,IMAGE,14)
              LINEP1=NLINE+1
```

```
        DEFINE FILE 20 (LINEP1,640,U,IVAR1)
        CALL ASSIGN (21,IOUT,14)
        DEFINE FILE 21 (LINEP1,640,U,IVAR2)
C       NOTE:  EXTRA RECORD IN THIS FILE MAY BE USED FOR COMMENTS ENTRY.
C       *************************************************************
C       COMPUTE DATA SCALE FACTOR TO ALLOW A MAXIMUM DATA VALUE OF 1024.
C       *************************************************************
        DO 10 I=1,NLINE
        READ (20'I) (Z(J),J=1,320)
        DO 12 IZ=1,319,2
        IF (Z(IZ).GE.100000000000.) GO TO 12
        IF (Z(IZ+1).GE.100000000000.) GO TO 12
C       THE TWO PRECEEDING STATEMENTS ARE USED TO
C          REMOVE THE VALUES STORED FOR TRANSDUCER DESIGNATION FROM CONTENTION
C          FROM RECONSTRUCTED IMAGE MAXIMUM VALUES.
        RELMAX=AMAX1(Z(IZ),Z(IZ+1),RELMAX)
   12   CONTINUE
   10   CONTINUE
        SCALE=RELMAX/1024.
  380   WRITE (7,320) SCALE
  320   FORMAT (' THE SCALE FACTOR IS ',F5.2)
        WRITE (7,330)
  330   FORMAT (' IS THIS VALUE ACCEPTABLE?',/,' Y OR N ?',/,' >')
        READ (7,340) IANS
  340   FORMAT (A1)
        IF (IANS.NE.N) GO TO 350
        WRITE (7,360)
  360   FORMAT (' ENTER DESIRED SCALE FACTOR **F5.2 FORMAT**',/,' >')
        READ (5,370) SCALE
  370   FORMAT (F5.2)
        GO TO 380
C       DEFINE IMAGE LINE NUMBER.
  350   WRITE (7,2300)
 2300   FORMAT (' PROCESSING HAS BEGUN . . .')
        K1=161-NPTS/2
        K2=160+NPTS/2
        DO 11 I=1,NLINE
        READ (20'I) (Z(J),J=1,320)
C       DEFINE NUMBER OF ELEMENT WITHIN LINE.
        DO 20 K=K1,K2
        IF ((Z(K)/SCALE).GE.1024.) GO TO 2256
        NUM=IFIX((Z(K)/SCALE)+0.5)
        GO TO 2257
 2256   NUM=1024
 2257   IHIST(NUM)=IHIST(NUM)+1
   20   CONTINUE
   11   CONTINUE
        MAXHST=0
        DO 510 I1=1,1024,2
        MAXHST=MAX0(IHIST(I1),IHIST(I1+1),MAXHST)
  510   CONTINUE
C       *****GRAPHICS*****
        CALL IWIND (20,1004,20,740)
        CALL RWIND (0.,1024.,0.,FLOAT(MAXHST))
```

```
        CALL CWIND (20,1004,20,740)
        CALL WAIT(6)
        CALL PAGE
        CALL MOVE (1.,FLOAT(IHIST(1)))
        DO 500 M=1,1024
        CALL DRAW (FLOAT(M),FLOAT(IHIST(M)))
500     CONTINUE
        CALL MOVE (0.0)
        CALL DRAW (0.,FLOAT(MAXHST))
        CALL MOVE (0.,0.)
        CALL DRAW (1024.,0.)
        CALL MOVE (5.,FLOAT(MAXHST))
        CALL AMODE
        WRITE (6,400) IMAGE,SCALE,MAXHST
400     FORMAT (' HISTOGRAM OF IMAGE FILE ',7A2,/,'   DATA SCALE ',
     1'FACTOR EQUALS ',F5.2,/,3X,'X-AXIS RANGE:  0-1024',/,
     13X,'Y-AXIS RANGE:  0-',I5)
        READ (5,410) ICHAR
410     FORMAT (A1)
C       ******************************
C       CUMULATIVE DISTRIBUTION FUNCTION.
C       ******************************
C       FORMATION OF CDF (FOR 320 X 'NLINE' PIXEL DISPLAY).
C       CDF(1)=(FLOAT(IHIST(1)))/(320.*FLOAT(NLINE))
C
C       ...........................................
C       FORMATION OF CDF (FOR 'NPTS' X 'NLINE' PIXEL DISPLAY).
        CDF(1)=(FLOAT(IHIST(1)))/(NPTS*FLOAT(NLINE))
C       ...........................................
        DO 420 L=2,1024
        CDF(L)=CDF(L-1)+(FLOAT(IHIST(L)))/(NPTS*FLOAT(NLINE))
420     CONTINUE
C       ****GRAPHICS*****
        CALL WAIT(6)
        CALL INIT
        CALL WAIT(6)
        CALL IWIND (20,1004,20,740)
        CALL RWIND (0.,1024.,0.,1.)
        CALL CWIND (20,1004,20,740)
        CALL MOVE (1.,CDF(1))
        DO 430 MN=2,1024
        CALL DRAW (FLOAT(MN),CDF(MN))
430     CONTINUE
        CALL MOVE (0.,0.)
        CALL DRAW (0.,1024.)
        CALL MOVE (0.,0.)
        CALL DRAW (1024.,0.)
        CALL MOVE (5.,1.)
        CALL AMODE
        WRITE (6,440) IMAGE,SCALE
440     FORMAT (' CDF OF IMAGE FILE ',7A2,/,'   DATA SCALE ',
     1'FACTOR EQUALS ',F5.2,/,3X,'X-AXIS RANGE:  0-1024',/,
     13X,'Y-AXIS RANGE:  0-1')
        READ (5,411) ICHAR
411     FORMAT (A1)
```

```
        WRITE (7,450)
 450    FORMAT (' ENTERING DATA HISTOGRAM EQUALIZATION MODE')
        DO 900 LINE=1,NLINE
C       READ IN ONE FULL LINE OF IMAGE DATA.
        READ (20'LINE) (Z(K),K=1,320)
C       ***************************************************
C       TABLE LOOK-UP FOR REASSIGNMENT OF GRAY VALUES.
C       ***************************************************
        DO 910 K=K1,K2
        IF ((Z(K)/SCALE).GE.1024.) GO TO 2259
        Z(K)=CDF(IFIX(((Z(K))/SCALE)+0.5))
        GO TO 2258
 2259   Z(K)=CDF(1024)
C       Z(K) NOW EQUALS A VALUE BETWEEN 0. AND 1.
 2258   Z(K)=(Z(K)*1023.)
C       Z(K) NOW EQUALS A VALUE BETWEEN 0. AND 1023.
C       DATA IS NOW PROPERLY SCALED FOR DIRECT CT/T DISPLAY.
 910    CONTINUE
C       WRITE TRANSFORMED VALUES INTO A NEW IMAGE FILE.
        WRITE (21'LINE) (Z(K),K=1,320)
 900    CONTINUE
        WRITE (21'LINEP1) (IDESCR(K),K=1,160)
        STOP 'HISTOGRAM EQUALIZATION OF F.S.I. IMAGE DATA FILE'
        END
```

B-8. SIMULATED DATA GENERATION

DATGN3.FOR
SQUARE.FOR
POINT.FOR

THIS ROUTINE GENERATES SIMULATED DATA FOR 3 POINT SCATTERERS AT
LOCATIONS (80,240), (160,160) AND (240,80).

6-OCT-78
DATGN3.FOR   2 2-JAN-78

```
        DIMENSION X(8),Y(8)
        R=1
        NT=8
        PI2=6.2831853072
        CALL ASSIGN (15,'SIM3PT.DAT',0,'NEW','CC')
        DO 310 M=1,NT
        X(M)=R*COS((PI2*(M-1))/NT)
        Y(M)=R*SIN((PI2*(M-1))/NT)
        X(M)=(X(M)*(160./R))+160.
        Y(M)=(Y(M)*(160./R))+160.
        X(M)=INT(X(M)+0.5)
310     Y(M)=INT(Y(M)+0.5)
        DO 200 I=1,NT
        DO 210 J=I,NT
        XT=X(I)
        YT=Y(I)
        XR=X(J)
        YR=Y(J)
        IIY=320
        DO 203 IIX=80,240,80
        IIY=IIY-80
        DST=SQRT((XT-IIX)**2.+(YT-IIY)**2.)+
     1SQRT((XR-IIX)**2.+(YR-IIY)**2.)
        WRITE (15,111) DST
111     FORMAT (1X,F6.2)
D       WRITE (6,112)I,J,IIX,IIY,DST
112     FORMAT (1X,I3,3X,I3,5X,I3,3X,I3,5X,F6.2)
203     CONTINUE
210     CONTINUE
200     CONTINUE
        STOP '---3 PT. PER SIGNAL DATA GENERATION FOR PSI SIMULATION-----'
        END
```

THIS PROGRAM GENERATES DATA FOR RECONSTRUCTION OF A SIMULATED SQUARE
ARRAY OF SCATTERERS BEING SCANNED BY AN 8 TRANSDUCER ARRAY.

6-OCT-78
SQUARE.FOR   3 10-FEB-78


```
C       PSI ARTIFICIAL DATA GENERATION FOR SOLID SQUARE
C       8 TRANSDUCERS
C       IMAGE OBJECT - SQUARE
        DIMENSION X(8),Y(8),IZ(320),NAME(7)
        R=1.
        NT=8
        PI2=6.2831853072
        IREC=0
        WRITE (7,500)
500     FORMAT (' ENTER NAME OF DATA FILE IN FORM',
     1' DK1:SIMU##.DAT',/,' >')
        READ (5,510) NAME
510     FORMAT (7A2)
        NUMREC=NT*(NT+1)/2
        CALL ASSIGN (15,NAME,14)
        DEFINE FILE 15 (NUMREC,640,U,IVAR1)
        WRITE (7,520)
520     FORMAT (' ENTER COORDINATES OF "Y" BOUNDS AND "X" BOUNDS',
     1' AS <IY1,IY2,IX1,IX2>.')
        READ (5,530) IY1,IY2,IX1,IX2
530     FORMAT (4(I3,1X))
      . WRITE (6,540) IY1,IY2,IX1,IX2
540     FORMAT (' IY1=',I3,3X,'IY2=',I3,6X,'IX1=',I3,3X,'IX2=',I3)
        DO 300 M=1,NT
        X(M)=R*COS((PI2*(M-1))/NT)
        Y(M)=R*SIN((PI2*(M-1))/NT)
        X(M)=(X(M)*(160./R))+160.
        Y(M)=(Y(M)*(160./R))+160.
300     CONTINUE
        DO 200 I=1,NT
        DO 210 J=1,NT
        IREC=IREC+1
        XT=X(I)
        YT=Y(I)
        XR=X(J)
        YR=Y(J)
        DO 100 K=1,320
        IZ(K)=0
100     CONTINUE
C       CAN ENTER SCATTER COORDINATES EITHER BY DO LOOP OR FROM A FILE.
        DO 310 IY=IY1,IY2
        DO 320 IX=IX1,IX2
        DST=SQRT((XT-IX)**2.+(YT-IY)**2.)+SQRT((XR-IX)**2.+(YR-IY)**2.)
        IDIST=INT((DST/2.)+0.5)
        IZ(IDIST)=64
320     CONTINUE
310     CONTINUE
        WRITE (15'IREC) (IZ(IJK),IJK=1,320)
210     CONTINUE
200     CONTINUE
        STOP 'PSI DATA GENERATION FOR SQUARE ARRAY OF SCATTERERS.'
        END
```

PROGRAM TO GENERATE DATA AN IDEAL SINGLE POINT IMAGE (64X64) FOR USE
WITH RECONSTRUCTED IMAGE IN PERFORMING POINT-SPREAD
FUNCTION ANALYSIS AND DETERMINATION OF A PSI DECONVOLUTION FUNCTION.

```
   6-OCT-78
  POINT .FOR     1 17-MAY-78


C       PROGRAM TO CREATE A 320X320 UNFORMATTED IDEAL PT. IMAGE.
        DIMENSION Z(320),IDESCR(10)
        DATA Z/320*0./
        DATA IDESCR/2HSI,2HNG,2HLE,2H P,2HOI,2HNT,2H I,2HMA,2HGE,2H. /
        CALL ASSIGN (10,'DK1:SPOINT.DAT',14)
        DEFINE FILE 10 (65,640,U,IVAR1)
        DO 500 I=1,64
        WRITE (10'I) (Z(J),J=1,320)
  500   CONTINUE
        Z(160)=1000.
        WRITE (10'32) (Z(J),J=1,160)
        WRITE (10'65) (IDESCR(I),I=1,10)
        STOP 'GENERATION OF A SINGLE POINT IMAGE'
        END
```

APPENDIX C. TRANSDUCER CHARACTERIZATION DATA

C-1. PANAMETRICS NON-FOCUSED TRANSDUCERS

The Panametrics transducers used were originally specified as 5 MHz center frequency, half inch element diameter, and as broadband as possible. The following material is the resultant characterization data for the pair of transducers purchased. Some portions of this data were supplied by Panametrics, Inc., with the remaining portions obtained at GE. The transducer element material is lead metaniobate.

PANAMETRICS 221 CRESCENT STREET, WALTHAM, MASSACHUSETTS 02154 / 617 899-2719 TELEX: 923406

IMMERSION TRANSDUCER ANALYSIS FORM

Part No. _V-09_ . Serial No. _15284_ . Frequency _5.0_ MHz.

Size: _0.5_ " diameter; _—_ " by _—_ ". Cable: RG- _58/_ , length _8_ ft.

Water path _1.0_ ". Focussed at _—_ ". Design focal length _—_ ".

Echo from front surface of _____ " thick fused silica.
_____ " diameter steel ball.

───────────────────────────────TEST INSTRUMENTATION───────────────────────────────

Panametrics	5052PR	Pulser Receiver
Panametrics	5052G	Stepless Gate
Tektronix	7704A	Oscilloscope System
with	7A26	Dual Trace Amplifier
	7B53A	Dual Time Base
	7L12	Spectrum Analyzer

Center frequency is determined by
multiplying the horizontal scan width
(4) by the number of divisions to the
spectrum peak.

Waveform

Pulser Receiver Settings:

  Energy Setting _1_ .

  Receiver Attenuation _____ dB.

  Receiver Damping _50_ ohms.

Oscilloscope Settings:

  1-Vertical Sensitivity/div.

  2-Horizontal Sweep Rate/div.

  3-Scale Format.

Spectrum Analysis

Oscilloscope Settings:

  4-Horizontal Scan Width/div.

  5-Resolution.

  6-Input Attenuation.

0.707 max

Technician _____

Date _____

Figure C-1. Data supplied by Panametrics, Inc. for transducer #15289

PANAMETRICS 221 CRESCENT STREET, WALTHAM, MASSACHUSETTS 02154 / 617 899-2719 TELEX: 923406

IMMERSION TRANSDUCER ANALYSIS FORM

Part No. _1309_. Serial No. _15291_. Frequency _5.0_ MHz.

Size: _0.5_ " diameter; _—_ " by _—_ ". Cable: RG- _59/_, length _1_ ft.

Water path _1.0_ ". Focussed at _—_ ". Design focal length _—_ ".

Echo from front surface of _1.0_ " thick fused silica.
_____" diameter steel ball.

_____TEST INSTRUMENTATION_____

Panametrics	5052PR	Pulser Receiver	
Panametrics	5052G	Stepless Gate	
Tektronix	7704A	Oscilloscope System	
with	7A26	Dual Trace Amplifier	
	7B53A	Dual Time Base	
	7L12	Spectrum Analyzer	

Center frequency is determined by
multiplying the horizontal scan width
(4) by the number of divisions to the
spectrum peak.

Waveform

Pulser Receiver Settings:

Energy Setting _1_.

Receiver Attenuation _____ dB.

Receiver Damping _120_ ohms.

Oscilloscope Settings:

1-Vertical Sensitivity/div.

2-Horizontal Sweep Rate/div.

3-Scale Format.

Spectrum Analysis

Oscilloscope Settings:

4-Horizontal Scan Width/div.

5-Resolution.

6-Input Attenuation.
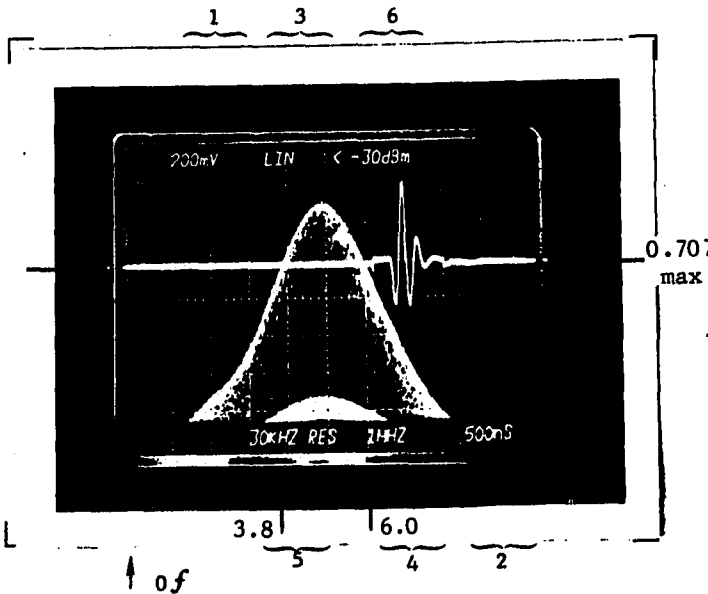
Technician _____

Date _____

Figure C-2. Data supplied by Panametrics, Inc. for transducer #15291

TABLE C-1. ELECTRICAL IMPEDANCE DATA FOR PANAMETRICS TRANSDUCER #15289 TAKEN 7/28/77

	FREQ. (f) (MHz)	H.P. IMPED. METER MAG.	H.P. IMPED. METER PHASE	SERIES RESIST. (Rs) (Ω)	SERIES REACT. ($-X_S$) (Cs)	EQUIV. SERIES CAPAC. (C_S) (pF)	PARALLEL CONDUCT. (G) ($\times 10^{-3}$ ℧)	PARALLEL SUSCEPT. (B) ($\times 10^{-3}$ ℧)	PARALLEL RESIST. (R) (Ω)	PARALLEL CAPAC. (C) (pF)
	1	138.0	-86°	9.63	137.66	1156	0.51	7.23	1978.3	1150
AIR	2	71.0	-76.5	16.58	69.04	1153	3.29	13.70	304.1	1090
LOADING	3	49.0	-68	18.36	45.43	1168	7.65	18.92	130.8	1004
	4	40.5	-60	20.25	35.07	1134	12.35	21.38	81.9	851
	5	34.2	-60	17.10	29.62	1075	14.62	25.32	68.4	806
	6	30.2	-50.2	19.33	23.20	1143	21.20	25.44	47.2	675
	7	29.5	-48.3	19.62	22.03	1032	22.55	25.31	44.4	575
	8	26.8	-48	17.93	19.91	999	24.97	27.73	40.05	552
	9	24.3	-46	16.88	17.48	1012	28.59	29.60	34.98	523
	10	22.4	-42.5	16.51	15.13	1052	32.91	30.16	30.38	480
	1	139.0	-85	12.11	138.47	1149	0.63	7.17	1595.00	1141
WATER	2	71.0	-76.5	16.57	69.04	1153	3.29	13.70	304.10	1090
LOADING	3	49.5	-68.5	18.14	46.05	1152	7.40	18.80	135.10	997
	4	39.5	-61	19.15	34.55	1152	12.27	22.14	81.50	881
	5	34.5	-56	19.29	28.60	1112	16.21	24.03	61.70	765
	6	31.0	-51	19.51	24.09	1101	20.30	25.07	49.26	664
	7	29.0	-49	19.03	21.89	1039	22.62	26.02	44.20	592
	8	26.5	-48	17.73	19.69	1010	25.25	28.04	39.60	558
	9	24.2	-45.8	16.87	17.35	1019	28.81	29.62	34.71	524
	10	22.4	-42.5	16.51	15.13	1052	32.91	30.16	30.38	480

TABLE C-2. ELECTRICAL IMPEDANCE DATA FOR PANAMETRICS TRANSDUCER #15291 TAKEN 7/28/77

	FREQ. (f) (MHz)	H.P. IMPED. METER MAG.	H.P. IMPED. METER PHASE	SERIES RESIST. (Rs) (Ω)	SERIES REACT. ($-X_s$) (C_s)	EQUIV. SERIES CAPAC. (C_s) (pF)	PARALLEL CONDUCT. (G) ($\times 10^{-3}$ ℧)	PARALLEL SUSCEPT. (B) ($\times 10^{-3}$ ℧)	PARALLEL RESIST. (R) (Ω)	PARALLEL CAPAC. (C) (pF)
	1	135.0	-90°	0.00	135.00	1179	0.00	7.41	∞	1179
AIR	2	63.5	-87.5	2.77	63.44	1254	0.69	15.73	1456	1252
LOADING	3	44.0	-84.5	4.22	43.8	1211	2.18	22.62	459.1	1200
	4	33.0	-80.5	5.45	32.55	1222	5.00	29.89	199.9	1189
	5	26.5	-78.5	5.28	25.97	1226	7.52	36.98	132.9	1177
	6	22.5	-76.0	5.44	21.83	1215	10.75	43.12	93.01	1144
	7	20.0	-74.5	5.35	19.27	1180	13.36	48.18	74.84	1095
	8	17.0	-76.5	4.02	16.72	1189	13.57	56.53	73.68	1124
	9	14.5	-76.5	3.39	14.10	1254	16.10	67.06	62.11	1186
	10	12.2	-75.8	2.99	11.83	1345	20.11	79.46	49.73	1265
	1	136.0	-90.0	0.00	136.00	1170	0.00	7.35	∞	1170
WATER	2	67.5	-89.5	0.59	67.50	1179	0.13	14.8	7735	1179
LOADING	3	43.8	-85.0	3.82	43.63	1216	1.99	22.74	502.5	1207
	4	33.5	-79.0	6.39	32.88	1210	5.70	29.30	242.9	1166
	5	27.5	-83.5	3.11	27.32	1165	4.12	36.13	242.9	1150
	6	21.5	-76.5	5.02	20.91	1269	10.86	45.20	92.10	1200
	7	20.0	-74.3	5.41	19.25	1181	13.53	48.13	73.91	1094
	8	17.7	-77.0	3.98	17.25	1154	12.71	55.05	78.68	1095
	9	14.8	-77.5	3.20	14.45	1223	14.62	65.97	68.38	1167
	10	12.6	-76.3	2.98	12.24	1300	18.80	77.11	53.20	1227
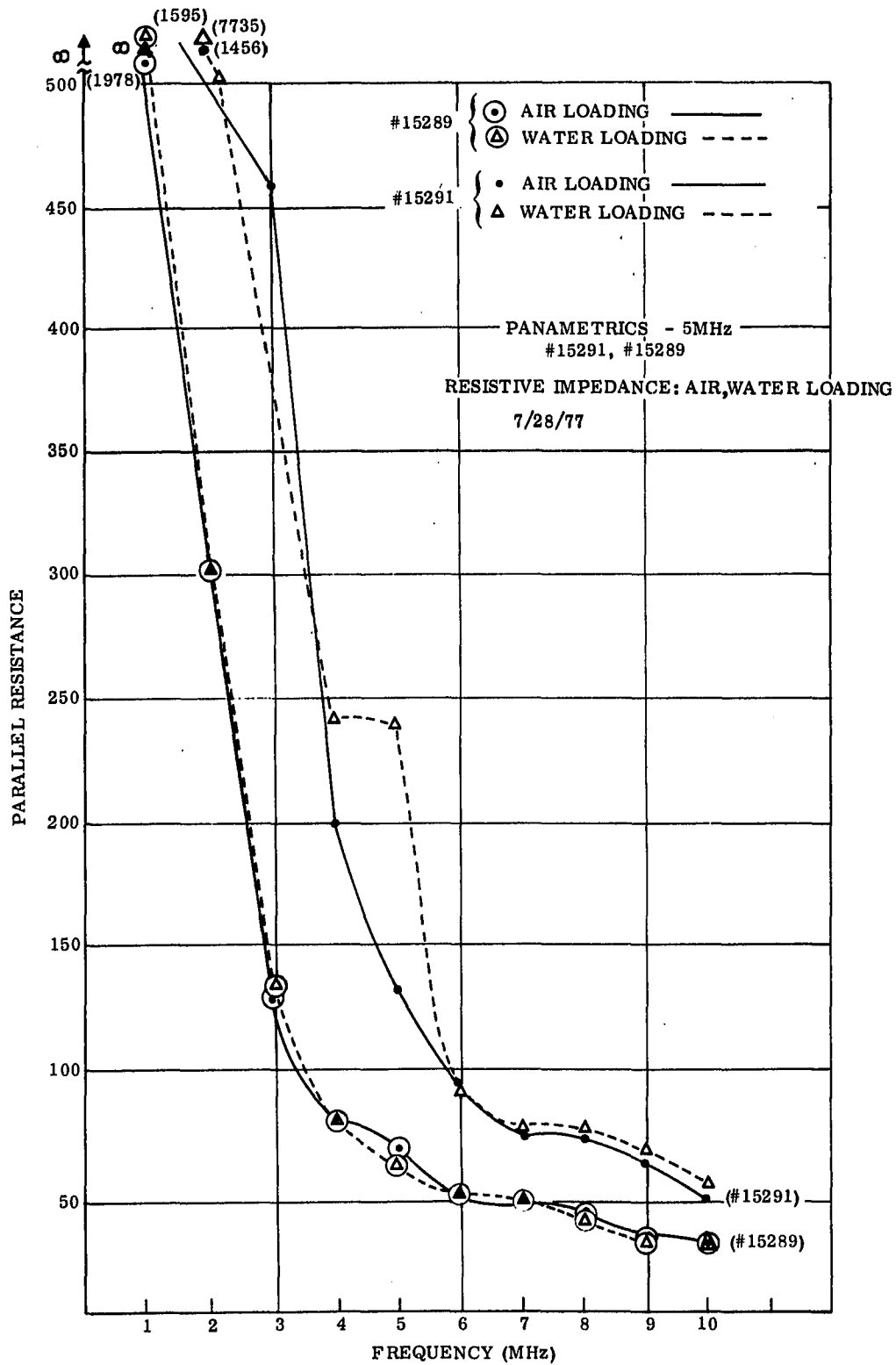
Figure C-3. Equivalent electrical parallel input resistance measured on
Panametrics transducers #15289 and #15291 using H.P. vector
impedance meter, for cases of air and water mechanical loading
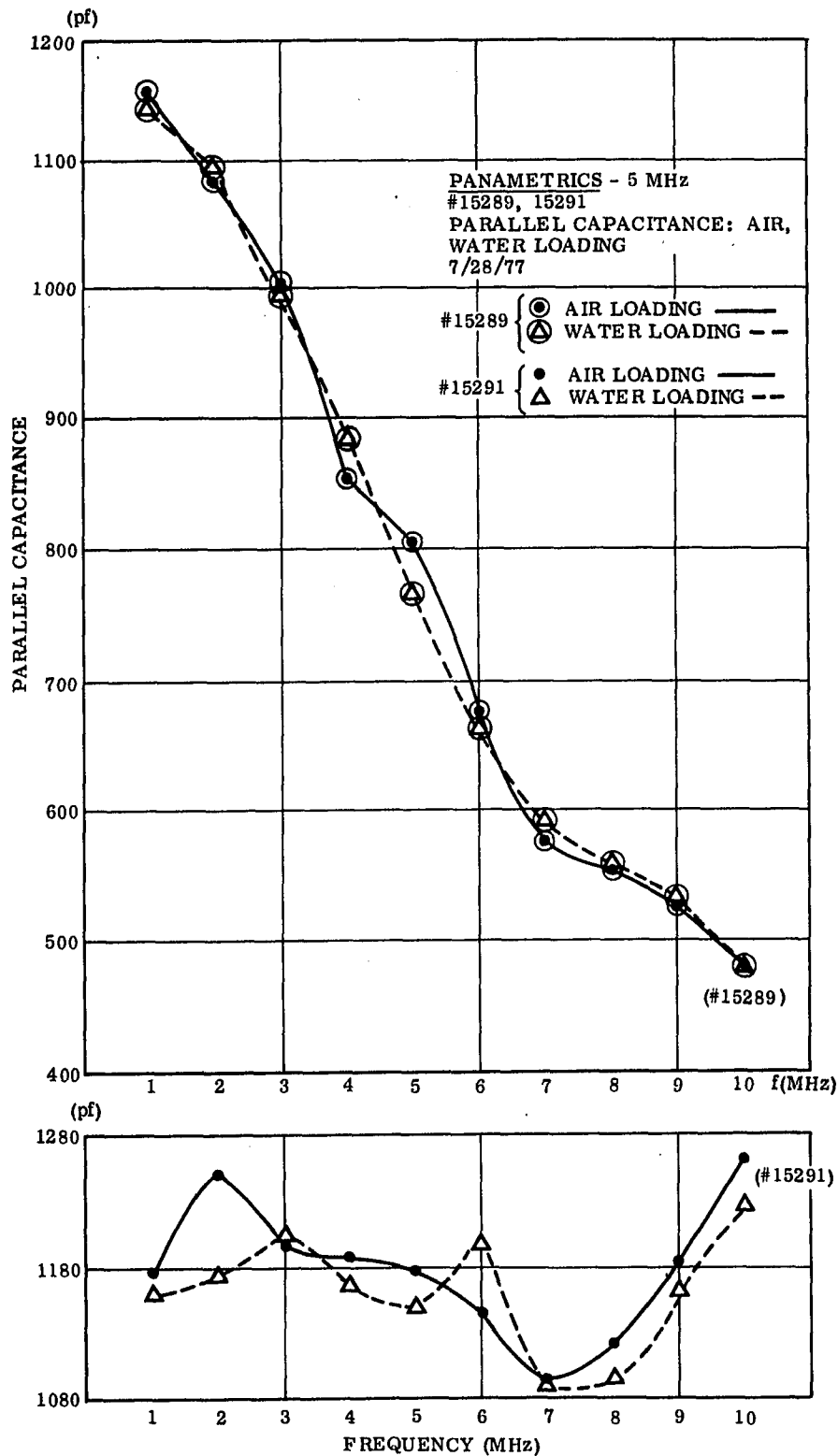
Figure C-4. Equivalent electrical parallel input capacitance measured on Panametrics transducers #15289 and #15291 using H.P. vector impedance meter, for cases of air and water mechanical loading

C-2. KB-AEROTECH FAN BEAM TRANSDUCERS

The fan beam transducers, purchased from KB-Aerotech were originally specified as:

- Special paintbrush transducer, 5.0 MHz

- 1/2" × 1/2", cylindrically convex ceramic

- Highly damped (maximum possible - 3 dB bandwidth on best effort basis)

- Delrin case per KB-Aerotech dimensions

- UHF connector centered in back of case

- Field (sound beam) characteristics to be attempted on a best effort basis

- 30 beam divergence at 3 dB level.

The remaining material in this section is comprised of characterization data for the two fan beam transducers received. This data was supplied by both KB-Aerotech and the U.S. Bureau of Radiological Health. The transducer element material is lead metaniobate.
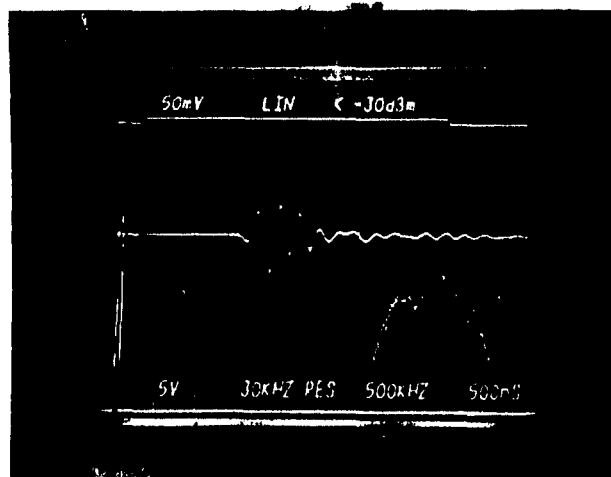
(a)
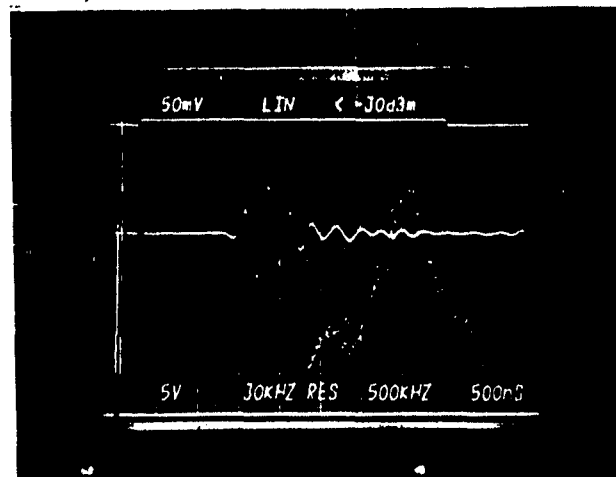
(b)

Figure C-5. Fan beam pulse and bandwidth data for transducers (a) 47264H and
(b) 47265H as supplied by KB-Aerotech

TRANSDUCER MODEL # : *SPECIAL* ½ x ½ *PRINT.* ___5___ MHZ _____ MM DIAMETER _____ FOCUS   SCALE: | ℂM |

SERIAL # : ___47264 H___

ATTENUATION SETTING: ___0___ dB

PLOTTED BY: ___*Plm*___

DATE: ___*3-12-78*___

TARGET: ___*6 m m steel ball   4" water path*___

INSTRUMENTATION: KB-AEROTECH UTA-3

MFE x-y RECORDER

Figure C-6. Fan beam profile (#47264H) at 4" from 6 mm steel ball

TRANSDUCER MODEL # : _SPECIAL PAINTBRUSH_ ___5_ MHZ _½ x ½_ MM DIAMETER _____ FOCUS   SCALE: | ICM |
SERIAL # : _47265 H_
ATTENUATION SETTING: __O__ dB   TARGET: _6 m m steel ball @ 4" water_
PLOTTED BY: ___PKM___   INSTRUMENTATION: KB-AEROTECH UTA-3 ---- _put_
DATE: ____3-12-78____   MFE x-y RECORDER
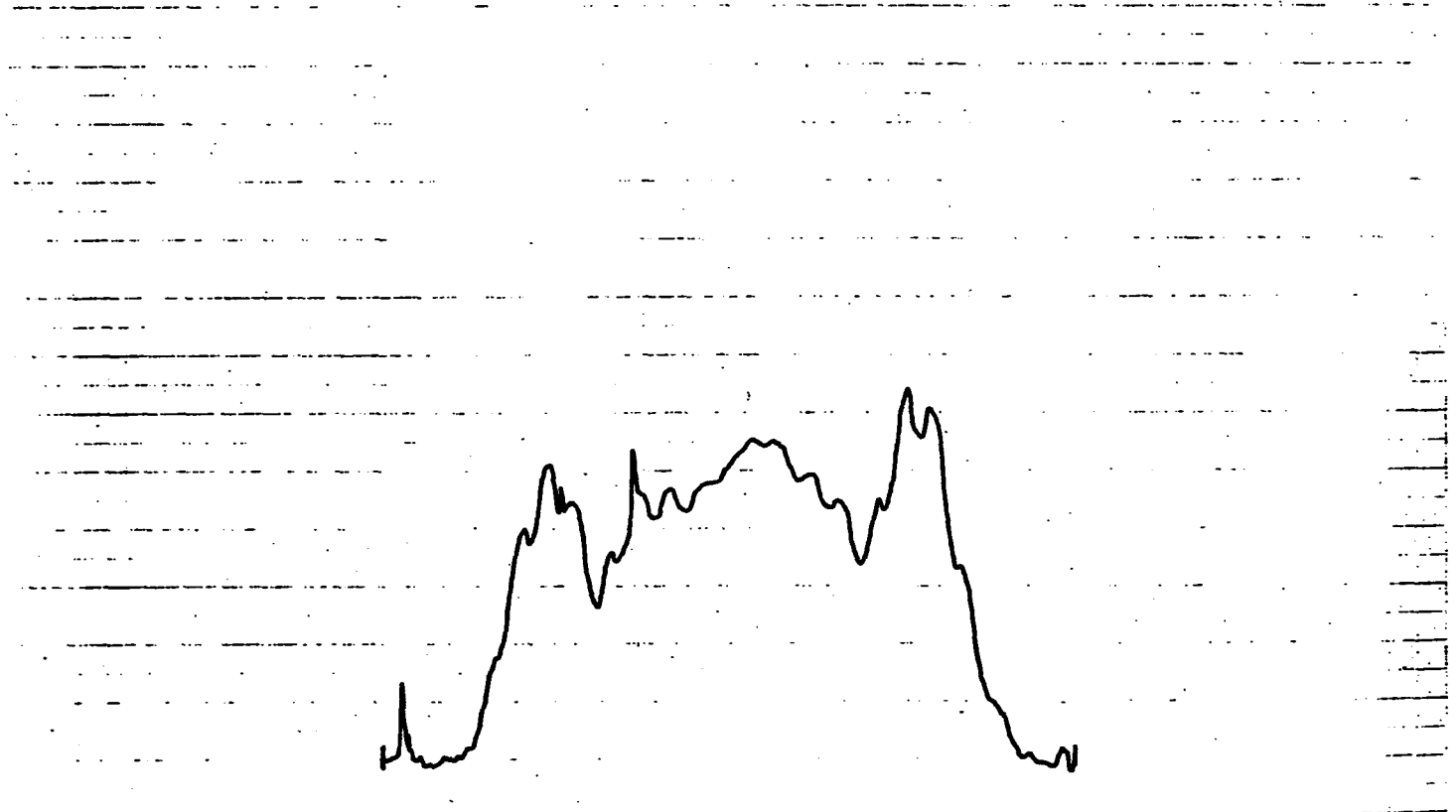
Figure C-7. Fan beam profile (#47265H) at 4" from 6 mm steel ball

	BEAM PROFILE
	AM219C77

TRANSDUCER MODEL # : _____   _5.0_ MHZ   _____ MM DIAMETER   _____ FOCUS   SCALE: | ᴵᶜᴹ |
SERIAL # : _47264 H_____
ATTENUATION SETTING: __O__ dB   TARGET: _6mm steel ball_ at _12"water path_
PLOTTED BY: _____PRm_____   INSTRUMENTATION: KB-AEROTECH UTA-3
DATE: ___4-12-78_____   MFE x-y RECORDER

8.3 mN

5.0 mN

4.1 mN
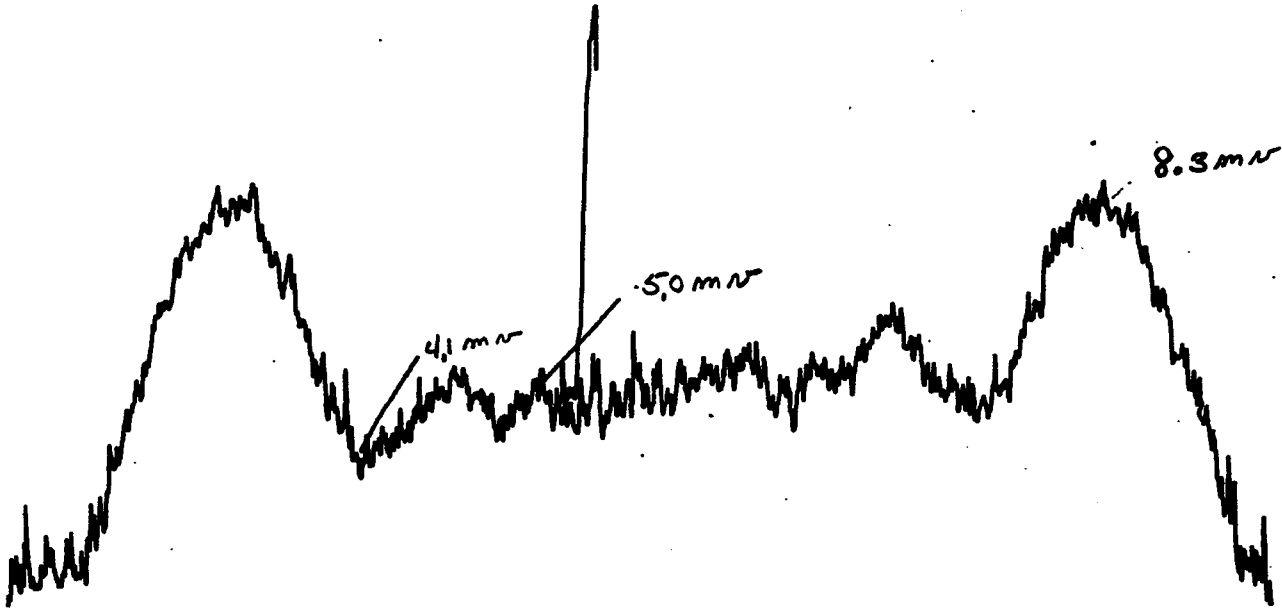
Figure C-8. Fan beam profile (#47264H) at 12" from 6 mm steel ball

Figure C-9. Fan beam profile (#47265H) at 12" from 6 mm steel ball

BEAM PROFILE

TRANSDUCER MODEL # ___SPECIAL___   ___5.0___ MHz   ___ A.E.D.   ___-6 db FOCAL ZONE

SERIAL # ___47264___   BEAM WIDTH SCALE [☐ 1CM   ☐ ⊢ 1CM ⊣]

ATTENUATION SETTING ___O db___ (35 db gain) dB   TARGET ___6 mm steel ball @ #6" water path___

PLOTTED BY ___PAM___   INSTRUMENTATION: KB-AEROTECH UTA, MFE x-y RECORDER

DATE ___7-28-78___

Figure C-10. Fan beam profile (#47264, with thin epoxy face) at 6" from 6 mm steel ball

KB-AEROTECH
TRANSDUCER TECHNOLOGY CENTER
Division of Krautkramer-Branson, Incorporated

BEAM PROFILE

TRANSDUCER MODEL # _____SPECIAL_____   _5.0_ MHz   _____A.E.D.   _____-6 db FOCAL ZONE

SERIAL # _____47265_____   BEAM WIDTH SCALE ☐ 1CM ☐ 1CM

ATTENUATION SETTING _O db (35db gain)_ dB   TARGET _6mm steel ball @ 6" water path_

PLOTTED BY _____PHm_____   INSTRUMENTATION: KB-AEROTECH UTA, MFE x-y RECORDER

DATE _____7-25-78_____

Figure C-11. Fan beam profile (#47265, with thin epoxy face) at 6" from 6 mm steel ball

The remaining material in this section is an exact reproduction of data collected by the U.S. Bureau of Radiological Health in Rockville, MD, and was obtained with the appreciated efforts of Mr. Michael Haran, Research Physicist.

DEPARTMENT OF HEALTH, EDUCATION, AND WELFARE
PUBLIC HEALTH SERVICE
ROCKVILLE, MARYLAND 20852

June 16, 1978

Lawrence D. Nadel
Electronics Laboratory
General Electric Company
Syracuse, N.Y. 13221

Dear Larry:

Enclosed is the data on the two transducers you asked my to evaluate.
First let me explain how the data were taken and displayed.

The ultrasonovision system, briefly described in the enclosed reprint,
measures the particle displacement amplitude normal to the plane of the
pellicle. The orientation of the pellicle is normal to the ultrasonic
beam axis so that a cross-sectional view of the field is recorded. Since
the reprint was published, the ultrasonovision has been interfaced to a
computer for data collection and display.

To evaluate your transducers, measurements of the field were taken at
32 evenly spaced locations down the beam axis. The spacing between the
planes was 0.5 cm and each plane of data contains 32 X 32 picture elements
(pixels). The plane dimensions are 7 X 7 cm. As can be seen in figure 1,
a volume of data are collected on the displacement amplitude of the field.

To analyze the data, a specific line is selected from each frame (e.g. line
16). These lines are used to construct a new frame showing the behavior of
the field as a function of distance from the source (see figure 2). Contour
plots are then made of the data at selected levels of displacement amplitude.

A 90 degree view can be obtained by selecting vertical lines from each of
the data frames and plotting the contours of this plane (figure 3).

For your transducers, the distance of the first plane to the transducer
was 1.0 cm and the last (32nd) plane was 16.5 cm from the transducer. The
data are stored in frames G1X01 through G1X32 and G2X01 through G2X32 for
the transducers having serial numbers 47265H and 47264H, respectively.
Contours were plotted every 5 db with respect to peak within the entire
data volume. The voltage applied to the transducer was 24V peak to peak
at 5.00 MHz for 30 μs with a 2k repetition rate.

I have provided you with six plots of each transducer. The first two are
isometric and contour plots of the beam cross-section at a distance of
1.0 cm from the transducer face. The next three are contour plots of lines
15, 16 and 17 showing the spreading of the beam as it leaves the source.

The last is a contour plot of the vertical view of the field as it leaves the source. It was impossible to assure the transducer axis would be normal to the plane of the pellicle and this may be reflected in the plots.

The transducer used for the G2X data series (s/n 47264H) clearly had problems. Much of the left side is not radiating and this is reflected in a "half-fan" shaped beam. The reduced aperture also results in a more smoothly varying field simply because the far-field transition has been brought closer to the source. It would appear that the loss of the outer laminar layer is indicative of poor bonding in the transducer. Dead areas in transducers frequently mean separation between the crystal and the front laminae.

The other transducer (s/n 47265H) radiates much more uniformly by comparison. The contour plot of the plane at 1.0 cm shows the diffraction effects of the edges of the crystal though they are not equal. The contour plots of lines 15, 16 and 17 show the jumbled amplitudes of a near-field and some side lobe structure.

If you have any questions about the way the data were taken or how to interpret these plots, please call me.

Sincerely yours,

Michael E. Haran
Research Physicist
Acoustics Branch
Division of Electronic Products
Bureau of Radiological Health

frame G1XØ1
frame G1XØ2
frame G1XØ3

UP

ACOUSTIC
AXIS

RIGHT

LEFT

DOWN

AEROTECH

NOTE THE ORIENTATION
OF THE LABELING

0.5 cm
SPACING
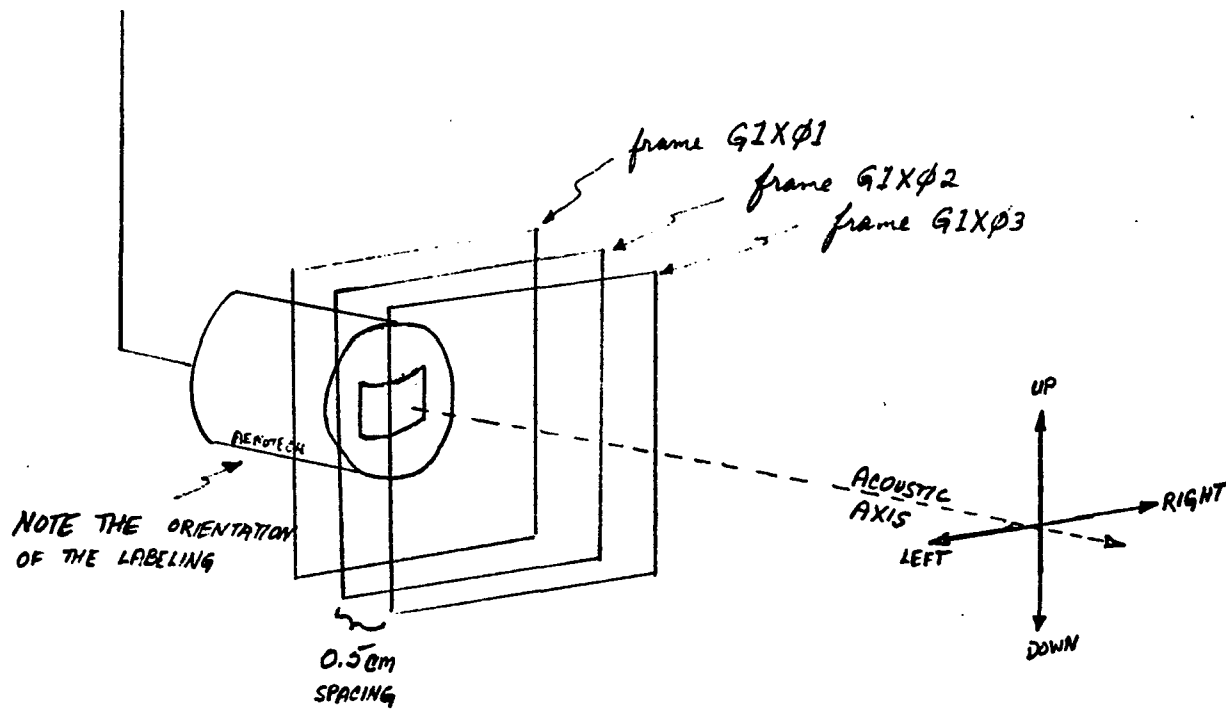
Figure 1

Figure C-12. Sample BRH ultrasonovision transverse imaging (i.e. frame) planes

"LINE 16" PLANE
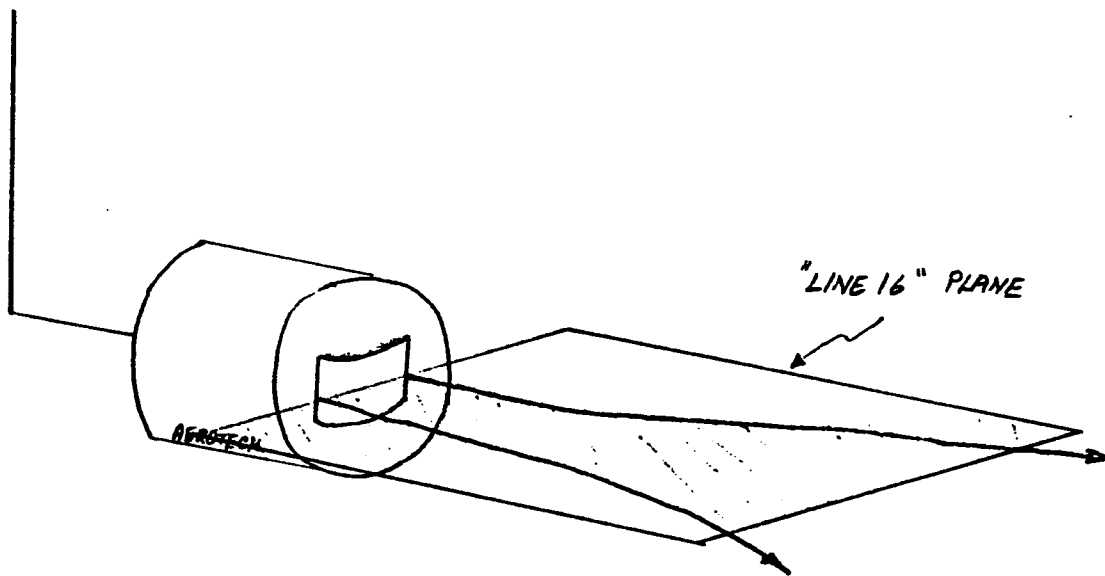
FIGURE 2

Figure C-13. Sample BRH ultrasonovision horizontal, longitudinal (i.e. line) imaging plane

"PIXEL 16" PLANE
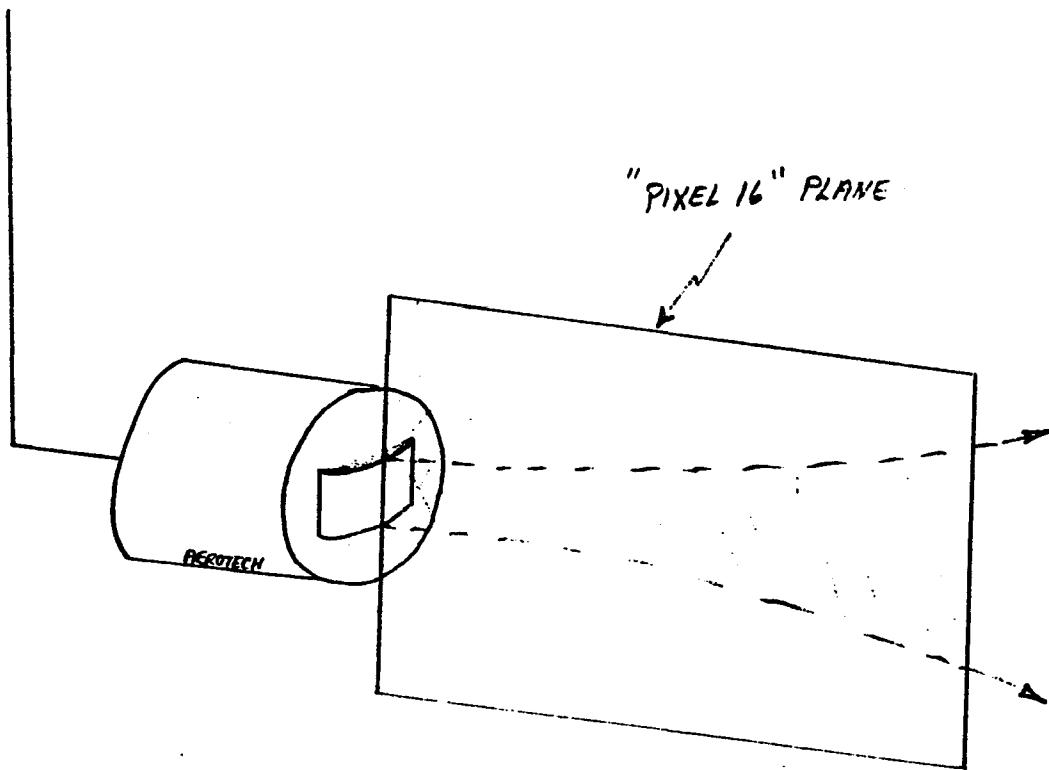
FIGURE 3

Figure C-14. Sample BRH ultrasonovision vertical, longitudinal (i.e. pixel) imaging plane
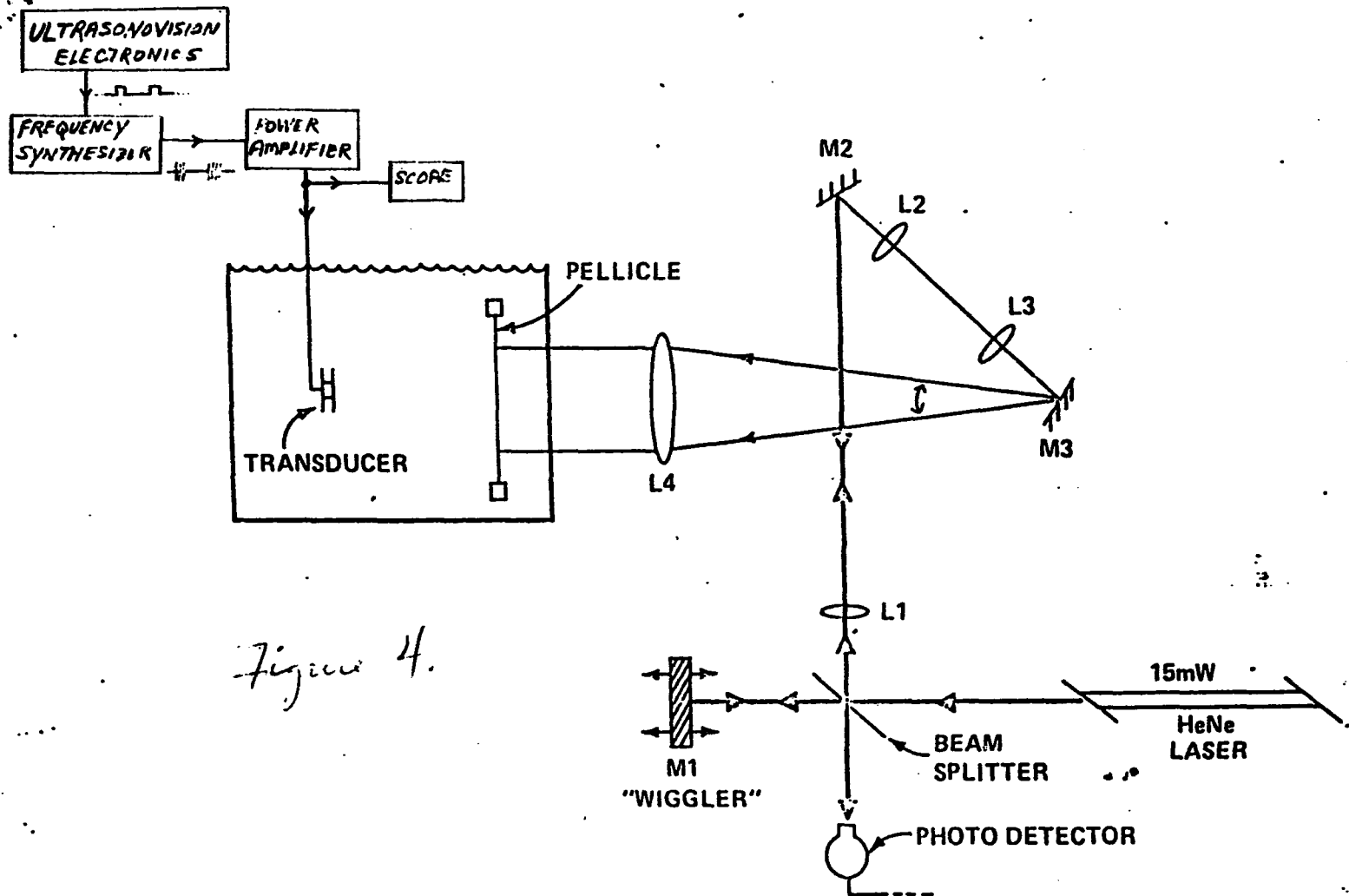
Figure C-15. Block diagram of BRH ultrasonovision beam profiling system

COMMENT SECTOR - ULTRASONOVISION DATA

FILE NAME;
    G2X01

NUMBER OF PIXELS PER LINE;
    32

NUMBER OF LINES PER FRAME;
    32

X-DIMENSION IN CM;
        7.0000

Y-DIMENSION IN CM;
        7.0000

DATA TAKEN WITH THE WIGGLER SYSTEM.

DATE OF TEST;
    6/15/78

MANUFACTURER;
    AEROTECH (GE OWNED)

MODEL OR TYPE;
    CYLINDRICAL SECTION; FAN BEAM FOR TOMOGRAPHY APPL.

SPECIFICATIONS;
    5MHZ/0.5X0.5 IN.   (S/N 47264H)

SOURCE USED;
    ULTR+FR.SYN+50W AMPL

DISTANCE FROM SOURCE IN CM;
        1.0000

PULSE DURATION IN MICROSECONDS;
        30.0000

VOLTAGE APPLIED;
        24.0000

REPETITION RATE IN KHZ;
        2.0000

PEAK DISPLACEMENT IN CM ;
        .0000E+00

    PERCENT OF PEAK INTENSITY;
        0

    SPATIAL AVERAGE INTENSITY IN WATTS/CM**2;
        .0000E+00

    BEAM AREA IN CM**2;
        .0000E+00
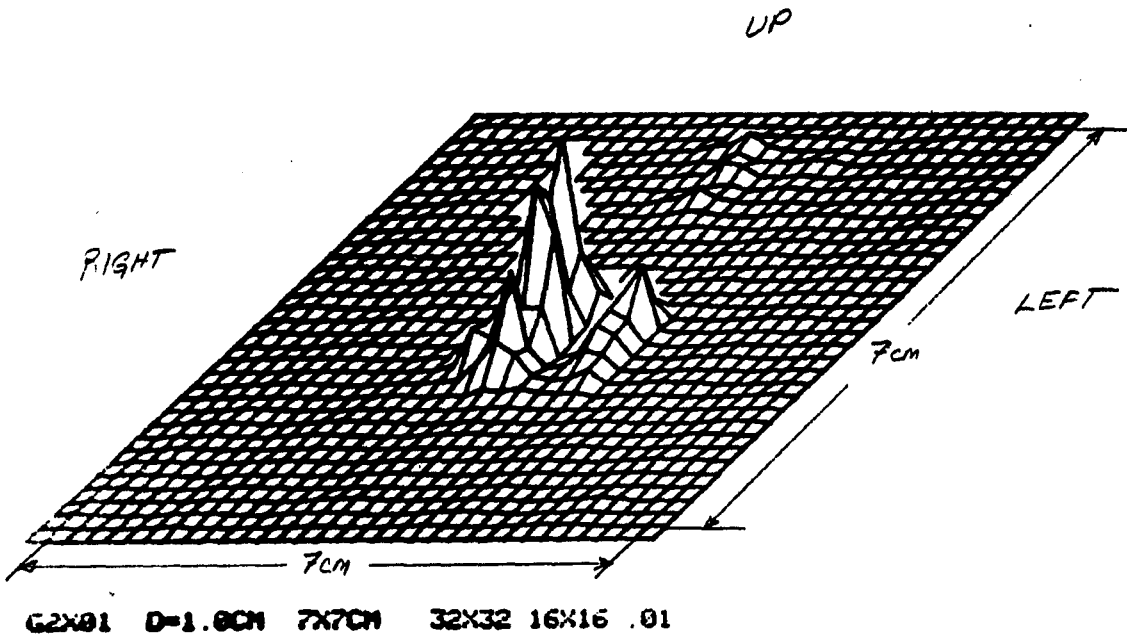
Figure C-16. Isometric plot of transverse acoustic field 1 cm from transducer (S/N 47264H). Note "half-fan" pattern as compared with Figure C-22.
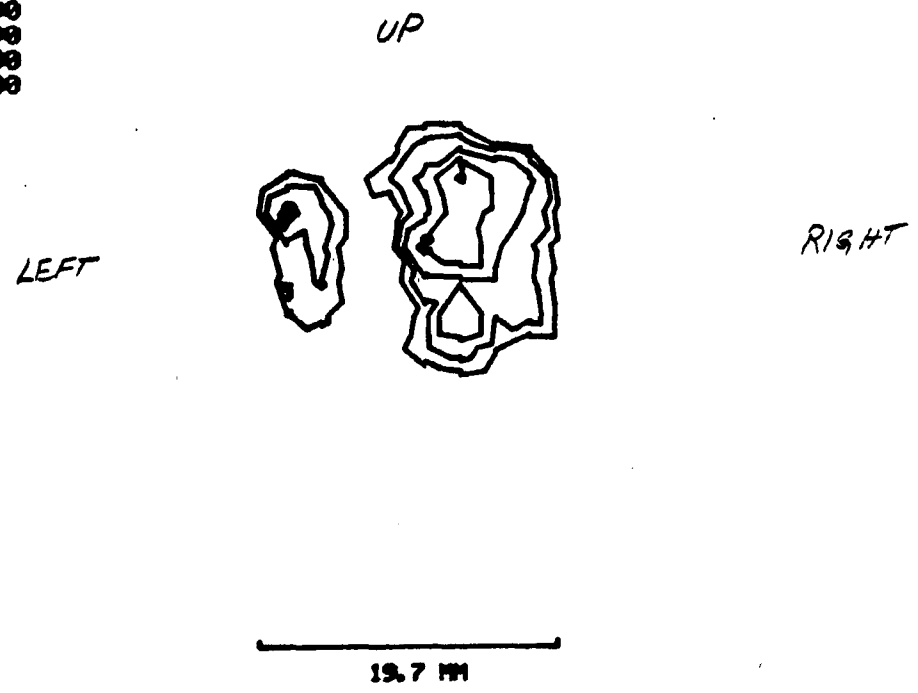
Figure C-17. Contour plot of transverse acoustic field 1 cm from transducer (S/N 47264H)
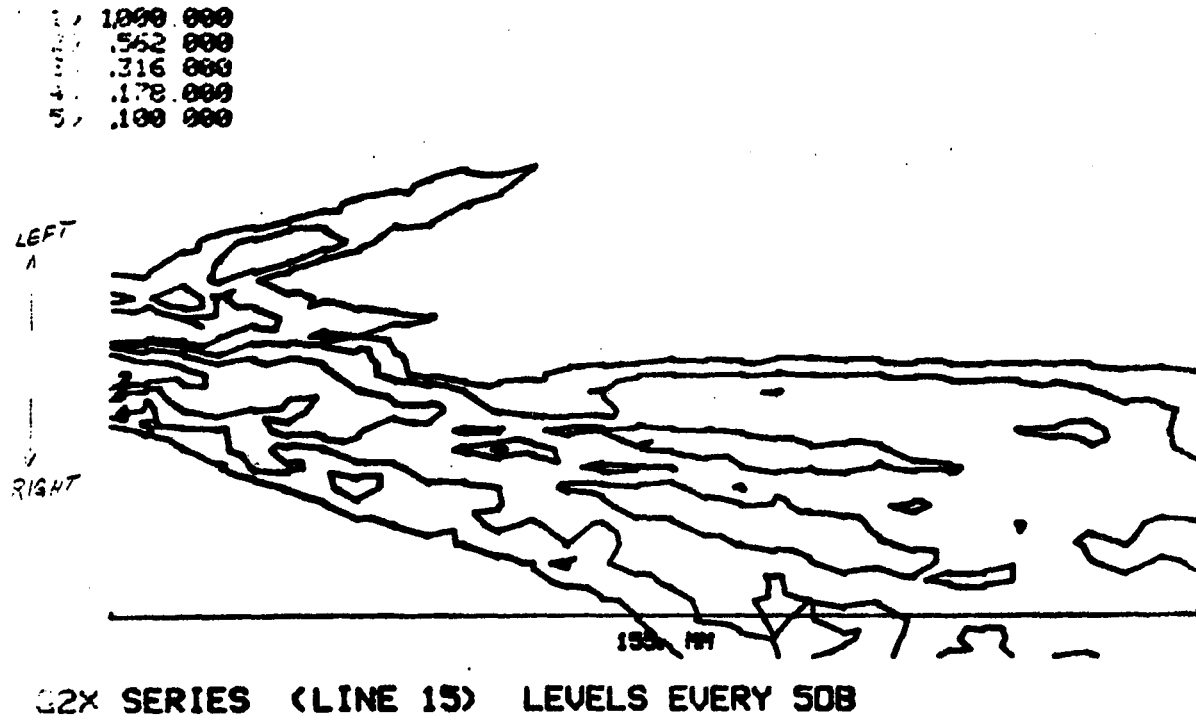
Figure C-18. Horizontal plane contour plot ("line 15") for S/N 47264H fan beam

1 : 1.000 000
2 : .562 000
3 : .316 000
4 : .178 000
5 : .100 000

LEFT

RIGHT
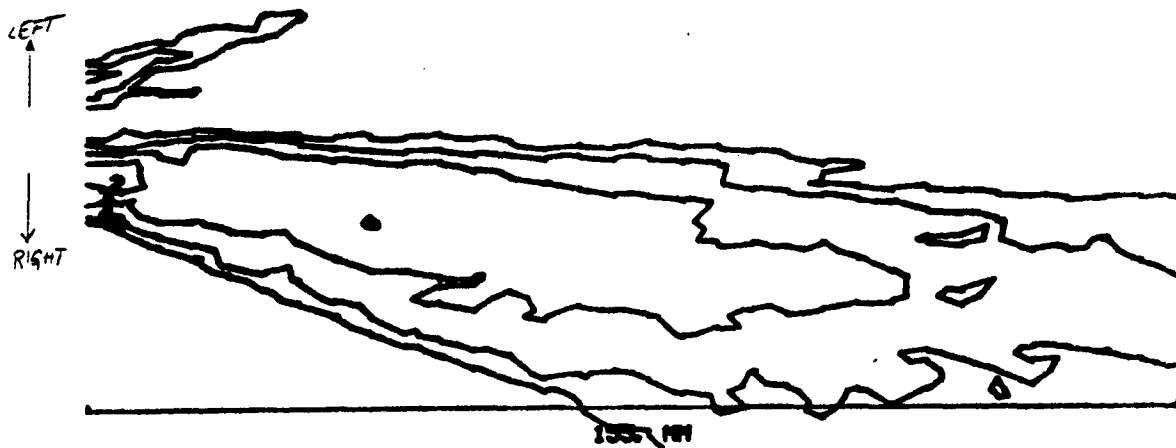
G2X SERIES (LINE 16)   LEVELS EVERY 5DB

SMALLER RADIATING SOURCE BRINGS
FAR FIELD CLOSER TO TRANSDUCER.

Figure C-19. Horizontal plane contour plot ("line 16") for S/N 47264H fan beam

1) 1,000.000
2) .562.000
3) .316.000
4) .178.000
5) .100.000

LEFT

RIGHT

195. MM
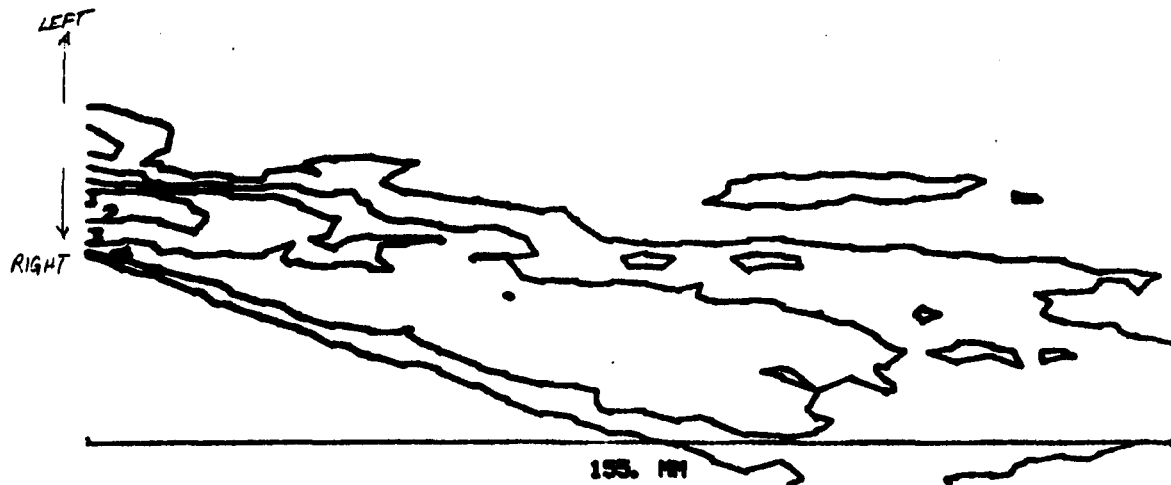
G2X SERIES (LINE 17)   LEVELS EVERY 5DB

Figure C-20. Horizontal plane contour plot ("line 17") for S/N 47264H fan beam

Figure C-21. Vertical plane contour plot ("pixel 16") for S/N 47264H fan beam

COMMENT SECTOR - ULTRASONOVISION DATA

FILE NAME:
    G1X01

NUMBER OF PIXELS PER LINE:
    32

NUMBER OF LINES PER FRAME:
    32

X-DIMENSION IN CM:
        7.0000

Y-DIMENSION IN CM:
        7.0000

DATA TAKEN WITH THE WIGGLER SYSTEM.

DATE OF TEST:
    5/14/78

MANUFACTURER:
    AEROTECH(G.E. OWNED)

MODEL OR TYPE:
    CYLINDRICAL SECTION; FAN BEAM FOR TOMOGRAPHY APPL.

SPECIFICATIONS:
    5MHZ/0.5X0.5 IN. (S/N 47265H)

SOURCE USED:
    ULTR+FR.SYN+50W AMPL

DISTANCE FROM SOURCE IN CM:
        1.0000

PULSE DURATION IN MICROSECONDS:
        30.0000

VOLTAGE APPLIED:
        24.0000

REPETITION RATE IN KHZ:
        2.0000

PEAK DISPLACEMENT IN CM :
        .0000E+00

    PERCENT OF PEAK INTENSITY:
        0

    SPATIAL AVERAGE INTENSITY IN WATTS/CM**2:
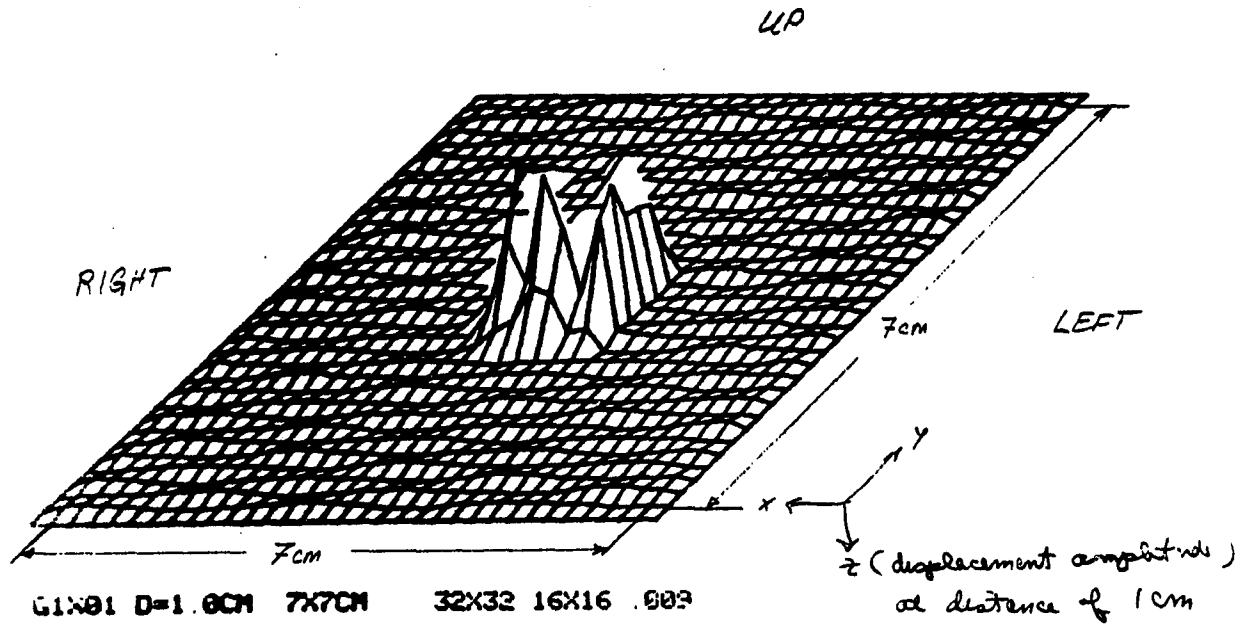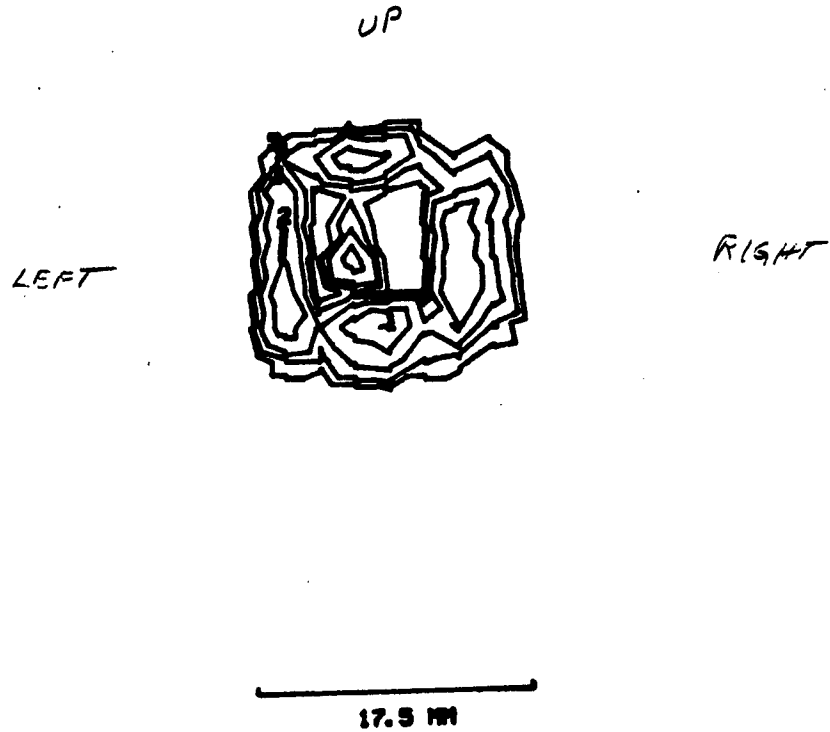   .0000E+00

    BEAM AREA IN CM**2:
        .0000E+00

UP

RIGHT

LEFT

7cm

Y

X

z (displacement amplitude) at distance of 1 cm

7cm

G1X01 D=1.0CM 7X7CM 32X32 16X16 .003

Figure C-22. Isometric plot of tranverse acoustic field 1 cm from transducer (S/N 47265H)

UP

LEFT

RIGHT

```
1: 1.000 000
2: .562 000
3: .316 000
4: .178 000
5: .100 000
```

17.5 MM

G1X01 D=1.0CM

CONTOUR OF DISPLACEMENT AMPLITUDE
... THAT COMPONENT NORMAL TO PELLICLE.

Figure C-23. Contour plot of transverse acoustic field 1 cm from transducer
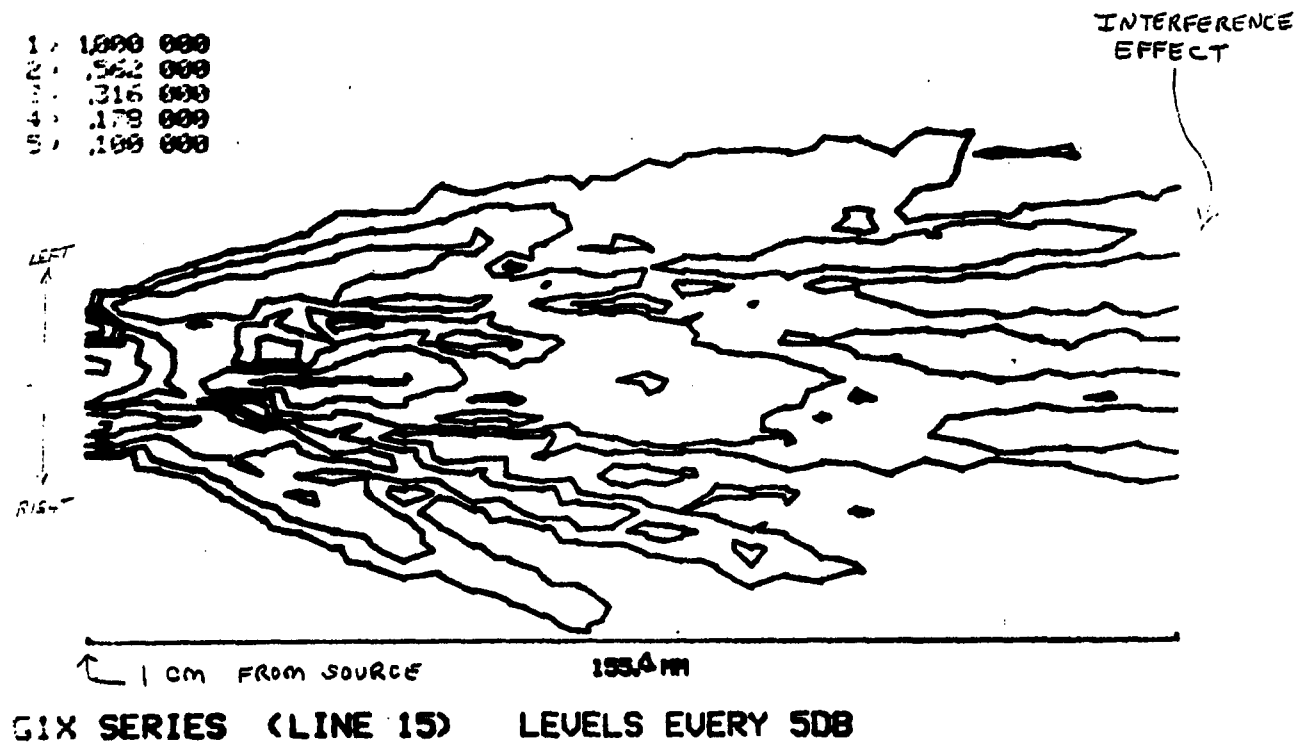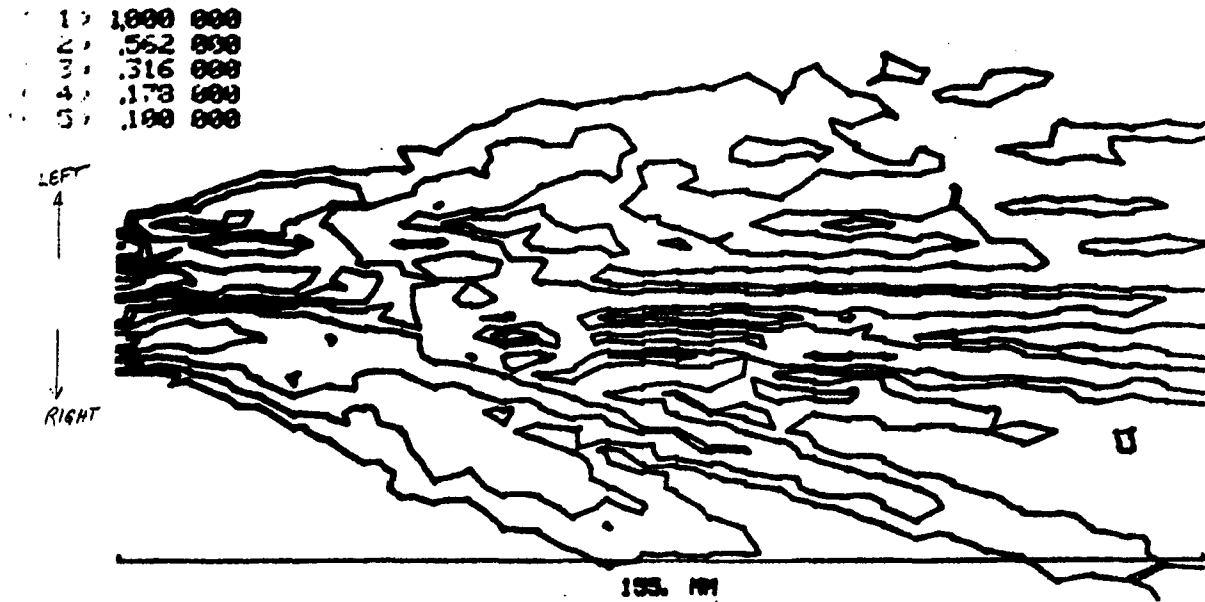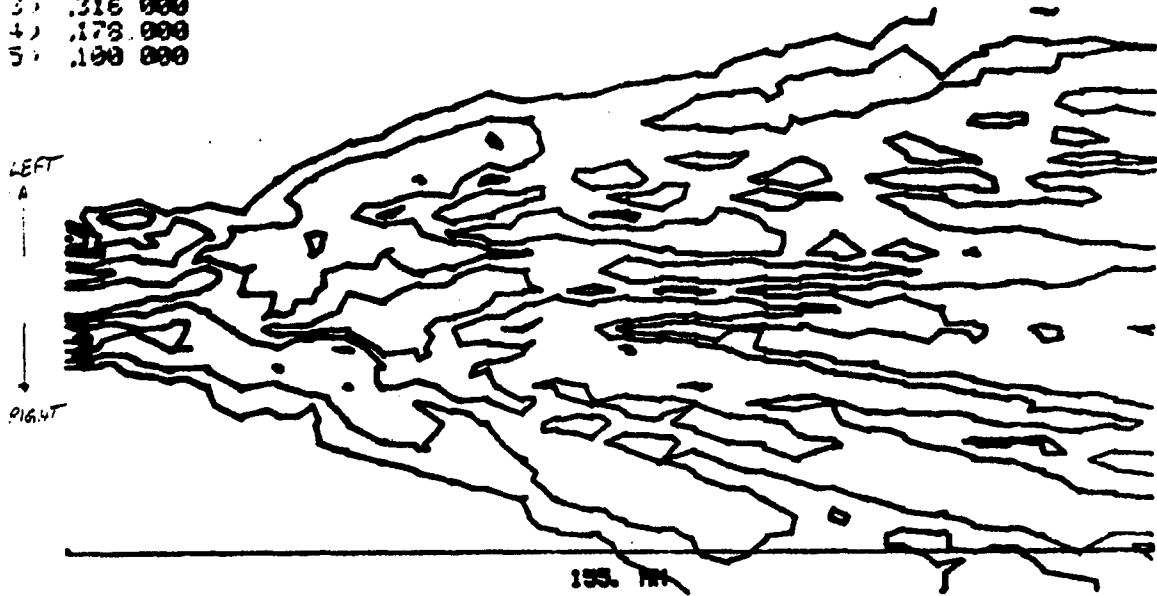(S/N 47265H)

Figure C-24. Horizontal plane contour plot ("line 15") for S/N 47265H fan beam

Figure C-25. Horizontal plane contour plot ("line 16") for S/N 47265H fan beam

GIX SERIES (LINE 17) LEVELS EVERY 5DB

Figure C-26. Horizontal plane contour plot ("line 17") for S/N 47265H fan beam
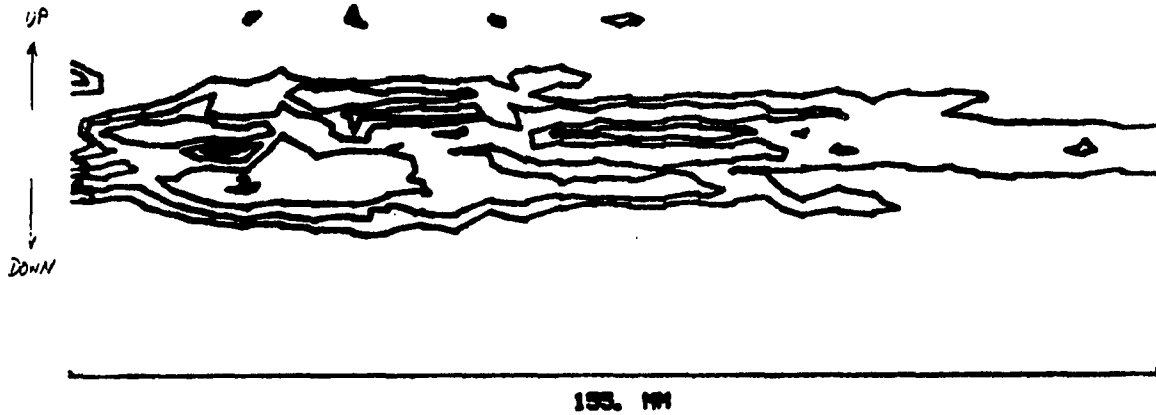
1) 1.000.000
2) .562.000
3) .316.000
4) .178.000
5) .100.000

UP

DOWN

155. MM

GIX SERIES (PIXEL 16)   LEVELS EVERY 5DB

Figure C-27. Vertical plane contour plot ("pixel 16") for S/N 47265H fan beam

Figure C-28 shows a beam profile of a plane, circular source (2.25 MHz/ 13 mm diameter). The sound travels from left to right with the transducer face being 4 mm from the beginning of the pattern. Part (b) of the figure has a 1:1 scale while part (a) has an expanded vertical scale. This figure is included strictly for a basis of comparison with a conventional transducer.

TSC Series (Line 18) 5DB Contours

(1) 1000
(2) 562
(3) 316
(4) 178
(5) 100·
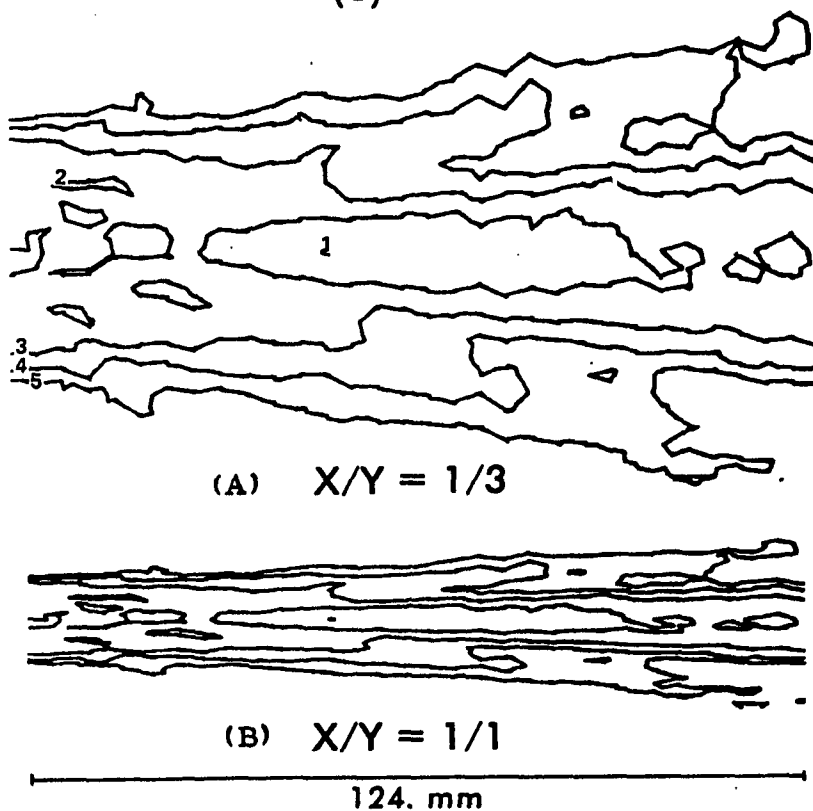

(A)   X/Y = 1/3

(B)   X/Y = 1/1

124. mm

Figure C-28. Typical ultrasonovision beam profile (shown for general comparison) for a plane, circular source (2.25 MHz, 13 mm diameter)

The remaining data was collected by the BRH on the fan beam transducer which exhibited the "full-fan" pattern. This data gives an indication of the fan beam total power output.

DEPARTMENT OF HEALTH, EDUCATION, AND WELFARE
PUBLIC HEALTH SERVICE
ROCKVILLE, MARYLAND 20852

July 6, 1978

General Electric
Bldg 3-229
Electronics Park
Syracuse, N. Y. 13201
Attn: Lawrence Nadel

Dear Mr. Nadel:

Enclosed please find the data from a calibration of your transducer s/n 47265H. A gated RF signal was used with a 5 MHz cw source, and a gating pulse of 1 khz rep rate, and 100 µsec pulse duration, for a duty cycle of 10%. The data is as follows:

Peak to Peak volts	RMS volts	Ultrasonic power
9.2V	1.0V	120 µ watts
18.5V	2.0V	400 µ watts
23.0V	2.5V	620 µ watts
28.0V	3.0V	970 µ watts
33.0V	3.5V	1.31 m watts
38.0V	4.0V	1.72 m watts

This data was taken using a Cahn electronic balance with a resolution of 30 µ watts. The distance from transducer to target was 3.2 cm and from Mike's data this indicates a beam diameter of 3.5 cm. The target has a diameter of 4.8 cm so the entire beam is intercepted by the target. The error due to non plane wave nature of the beam is less than 2%.

Sincerely,

Ronald A. Robinson
Staff Engineer, Acoustics Br.
5600 Fishers Lane - Room 749
Rockville, Md. 20857
(301) 443-6113

P. S.

also enclosed is a linear regression graph of the data. I hope this data will be useful to you in your work. If I can be of further assistance please let me know
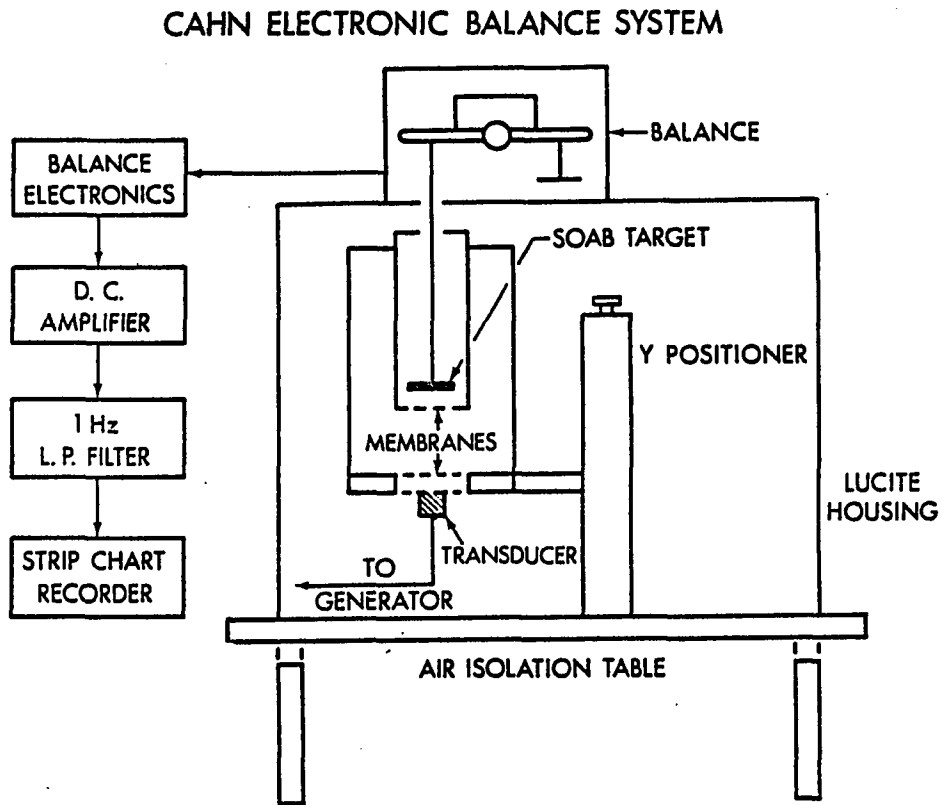
RAR

CAHN ELECTRONIC BALANCE SYSTEM

Figure C-29. Cahn electronic balance system used to measure ultrasonic output power
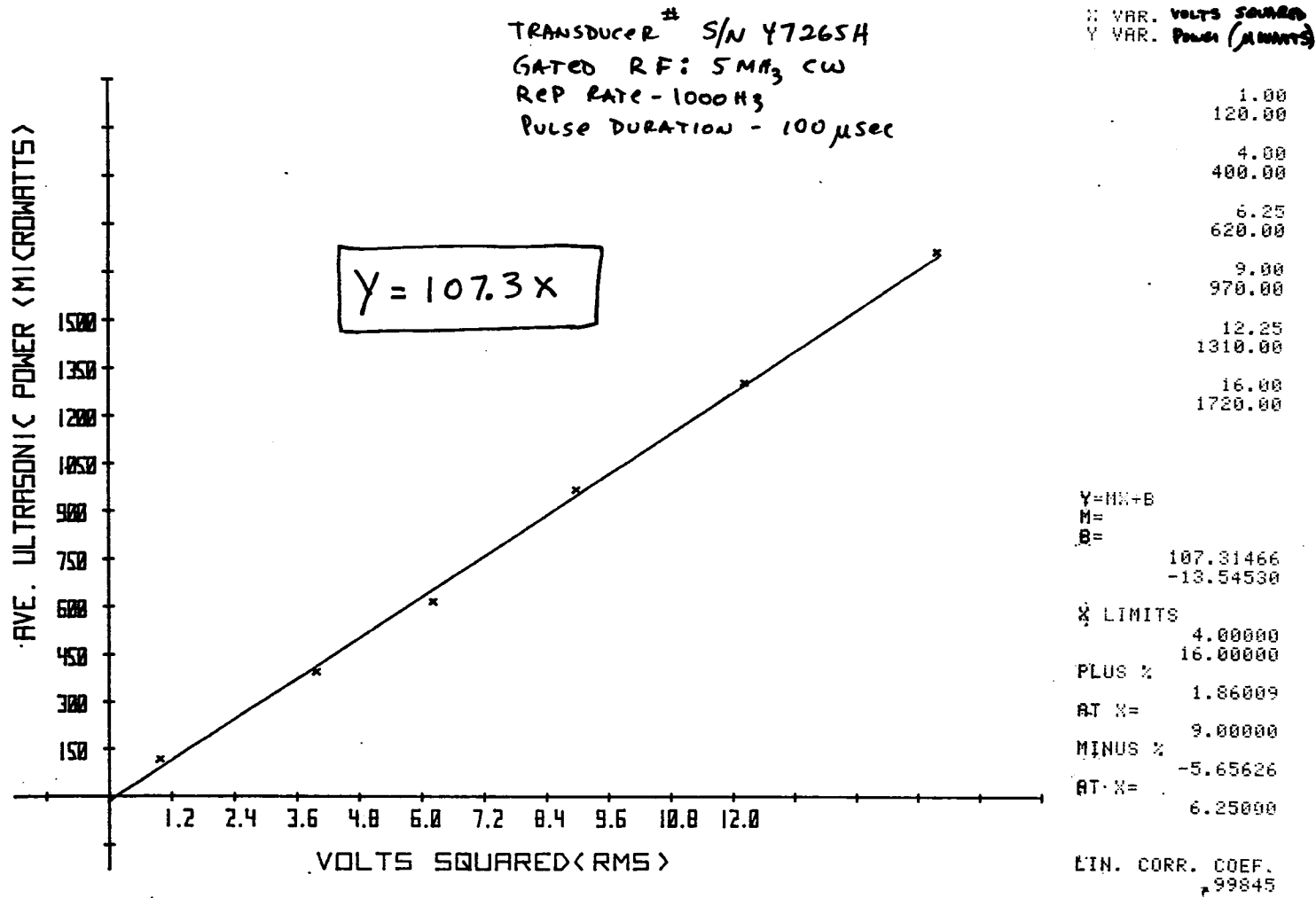
Figure C-30. Output power versus input voltage squared for S/N 47265H as
determined by the BRH Cahn electronic balance

REFERENCES

[1] Liboff, A.R. and Terry, F., Pulse Scatter Imaging (Revised), General Electric Company, Electronics Laboratory, Syracuse, N.Y., Report No. R77ELS036, August, 1977.

[2] Graff, Karl F., "Ultrasonics Historical Aspects", IEEE 1977 Ultrasonics Symposium Proceedings, IEEE Cat. #77CH1264-ISU, New York, 1977.

[3] Lord Rayleigh, Theory of Sound, Dover Publications, New York, 1945.

[4] Firestone, Floyd A., "The Supersonic Reflectoscope, an Instrument for Inspecting the Interior of Solid Parts by Means of Sound Waves", Journal of the Acoustical Society of America, 17(3), January, 1946, pp. 287-299.

[5] Posakony, Gerald J., "A Look to the Past -- A Look to the Future", Materials Evaluation, December 1976, pp. 10A-21A.

[6] Smith, James J., M.D., "The Use of Supersonic Waves in Clinical Diagnosis", Journal of Clinical Ultrasound, 4(6), December, 1976, p. 376.

[7] Ohio State University, Bio-Medical Engineering Center, Columbus, Ohio.

[8] "Statement on Mammalian In Vivo Ultrasonic Biological Effects - August 1976", Journal of Clinical Ultrasound, 5(1), February 1977, pp. 2-3.

[9] Gordon, R., Herman, G.T., and Johnson, S.A., "Image Reconstruction From Projections", Scientific American, 233(4), October 1975, pp. 56-68.

[10] Glusick, Robert E., unpublished material, General Electric Company, Electronics Laboratory, Syracuse, N.Y.

[11] McMaster, Robert C., editor, Non-Destructive Testing Handbook, Vol. II, The Ronald Press, New York, 1959.

[12] McDicken, W.N., Diagnostic Ultrasonics: Principles and Use of Instruments, John Wiley and Sons, New York, 1976.

[13] Wells, P.N.T., <u>Biomedical Ultrasonics,</u> Academic Press, London, 1977.

[14] Hussey, Matthew, <u>Diagnostic Ultrasound,</u> John Wiley and Sons, New York, 1975.

[15] Goldberg, Barry B., <u>Abdominal Gray Scale Ultrasonography,</u> John Wiley and Sons, N.Y., 1977.

[16] Faran, James J., Jr., "Sound Scattering by Solid Cylinders and Spheres", <u>J. Acoust. Soc. Am.</u>, 23(4), July 1951, pp. 405-418

[17] Davis, C.M., et. al., "Acoustic Scattering From Silicone Rubber Cylinders and Spheres", <u>J. Acoust. Soc. Am.</u>, 63(6), June 1978, pp. 1694-1698.

[18] Alkier, K.W., "Underwater Acoustic-Backscattering and Echo Structure Characteristics for a Thin Stiffened Plate", <u>J. Acoust. Soc. Am.</u>, 63(3), March 1978, pp. 704-708.

[19] Tittman, B.R., "Mode Conversion and Angular Dependence for Scattering From Voids in Solids", <u>1975 IEEE Ultrasonics Symposium Proceedings,</u> pp. 111-115.

[20] Fay, B. et. al., "Studies of Inhomogeneous Substances by Ultrasonic Backscattering", <u>Ultrasound in Medicine and Biology,</u> 2(3), June 1976, pp. 195-198

[21] Lerner, R.M., et. al., "Ultrasound Diffraction and Fourier Optical Determination of Average Scatterer Spacing in a Random Medium", <u>Appendix II: Tissue Characterization With Ultrasound - NSF Project APR 75 - 14890/R.C. Waag - PI,</u> Univ. of Rochester, April 1976.

[22] Lee, Paul P.K., "Swept-Frequency Diffraction of Ultrasound by Cylinders and Arrays", <u>Appendix III: NSF Project Report APR 75-14890,</u> Univ. of Rochester.

[23] Shung, K.R., and Reid, J.M., "Ultrasonic Scattering From Tissues", <u>1977 IEEE Ultrasonic Symposium Proceedings,</u> pp. 230-233.

[24] Gramiak, R. et. al., "Diffraction Characterization of Tissue Using Ultrasound", <u>1976 IEEE Ultrasonics Symposium Proceedings,</u> pp. 60-63.

[25] Senapti, N. et. al., "A Study of the Scattering of Sub-Millimeter Ultrasound From Tissues and Organs", <u>1972 IEEE Ultrasonics Symposium Proceedings,</u> pp. 59-63.

[26] Shung, Koping K., et. al., "Angular Dependence of Scattering of Ultrasound From Blood", <u>IEEE Transactions on Biomedical Engineering,</u> 24(4), July 1977, pp. 325-331.

[27] Gore, J.C., and Leeman, S., "Ultrasonic Backscattering From Human Tissue: A Realistic Model", Physics in Medicine and Biology, 22(2), 1977, pp. 317-326.

[28] Waag, R.C., et. al., "Swept-Frequency Ultrasonic Determination of Tissue Macrostructure", NBS Proceedings of Seminar on Ultrasonic Tissue Characterization, May 1975, pp. 213-228.

[29] Waag, R.C., and Lerner, R.M., "Tissue Macrostructure Determination With Swept-Frequency Ultrasound, 1973 IEEE Ultrasonics Symposium Proceedings, pp. 63-66.

[30] Waag, R.C., et. al., "Angle Scan and Frequency Swept Ultrasonic Scattering Characterization of Tissue", NBS Proceedings of the 2nd International Symposium on Ultrasonic Tissue Characterization, June 1977 (pre-print).

[31] Waag, R.C., et. al., "Ultrasonic Diffraction Characterization of Tissue", Ultrasound in Biomedicine, ed. by D.N. White, Research Studies Press, Forest Grove, Ore., 1978.

[32] Lele, P.P., et. al., "Tissue Characterization by Ultrasonic Frequency - Dependent Attenuation and Scattering", Proceedings of NBS Seminar on Ultrasonic Tissue Characterization, May 1975, pp. 167-196.

[33] Shung, K.K. et. al., "The Scattering of Ultrasound by Red Blood Cells", Proceedings of NBS Seminar on Ultrasonic Tissue Characterization, June 1975, pp. 207-212.

[34] Waag, R.C., et. al., "Tissue Macrostructure From Ultrasound Scattering", Proceedings of the Conference on Computerized Tomography in Radiology, April 1976, pp. 175-186.

[35] Hill, C.R., Frequency and Angular Dependence of Ultrasonic Scattering From Tissue", Proceedings of NBS Seminar on Ultrasonic Tissue Characterization, May 1975, pp. 197-206.

[36] Hueter, Theodore and Bolt, Richard, Sonics, John Wiley and Sons, Inc., New York, 1955.

[37] Clevite Corporation, "Piezoelectric Technology Data for Engineers", Bedford, OH, 1965.

[38] Linden Labs., Inc., "Application Notes - Volume 1 - Piezoceramics", State College, PA, 1976.

[39] Automation Industries, Inc., "What You Should Know About Automatic Search Units", Danbury, CT, 1971.

[40] Bennet, S.D., and Chambers, J., "Novel Variable - Focus Ultrasonic Transducer", Electronics Letters, 13(4), February 17, 1978, pp. 110-111.

[41] Murayama, N., et. al., "The Strong Piezoelectricity in Polyvinylidene Fluoride (PVDF)", Ultrasonics, January 1976, pp. 15-23.

[42] Heyman, Joseph S., and Cantrell, John H., Jr., "Application of an Ultrasonic Phase Insensitive Receiver to Material Measurements", 1977 IEEE - Ultrasonic Symposium Proceedings, IEEE Catalog #77CH1264-1SU, pp. 124-128.

[43] Frederick, Julian R., Ultrasonic Engineering, John Wiley and Sons, Inc. New York, 1965.

[44] Berlincourt, Don A., et. al., "Piezoelectric and Piezomagnetic Materials and Their Function in Transducers", Physical Acoustics, Vol. 1(A), edited by Warren P. Mason, Academic Press, New York, 1964.

[45] Foster, F.S., and Hunt, J.W., "The Design and Characterization of Short Pulse Ultrasound Transducers", Ultrasonics, 16(3), May, 1978, pp. 116-122

[46] Krautkramer, Josef and Krautkramer, Herbert, Ultrasonic Testing of Materials, 2nd ed., Springer Verlag, NY, 1977.

[47] King, Donald, editor, Diagnostic Ultrasound, C.V. Mosby Co., St. Louis, 1974.

[48] Hubelbank, Mark, Computer Enhancement of Ultrasound Images, Doctoral Dissertation, Massachusetts Institute of Technology, Aug. 1972.

[49] Freimanis, Atis K., "The Biological Effects of Medically Applied Ultrasound and Their Causes", CRC Critical Reviews in Radiological Sciences, Chemical Rubber Co., Cleveland, December 1970, pp. 639-652.

[50] Gregg, E.C., "Ultrasonics: Biologic and Medical Effects", Medical Physics, Ed. by Otto Glasser, Year Book Publishers, Inc., Chicago, 1960.

[51] Baum, Gilbert, Fundamentals of Medical Ultrasonography, G.P. Putnam's Sons, N.Y., 1975.

[52] Coleman, D.J., Katz, L. and Lizzi, F.L., "Isometric, Three-Dimensional Viewing of Ultrasonograms", Archives of Ophthalmology, Vol. 93, December 1975, pp. 1362-1365.

[53] von Ramm, Olaf T., and Thurstone, Frederick L., "Cardiac Imaging Using a Phased Array Ultrasound System", Circulation, 53(2), February 1976, pp. 258-267.

[54] Pederson, Jan Fog and Nartheved, Allan, "An Ultrasonic Multitransducer Scanner for Real Time Heart Imaging", Journal of Clinical Ultrasound, 5(1), February, 1977, pp. 11-15.

[55] Walter, J.T., and Meindl, J.D., "A Digitally Controlled CCD Dyna-mically Focused Phased Array", 1975 IEEE Ultrasonics Symposium Proceedings, IEEE Cat. #75CHO994-4SU, pp. 80-83.

[56] Beaver, William L., "A Method of Three-Dimensional Electronic Focusing and Beam Steering Using Electronic Delay Lines", 1975 IEEE Ultrasonics Symposium Proceedings, IEEE Cat. #75CHO994-4SU, pp. 88-90.

[57] Dussik, K.S., "Possibility of Using Mechanical High Frequency Vibration as a Diagnostic Aid", Journal of Neurological Psychiatry, Vol. 174, pp. 153-168.

[58] Meindl, James D., Integrated Electronics for Acoustic Imaging Arrays, Stanford University Electronics Laboratory, October, 1975.

[59] Wells, P.N.T., "Ultrasonics in Medicine and Biology", Physics in Medicine and Biology, 22(4), 1977, pp. 629-699.

[60] Smith, James M., "A Survey of Advanced Techniques for Acoustic Imaging", Army Materials and Mechanics Research Center, Watertown, MA, NTIS No. ADA048039, August, 1977.

[61] Devey, Gilbert B., and Wells, Peter N.T., "Ultrasound in Medical Diagnosis", Scientific American, May, 1978, pp. 98-111.

[62] Erikson, Kenneth R., et. al., "Ultrasound in Medicine – A Review", IEEE Transactions on Sonics and Ultrasonics, Vol. SU-21, No. 3, July, 1974, pp. 144-170.

[63] Linzer, Melvin, Editor, Ultrasonic Tissue Characterization, National Bureau of Standards, Publication No. 453, Gaithersburg, MD, October, 1976.

[64] VanEtten, J.P., "Loran-C System and Product Development", (ITT) Electrical Communication, 45(2), 1970, pp. 100-115.

[65] Pierce, J.A., et. al., Loran, McGraw-Hill Book Co., New York, 1948.

[66] Kazel, Sidney, "Multilateration Radar", Proceedings of the IEEE, October, 1972, pp. 1238-1239.

[67] "Seismic Exploration for Oil and Gas", McGraw-Hill Encyclopedia of Science and Technology, Vol. 12, 1977, pp. 190-193.

[68] Dow, J. and Brown, R., "Isochrone Convergence Imaging of Pulse Echoes", Ultrasonics, May, 1977, pp. 129-135.

[69] Shepp, L.A., and Kruskal, J.B., "Computerized Tomography: The New Medical X-Ray Technology", The American Mathematical Monthly, 85(6), June-July, 1978, pp. 420-439.

[70] Scudder, Henry J., "Introduction to Computer-Aided Tomography", Proc. of the IEEE, 66(6), June 1978, pp. 628-637.

[71] Brooks, R.A., and DiChiro, G., "Principles of Computer Assisted Tomography (CAT) in Radiographic and Radioisotopic Imaging", Physics in Medicine and Biology, 21(5), 1976, pp. 689-732.

[72] Glover, G.H., "Computerized Time-of-Flight Ultrasonic Tomography for Breast Examination", General Electric Company Report #76CRD164, Schenectady, NY, 7/76.

[73] Glover, G.H., and Sharp, J.C., "Reconstruction of Ultrasound Propagation Speed, Distributions in Soft Tissue: Time of Flight Tomography", IEEE Transactions on Sonics and Ultrasonics, Vol. SU-24, No. 4, 7/77, pp. 229-234.

[74] Greenleaf, J.F., et al., "Algebraic Reconstruction of Spatial Distributions of Acoustic Velocities in Tissue From Their Time-of-Flight Profiles", Acoustical Holography - Volume 6, Plenum Press, NY, pp. 71-90.

[75] Carson, P.L., Oughton, T.V., and Hendee, W.R., "Ultrasound Transaxial Tomography By Reconstruction", Dept. of Radiology, Univ. of Colorado Medical Center, Report, copy received 4/20/77.

[76] Herman, Gabor T., and Lent, Arnold, "ART: Mathematics and Applications", J. Theor. Biol, Vol. 42, 1973, pp. 1-32.

[77] Edelheit, Lewis S., Herman, Gabor T., and Lakshminarayanan, A.V., "Reconstruction of Objects From Diverging X-Rays", Medical Physics, 4(3), May/June, 1977, pp. 226-231.

[78] Chivers, R.C., and Hill, C.R., "A Spectral Approach to Ultrasonic Scattering From Human Tissue", Physics in Medicine and Biology, 20(5), 1975, pp. 797-815.

[79] Winter, T.G., et. al., "On Driving a Transducer to Produce Pulses Shorter Than the Natural Period of the Transducer", Ultrasonics, 13(3), May, 1975, pp. 110-112.

[80] Foster, F.S., and Hunt, J.W., "The Design and Characterization of Short Pulse Ultrasound Transducers", Ultrasonics, 16(3), May, 1978, pp. 116-122.

[81] Desilets, Charles S., et. al., "The Design of Efficient Broad-Band Piezoelectric Transducers", IEEE Transactions on Sonics and Ultrasonics, SU-25(3), May, 1978.

[82] Furgason, E.S., et. al., "Application of Random Signal Correlation Techniques to Ultrasonic Flaw Detection", Ultrasonics, 13(1), January, 1975, pp. 11-17.

[83] Cho, Z.H., "General Views on 3-D Image Reconstruction and Computerized Transaxial Tomography", <u>IEEE Transactions on Nuclear Science</u>, Vol. NS-21, June, 1974, pp. 44-71.

[84] Budinger, T.F., and Gullberg, G.T., "Three-Dimensional Reconstruction in Nuclear Medicine Emission Imaging", <u>IEEE Transactions on Nuclear Science</u>, NS-21(3), 6/74, pp. 2-20.

[85] Cho, Z.H., et. al., "A Comparative Study of 3-D Image Reconstruction Algorithms With Reference to Number of Projections and Noise Filtering", <u>IEEE Transactions on Nuclear Science</u>, Vol. NS-22, February, 1975, pp. 344-358.

[86] Cho, Z.H., and Tsai, C.M., "Computer Algorithms and Detector Electronics for the Transmission X-Ray Tomography", <u>IEEE Transactions on Nuclear Science</u>, NS-21(1), 1974, pp. 218-227.

[87] Brunal, J., et. al., "Déconvolution Analogique en Imagerie Par Ouverture Codée Appliquée à la Médicine Nucléaire", <u>Optica Acta</u>, 25(2), pp. 113-124.

[88] Mezrich, R.S., "System for Visualizing and Measuring Ultrasonic Wavefronts", <u>RCA Review</u>, Vol. 35, December, 1974, pp. 483-519.

[89] Haran, M.E., "Optical Interferometric Measurements of Ultrasonic Radiation and Its application to Medicine", Bureau of Radiological Health Report, NBS SP456 (1976), pp. 285-297.

[90] Furason, E.S., et. al., "Application of Random Signal Correlation Techniques to Ultrasonic Flaw Detection", <u>Ultrasonics</u>, 13(1), January, 1975, pp. 11-17.

[91] Sackman, George L., et. al., <u>An Introduction to Acoustic Signal Processing</u>, Chapter VIII, Naval Postgraduate School, Monterrey, CA, NTIS #ADA050010, November, 1977.

[92] Andrews, H.C. and Hunt, B.R., <u>Digital Image Restoration</u>, Prentice-Hall, Inc., Englewood Cliffs, NJ, 1977.

[93] Andrews, Harry C., editor, <u>Tutorial and Selected Papers on Digital Image Processing</u>, IEEE Computer Society, IEEE #EH0133-9, 1978.

[94] Gonzalez, Rafael C. and Wintz, Paul, <u>Digital Image Processing</u>, Addison-Wesley Pub. Co., Reading, MA, 1977.

[95] Toriwaki, Jun-Ichiro and Fukumura, Teruo, "Extraction of Structural Information From Grey Pictures", <u>Computer Graphics and Image Processing</u>, No. 7, 1978, pp. 30-51.

[96] Cahill, P.T., Ornstein, E. and Ho, S.L., "Edge Detection Algorithms in Nuclear Medicine", IEEE Transactions on Nuclear Science, NS-23(1), February, 1976, pp. 555-559.

[97] Andrews, Harry C., Computer Techniques in Image Processing, Academic Press, New York, 1970.